

Evaluation of MDCK suspension cell lines for influenza A virus production: media, metabolism, and process conditions

Dissertation

zur Erlangung des akademischen Grades

Doktoringenieur

(Dr.-Ing.)

von

Dipl.-Biol. (t.o.) Thomas Bissinger

geboren am

12. April 1986 in Ulm

genehmigt durch die Fakultät für Verfahrens- und Systemtechnik
der Otto-von-Guericke-Universität Magdeburg

Promotionskommission:

Prof. Dr.-Ing. Andreas Seidel-Morgenstern	(Vorsitz)
Prof. Dr.-Ing. Udo Reichl	(Gutachter)
Prof. Alan Dickson, PhD	(Gutachter)
Dr.-Ing Boris Hundt	(Gutachter)

eingereicht am: **29. Juni 2020**

Promotionskolloquium am: **28. Oktober 2020**

Kurzfassung

Infektionen mit Influenza-Viren sind nicht nur eine Bedrohung für die Gesundheit von Millionen Menschen, sondern haben auch erhebliche Auswirkungen auf die lokale und globale Wirtschaft. Die Kontrolle und Prävention von Grippe Epidemien hängt von der Verfügbarkeit wirksamer und sicherer saisonaler- und pandemischer Impfstoffe ab, welche hauptsächlich aus inaktivierten Influenzaviruspartikeln hergestellt werden. Die derzeitigen Produktionsprozesse basieren hierbei stark auf Hühnereiern als Substrat für die Virusvermehrung. Trotz der Unterschiede in den Oberflächenantigenen der saisonalen Virus-Subtypen, sind die Impfstoffhersteller gut gerüstet, um der periodischen Nachfrage nach Impfstoffdosen nach zu kommen. Angesichts der steigenden Nachfrage nach Grippeimpfstoffen in den Schwellenländern und des Bedarfs an Milliarden von Impfstoffdosen im Falle einer plötzlichen Pandemie, könnte die traditionelle Impfstoffherstellung jedoch an ihre Grenzen stoßen. Der Einsatz von zellkulturbasierten Produktionsprozessen ermöglicht eine schnelle Fertigung sowohl in großtechnischen als auch in mittelgroßen Anlagen, unabhängig von Hühnereiern. Um eine effiziente zellkulturbasierte Fertigung zu ermöglichen, sind optimierte Produktionsprozesse erforderlich. Hier können neue Zellkulturmedien, gut charakterisierte Produktionszelllinien und neue Zellkulturprozesstechnologien helfen, Produktionsbarrieren zu überwinden und sichere, effiziente und kostengünstige Grippeimpfstoffe anzubieten.

Diese Arbeit konzentriert sich auf die Evaluierung von MDCK-Suspensionszelllinien für die Herstellung von zellkulturbasierten Grippeimpfstoffen. Wachstum, Stoffwechsel und Produktivität verschiedener MDCK-Suspensionszelllinien in einer Variation der Kultivierungsmedien wurden bewertet, um einen Batchprozess zu entwickeln, welcher bei sehr hohen Zellkonzentrationen maximale Virusausbeuten ermöglicht. Darüber hinaus wurden die Auswirkungen der Influenzavirusinfektion auf den zentralen Energie- und Kohlenstoffmetabolismus der MDCK-Suspensionszellen analysiert, um potenzielle metabolische Engpässe zu identifizieren, die die Replikation des Influenzavirus begrenzen könnten.

Im ersten Teil dieser Arbeit wurde eine MDCK-Suspensionszelllinie an ein neues Kultivierungsmedium adaptiert, welches ein schnelleres Zellwachstum, eine höhere Zellkonzentration und einen höheren Influenzavirus Titer als vergleichbare Medien ermöglichte. MDCK-Zellen wuchsen als Einzelzellensuspension mit einer Verdoppelungszeit von weniger als 20

Stunden und erreichten Zellkonzentrationen von über 10×10^6 Zellen/mL im Batch-Betrieb. Influenza A-Virus Titer von Batchinfektionen, lagen bei 3,6 lg(HAU) für die gesamten Viruspartikel und 10^9 TCID₅₀/mL für infektiöse Viruspartikel. Zusätzlich wurde eine Kultivierung mit hoher Zelldichte im Semi-Perfusionsmodus durchgeführt, wobei Zellkonzentrationen von bis zu 60×10^6 Zellen/mL möglich waren. Mit dieser Technologie wurden Virustiter von 4,5 lg(HAU) erreicht, die höchsten bisher in Zellkultur gemessenen Titer.

Im zweiten und dritten Teil dieser Arbeit wurden vier MDCK Suspensionszelllinien verglichen, um die Auswirkungen von Medium und Zelllinie auf das Zellwachstum, den Stoffwechsel und die Virusproduktion zu untersuchen. Die MDCK-Zelllinie aus der amerikanischen Zellbank (ATCC), kultiviert in einem neuen chemisch definierten Medium, war den anderen getesteten Zelllinien deutlich überlegen. Dies führte zu der Entwicklung eines skalierbaren Fed-Batch-Prozesses für die Herstellung von Grippeimpfstoffen. Durch optimale Skalierbarkeit, sehr guten Wachstumseigenschaften, optimierter Mediumsnutzung und einer maximalen Zellkonzentration von 12×10^6 Zellen/mL, waren sehr hohe Influenzavirus-Titer von 3,6 lg(HAU) und 2×10^9 TCID₅₀/mL möglich. Eine geschätzte Produktivität von bis zu 600 Impfstoffdosen pro Liter innerhalb von nur 4 bis 5 Tagen Kultivierungszeit machte diesen Prozess sowohl im Vergleich zu anderen zellbasierten Prozessen als auch gegenüber der eierbasierten Produktion überlegen.

Der letzte Teil dieser Arbeit konzentrierte sich auf die detaillierte Analyse des Stoffwechsels der MDCK-Suspensionszelle während des Zellwachstums und nach der Infektion mit Influenzaviren. Extra- und intrazelluläre Metaboliten und die Replikation des Influenzavirus bei Infektionen mit hoher MOI wurden in zwei Versuchsreihen untersucht. Eine synchrone Zellinfektion führte zu einem schnellen Stopp des Zellwachstums. Nach einem kurzen Zeitintervall der Virusvermehrung von nur 12 Stunden, setzte die virusinduzierte Apoptose ein, welche zu einem schnellen Zelltod führte. Innerhalb dieser Zeit waren sowohl der zellspezifische Glukoseverbrauch als auch die Laktatsekretion leicht erhöht. Es wurden einige Veränderungen in den intrazellulären Metabolitpools der Glykolyse gefunden, was auf eine Wirkung der Virusinfektion auf diesen Stoffwechselweg hinweist. Für die Energiemetaboliten (ATP, ADP, AMP), die Energieladung und die Metabolitpools des TCA-Zyklus wurden jedoch keine größeren Veränderungen gefunden.

Insgesamt gibt diese Arbeit einen tieferen Einblick in den Stoffwechsel von MDCK-Suspensionszellen, insbesondere nach der Infektion mit Influenzaviren. Obwohl kein klarer metabolischer Engpass für die Vermehrung der Influenzaviren identifiziert werden konnte, gab es einige Hinweise auf eine veränderte Glykolyse in infizierten MDCK-Suspensionszellen. Insgesamt waren die metabolischen Auswirkungen von Influenza-A-Virusinfektionen jedoch begrenzt.

Darüber hinaus wurden zwei neuartige, hochproduktive Verfahren zur Herstellung von Influenzaviren entwickelt. Hier wurden, mittels neuer Kultivierungsmedien, MDCK Suspensionszelllinien generiert, welche in Kombination mit modernster Kultivierung- und Prozesstechnologie den Virustiter und die Produktivität deutlich erhöhten. Diese Arbeit könnte der erste Schritt zu einem verbesserten, weit verbreiteten und kostengünstigen MDCK-basierten Grippeimpfstoff sein, der idealerweise in einem intensivierten Verfahren mit hoher Zelldichte hergestellt wird.

Abstract

Human influenza virus infections are not only a threat for the health of millions of people but have a significant impact on local and global economies as well. Control and prevention of rapid influenza spread depend on the availability of efficacious and safe seasonal and pandemic vaccines, made primarily from inactivated influenza virus particles. Current influenza virus production processes rely heavily on embryonated chicken eggs as substrate for virus propagation. Manufacturers are well prepared to respond to seasonal demands for vaccine doses, despite the differences in surface antigens and virulence of virus subtypes. However, with raising demand for influenza vaccines in developing countries and the need for billions of vaccine doses in case of a sudden pandemic, traditional vaccine manufacturing might reach its limits. With the use of cell culture-based facilities, egg independent virus production enables fast manufacturing both in large scale and medium sized single use facilities. To enable efficient cell culture-based manufacturing, optimized production processes are needed. Here, cell culture media, well characterized production cell lines, and state of the art cell culture process technologies can help to overcome production barriers and provide safe, efficient, and affordable influenza vaccines.

This work focuses on the evaluation of MDCK suspension cell lines for the production of cell culture-based influenza vaccines. Growth, metabolism and productivity of different MDCK suspension cell lines in various cultivation media were evaluated to suggest an improved, highly productive process with very high cell concentrations. Additionally, effects of influenza virus infection on the central energy and carbon metabolism on the MDCK suspension cells was analyzed to identify potential metabolic bottleneck that could limit influenza virus replication.

In the first part of this thesis a MDCK suspension cell line was adapted to a new cultivation medium which enabled faster cell growth, higher cell concentration and higher influenza virus titer. MDCK cells grew as single cell suspension with a doubling time of less than 20 h achieving cell concentrations over 10×10^6 cells/mL in batch mode. Influenza A virus titer obtained in batch infections were 3.6 lg(HAU) for total- and 10^9 TCID₅₀/mL for infectious virus particles, respectively. Additionally, high cell density cultivations were performed in semi-perfusion mode, where cell concentrations of up to 6×10^7 cells/mL were possible. Using this technology a virus titer of 4.5 lg(HAU) were reached, which was the highest titer ever reported so far.

In the second and third part of this thesis, four MDCK suspension cell lines were evaluated to investigate the impact of medium, and cell line on the cell growth, metabolism and virus production. The MDCK cell line from the American cell bank (ATCC), cultivated in a new chemically defined medium was identified to be superior to the other tested cell lines and media. The superior characteristics of this cell line were used to design and evaluate a scalable fed-batch process for the manufacturing of influenza vaccines. Due to optimal scalability, superior growth, optimized medium use and maximal cell concentration of 12×10^6 cells/mL very high influenza virus titers of 3.6 lg(HAU) and 2×10^9 TCID₅₀/mL were achieved. An estimated productivity of up to 300 vaccine doses per liter of harvest broth within 4 to 5 days of manufacturing made this process superior not only to other cell-based processes but to egg-based production as well.

The last part of this work focused on the deeper analysis of the metabolism of MDCK suspension cell during a cell growth phase and upon influenza virus infection. Extra- and intracellular metabolites and influenza virus replication in high MOI infections were monitored in two sets of experiments. A synchronous cell infection stopped cell growth almost immediately limiting virus replication to about 12 h until virus-induced apoptosis resulted in fast cell death. Within this time period cell specific glucose consumption as well as lactate secretion was slightly increased. Some alterations were found in the intracellular metabolite pools of the lower glycolysis indicating an effect of virus infection on this pathway. However, no changes were found for energy metabolites (ATP, ADP, AMP), energy charge and the metabolite pools of the TCA cycle.

Overall, this thesis gives a deeper insight in the metabolism of MDCK suspension cells, especially upon influenza virus infection. Even though no clear metabolic bottleneck has been identified, there was some evidence for an altered glycolysis in infected MDCK suspension cells. However, the overall metabolic effects of influenza A virus infections were limited. Furthermore, two novel highly productive processes for influenza vaccine manufacturing were designed. Here, new cultivation media for MDCK suspension was combined with modern cultivation and process technologies to maximize virus titers and productivity. This work might be the first step towards an improved, widely available, and affordable MDCK-based influenza vaccine ideally produced in intensified high cell density processes.

Content

Abbreviations.....	XIII
Symbols	XVII
List of figures.....	XIX
List of tables.....	XXI
1 Introduction	1
2 Theoretical background	5
2.1 Influenza disease and virology	5
2.1.1 Virus structure & viral replication	6
2.1.2 Influenza A virus antigens.....	6
2.1.3 Pandemic and seasonal influenza.....	9
2.2 Influenza vaccines	11
2.2.1 Viral vaccines: past, present & future	11
2.2.2 Influenza vaccine manufacturing.....	12
2.2.3 MDCK cells for influenza virus propagation.....	14
2.3 Metabolism of mammalian cell culture.....	16
2.3.1 The central carbon metabolism in brief	16
2.3.2 Metabolomics: the analytical tool set	23
2.3.3 Metabolomics in mammalian cell culture processes.....	24
2.3.4 Metabolic effects of virus infections	25
3 Materials and methods.....	27
3.1 Cell culture	27
3.1.1 Media and cell lines.....	27
3.1.2 Cultivation of MDCK suspension cells.....	29
3.1.3 Cell culture analytics.....	31
3.2 Influenza A virus infection	33
3.2.1 Seed viruses.....	33
3.2.2 Infection conditions.....	33

3.2.3	Analytics for influenza virus particles and infected cells	35
3.2.4	Viral antigen content and host cell contaminants.....	37
3.3	Metabolic profiling of MDCK suspension cells	38
3.3.1	Quenching	38
3.3.2	Metabolite extraction & recovery	40
3.3.3	Metabolite quantification by LC-MS.....	41
3.4	Calculations and statistics	43
3.4.1	Calculations	43
3.4.2	Errors and statistics	45
4	Results and discussion	47
4.1	A new medium for influenza virus production	47
4.1.1	Adaptation of MDCK suspension cells to Xeno-SFM	47
4.1.2	MDCK.Xe.E: cell growth and influenza A virus production	49
4.1.3	Cultivation and infection of MDCK.Xe.E cells at high cell density.....	51
4.1.4	Summary: MDCK.Xe.E cells for influenza A virus production	54
4.2	Comparison of MDCK cell lines for influenza A virus production	55
4.2.1	Adaptation of MDCK.Xe.A to Smif8 medium.....	55
4.2.2	Cell growth and metabolism	56
4.2.3	Infection and influenza A virus production using different MDCK cell lines.....	61
4.2.4	The optimal cell line for influenza A virus production.....	63
4.3	Influenza A virus production in laboratory scale bioreactors.....	65
4.3.1	Optimization of stirred tank bioreactor cultivations	66
4.3.2	MDCK.Xe.A cells in stirred tank system: growth and metabolism.....	67
4.3.3	MDCK.Xe.A cells in stirred tank system: influenza A virus production	75
4.3.4	Process performance in stirred tank bioreactors	79
4.4	Metabolic profiling of MDCK suspension cells	82
4.4.1	Evaluation of quenching methods for MDCK.S8.E and MDCK.Xe.E cells	83
4.4.2	Cell growth and extracellular metabolites of MDCK.S8.E cells.....	89
4.4.3	Influenza A virus replication in MDCK.S8.E cells.....	93
4.4.4	Dynamics of intracellular metabolite pools in MDCK.S8.E cells	95
4.4.5	Overall effects of influenza A virus infection on MDCK metabolism	102
5	Conclusion.....	103

6	Outlook	107
7	References.....	109
8	Appendix	127
8.1	Cultivation media for MDCK suspension	127
8.2	LC-MS measurement.....	129
8.3	Error estimation: TCID ₅₀ assay	132
8.4	Error estimation: HA assay	133

Abbreviations

1,3PG	1,3-Bisphosphoglycerate
3PG	3-Phosphoglycerate
AA	Amino acids
ACCoA	Acetyl-CoA
ADP	Adenosine diphosphate
AEC	Adenylate energy charge
AE-HPLC	Anion exchange HPLC
Ala	Alanine
AMBIC	Ammonium bicarbonate
AMP	Adenosine monophosphate
AMPK	AMP-activated protein kinase
APR	Influenza A/Puerto Rico/8/34(H1N1) virus
Asp	Aspartate
ATCC	American Type Culture Collection
ATF	Alternating tangential flow filtration
ATP	Adenosine triphosphate
BHK	Baby hamster kidney
BSA	Bovine serum albumin
Cas9	CRISPR associated protein 9
CDC	Centers for Disease Control and Prevention
CDM	Chemically defined medium
CE	Capillary electrophoresis
CHO	Chinese hamster ovary
Cit	Citrate
CO₂	Carbon dioxide
CoA	Coenzyme A
CoA	Coenzyme A
CQ	Centrifugation quenching
CRISPR	Clustered regularly interspaced short palindromic repeats
CS	Citrate Synthase
CSVY	Cell specific virus yield
DAPI	4',6-Diamidino-2-phenylindole dihydrochloride
DHAP	Dihydroxyacetone phosphate
DIP	Defective interfering particles
DNA	Deoxyribonucleic acid
DO	Dissolved oxygen
DQ	Direct quenching
E4P	Erythrose 4-phosphate
ECACC	European Collection of Authenticated Cell Cultures

Abbreviations

ECE	Embryonated chicken eggs
ECUST	East China University of Science and Technology
EPO	Erythropoietin
ExpI/II	Experiment I/II of metabolic profiling
F_{1,6}BP	Fructose 1,6-bisphosphate
F6P	Fructose 6-phosphate
FACS	Fluorescence-activated cell sorting
FCS	Fetal calf serum
FQ	Filtration quenching
Fum	Fumarate
FVIII	Factor VIII (blood clotting protein)
G6P	Glucose 6-phosphate
GalNac	N-Acetylgalactosamine
GAP	Glyceraldehyde 3-phosphate
GC	Gas chromatography
GDH	Glutamate dehydrogenase
Glc	Glucose
GlcNac	N-Acetylglucosamine
Gln	Glutamine
Glu	Glutamate
GLUT	Glucose transporter
HA	Hemagglutinin
HCD	High cell density
HC-DNA	Host cell DNA
HCP	Host cell protein
HEK	Human embryo kidney
HIF-1	Hypoxia-inducible factor 1
HILIC	Hydrophilic interaction chromatography
HK	Hexokinase
hpi	Hours post infection
HPLC	High-performance liquid chromatography
IAV	Influenza A virus (i.e. A/Puerto Rico/8/34(H ₁ N ₁))
ICit	Isocitrate
Lac	Lactate
LC-MS	Liquid chromatography–mass spectrometry
LDH	Lactate dehydrogenase
lg	Common logarithm
LOD	Limit of detection
LOQ	Limit of quantification
M_{1/2}	Matrix protein 1/2
mAb	Monoclonal antibody
Mal	Malate
MDCK	Madin-Darby canine kidney
MDCK.S8.A	MDCK cell line adapted to Smif8 medium (ATCC origin)
MDCK.S8.E	MDCK cell line adapted to Smif8 medium (ECACC origin)

MDCK.Xe.A	MDCK cell line adapted to Xeno medium (ATCC origin)
MDCK.Xe.E	MDCK cell line adapted to Xeno medium (ECACC origin)
MDH	Malate dehydrogenase
MeOH	Methanol
MFA	Metabolic flux analysis
Milli-Q water	Milli-Q® ultrapure water (Type 1)
MM	Master mix (metabolite standard)
MOI	Multiplicity of infection
MPC	Mitochondrial pyruvate carrier
MPI	Max Planck Institute for Dynamics of Complex Technical Systems
MS	Mass spectrometer or mass spectrometry
mTOR	Mammalian target of rapamycin
NA	Neuraminidase
NADP	Nicotinamide adenine dinucleotide phosphate (oxidized)
NADPH	Nicotinamide adenine dinucleotide phosphate (reduced)
NIBSC	National Institute for Biological Standards and Control
NMR	Nuclear-magnetic-resonance
NP	Nucleoprotein
NSo	Murine myeloma cell line
O.D.	Outer diameter
OAA	Oxaloacetate
Oxphos	Oxidative phosphorylation
PBS	Phosphate buffered saline
PC	Pyruvate carboxylase
PD	Pyruvate dehydrogenase complex
PDK	Pyruvate dehydrogenase kinase
PEP	Phosphoenolpyruvate
PFK	Phosphofructokinase
PK	Pyruvate kinase
PPP	Pentose phosphate pathway
Pyr	Pyruvate
QqQ	Triple quadrupole
QTOF	Quadrupole Time-of-Flight
R5P	Ribose 5-phosphate
rcf	Relative centrifugation force
RNA	Ribonucleic acid
RPC	Reverse phase chromatography
rpm	Revolutions per minute
RT	Room temperature
RU5P	Ribulose 5-phosphate
S7P	Sedoheptulose 7-phosphate
SD	Standard deviation
SDS-PAGE	Sodium dodecyl sulfate polyacrylamide gel electrophoresis
SF	Shake flask
SF9	Insect cell line from <i>Spodoptera frugiperda</i>

Abbreviations

SFM	Serum-free medium
SIM	Single ion monitoring
SOP	Standard operating procedure
SRID	Single radial immunodiffusion
STD	Standard
STR	Stirred tank bioreactor
STY	Space time yield
Suc	Succinate
SucCoA	Succenyl-CoA
TCA	Tricarboxylic acid cycle
TCID₅₀	50% Tissue Culture Infective Dose
TFF	(Unidirectional) tangential flow filtration
UDP	Uridine diphosphate
UK	United Kingdom
USA	United States of America
VLP	Virus like particle
VRNP	Viral ribonucleoprotein
WHO	World Health Organization
X_{5P}	Xylulose 5-phosphate
αKG	α-ketogluterate
β-PL	β-propiolactone

Symbols

Symbol	Name	Dimension
AEC	Adenylate energy charge	–
AXP	Adenylate concentration	μM
CEry	Erythrocyte concentration	Erythrocytes/mL
CM _{analyte}	Metabolite concentration in analyte	μM
CM _{cell}	Intracellular metabolite concentration	μM
C _{S/P}	Substrate/product concentration	mM
CSPR	Cell specific perfusion rate	pL/(cell h)
CSVY _{HA}	Cell specific virus yield (HA based)	Virions/cell
CSVY _{TCID}	Cell specific virus yield (TCID ₅₀ based)	Virions/cell
CV _T	Total virus particle concentration	Virions/mL
d _i	Cell diameter of size category	μm
HA	Hemagglutination titer	lg(HAU)
HA _{acc}	Accumulated HA-titer	lg(HAU)
HA _P	HA-titer in permeate	lg(HAU)
HA _S	HA-titer in shake flask	lg(HAU)
HAU	Hemagglutination unit	HAU
N	Sample size	–
N _i	Cell number of size category i	–
N _{tot}	Total cell number of analyzed cell population	–
P	Total amount of product	g
q _{S/P}	Specific consumption/production rate	fmol/(cell h)
STY	Space time yield	Virions/(L day)
STY _{VD}	Space time yield (vaccine doses)	Doses/(L day)
TCID ₅₀	50% Tissue Culture Infective Dose	infectious virions/mL or TCID ₅₀ /mL
t _D	Doubling time	h
t _P	Total process time	day
T _v	Virus titer	Virions/mL
T _{vacc}	Accumulated virus titer	HAU or TCID ₅₀ /mL
T _{vP}	Virus titer in permeate	HAU or TCID ₅₀ /mL
T _{vS}	Virus titer in shake flask	HAU or TCID ₅₀ /mL
V _C	Cultivation volume	L
VCC	Viable cell concentration	Cells/mL
VCC _{max}	Maximal viable cell concentration	Cells/mL

Symbols

V_{cell}	Average cell volume	μL
V_{CV}	Viable cell volume per cultivation volume	$\mu\text{L}/\text{mL}$
V_{P}	Perfusion volume	mL
V_{R}	Reactor volume	mL
V_{rec}	Reconstitution volume	μL
V_{s}	Sample volume of cell suspension	mL
V_{W}	Working volume	mL
$Y_{\text{P/S}}$	Conversion ratio: product / substrate	–
z	Sample value	–
Δt	time interval between perfusion steps	h
μ	Specific cell growth rate	h^{-1}
σ_{f}	Standard deviation of function f	value of f
σ_{s}	Sample standard deviation	–

List of figures

Figure 1: Influenza A virus particle with depiction of viral proteins and segmented genome	8
Figure 2: Intracellular influenza A virus replication cycle.....	8
Figure 3: Energy and redox balance of glycolysis.	17
Figure 4: Truncated tricarboxylic acid cycle.....	20
Figure 5: Overview of the simplified central carbon metabolism for mammalian cells	22
Figure 6: Adaptation of MDCK.S8.E cells from Smif8 to Xeno-SFM medium (MDCK.Xe.E).	48
Figure 7: Cell growth and influenza A virus production of MDCK.Xe.E cells in Xeno-SFM.	50
Figure 8 Influenza A virus production with MDCK.Xe.E cells in high cell density culture.	53
Figure 9: Adaptation of MDCK.Xe.A cells to Smif8 medium.	56
Figure 10: Growth and cell properties of MDCK cell lines in different cultivation media.....	58
Figure 11: Main extracellular metabolites of MDCK cell lines in different cultivation media.	59
Figure 12: Metabolic rates and conversion ratios of main metabolites for different MDCK cell lines.....	60
Figure 13: Influenza A virus production in different MDCK suspension cell lines.....	62
Figure 14: Schematic overview of evaluated production process for influenza A virus.	65
Figure 15: Optimization of stirred tank cultivation conditions for MDCK.Xe.A cells.....	67
Figure 16: Cell count and properties of MDCK.Xe.A cells in three parallel stirred tank bioreactors.	69
Figure 17: Process parameters of MDCK.Xe.A cell cultivations in three parallel bioreactors.....	70
Figure 18: Main extrac. metabolites of MDCK.Xe.A cell cultivations in three parallel bioreactors.	71
Figure 19: Metabolic rates of MDCK.Xe.A cell cultivations in three parallel bioreactors.....	72
Figure 20: Selected amino acids of MDCK.Xe.A cell cultivations in three parallel bioreactors.	73
Figure 21 Extracellular amino acids of MDCK.Xe.A cell cultivations in three parallel bioreactors.	74
Figure 22: Influenza A virus infection of MDCK.Xe.A cell cultivations in parallel bioreactors.	77
Figure 23: Total protein and DNA profiles of MDCK.Xe.A cells cultivations in parallel bioreactors.	78
Figure 24: Experimental set-up for metabolic profiling of MDCK.S8.E cells.....	82
Figure 25: Experimental design for the evaluation of quenching methods.	83
Figure 26: Energy charge and adenylate recovery of quenched MDCK suspension cells.....	85
Figure 27: Intracellular metabolites of glycolysis for quenched MDCK suspension cells.....	86
Figure 28: Intracellular metabolites of TCA for quenched MDCK suspension cells.	87
Figure 29 Cell concentration, cell size and viability for IAV infected and mock infected MDCK cells.....	91
Figure 30: Main extracellular metabolites for IAV infected and mock infected MDCK cells.....	92
Figure 31: Specific metabolic rates of main metabolites for infected and mock infected MDCK cells.	93
Figure 32 Influenza A virus titer and image stream analysis of infected MDCK cells.....	94
Figure 33: Intracellular metabolite pools of energy metabolites in MDCK cells.	96

Figure 34: Intracellular metabolite pools of glycolytic metabolites in MDCK cells.	98
Figure 35: Intracellular metabolite pools of TCA metabolites in MDCK cells.	100
Figure 36: Intracellular metabolite pools of nucleotide sugars and ribose-P in MDCK cells.	101
Figure 37: Chromatogram of the used metabolite standard used for LC-MS analysis.....	131

List of tables

Table 1: Cultivation media for MDCK suspension cells	28
Table 2: Origin and background of the used MDCK suspension cell lines.	29
Table 3: Routine cultivation conditions of MDCK suspension cell lines in shake flasks.	30
Table 4: Settings used for counting MDCK suspension cells with the Vi-Cell XR cell counter.	32
Table 5: Influenza A seed viruses adapted to different cell lines	33
Table 6: Overview of the infection conditions used in the different experiments.....	35
Table 7: Solutions used for washing, quenching and metabolite extraction.	38
Table 8: KOH-gradient for the separation of intracellular metabolites by AE-HPLC.	41
Table 9: Dilutions used as external standards for quantitative LC-MS measurements.	42
Table 10: Comparison of influenza A virus production in batch and semi-perfusion culture.....	52
Table 11 Cellular growth performance and influenza virus productivity for MDCK cell lines.	64
Table 12: Comparison of metabolic activity of MDCK cells between bioreactor and shake flask.	81
Table 13: Bioreactor and shake flask process performance for influenza A virus production.	81
Table 14: Overview of equipment and time necessary for the different quenching methods.	84
Table 15: Overview of single ion monitoring channels for metabolite quantification by MS.....	129
Table 16: Metabolite standard mix used as standard for LC-MS analysis.	130

1 Introduction

The rise of mammalian cell culture in the biopharmaceutical industry started with the first polio vaccine 60 years ago [1]. Since Jonas Salk introduced his innovative vaccine produced in Vero cell culture, this field has gone through some major transformations. Despite the fact that many viral vaccines are still produced in similar processes [2], recombinant proteins attracted more interest as pharmaceutical compounds in the 1980s and are now the major commercial cell culture-based products [3-5]. Due to the huge demand for complex therapeutic proteins (e.g. mAb, EPO, FVIII) advanced production processes and cell line development, led to massive improvements in manufacturing [6-8]. With the growing need for viral vaccines and the development of new therapeutic applications using viral vectors, viral biopharmaceutical products are also getting greater attention both in academia and industry [9,10]. Today, this field is benefitting from technologies developed for mammalian cell lines used for recombinant protein expression (CHO, NS0, BHK and HEK293). Similar production standards, concerning process modes, cell line performance and media development are needed [11]. As for recombinant proteins, manufacturing of viral products is moving from processes based on adherent cells to single cell suspensions in serum-free or chemically defined media [12-15]. Suspension cells ease scale-up for production and enable small-scale cultivation for screening in high throughput [16,17]. Furthermore, suspension cells are increasingly used in intensified processes like continuous, fed-batch or perfusion mode to boost productivity significantly and reduce development as well as manufacturing costs [18-21]. In the same way as bioreactor based production has transformed in the recent decades, purification trains for recombinant proteins and viruses have improved massively to speed up purification of products and enable integrated manufacturing [7,22-24]. Today many manufacturing options are available for fast, cheap and safe cell culture-based production, both in traditional stainless steel and single-use facilities [5,25-27].

Despite positive examples of modern cell culture-based manufacturing processes for vaccines and viral vectors no general platform technology has prevailed in a similar manner to platform technologies for recombinant protein production [28-31]. Differences in host cells, product properties, availability of cultivation media and purification systems demands for additional research in this highly interdisciplinary area. Influenza vaccine manufacturing is one example where the transition from traditional manufacturing to modern cell culture-based systems are still limited.

Approximately 90 % of the 500 million annual influenza vaccine doses are still produced in embryonated chicken eggs (ECE) despite many attempts and some successes of cell culture-based manufacturing [32,33]. Even though egg-based flu vaccines dominate the seasonal vaccine manufacturing, they are considered less suitable for pandemic influenza vaccine production [34]. Apart from common disadvantages like slow manufacturing, poor scalability and limitations in ECE supply [35], egg-derived vaccines might be less protective against some influenza virus strains [36-38]. Higher production and investment costs, patent and legal restrictions or technical expertise might be the main barrier for changing from eggs to cell culture. Mammalian Vero and Madin-Darby canine kidney (MDCK) cell lines (Influvac[®], Optaflu[®]/ Flucelvax[®], Preflucel[®]) as well as the insect cell line SF9 (FluBlock[®]) have been licensed for commercial human influenza vaccine manufacturing [35,39,40]. Additionally, HEK293 and other cell lines like Per.C6[®], EB66[®], CAP[®], AGE1.CR[®] were evaluated as a cell substrate for influenza virus propagation [35,41-43]. However, with a cell specific virus yield (CSVY) exceeding 10,000 virions/cell, MDCK remain the most productive cell line for influenza viruses [44]. MDCK cells are easily accessible[45], are widely used in influenza research and are already applied successfully in vaccine manufacturing [31]. Initially, MDCK cells were cultivated as adherent cells on microcarriers [46-49]. Further cell line and media development led to MDCK suspension cell lines, used both in academia [50-53] and industry [54]. For MDCK cells growing in suspension however, disadvantages like low specific growth rate (μ), low cell density and cell aggregates have been reported [51-53,55]. For large-scale manufacturing, fast cell growth, high maximal cell density and high cell specific productivity are crucial in order to reduce time to reach the needed production scale and maximize virus titer. Cell line and medium development have the potential to improve not only cellular performance, but to boost overall productivity as well.

Furthermore, it is to be noted that advanced process optimization and intensification technologies can be applied to maximize the productivity of MDCK-based processes and reduce production costs. For process optimization many aspects of the cultivation environment and the cellular response regarding product yield and product quality have to be considered [56,57]. Today's process analytical and optimization technologies are not only limited to empirical approaches, but are moving to a more rational understanding using omics technology [58-61]. Besides the very established genomics [62,63], transcriptomics [64,65] and proteomics [63,66], the use of metabolomics technologies in the biopharmaceutical industry is growing for process characterization, optimization and troubleshooting [67-69]. This most recent member of the omics family captures the cellular intracellular metabolite pools, consumption/production rates or intracellular metabolite fluxes to obtain an impression of the metabolic status of the cell [70,71].

Metabolite fluxes and pools react almost instantly to external and internal stimulations making them good process indicators on the one hand but are complicating the exact determination of the pool compositions on the other hand. Despite a growing application of this technology in the culture of Chinese hamster ovary (CHO) cells [60,72-75], there are very few metabolic analyses for viral production processes [76-79]. No metabolic analysis concerning the dynamics of intracellular metabolite pools during cell growth and virus replication has been described for MDCK suspension cells.

This work has the aim to shed some light on the metabolic profile of MDCK suspension cells during a standard batch cultivation and an influenza A virus infection. With the help of LC-MS based metabolomics, the dynamics of the different metabolite pools, especially of the glycolysis and of the citric acid cycle, might give deeper insights in substrate conversion and reveal potential metabolic bottlenecks. In order to analyze the effect of viral infection in this scenario, standard infection used for industrial virus propagation is not suitable (low MOI and trypsin addition), therefore, a more artificial infection condition (MOI 10 & no trypsin) was used. Furthermore, a new cultivation medium provided by a cooperation partner from the East China University of Science and Technology (ECUST) was evaluated for the cultivation of MDCK cells in suspension. Effects of the original (Smif8) and new medium (Xeno) on cellular growth, morphology, metabolism and influenza A virus productivity were analyzed for several MDCK suspension cell lines. The final aim was to identify the best performing host cell line to establish and characterize a scalable cell culture-based production process for an influenza vaccine candidate.

2 Theoretical background

This chapter introduces influenza virology, influenza vaccine manufacturing, mammalian metabolism and metabolomics in brief. This will give the knowledgeable reader the necessary background and literature to follow subsequent explanations. General information concerning influenza disease or virology was taken from two book chapters [80,81] and a review [82]. Metabolic pathways of central carbon metabolism and their role for cultured animal cells are summarized from two book chapters [83,84].

2.1 Influenza disease and virology

Influenza viruses can be separated into four genera, all belonging to the *Orthomyxoviridae* family: *Influenzavirus A*, *Influenzavirus B*, *Influenzavirus C* and *Influenzavirus D*, of which A, B and C are viral human pathogens. Influenza virus infections are the cause of a disease phenotype called flu or influenza. In humans, influenza viruses primarily infect cells of the upper respiratory system (nose, throat and bronchi) leading to cough, runny nose, fatigue, fever, headache, muscle pain and in some cases gastrointestinal problems. Extended viral infections of the lower respiratory tract and secondary bacterial infections can lead to severe and sometimes fatal respiratory complications. Influenza C viruses are rarely isolated from infected patients and play a very small role in the influenza disease. Influenza A and B viruses cause seasonal global infection waves, both in northern and southern hemispheres. These seasonal infections are caused by multiple influenza A and B virus subtypes with varying virulence. All influenza A virus (IAV) subtypes can be found in wild aquatic birds, which are considered the main reservoir for IAV. In some cases, avian influenza viruses can evolve to new human pathogenic viruses, which can cause epidemic or even pandemic infections of only a single IAV subtype. Due to the importance for pandemic infections, this work mainly focuses on viruses of the genus *Influenzavirus A*.

2.1.1 Virus structure & viral replication

Influenza A virus is an enveloped virus with a segmented negative-sense RNA genome. The lipid membrane harnesses the proton ion channel: matrix protein 2 (M₂) and two main glycoproteins: hemagglutinin (HA) and neuraminidase (NA), which form the main viral antigens. Three HA proteins form a functional protein complex (homotrimer) which assembles in the virus membrane. The structural protein “matrix protein 1” (M₁) forms a capsid structure below the lipid membrane. The viral genome, comprised of eight genomic RNA segments (vRNA), is stored in the virus core as protein complexes of vRNA, nuclear protein (NP), and the RNA polymerase complex (PB₁, PB₂ and PA) called viral ribonucleoproteins (vRNPs). Each of the genome segments, ranging from 0.9 to 2.3 kb, encodes for at least one viral protein. Using different splicing products (segment 7 & 8) and multiple open reading frames (segment 2, 3 & 7), the total influenza virus proteome can encompass 17 proteins and polypeptides [85].

Influenza virus particles are mostly spherical with a diameter between 80-100 nm, but also longer filamentous viruses are found in clinical isolates [86]. HA surface proteins bind sialic acid sugars of host glycoproteins (α _{2,6} for mammalian; α _{2,3} for avian) to attach the virus to the host membrane, leading to endocytosis of the virus. The acidification of the virus containing lysosome induces the HA mediated fusion of the endosome and the virus membrane, releasing the vRNAs into the cytoplasm. The viral genome segments are transported into the nucleus, where the transcription of viral mRNA and the replication (via viral cRNA) is initiated. Viral protein expression takes over the host protein expression system in the cytoplasm and newly expressed viral proteins, and vRNA complexes assemble on the cellular surface to create new virus particles. Viral NA surface proteins have sialidase activity, which releases viral particles bound to host cell glycoproteins. Neuraminidase inhibitors (oseltamivir, zanamivir, peramivir) are used as antivirals to block viral release and reduce viral distribution [87,88]. HA-trimers, in their initial inactive form (HA₀), have to be cleaved enzymatically into two polypeptides (HA₁ & HA₂) to form a fully active protein complex [89]. *In vivo* tissue-specific or ubiquitous host proteases are responsible for HA activation, and *in vitro* unspecific serine proteases (e.g. trypsin) are added for successful virus infection in cell culture [90-92]. Specific protease inhibitors (e.g. aprotinin) are also suggested as potential antiviral treatment for influenza virus infections [93].

2.1.2 Influenza A virus antigens

Unique for influenza virus A subtypes is the high variability in the main antigenic proteins HA and NA. In total, 18 antigenically different HA and 11 NA serotypes have been identified, which theoretically could reassort to create 198 different subtypes, of which 131 were already detected in

nature [82,94]. However, this reassortment can only occur in coinfections of two or more different IAV subtypes. Therefore, direct contact of human and livestock is needed for cross-species reassortment. This can create new, highly pathogenic influenza virus subtypes, leading to massive global infection waves. Interestingly the five major influenza pandemics only had a limited set of HA (H1, H2, H3) and NA (N1 & N2) serotypes, indicating some restrictions of the serotype profile for successful human reassortment. In addition to reassortment, a high mutation rate in the HA and NA genome, especially in mammalian host, results in a strong variation of the main antigens over time. Despite these variations in amino acid sequence, explicitly in the variable head region, structure and function of the HA and NA proteins seem to be rather stable. In wild aquatic birds the HA and NA sequence seems to be more conserved, indicating a good viral adaptation to their main reservoir. Due to this antigenic shift, human influenza viruses are classified by HA and NA subtypes as well as by place and date of isolation. For instance, the very common laboratory strain influenza A/Puerto Rico/8/34(H1N1) was the isolate number 8 of a human H1N1 subtype, obtained 1934 in Puerto Rico. If the virus is isolated from non-human species, this is indicated in the virus classification as well (e.g. influenza A/chicken/Hong Kong/220/97(H5N1)). In addition to variations in protein sequence, differences in the glycosylation of HA and NA increase antigenic complexity even more. Since glycosylation highly depends on the host cell glycosylation machinery (endoplasmatic reticulum & golgi apparatus), viral glycan structures are host cell dependent [95,96]. Furthermore, host independent variations of antigen glycan structures and glycosylation sites were described for different H1N1 serotypes [97,98]. Due to the complexity of viral glycosylation, the direct effects of the glycan structure on activity, virulence, antigenicity and immune evasion is not well understood. It seems that the complex glycosylation pattern can mask viral antigens to evade detection by the host immune system [99-101]. For an effective vaccine design, glycosylation might play an important role and should be considered for selection of host cell systems [38,102].

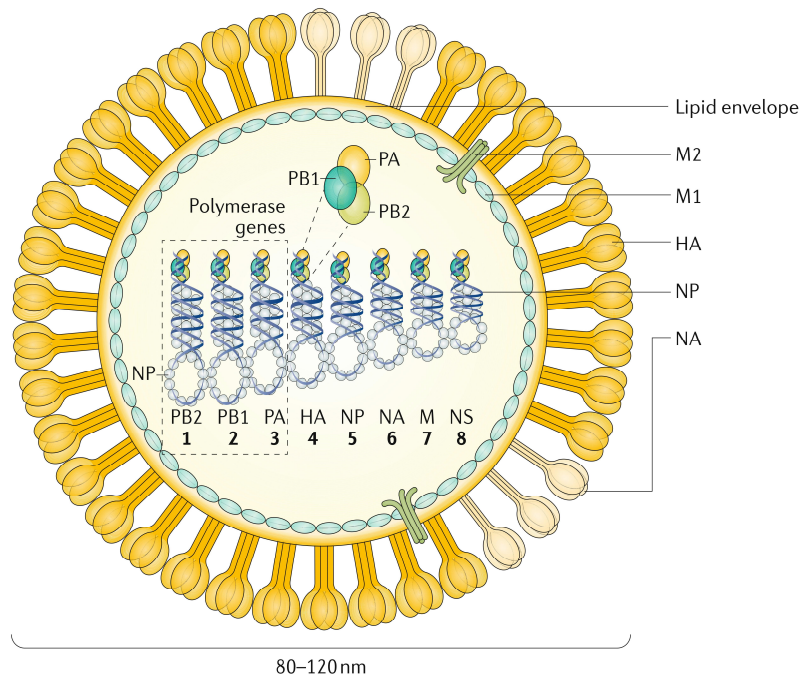


Figure 1: Influenza A virus particle with depiction of viral proteins and segmented genome

The main antigenic surface proteins hemagglutinin (HA) and neuraminidase (NA) are embedded in the lipid membrane. Matrixprotein 1 (M1) separates the virus shell from the core with the eight segments of the viral genome. Genomic RNAs form with the nucleoprotein (NP) and the polymerase complex (PA, PB1 & PB2) a functional unit, the vRNP (viral ribonucleoprotein) complex.

This figure was reprinted from Kramer et al. [82] by permission of the Springer Nature Group.

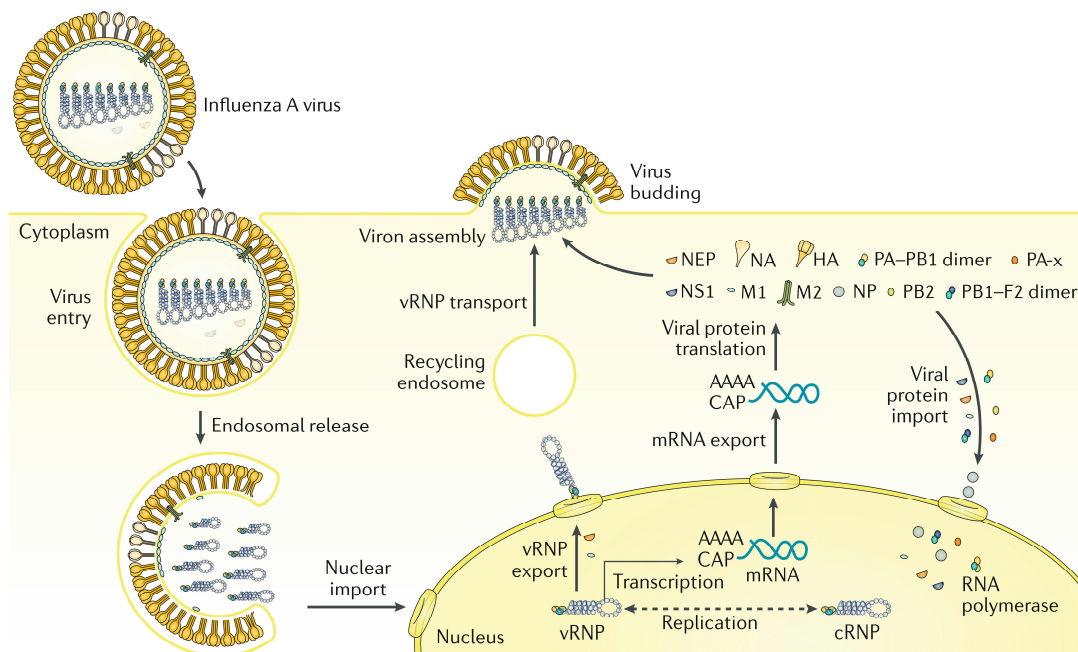


Figure 2: Intracellular influenza A virus replication cycle

After viral entry and acidification of the endosomal compartment, vRNPs are released into the cytoplasm and transported to the nucleus. Transcription and translation of viral proteins take place in the nucleus and cytoplasm, respectively. Viral proteins and duplicated vRNP complexes assemble at the cell membrane to new virus particles.

This figure was reprinted from Kramer et al. [82] by permission of the Springer Nature Group.

2.1.3 Pandemic and seasonal influenza

Reassortment between influenza A virus subtypes of different species can create new, highly pathogenic subtypes with various antigenic profiles. Due to the lack of preexisting immune protection against similar virus strains, these virus infections can have a higher mortality compared to reoccurring virus subtypes. Infections can spread over large regions or over the whole world creating an influenza pandemic with massive global economic and health impact. The most serious influenza pandemic recorded from 1918 to 1919 was the “Spanish flu”. It is estimated that 50 to 100 million people died as a result of respiratory illnesses caused by a single influenza virus subtype (H₁N₁). Both World War I and the lack of antibiotics to treat secondary bacterial infections could have sustained high pathogenicity (mortality rate: 2-5%) of this pandemic virus strain. Since the Spanish flu, three less severe pandemics with global impact have been recorded. The “Asian influenza” of the subtype H₂N₂ originated 1957 in south China and spread subsequently over the northern hemisphere resulting in 1-2 million deaths. Rapid development of a vaccine and the availability of antibiotics for treatment of secondary infections limited the spread and mortality of this pandemic. In 1968, the Hong Kong influenza emerged from southern Asia and was an H₃N₂ subtype. In the following two years, the highly infectious virus spread rapidly, leading to 1-4 million deaths. Even though a vaccine was developed, it was not produced and distributed fast enough before the pandemic peak. In 2009, the pandemic subtype H₁N₁ as a triple reassortment between an avian, swine and human influenza virus appeared in Mexico. Despite rapid spread of this pandemic virus subtype, the death rate was not higher than that caused by usual seasonal infections. A higher cross protection with other seasonal H₁N₁ subtypes might have been the reason. Even though no influenza pandemic has been reported since 2009, other outbreaks of highly pathogenic avian influenza subtypes (e.g. H₅N₁) have been registered, and other influenza subtypes with potential for new pandemic infections have been identified [103].

Pandemic virus subtypes continue to circulate globally as seasonal viral subtypes for many years after the epidemic. However, further host adaptation and antigenic shift of the original virus can lead to the emergence of antigenically different viruses, which are not covered by potential pandemic vaccines. Additionally, this antigenic shift is not only limited to influenza A viruses, creating the need for continuous adaptation of influenza vaccines against the most prevalent Influenza A and B viruses every year. Globally, influenza related diseases occur in annual oscillation during the respective winter seasons in almost every country. Influenza virus infections typically peak between January and March in the northern hemisphere and between June and August in the southern hemisphere [104]. Due to infections in this massive scale, influenza virus-related diseases are responsible for 3–5 millions of severe illnesses and associated with 290,000–650,000 annual

deaths worldwide [105,106]. In 1952, the World Health Organization (WHO) implemented influenza surveillance systems to monitor present influenza virus subtypes and predict the most predominant influenza A and B virus antigens for the upcoming season. Two influenza A and two influenza B subtypes are selected for seasonal vaccination campaigns in order to minimize influenza spread, limit health risks and reduce its economic burden.

2.2 Influenza vaccines

2.2.1 Viral vaccines: past, present & future

Despite rising skepticism towards vaccination in parts of society during the 21st century, there is no question in the scientific community that vaccination is the most successful preventive measure against viral infections [107,108]. In many cases, viral infectious diseases are hardly treatable and can have very significant effects not only on the individual health, but also on society [108]. The most successful viral vaccine was also the first one. When Edward Jenner introduced his revolutionizing smallpox vaccine in 1796, nobody imagined that this would lead to the eradication of smallpox in 1980, almost 200 years later [109,110]. Since then much has changed. New vaccine types as well as production technologies were developed, and this field will continue to change in the future [108]. Early vaccines (until the 1940s) were limited to attenuated virus strains (smallpox, rabies, yellow fever), isolated either from animal tissue or chicken embryos [110-112]. The use of similar virus strains or the adaptation to other species and tissues through repeated passaging created these less infectious vaccine strains [113,114]. With the development of the first influenza vaccine in 1935, it was shown that also inactive virus particles are able to create sufficient protection against viral infections [115]. The development of sterile cell culture in the 1940s revolutionized the vaccine manufacturing field, and was rapidly applied for the first polio vaccine in 1955 [1,116]. First as an inactivated vaccine and later as attenuated oral version, these polio vaccines soon led to a major decline of poliomyelitis, and today the eradication of this disease is imminent [117]. The success of cell culture technology for virus propagation led to the development of many new vaccines in the second half of the 20th century (measles, mumps, rubella varicella, hepatitis A), and its application for new versions of already developed vaccines (smallpox, rabies & influenza) [118]. Additionally, huge improvements in genetic engineering led to the development of the first recombinant vaccine for hepatitis B in 1986, when viral antigens were expressed from a viral transgene in yeast [119]. This technology led to the development of other revolutionary vaccines in the 21st century, when genetic engineering not only allowed the expression of viral antigens as VLPs (human papillomavirus in 2006, influenza in 2013), but also enabled the design of chimeric viruses based on established vaccine strains (Japanese encephalitis in 2009, Ebola in 2016, Dengue fever in development) [120-123]. Today's modern vaccine technologies are clearly moving towards a more rational design of viral vaccine strains manufactured with modern cell culture based technologies [108]. However, older production technologies (e.g. embryonated chicken eggs) are still in place and are a major part of current manufacturing capacity, but might be replaced gradually over time.

In the future, there might be an additional vaccination strategy solely based on the nucleotide sequence called RNA- or DNA-vaccines. With this technology, plasmid DNA or mRNA is introduced to the tissue of the patient to express immunologically active compounds in situ [124,125]. DNA- or RNA vaccines have a huge potential as platform technology for many vaccines against viral diseases and many potential candidates are in clinical trials [126,127]. However, many of these vaccines failed to demonstrate sufficient efficacy so far, and no commercial product has been approved by the regulatory authorities yet (2019) [126-128].

2.2.2 Influenza vaccine manufacturing

Influenza vaccines are one of the oldest viral vaccines and have been produced with major commercial success for over 80 years [115,129]. Due to high variability of the viral antigens, millions of vaccine formulations have to be adapted, tested and produced every year. In order to enable large scale production in very short time, established platform technologies are crucial to streamline vaccine development and manufacturing [130,131]. Inactivated influenza virions propagated in embryonated chicken eggs have been the sole production platform for over 60 years, until cell culture-based and live attenuated vaccines were approved in 2001 and 2003, respectively [132,133]. Huge automated and semi-automated production facilities enable the handling of thousands of eggs simultaneously in order to manufacture millions of vaccine doses. Egg-based production depends heavily on ECE supply, is limited in scalability and has a contamination risk for egg-derived allergens [134]. Although modern animal cell culture has proven to enable safe vaccine manufacturing in chemically defined medium [35] and extensive research has been dedicated to this field, cell culture-based vaccines have not been able to play a major role in the global manufacturing capacity yet [134]. Until recently, all influenza vaccines contained inactivated virus subunits or attenuated virions as antigens. Only in 2013, the first recombinant influenza vaccine was introduced, using the baculovirus expression system in insect cells [120,135]. This allowed the expression of the isolated seasonal HA-antigen recommended by the WHO without the generation of influenza virus strains for vaccine production. Differences in posttranslational modification and lack of other immunogenic antigens (e.g. NA) might make this vaccine less immunogenic and more HA antigen seems to be needed for sufficient protection [136,137]. Unfortunately, even with higher antigen content, no sufficient protection is achieved for children using this vaccination strategy [138].

For viral vaccines, influenza seed viruses are usually a reassortment of high-growth virus strains and the circulating virus strains containing viral antigens HA and NA set by the WHO. Today, this egg-based reassortment is complemented by reverse genetics for a directed virus design and to omit egg adaptation [139,140]. The virus subtype A/Puerto Rico/8/34(H1N1) is considered the most suitable backbone for viral influenza A vaccine strains, and is commonly used as reference strain in influenza research and process development [141,142]. The generated seed viruses are adapted in multiple passages with low MOI to the host system (ECE or cells) and are used to infect eggs or cell culture. Viruses proliferate and infect the cell population or tissue of the ECE and virus particles are harvested between 24 and 96 h depending on virus strain and cultivations system [52,143-145]. Traditionally, ultracentrifugation is used for virus purification, but also advanced chromatographic methods were developed for the purification of cell culture-based virus particles [146]. Influenza virions are chemically inactivated by β -propiolactone (β -PL) or formaldehyde treatment. Purified, inactivated and formulated full virions can already be applied as final product. However, the disruption of the virus particles with detergents (splitting) followed by additional enrichment of viral antigens (HA, NA) and further purification steps are commonly applied to generate the final product [147,148]. A vaccine dose for inactive influenza vaccines is usually defined by the HA-antigen amount for a monovalent dose. In most cases one dose contains 15 μ g of HA antigen, higher doses are used for elderly patients (60 μ g) or recombinant HA antigen (45 μ g), smaller doses were used in pandemic vaccines containing modern adjuvants (3.75 μ g in Celtura[®]) [149,150]. Immunological active HA-antigen content is determined by single radial immunodiffusion (SRID) assay with strain specific antibodies and antigen standards provided by the regulatory agencies (e.g. NIBSC, CDC) [151]. For cell culture derived vaccines, limits for host cell DNA (HC-DNA) and host cell protein (HCP) are defined by the regulatory authorities as 10 ng of HC-DNA and 100 μ g of total protein (viral protein & HCP) per vaccine dose, respectively [152]. Newly developed membrane-based chromatographic resins for virus particles are able to improve purification speed and efficiency for a more productive influenza virus production train [153,154]. To deliver huge masses of vaccines in a potential pandemic influenza scenario, cell culture-based influenza vaccine manufacturing might be crucial to facilitate fast, intensified, large scale production for maximized productivity [155,156]. In recent years, many suspension cell lines were characterized and tested as potential virus substrate for vaccine manufacturing [41,42,53,157,158]. This enabled the implementation of perfusion technology for the development of intensified vaccine processes in high cell density processes using filtration retention devices in alternating tangential flow filtration (ATF) and unidirectional tangential flow filtration (TFF) mode [159-162]. Further research in this field will be necessary to improve overall productivity and make cell culture-based vaccines more competitive in comparison to egg-based production systems.

In the future, current manufacturing technologies of influenza vaccines might be complemented with universal peptide vaccines providing protection against many influenza virus subtypes [163]. Here, peptide sequences of the more conserved stalk region of the HA-antigen or other viral proteins are targeted, potentially leading to a broad protection. Additionally, DNA [164] and RNA [165] vaccines might facilitate even faster production and cheaper vaccines due to the easy production independent of virus subtype. However, both universal and DNA/RNA vaccines still have to proof clinical efficacy and commercial success until their application.

2.2.3 MDCK cells for influenza virus propagation

Madin-Darby Canine Kidney (MDCK) cells were isolated in 1958 by S.H. Madin and N.B. Darby from the kidney epithelium of the distal tubulus of a female adult cocker spaniel (*Canis lupus familiaris*). Depending on passage history and origin, MDCK cells have a more or less pronounced hyperdiploid karyotype with up 90 chromosomes per cell. The “parental” cell line has a normal canine karyotype ($2n= 78$) with an additional metacentric autosome [166]. From the beginning, MDCK cells were considered as substrate for virus replication, but due to its prominent epithelial characteristics, they were commonly used as model to study epithelial phenotype in vitro, too [167]. MDCK cells are susceptible to a wide range of important viral human pathogens, of which influenza viruses (A, B & C) are the most prominent ones [166]. Due to the fast cell growth, robustness and high virus productivity, MDCK cells became the major cell line for influenza virus propagation and research [35,168]. Two parental MDCK cell lines, one American (ATCC) and one European (ECACC), dominate the influenza virus field. The European MDCK cell line (ECACC 84121903) is predominately used by European research groups, and the American MDCK (NBL-2) cell line (ATCC CCL-34) is used all over the world, with a focus in North America and Asia [45]. In 2001, the first cell culture-derived influenza vaccine (Influvac®) was approved for the European market using adherent MDCK cells (ATCC CCL-34) as substrate for influenza virus propagation [169]. After discontinuing the use of Vero cells in 2012 (Preflucel®) MDCK cells are the only cell line used for commercial human influenza virus production (2019). For large scale production, MDCK cells were initially cultivated as adherent cells on microcarriers [46-49], but further cell line development led to the first suspension cell line in 1997 [54]. This “MDCK 33016” cell line was adapted to suspension from an adherent CCL-34 (ATCC) cell line and was first used by Novartis for the manufacturing of seasonal influenza vaccines (Optaflu®), commercialized in 2007 [31]. The same cell line is still used today for vaccine production (Flucelvax®) by Seqirus in the USA [170]. Roughly ten years after the first description of MDCK suspension cells, academic research groups developed similar cell lines [51-53] both from ATCC and ECACC progenitors. For these cell lines, however, disadvantages like low growth rate, low cell density and cell aggregates have limited their use for commercial

manufacturing [55]. The MDCK suspension cell line MSCK.SUS2, in particular, was extensively characterized for influenza A virus production by our research group, but limitations in scalability to STR systems restricted their use from larger scales or intensified processes [44,53,55,162,171]. In 2015, a new serum-free cultivation medium was developed in a Chinese academic/industry cooperation, which enabled high growth rates of single cell suspension MDCK cells in stirred tank bioreactors [50,172]. Due to higher cell concentrations, improved influenza A virus titers were achieved within shorter process time.

2.3 Metabolism of mammalian cell culture

Over billions of years, evolution has formed an almost infinite network of metabolites, enzymes, co-factors and reactions creating the diversity of our global ecosystem [173,174]. Every species, tissue and even individual cell has its own, characteristic metabolism, which interacts with internal and external stimuli [175]. More conserved metabolic pathways (e.g. glycolysis & tricarboxylic acid cycle) can also be found in many species or even in almost all living organism [173,174]. The central carbon metabolism is a highly conserved metabolic pathway and follows the same or similar reactions to provide energy as well as metabolic precursors for growth, replication and maintenance [176]. In culture, cells lack the tissue characteristic and have a more equal distribution of cell morphology. Compared to primary cells growing in a tissue environment, cultivated cells are stripped of many intercellular control mechanisms and have a much higher (sometimes indefinite) proliferation capacity [177]. These changes affect the metabolism as well, and make central carbon metabolism of cells in culture unique compared to cells growing in healthy tissue. Not surprisingly, similar metabolic characteristics have been found in immortalized cells used in cell culture and tumor cells [178-180]. Despite decades of research in the field of metabolism or metabolomics, many aspects of the central carbon metabolism remain unclear. Primarily, the dynamics of this network and its complex control mechanisms appear to be very flexible. Especially in continuously growing cells, flexible metabolic networks enable an efficient adaptation of the cell metabolism to different cultivation conditions. Cultivated cells face continuously changing environmental conditions (e.g. substrates, products, pH, osmolarity, etc.) leading to highly dynamic activity (i.e. fluxes, pools) within the metabolic networks of even conserved pathways.

2.3.1 The central carbon metabolism in brief

The central carbon metabolism of animal cells can be divided into four parts, which are tightly connected over several metabolic pathways. When we look at the central carbon metabolism, we will primarily consider the metabolic pathways used for processing the main substrates in cell culture: glucose, glutamine, and to some extent pyruvate (Figure 5). Various nonessential amino acids (i.e. alanine, glutamate, and aspartate) are involved in these pathways as substrates or by-products as well, but play a smaller role overall. Essential amino acids are mostly used as substrate for protein biosynthesis and are barely used for biosynthesis of other intermediates or as energy substrates.

Glycolysis

Glucose is the main energy substrate for many cell lines and plays a major role for energy supply and as carbon backbone for several anabolic pathways. Ubiquitously expressed transporter family GLUT transports glucose into the cell. Different tissue specific isoforms are described, but for many cell lines GLUT₁ is the prominently expressed type. An overexpression of GLUT₁ is observed not only for production cell lines, but also for cancer cells [181]. Overall, several metabolic dysregulations are found in continuously growing cells, including cancer cells, creating similar metabolic phenotype of high glucose and glutamine consumption with high lactate production. Otto Warburg described this phenomena 60 years ago, where he observed high anaerobic glycolysis activity in cancer cells even in aerobic environments [178,182].

Intracellular glucose is immediately phosphorylated by hexokinase (HK) to glucose 6-phosphate (G6P), which activates the sugar for following reactions and captures it in the cell due to the negative charge of the phosphate group. After an isomerization to fructose 6-phosphate (F6P), an additional phosphate is transferred from ATP by the phosphofructokinase to build the double activated sugar fructose 1,6-bisphosphate (F16BP). This sugar is subsequently split into two activated interchangeable C₃ isomers of which only the glyceraldehyde 3-phosphate (GAP) is used for downstream reactions (Figure 5). In this “upper” part of glycolysis, 2 ATPs are used to create 2 activated C₃ molecules, which are oxidized in following steps. By oxidizing the aldehyde to a carbonate, enough energy is generated to bind one phosphate and generate 1,3-bisphosphoglycerate (1,3PG). Subsequently, the stored energy is used to generate ATP and 3-phosphoglycerate (3PG). Via the intermediate 2-phosphoglycerate (2-PG), highly-activated phosphoenolpyruvate (PEP) is generated with enough energy to produce another ATP and pyruvate (Pyr). Overall, two net ATP and NADH are generated from one glucose molecule by oxidizing it to two molecules of pyruvate (Figure 3).

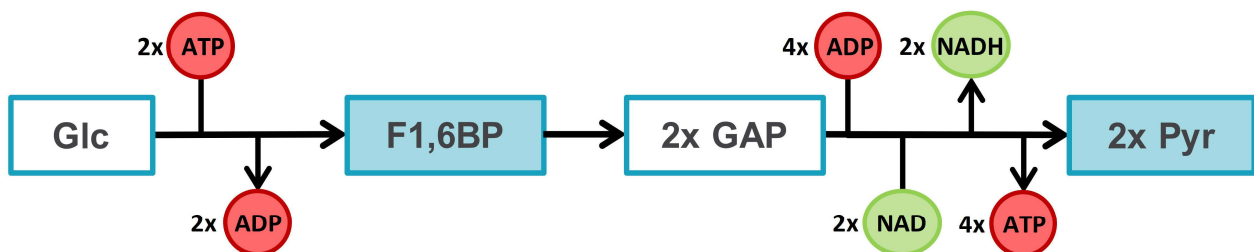


Figure 3: Energy and redox balance of glycolysis.

Simplified pathway of glycolysis with the consumption and production of ATP/ADP and the redox metabolites NAD/NADH. Net balance of the glycolysis from glucose to pyruvate.

If the generated NADH cannot be oxidized sufficiently in the mitochondria, it needs to be regenerated in the cytoplasm to maintain redox potential and glycolysis. In this case, pyruvate can be reduced to lactate (Lac) by the lactate dehydrogenase (LDH), where NADH is consumed without the need of oxidative phosphorylation in the mitochondria. Lactate is excreted into the medium as one of the main by-products of animal cell culture (Figure 5). Under certain conditions (e.g. glucose limitation), lactate can be used as a substrate, oxidized to pyruvate and used in downstream reactions (i.e. TCA). Furthermore, pyruvate is used as an additional substrate in some cultivation media, which can be transported into the cell with the same transporter as lactate. It is either used to regenerate excessive cytosolic NAD or can be used in other downstream pathways of glycolysis without the need of NADH regeneration (e.g. alanine synthesis). Here, pyruvate is used as reaction partner for an amino group (aminotransferase) from another amino acid substrate (e.g. glutamate) to avoid ammonium accumulation.

The glycolytic flux is regulated by specific key enzymes: the glucose transporter (GLUT₁), the phosphofruktokinase (PFK) and the pyruvate kinase (PK). On a molecular level, PFK functions as the main driver dividing metabolic fluxes between lower glycolysis, pentose-phosphate, glycogen and hexosamine metabolism. It has three activator sites, for AMP, ADP and fructose 2,6-bisphosphate as well as three inhibitor sites for ATP, citrate and 3PG. Furthermore, GLUT₁, PFK and PK are regulated globally by the AMPK/mTOR/HIF-1 pathway, which is altered in immortalized cells to function as an insulin independent activator both for cell growth and increased glycolytic activity [183,184]. This “dysregulation” enables fast, unrestricted cell growth linked to high anaerobic glycolysis rate even under aerobic conditions (Warburg effect) and high production of lactate.

Pentose phosphate pathway (PPP)

The pentose phosphate pathway is a very important anabolic pathway for all cell types. It provides reducing agents (NADPH) and activated sugars of different sizes (C₃-C₇) as precursors for biosynthesis reactions (e.g. fatty acids, amino acids and nucleotides). This pathway is closely linked to upper glycolysis over the common intermediates F6P and GAP, which can function both as substrates and as products of the pathway (Figure 5). In the oxidative part of the PPP, fructose-6-P is oxidized over 6-phosphogluconate to ribulose 5-phosphate (RU₅P) where NADPH is generated. In the non-oxidative part of the PPP, two C₅ isomers, ribose 5-phosphate (R₅P) and xylulose 5-phosphate (X₅P), are generated, and all three isomers are transformed in a series of reactions to erythrose 4-phosphate (E₄P), sedoheptulose 7-phosphate (S₇P), GAP and F6P. Within these, ribose 5-phosphate is the most important precursor of the PPP for the biosynthesis of nucleotide

containing biopolymers (RNA & DNA) and free nucleotides. Detailed descriptions of the PPP is summarized in two recent reviews [185,186].

Tricarboxylic acid cycle

The tricarboxylic acid cycle (TCA) is arguably the most complex metabolic pathway of the central carbon metabolism. The TCA operates as catabolic center of substrate oxidation for aerobic energy production and its intermediates are involved in many anabolic reactions. The TCA is located in the mitochondria of the cell, and the substrates and products have to be transported in the mitochondrial lumen via transport proteins. Pyruvate is the key link between glycolysis and TCA and is transported in the mitochondria over the mitochondrial pyruvate carrier (MPC). The MPC activity can vary between cell lines. Very low activity was reported for some cancer cell lines, where uncoupling the TCA from glycolysis might be the main reason for the Warburg effect [187]. Mitochondrial pyruvate can enter the TCA carboxylated as oxaloacetate (OAA) in an anaplerotic reaction or it is oxidized by the pyruvate dehydrogenase complex (PD) and transferred to a coenzyme A (CoA) to form an acetyl-CoA. The acetyl component of acetyl-CoA enters the TCA over the citrate synthase (CS) which transfers the acetyl group to OAA and forms citrate (Cit). In a full circular reaction system, the acetyl group is oxidized completely, and oxaloacetate is regenerated (Figure 5). The arising NADH is used in the presence of oxygen to fuel ATP production in the mitochondrial oxidative phosphorylation (oxphos). That way a much higher amount of ATP (~30 ATP/glucose) can be generated compared to the anaerobic glycolysis (~2 ATP/glucose). In addition to reduced pyruvate transport, it appears that PD activity controlled over pyruvate dehydrogenase kinase (PDK) is rather low. PDK expression is controlled by HIF-1 which is overexpressed in many immortalized and cancer cells. Furthermore, TCA intermediates are involved in anabolic reactions and are removed from the cycle for biomass formation, leading to an interruption of cyclic TCA activity and the need for high anaplerotic reactions (Figure 4). Specifically citrate is used for the fatty acid synthesis in the cytoplasm. Citrate is transported to the cytoplasm, where with the help of ATP one acetyl is transferred to CoA to form acetyl-CoA and oxaloacetate. The OAA is reduced to malate which can be shuttled back to the mitochondria against the export of citrate. The acetyl group of cytosolic acetyl-CoA is used as precursor for the fatty acid synthesis, indispensable for biomass formation (phospholipids) [188]. Due to the high efflux of citrate from the mitochondrial lumen and rather low citrate synthesis from OAA the TCA is truncated. It seems that there is even an inversion of the normal isocitrate dehydrogenase catalyzed reaction, where citrate is generated from α -ketoglutarate, as well.

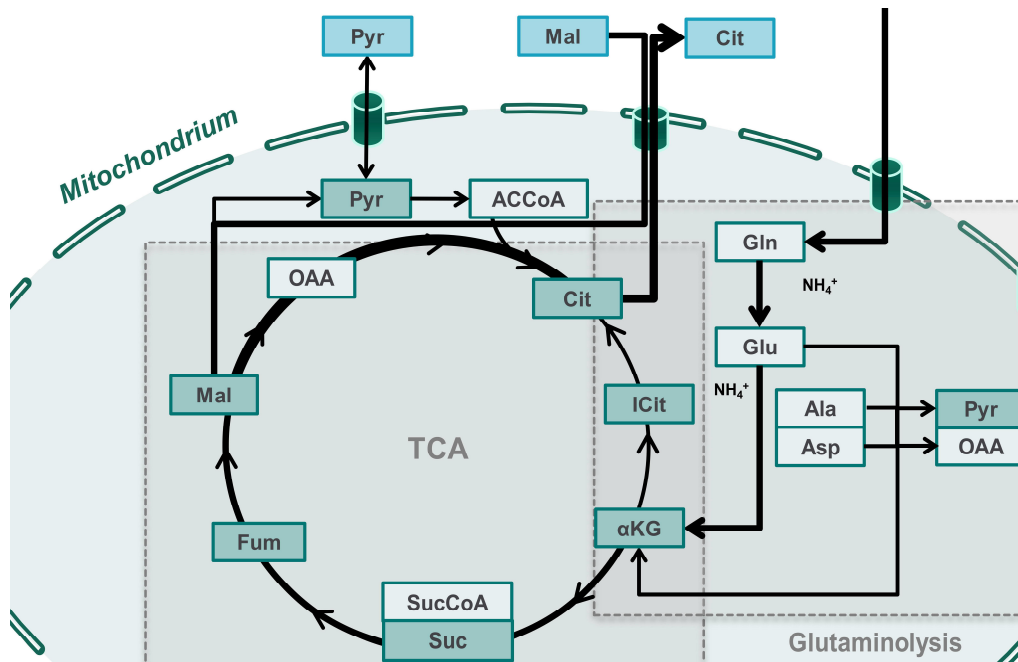


Figure 4: Truncated tricarboxylic acid cycle.

A truncated TCA cycle is potentially uncoupled from the glycolysis and mainly fed over glutamine (Gln) derived α -ketoglutarate (α KG). The TCA can be truncated leading to high citrate (Cit) synthesis rate both from malate (Mal) and α KG (inverted cycle). High activity of the citrate-malate shuttle ensures precursor supply for lipid biosynthesis in the cytoplasm.

Glutaminolysis

In addition to glucose, immortalized cells rely heavily on glutamine as substrate for cell growth. Like any other amino acid, glutamine is needed as a precursor for protein biosynthesis, but is also used as additional substrate to fuel the central carbon metabolism via the glutaminolysis (Figure 4). For many cell lines (i.e. MDCK cells), 40-50 % of the overall consumed amino acids is glutamine, whereas only 4-5 % of the mammalian proteome (i.e. *homo sapiens*) accounts for glutamine [189]. Other essential and nonessential amino acids are consumed much more in balance with their respective use for protein biosynthesis. Various glutamine transporters were described with an altered activity in immortalized and tumor cells [190]. Intracellular glutamine can be deaminated by the glutaminase to glutamate (Figure 5). In mammalian cells, glutaminase is expressed both in the cytoplasm and the mitochondria. However, to explain the extensive glutamate production during MDCK cultivation the primary glutaminase activity is presumed to be in the mitochondria (Figure 5), as already described for CHO cells [191,192]. Mitochondrial glutamate is converted to α -ketoglutarate either by transamination or oxidative deamination. In the transamination, the amino group is transferred to a keto acid (i.e. pyr or OAA) producing α -KG and alanine or aspartate. The transamination reaction is also active in the cytoplasm generating glutamate, which is secreted into the medium. In some cases, ammonium recovery by an inverted glutamate dehydrogenase (GDH)

activity was also described [193]. Mitochondrial α -KG generated from glutamate is used in the TCA cycle and is considered the major α -KG source to fuel the truncated cycle. The α -KG is either reduced to citrate for fatty acid synthesis or partly oxidized to malate. The malic enzymes catalyze the transition from malate to pyruvate which can be secreted in the form of lactate.

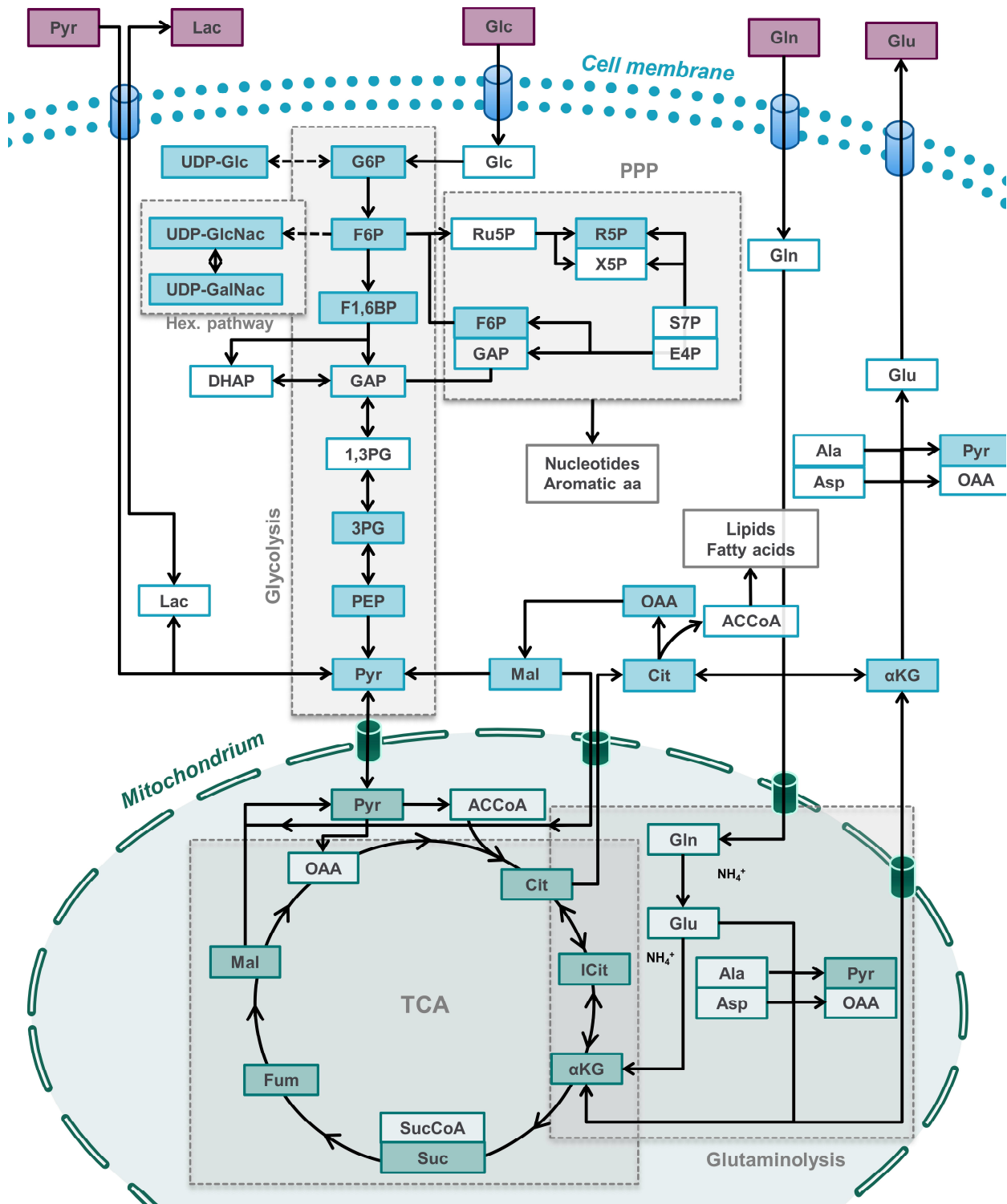


Figure 5: Overview of the simplified central carbon metabolism for mammalian cells

Extracellular metabolites (red) are transported to the cytoplasm over transporters in the cell membrane. Cytosolic metabolites (blue) are involved in glycolysis and associated metabolic pathways of pentose phosphate pathway (PPP) as well as hexosamine pathway. Key metabolites are transported to the mitochondria compartment. Mitochondrial metabolites (green) are involved in the glutaminolysis and the tricarboxylic acid cycle (TCA). Light colored squares: not quantified; dark coloured squares: quantified metabolites.

2.3.2 Metabolomics: the analytical tool set

Quantitative metabolomics has the (idealistic) goal of capturing and quantifying a comprehensive set of intra- and/or extracellular metabolites fast, reproducible, precise and sensitive. Today, after many years of technological improvements in this field, it is clear that there is no single technology able to achieve this goal. Metabolites are too heterogeneous in their chemical properties, concentration and stability to enable the direct quantification of the whole metabolome with one platform technology [194]. In contrast to genomics, transcriptomics and proteomics, where molecules have very similar chemical subunits (i.e. nucleotides, peptides), metabolomics covers a vast range of organic compounds with very different chemical properties (e.g. hydrophobicity, polarity, charge, molecular weight) [194-197]. Furthermore, concentrations of intracellular metabolites range from highly abundant (mM) to scarcely detectable (nM), and are found in very dynamic pool compositions with fast turnover rates [198]. For the quantification of some metabolites, we face an additional challenge of stability, leading to metabolite alteration either due to sample preparation or analytics [199]. For these metabolites, fast arrest of metabolite turnover (quenching) and gentle sample treatment (i.e. extraction) is crucial to obtain valid metabolite quantities [200]. In many cases, the development of technologies for quantification of metabolites was very much driven by the application and the metabolites of interest. Therefore, many different technologies are utilized, depending on the metabolite type and concentration of the metabolites as well as the used organism or cell type. Initial studies were using basic high-performance liquid chromatography (HPLC), gas chromatography (GC) or capillary electrophoresis (CE) to separate and detect metabolites according to their respective chemical properties [201-204]. Additional pre-treatment of metabolites by derivatization helped to separate and quantify metabolite families with similar functional groups (e.g. amino acids) [205,206]. Massive technological advances for all these analytical tools increased sensitivity, separation, speed, and reduced sample and eluent quantity [207]. One technological breakthrough for metabolomics, however, was the development of high-performance mass spectrometry (MS) [208,209]. This enabled the detection and quantification of many metabolites with different chemical properties based on their mass to charge ratio. Furthermore, the identification and quantification of metabolites in mixture by mass, ionization and fragmentation properties creates an additional dimension to upstream chromatographic or electrophoretic separation [210,211]. Parallel to MS-based quantification methods, the noninvasive nuclear-magnetic-resonance (NMR) method is growing as an alternative technology for direct quantitative metabolite analysis. Despite some advantages and current technological improvements, NMR is not able to match the sensitivity, spectral diversity and throughput achieved with MS-based methods and will not be discussed in detail here [69,212,213].

Today, the combination of HPLC or GC with mass spectrometry for identification, mass-separation and quantification is considered the method of choice for a highly sensitive analysis of intra- and extracellular metabolites. MS-based analytical methods enable isotopic labeling, where labeled metabolites are used as internal standards for more accurate quantification or in pulse-chase experiments for the determination and quantification of intracellular metabolite fluxes [198,214,215]. For metabolic profiling, reverse phase chromatography (RPC) and hydrophobic interaction chromatography (HILIC) coupled to high performance tandem mass spectrometry (i.e. QqQ-MS, QTOF-MS and hybrid ion trap) showed excellent results for the quantification of many intracellular metabolites in a high throughput manner [216-220]. This technology can be applied to quantify a predefined set of already known metabolites (targeted metabolomics) [221,222] or for identification and quantification of undefined metabolites based on their molecular weight and fragmentation characteristics (untargeted metabolomics) [223-225]. Historically, RPC and HILIC methods had problems separating sugar phosphate isomers which are the most important compounds of glycolytic pathways. In this respect ion-chromatography showed much better separation performance for sugar phosphates and nucleotide sugars relevant in the primary carbon metabolism and hexosamine pathway [201,226].

2.3.3 Metabolomics in mammalian cell culture processes

Metabolomics, specifically metabolic profiling is a relatively young field applied in bioprocess analysis and optimization. Metabolic flux analysis (MFA) based on extracellular metabolites was the first attempt to shed light on the intracellular metabolic reactions in mammalian cells [227]. ¹³C labeled isotopes, analyzed by NMR or MS, enabled the indirect quantification of intracellular metabolic fluxes and gave the opportunity to analyze more complex metabolic networks [228-231]. With the development of advanced MS-based analytical technologies, metabolic profiling was applied for both adherent and suspension cells [232-235]. In processes development, metabolic profiling is combined with mathematical modeling for systematical analysis in order to identify metabolic bottlenecks. Metabolic analyses led to some targets for metabolic engineering [73,236,237]. Especially the “inefficient” Warburg metabolic phenotype was targeted in many studies to improve aerobic glycolysis and reduce the accumulation of undesired by-products (i.e. lactate & ammonium) [238,239]. Some of these studies demonstrate positive effects on by-product formation by GLUT5 (with fructose feeding), PC and MDH overexpression or by knock down/inhibition of LDH and PDK [180,240-242]. However, the overall success of reducing the Warburg effect for production cell lines by targeted metabolic engineering is rather limited [243]. With the exception of the overexpression of glutamine synthetase for cell selection, no metabolic engineering approach is applied in manufacturing processes, so far [244,245]. This might change in the near future thanks to

developments of more robust targets for genetic engineering and new gene editing technologies (i.e. CRISPR-Cas9) [246,247]. Nonetheless, the highly complex and flexible system of enzymes, metabolite pools, transporters and regulatory circuits is still not resolved to enable a rational engineering of the central carbon metabolism. Clonal cell selection indicate the existence of a metabolic improved genotype, but high intrinsic heterogeneity is leading to unstable cell population which might result in a loss of the desired phenotype in large scale production. As a consequence, advanced process control strategies, new cultivation techniques (e.g. perfusion) and new media are currently considered more efficient to limit the accumulation of by-products and subsequently improve overall process productivity [248-250].

2.3.4 Metabolic effects of virus infections

In comparison to the amount of metabolic studies conducted for diabetes, cardiovascular disorders cancer or CHO-based processes for recombinant protein production, virus-related metabolic research is rather limited. However, studying the impact of viral infection on the cellular metabolism of the host is important for a basic understanding of virus host interaction, or identification of metabolic bottlenecks that limit virus production. The latter is of special significance for cell culture-based viral vaccine production, as metabolic engineering could be considered for process optimization to maximize virus yields. Systemic metabolic analysis of different viruses showed complex effects both on central carbon metabolism and (for enveloped viruses) on lipid metabolism [251-258]. The elucidation of virus induced alterations of the cellular metabolism might reveal new antiviral drug targets for new therapeutic options [259]. Manchester & Anand provide a comprehensive overview of the current status of research concerning response of cellular metabolism to infections of major viral human pathogens [260]. Furthermore, the metabolism of immune cells is considered a potential drug target to support immune effector cells in their fight against viral infection. A metabolic boost of lymphocytes might not only be beneficial in acute infections, but in chronic viral infections suffering from low T-cell activity as well [261]. For influenza virus infections, however, only a limited amount of data is available to provide a clear picture of its influence on the host metabolism. The few studies, conducted in animal [262-265] and human [266] trials, demonstrated changes in amino acid, central carbon and lipid metabolism. These metabolic effects on the whole organism were only confirmed for the lipid metabolism in metabolic profiling analysis of in vitro infections [76,267]. In process-related metabolic analyses of cell culture systems used for virus production, studies have investigated direct virus effects on intracellular metabolic flux or pool composition [268-271]. For influenza virus production with MDCK cells, the majority of metabolic analysis focused on extracellular metabolites which are a reasonable indicator for overall metabolic performance and can be used for media optimization

[53,272-275]. Intracellular metabolic profiling, however, were only analyzed in one single study with adherent MDCK cells [76]. For future process intensification and large-scale manufacturing, understanding how MDCK suspension cells cultivated in chemically defined media respond to influenza A virus infections would be of fundamental importance. This could enable specific, tailor-made infection media to support virus propagation in the infection phase of a virus production process.

3 Materials and methods

3.1 Cell culture

3.1.1 Media and cell lines

Cultivation media

For the cultivation of MDCK suspension cells, three different media were analyzed and compared. First, the traditional medium Smif8, which was developed for the cultivation of MDCK suspension cells and has been used for many years at the MPI. A serum-free (Xeno-SFM) and chemically-defined version (Xeno-CDM) of another cultivation medium was acquired through a cooperation with the East China University of Science and Technology (ECUST) and the company Shanghai BioEngine (Table 1). All media were delivered as dry base powder, which was solved together with other ingredients (e.g. bicarbonate, glucose, etc.) in Milli-Q ultrapure water and sterile filtered (0.22 µm). Before use, glutamine and pyruvate were supplemented from a sterile filtered stock solution (200 mM).

Smif8 medium

Smif8 medium was prepared from a base medium powder acquired from University of Applied Science Emden-Leer through Prof. Klaus Scharfenberg. Medium powder (6.12 g/L), NaCl (5 g/L), sodium bicarbonate (2 g/L), glutamic acid (0.24 g/L) and glucose (3.66 g/L) were mixed as solids and solved together in the respective amount of Milli-Q water (90 % of final volume). Pluronic F68 (10 mL/L) and ethanolamine (2 µL/L) were added as liquid solutions. Sodium hydroxide solution (5 M aq) was added to adjust pH to 7.00. After all ingredients were completely dissolved, the medium solution was sterile filtered (0.2 µm filter) and stored at 4 °C. Before use, 20 mL/L of each glutamine and pyruvate solution were supplemented from a 200 mM sterile stock solution of the respective supplement. Detailed description of media preparation is provided in the appendix (8.1: Cultivation media for MDCK suspension).

Xeno-SFM/CDM medium

Xeno-SFM and Xeno-CDM medium were prepared from the respective base medium powder provided by Shanghai BioEngine Sci-Tech Co., LTD. The respective medium powder Xeno™-Soo1S (26.04 g/L) or Xeno™-CD001S (21.04 g/L) was added to required amount of Milli-Q water and mixed for 20-30 min. Sodium hydroxide solution (5 M aq) was added to adjust the pH to 6.5 ±0.2. Sodium bicarbonate (2 g/L) were added and medium was mixed for 10-20 min until all components were completely dissolved. Medium solution was sterile filtered (0.2 µm filter) and stored at 4 °C. Before use, 40 mL/L of glutamine solution was added from a 200 mM sterile glutamine stock solution. Detailed description of media preparation is provided in the appendix (8.1: Cultivation media for MDCK suspension).

Table 1: Cultivation media for MDCK suspension cells

Short name	Long name	Medium property	Supplement	Distribution
Smif8	Smif8 PGD 2x	Chemically defined Animal comp. free Protein free	Gln (4 mM) Pyr (4 mM)	Acquired from K. Scharfenberg, University of Applied Science Emden-Leer
Xeno-SFM	Xeno™-Soo1S	Serum-free Animal comp. free	Gln (8 mM)	Shanghai BioEngine Sci-Tech Co., LTD
Xeno-CDM	Xeno™-CD001S	Chemically defined Animal comp. free	Gln (8mM)	Shanghai BioEngine Sci-Tech Co., LTD

MDCK suspension cell line

In this work, four MDCK suspension cell lines were used in different experiments. Two cell lines were developed previously, and two were generated in the process of this work (Table 1). Here, a uniform nomenclature is used independent of other names used in literature.

Table 2: Origin and background of the used MDCK suspension cell lines.

Name	Other name	Medium	Origin	Adaptation	Proprietary
MDCK.S8.E	MDCK.SUS ₂	Smif8	MDCK (ECACC) #84121903	[53,171]	MPI / K. Scharfenberg
MDCK.Xe.E	MDCK.Xeno	Xeno	MDCK (ECACC) #84121903	This work	MPI
MDCK.Xe.A	ssf-MDCK	Xeno	MDCK NBI-2 (ATCC) ATCC CCL-34	[50,172]	ECUST
MDCK.S8.A	-	Smif8	MDCK NBI-2 (ATCC) ATCC CCL-34	This work	MPI / ECUST

3.1.2 Cultivation of MDCK suspension cells

Cultivation of MDCK cells in shake flasks

MDCK cells were cultivated in shake flasks (polycarbonate Erlenmeyer Flask, #431143/#431144, Corning®, USA) in a Multitron Pro incubator (Infors HT, Switzerland) at 37 °C and 5 % CO₂ atmosphere. MDCK cells were passaged every two to four days with a variable seeding density (0.4–1.0 × 10⁶ cells/mL) depending on passage schedule and cell line (Table 3). Growth and infection experiments of MDCK.S8.E cells for metabolic profiling experiments were performed using 500 mL shake flasks (#4113-0500, Nalgene™, Thermo Scientific, USA) with an initial cultivation volume of 200 mL at 150 rpm. In extended growth experiments, sterile Milli-Q water was added before every sampling point according to the weight reduction due to water evaporation (1–2 mL/d) in non-hydrated incubator.

Table 3: Routine cultivation conditions of MDCK suspension cell lines in shake flasks.

	MDCK.S8.E	MDCK.Xe.E	MDCK.Xe.A	MDCK.S8.A
Shake flask	125/250 mL	125/250 mL	125/250 mL	125/250 mL
Baffles +/-	+	+	-	-
V_w	50/100 mL	50/100 mL	30/60 mL	40/80 mL
Shaking speed	185 rpm	185 rpm	100 rpm	150 rpm
Inoculation [10 ⁶ cells/mL]	0.5–0.8	0.4–1.0	0.4–1.0	0.5–0.8
Passage frequency	3–4 days	2–3 days	2–3 days	2–3 days
Morphology	Aggregates	Single cell	Single cell	Small aggregates

V_w: working volume,

Cultivation of MDCK cells in semi-perfusion

For cultivation of MDCK.Xe.E cells at high cell density, semi-perfusion was used to simulate perfusion in shake flask experiments [276]. Cells in semi-perfusion were cultivated in 50 mL medium with standard cultivation conditions. In each perfusion step, cells were pelleted by centrifugation (400 × g, 10 min, RT) and up to two third (i.e. 33 mL) of the cultivation volume was removed and replaced with pre-warmed, fresh cultivation medium. With increasing cell concentration, more medium had to be replaced until a maximum replacement of 2/3 of working volume was reached. To continue the semi-perfusion, the time interval between medium replacements of working volume was decreased to realize an overall constant cell specific perfusion rate (CSPR). A constant cell specific growth rate of 0.027 h⁻¹ and a CSPR of 2.5 pL/(cell h) was used to calculate the perfusion volume of each perfusion step (Equation 1) or the time interval with fixed perfusion volume (Equation 2), respectively.

$$\frac{V_P}{V_W} = \frac{VCC \cdot CSPR \cdot (e^{\mu \Delta t} - 1)}{\mu} \quad (\text{Equation 1})$$

$$\Delta t = \frac{\ln\left(\frac{V_P}{V_W} \cdot \frac{\mu}{CSPR} \cdot \frac{1}{VCC} + 1\right)}{\mu} \quad \text{with} \quad \frac{V_P}{V_W} = \frac{2}{3} \quad (\text{Equation 2})$$

Cultivation of MDCK in stirred tank bioreactors

For process evaluation, MDCK.Xe.A cells were cultivated in up to four parallel 0.7 L DASGIP® vessel (#76DS0700ODSS, Eppendorf, Germany). All bioreactors were controlled by a DASGIP® Parallel Bioreactor System (#76DGo4CC, Eppendorf, Germany) using the DASware® control software (#76DGCS, Eppendorf, Germany). Temperature was controlled at 37 °C using a heat blanket. Variable gas flow of an air-oxygen mixture was used for aeration with a macrosparger controlling dissolved oxygen (DO) at 40 % of air saturation. The pH set point (growth: 7.0; infection: 7.2) was controlled using a CO₂ flow or by addition of 1 M NaOH, during the end of cultivation. For agitation, a single 30° pitched 3-blade stirrer (O.D. 50 mm) was used. Bioreactors were started with 400 mL working volume, which was reduced or increased during cultivation due to sampling and medium addition for infection, respectively. Overall, the working volume was between 300 and 600 mL. Approximately 50 mL of independent precultures (Erlenmeyer flask, 60 mL wv, 8–9 × 10⁶ cells/mL) were used to inoculate each bioreactor with an initial cell concentration of 1 × 10⁶ cells/mL.

Medium adaptation

Step-wise medium exchange was applied for the adaptation of the MDCK cells to Xeno and Smif8 medium, respectively. Over the first adaptation period, the content of new medium was increased by 10 % steps. During adaptation, MDCK cells were passaged by spinning down cells (300 × g, 5 min, RT) to adjust to 0.5–1.0 × 10⁶ cells/mL for inoculation and to limit carryover of old medium. Cells were resuspended in the new medium mixture (10 % carry over) and cultivated for three days. In case of poor cell growth, additional passages with the same medium mixture were performed to stabilize adaptation.

3.1.3 Cell culture analytics

Cell count and cell volume

Cell concentration, average cell diameter, cell viability and size distribution of cultured cells were determined using a Vi-CELL XR cell counter (#731050, Beckman Coulter, USA). These same settings were used for the determination of cell count for all MDCK suspension cells (Table 4). Due to cell aggregates, MDCK.S8.E cells were trypsinized prior to analysis. For this, one mL of cell suspension was centrifuged using a tabletop centrifuge (800 × g, 1 min, RT), 900 µL of supernatant was removed and the cell pellet was resuspended by adding 500 µL of trypsin-EDTA solution (1 ×). Cells were incubated for 10 min at 37 °C, mixed with 400 µL of FBS, triturated and analyzed.

Average cell volume was determined from the size distribution of the analyzed cells, assuming a spherical cell shape. The evaluated cell population (1,000–18,000 cells) was distributed into 140 size classes (i) with a corresponding cell diameter (d_i). The analysis software (Vi-CELL XR Cell Viability Analyzer 2.04, Beckman Coulter) considered cell sizes between 7 μm and 50 μm with diameter steps of 0.31 μm between each size class. The average cell volume of the sample was calculated from the cell volume of each size class (Equation 3). Viable cell volume (VCV) was determined by multiplying the average cell volume and the viable cell concentration (Equation 4). For the cell concentration measured with the Vi-CELL XR system an error (relative standard deviation) of 5 % was assumed [277].

$$\bar{V}_{cell} = \frac{\pi}{6} \cdot \sum_{i=1}^{140} \left(d_i^3 \cdot \frac{N_i}{N_{tot}} \right) \quad (\text{Equation 3})$$

$$VCV = VCC \cdot \bar{V}_{cell} \quad (\text{Equation 4})$$

Table 4: Settings used for counting MDCK suspension cells with the Vi-Cell XR cell counter.

Cell Type	MDCKSUSP	
Minimum diameter	7	μm
Maximum diameter	50	μm
Cell brightness	85	%
Cell sharpness	80	
Viable cell spot brightness	90	%
Viable cell spot area	4	%
Decluster degree	Medium	
Amount of size classes (i)	140	

Extracellular metabolites

Cell suspension was centrifuged at $300 \times g$ for 5 min at room temperature to remove cells and cell debris. Cell-free supernatant was either analyzed directly or stored at $-80 \text{ }^\circ\text{C}$ until respective analysis. Virus containing samples were inactivated in a heat block at $80 \text{ }^\circ\text{C}$ for 3 minutes prior to analysis. Concentration of glucose, glutamate, lactate, ammonium and lower levels of glutamine ($\leq 4 \text{ mM}$) were measured using a BioProfile 100 Plus analyzer (Nova Biomedical, USA) with three external standards. Higher levels of glutamine ($\leq 10 \text{ mM}$) as well as pyruvate were quantified using a Cedex Bio Analyzer (#0639554001, Roche Diagnostics, Germany). Amino acid concentrations

were determined with the “UPLC Amino Acid Analysis Solution” using an ACQUITY UPLC H-Class (#720003294en, Waters, USA). Medium osmolality was measured from a 10 μ L cell free sample using a vapor pressure osmometer (VAPRO[®] 5520, Wescor, USA).

3.2 Influenza A virus infection

3.2.1 Seed viruses

All infections were carried out using an influenza A/Puerto Rico/8/34(H1N1) strain, here referred to as “influenza A virus (IAV)” or “APR8”. The egg-based influenza A virus strain obtained from Robert Koch Institute (Amp. 3138, RKI, Germany) was propagated in adherent MDCK cells (#84121903, ECACC, UK) to generate the original seed virus adapted to adherent MDCK cells. Multiple sequential infection with low multiplicity of infection (MOI: 10^{-5}) were performed with all four cell lines for complete virus adaptation to the respective cells and medium (Table 5). Cell suspension was harvested for seed virus generation, centrifuged (300 \times g, 10 min, 4 $^{\circ}$ C) and supernatant was distributed in aliquots of 0.5 mL each. Seed viruses were stored at -80 $^{\circ}$ C.

Table 5: Influenza A seed viruses adapted to different cell lines

Name	Passages for adaptation	Cell line	Virus titer [TCID ₅₀ /mL]	Harvest
APR8_O	Original seed virus	MDCK adh ¹	1.1×10^9	-
APR8_SFM	1	MDCK.Xe.E ² in Xeno-SFM	1.3×10^9	27 hpi
APR8_S8E	5	MDCK.S8.E ³	1.5×10^9	30 hpi
APR8_XeE	5	MDCK.Xe.E ⁴	0.9×10^9	27 hpi
APR8_XeA	5	MDCK.Xe.A ⁴	1.8×10^9	30 hpi
APR8_S8A	5	MDCK.S8.A ³	0.9×10^9	27 hpi

¹ in serum-free V-medium, ² in Xeno-SFM medium, ³ in Smif8 medium, ⁴ in Xeno-CDM medium

3.2.2 Infection conditions

For infection of MDCK suspension cells with IAV, some variations concerning trypsin activity, MOI and media replacement were used. Whereas differences in trypsin activity were minor (10 – 30 U/mL), differences in MOI and media replacement were more significant. Infection strategies progressed over time (media replacement) or had to be adapted to the circumstances of the experiments (Table 6). All infections were performed with the same trypsin type (#27250018,

Thermo Scientific, USA) dissolved in PBS at a stock activity of 5000 U/mL and stored as aliquots at -20 °C. With exception of high MOI infection (MOI 10), thawed seed virus was serially diluted (1:10) with PBS until a convenient volume for the infection was reached (20 – 200 µL).

Metabolic profiling experiment

Infections performed for metabolic profiling experiments were not performed with the goal of reaching a virus production process with high viral titers and low seed virus consumption. Due to low cell density during infection ($2-3 \times 10^6$ cells/mL) and high MOI condition, no media replacement and trypsin addition was necessary. For virus infection, pure undiluted seed virus (APR8_O & APR8_SFM) was added (3–5 mL). For mock infection V-medium or Xeno-SFM medium was added, respectively.

Batch infection

For IAV production in batch mode, cells were cultivated for three days to accumulate enough biomass for infection. At time of infection, cells were either diluted by half with fresh medium or cells were spun down ($300 \times g$, 10 min, RT) and all the cells were resuspended in fresh medium in the same working volume as previously. Medium exchange allowed higher cell density and higher virus titer, whereas cell dilution is more applicable for large-scale manufacturing. After medium replacement, trypsin and diluted seed virus were added, depending on working volume and cell concentration, respectively. Except for seed virus production and virus adaptation (MOI: 10^{-5}) a standard MOI of 10^{-3} was used for batch infection (Table 6).

Semi-perfusion infection

At time of infection 90 % of the medium was replaced with fresh cultivation medium (Xeno-SFM) as described for the standard semi-perfusion steps. As for batch infection, trypsin and diluted seed virus was added, according to the required MOI and trypsin activity (Table 6). To keep trypsin activity stable throughout the whole infection phase, trypsin was added to the fresh perfusion medium (20 U/mL) for all following semi-perfusion steps post infection.

Table 6: Overview of the infection conditions used in the different experiments

Experiment	Cult. mode	Trypsin	MOI	Media replacement
MDCK.S8.E metabolomics	SF; batch	-	10	-
MDCK.Xe.E in Xeno-SFM	SF; batch	30 U/mL	10^{-3}	Media exchange
	SF; semiperf.	20 U/mL	10^{-1} & 10^{-3}	Media exchange
Seed virus	SF; batch	30 U/mL	10^{-5}	Dilution
MDCK.X/S8.E/A comparison	SF; batch	10 U/mL	10^{-3}	Dilution
MDCK.Xe.A	STR; batch	30 U/mL	10^{-3}	Dilution

3.2.3 Analytics for influenza virus particles and infected cells

Tissue Culture Infective Dose₅₀

For the quantification of infective influenza virus particles, a Tissue Culture Infective Dose₅₀ (TCID₅₀) assay was used as described by Genzel and Reichl [278]. Cell-free, sterile supernatant was stored until measurement at -80°C . Samples were thawed in a water bath before analysis. Multiple freeze-thaw cycles were not avoided. Confluent MDCK cells (#84121903, ECACC, UK) cultivated in 96-well plates were infected with a serial dilution of virus samples (100 μL) and incubated for 48 h (37°C , 5 % CO_2). MDCK cells were fixed with an ice-cold acetone solution (80 %), stained with an anti- influenza A/Puerto Rico/8/34(H1N1) HA serum (#03/242, NIBSC, UK) and an Alexa Fluor donkey anti-sheep IgG antibody (#A11015, Thermo Scientific, USA) as a secondary fluorescence label. Fluorescence positive and negative wells were counted using a fluorescence microscope (Axio Observer.A1, Zeiss, Germany) and infectious titer was calculated from eight replicates with the Spearman-Kärber method [279,280]. The infectious virus titer is expressed as TCID₅₀ units per milliliter: TCID₅₀/mL. Based on >100 measurement, within this thesis the error (relative standard deviation) of the TCID₅₀ assay was estimated to be 41 % (8.3 Error estimation: TCID₅₀ assay). The standard operating procedure (SOP) to determine the TCID₅₀ titer is available upon request from MPI (SOP: Instructions V/o8_Version2.1_english, 07.08.2019).

Hemagglutination activity assay

Influenza virus content was estimated by a hemagglutination activity (HA) assay as described previously [281]. Cell-free virus samples and standards were serially diluted with PBS in two dilution rows ($2^{(1-n)}$ & $2^{(0.5-n)}$ with n: 1 to 12) in 96-round-bottom-wells. Chicken erythrocyte solution (100 μL) was added with a concentration of 20×10^6 erythrocytes per mL to the diluted samples (100 μL) and incubated for 308 h at RT. Erythrocyte agglutination was evaluated using a plate reader (Infinite®

M200 microplate reader, Tecan Group, Switzerland) measuring the extinction at 700 nm. A curve fitting function of the resulting extinction data was used to determine the transition from agglutination to sedimentation. The dilution factor needed until agglutination stops, corresponds to the HA titer. The final virus titer is expressed as common logarithm (lg) of the hemagglutination units (HAU): lg(HAU). It was assumed that at the highest diluted sample with agglutination, virus and erythrocyte concentration are equal. The concentration of the total virus particles (CV_T) can be calculated using this assumption (Equation 5). Based on >100 measurement within this thesis the standard deviation of the HA assay was estimated to be 0.04 Lg(HAU) (8.4 Error estimation: HA assay), lower than the validated assay standard deviation of 0.08 Lg(HAU) reported previously [282]. This corresponds to an error (relative standard deviation) for the linear HA value, as well as total virus particles of 10 % (0.04 Lg(HAU)) or 19 % (0.08 Lg(HAU)). The standard operating procedure (SOP) to determine the hemagglutination titer is available upon request from MPI (SOP: V/05 HA-Assay, Version 2.2, 20.01.2011).

$$CV_T = CE_{Ery} \cdot HAU = 2 \cdot 10^7 \frac{1}{mL} \cdot 10^{HA} \quad (\text{Equation 5})$$

Imaging flow cytometry

The relative amount of infected and apoptotic cells was determined by imaging flow cytometry as previously described in detail [283]. MSCK.S8.E cells had to be trypsinized prior to sample treatment to assure single cell analysis and to prevent clogging of the ImageStream analyzer. For cell fixation, 1 mL of infected MDCK cells was mixed with paraformaldehyde to a final concentration of 2 % and incubated at 4 °C for 30 min. Cells were washed with PBS (300 × g, 10 min, 4 °C), added to 5 mL cold (−20 °C) 70 % ethanol and stored at −20 °C. For staining, fixed cells in ethanol were spun down (300 × g, 10 min, 4 °C) to remove storage solution. Cell pellet was washed twice with FACS-buffer (PBS containing 0.1 % BSA and 2 % glycine) and blocked in PBS containing 1 % BSA (30 min, 37 °C). vRNP positive cells were stained with a monoclonal mouse anti-NP antibody mAb61A5 [284] as a primary antibody, and Alexa Fluor 647-conjugated goat anti-mouse pAb (#A21235, Thermo Scientific, USA,) as a secondary antibody. All antibodies were incubated for 60 min at 37 °C in FACS-buffer. Between each incubation step, cells were washed twice with FACS-buffer (300 × g, 10 min, 4 °C). Shortly before analysis, nucleic DNA was stained with DAPI (50 mg/L, #6843-2, Carl Roth, Germany). Ten thousand single cells were analyzed with an ImageStream X Mark II (#100220, Merck, Germany) using a 60x objective lens. Image analysis was carried out with the IDEAS software

(version 6.1). The vRNP-positive cells were considered as infected and nucleic condensation and fragmentation was used as signs of apoptosis.

3.2.4 Viral antigen content and host cell contaminants

Virus antigen quantitation by single-radial immunodiffusion assay

The amount of the viral hemagglutinin surface antigen was quantified by single-radial immunodiffusion (SRID) assay as previously reported [285]. Samples were dialyzed as described before [153] and lyophilized using 1% sucrose as cryo-protectant. Resuspension was made by adjusting the HA content of the samples to the HA content of a reference standard produced in-house as described by Opitz et al. [286]. The assay setups consisted of a 7×7 diffusion matrix made out of a 1% agarose gel with 64 µg of influenza A/Puerto Rico/8/34(H1N1) antigen per mL (#03/242; NIBSC, UK).

Total protein and host cell DNA quantification

Total protein was estimated using a Bradford BioRad assay (#5000006, BioRad Laboratories, USA). The calibration curve was made with bovine serum albumin (#A3912, Sigma-Aldrich, Germany) in the range of 5–40 µg/mL. The concentration of dsDNA was estimated with a Quant-iT™ PicoGreen assay (#P7581, Life Technologies, Germany). The standard curve was made with lambda DNA (#D1501, Promega, USA) for the range of 4–250 ng/mL.

3.3 Metabolic profiling of MDCK suspension cells

3.3.1 Quenching

Quenching of suspension cells had to be performed as fast as possible to limit possible metabolite transition or decay. The quenching procedures used in this work were slightly changed from the original methods in order to improve comparability (explained later in detail). Suspension cells were cultivated in shake flask and sampled in mid exponential growth phase. For all quenching methods, 2 mL of cell suspension were used in triplicate, extracted, dried and analyzed simultaneously. All used solutions were prepared ahead using high grade components and precooled to the according temperature (Table 7). Quenched samples were stored at -80 °C for up to five days until metabolite extraction.

Table 7: Solutions used for washing, quenching and metabolite extraction.

Name	Solvent (v/v)	Additives (f.c.)	Temperature
Wash solution	MilliQ-water (100 %)	NaCl (9.0 g/L)	4 °C
Quench solution	Methanol (66.7 %) Chloroform (33.3 %)	-	-20 °C
Extraction solution	Methanol (47.4 %) MilliQ-water (52.6 %)	Tricine (2 mM)	4 °C
MeOH-AMBIC	Methanol (60.0 %) MilliQ-water (40.0 %)	AMBIC (8.5 g/L) HCl (pH adjust)	4/-40 °C
Chloroform	Chloroform (100 %)	-	-20 °C

Centrifugation quenching

For centrifugation quenching (CQ), cells were separated by g-force from the cultivation medium, washed and quenched. In order to achieve the shortest possible centrifugation time, centrifugation speed was optimized to guarantee total cell recovery. In the final method, 2 mL of cell suspension were transferred to a 2 mL reaction tube (Safe-Lock Tubes, 2.0 mL, Eppendorf AG) and then added to a precooled (4 °C) centrifuge (Biofuge Primo R, swing bucket rotor # 7592, Heraeus, Thermo Scientific, USA). Cell suspension was centrifuged at maximum acceleration until the centrifuge reached 2000 x g and stopped immediately (~30 s). The supernatant was decanted, and cell pellet was washed (wash solution). After a second centrifugation, the supernatant was removed thoroughly, 600 µL of quench solution was added, vortexed for five seconds and snap frozen in liquid nitrogen.

Filtration quenching

Filtration quenching (FQ) was adapted from previous descriptions [287-289] using a glass depth filter (Type A/D, #66220, Pall Corporation, USA) and a defined pressure, controlled with a vacuum controller (CVC3000, Vacuubrand, Germany). The pressure used for filtration was optimized to limit cell damage, while obtaining sufficient filtration speed. A glass vacuum filtration device (Schleicher & Schuell, Germany) was connected over the vacuum controller to a running vacuum pump (MZ2C, Vacuubrand, Germany). Before assembling the filter, the whole system (glassware, filter support) was flushed with wash solution, the vacuum regulator was zeroed to the air pressure and set to -20 mbar. The inserted glass fiber filter was washed with 5 mL of wash solution, and 2 mL of cell suspension was carefully added to the filter center. Cells were washed immediately with 5 mL of wash solution to remove medium components. The filter was quickly transferred to a 15 mL polypropylene tube (17/120 mm, CELLSTAR, Greiner, Germany) containing 1.2 mL of quenching solution, vortexed for five seconds and snap frozen in liquid nitrogen. Higher amount of quenching solution was necessary to compensate for excessive wash solution in the filter and prevent it from freezing.

Direct quenching

In the direct quenching (DQ) method, suspension cells were quenched in a methanol ammonium bicarbonate (MeOH-AMBIC) solution, and separated by centrifugation adapted from Sellick et al. [290]. To achieve a stable temperature of -40 °C for the MeOH-AMBIC solution, a thermostat was used (FP89-HL, JULABO, Germany) with silicone oil as a heat transfer liquid (KRYO 90, JULABO, Germany). The pH of MeOH-AMBIC solution was adjusted to pH 7.4 by adding 5 M HCl solution, 10 mL were transferred to 15 mL polypropylene tubes (17/120 mm, CELLSTAR, Greiner, Germany) and cooled in the cryostat to -40 °C (approx. 10 min.). 2 mL of the cell suspension was added to the MeOH-AMBIC solution, the tube was inverted twice and centrifuged for one minute at 3000 x g in a precooled (-20 °C) centrifuge (Sigma 4-16KS, swing bucket rotor #11650, Sigma Laborzentrifugen, Germany). The supernatant was carefully removed with a Pasteur pipette connected to a peristaltic pump, 600 µL of quenching solution was added, vortexed for 5 seconds and snap frozen in liquid nitrogen.

3.3.2 Metabolite extraction & recovery

Methanol-chloroform extraction

The extraction of metabolites was based on previous work for adherent cells [291] and suspension cells [292] and was slightly adapted to this application. During the extraction, all samples and solutions were stored on ice, and the centrifuge (Biofuge Primo R, swing bucket rotor # 7592, Heraeus, Thermo Scientific, USA) was precooled to 0 °C. QC and DQ samples were stored on ice for 5 min, vortexed and transferred to an extraction tube (Safe-Lock Tubes, 2.0 mL, Eppendorf) containing 500 µL of chloroform. 800 µL of extraction solution was added to the sample vials, vortexed and transferred to an extraction tube. The two phases (chloroform & MeOH-buffer) of the cell extract were mixed thoroughly (vortex, 20 s, max. speed), and the extraction tubes were centrifuged for 5 minutes at 16,000 x g. The upper hydrophilic layer (MeOH-buffer) was removed carefully and transferred to another extraction tube (E2). For the second extraction 800 µL of extraction buffer was transferred to the extraction tube (E1), followed by the same steps as the first extraction. The hydrophilic layers of the first and second extraction were pooled (E2), heated to 85 °C for 5 min and centrifuged for 10 min at 16,000 x g. The extracts were transferred to storage tubes (Safe-Lock Tubes, 2.0 mL, ambra, Eppendorf AG, Germany) and stored at -80 °C until drying.

FQ samples were stored on ice for 5 minutes, and the filter was transferred to a syringe barrel (10 ml, Omnifix Solo, B. Braun). 1200 µL of extraction buffer was transferred to the sample tube, vortexed and added to the syringe. Using a plunger, the liquid was removed from the filter. The liquid was added back to the same syringe barrel and the filtration process was repeated. The filtrate was split in equal amount into two extraction tubes (E1) containing 500 µL of chloroform, vortexed and centrifuged as described for QC and DQ. The filter extraction was repeated and the hydrophilic phase of both first and second extractions were pooled (E2) and proceeded as described for QC and DQ. For each sample, two storage tubes with extracted metabolites (~1.8 mL each) were stored at -80 °C until drying and pooled after reconstitution.

Drying and reconstitution

Metabolite extracts were dried at RT under nitrogen gas stream until no liquid was present in the sample (8–10 h). Samples were stored as dry powder until analysis, at -80 °C. On the day of analysis metabolites were solved in 300–800 µL of ultra-pure LC-MS grade water (Milli-Q Type 1 plus LC-Pak Polisher, Merck, Germany), vortexed and incubated at 4 °C for 15 min. For metabolic profiling of MDCK.S8.E cells, the reconstitution volume was adjusted to respective VCC of the sample. FQ samples were reconstituted in half of the volume used for DQ and CQ and the corresponding two

metabolite extracts were pooled to obtain the same final volume. Reconstituted samples were vortexed, centrifuged at 16,000 x g for 10 min at 4 °C and transferred to HPLC glass vials.

3.3.3 Metabolite quantification by LC-MS

Extracted metabolites were quantified with an ICS-5000 MSQ-plus system (Dionex, Thermo Scientific, USA) adapted from Ritter et al. [201]. Reconstituted metabolites (15 µL injection volume) were separated with two analytical anion-exchange columns (Dionex IonPac AS11, 2x250 mm, 30 °C) connected serially after an inline filter (35/5/0.45 µm) and a guard column (Dionex IonPac AG11, 2x50 mm). Potassium hydroxide (KOH) eluent (2-100 mM) was generated from ultra-pure water using an in line eluent generator (Dionex ICS-5000⁺ EG) with a constant eluent flow of 0.35 ml/min (\cong 2300 psi). Post column continuous eluent suppression (Dionex AERS 500, 2 mm) enabled highly sensitive detection of metabolites using a serial connected conductivity- (Dionex ICS-5000⁺ CD) UV- (Dionex ICS-Series VWD, single-channel, 260 nm) and MS-detector (MSQ Plus Mass Spectrometer). Over a high pressure valve the eluent could be directed either to the MS-detector or to waste. Eluent flow was directed to the MSQ from 2 to 6 min and from 9 to 53 min, due to the elution of high amount of chlorine ions at around 8 min. In order to shorten the run time and avoid negative gradient a new simplified gradient was developed. The run time was reduced by 10 minutes, and more robust separation was achieved by skipping declining KOH gradients used before [201]. Thirty metabolites were separated via the optimized gradient (Table 8), and quantified using an external standard mix of all the metabolites. Single ion monitoring was used to detect specific predetermined metabolite ions (Appendix: Table 15). As an example, the eluent profile of a standard (105) from the UV, conductivity and MS signal (total ion count) with an eluent overlay is shown in the appendix (Figure 37). Metabolite standard stock (Appendix: Table 16) stored at -80 °C was diluted with tricine buffer (10 mM tricine, 6 mM NaCl) and water to simulate the extraction matrix (Table 9). All standards and samples were measured as analytical triplicate.

Table 8: KOH-gradient for the separation of intracellular metabolites by AE-HPLC.

Time [min]	KOH [mM]	Curve ¹		Time [min]	KOH [mM]	Curve ¹
0 ²	2	5		33	50	5
5	6	5		41	86	5
10	10	3		41	100	5
15	14	3		46	100	5
18	22	1		46	2	5
27	30	7		53	2	5

¹ Curves 1 through 4 are convex, curve 5 is linear and curves 6 through 9 are concave; ² time of injection.

Table 9: Dilutions used as external standards for quantitative LC-MS measurements.

STD ID	Tricine-buffer	Metabolite-MM ¹	Water	e.g. [ATP] ²
155	845 µL	155 µL	–	310 µM
130	845 µL	130 µL	25 µL	260 µM
105	845 µL	105 µL	50 µL	210 µM
080	845 µL	80 µL	75 µL	160 µM
055	845 µL	55 µL	100 µL	110 µM
030	845 µL	60 µL (1:2)	95 µL	60 µM
020 ³	845 µL	40 µL (1:2)	115 µL	40 µM
010 ³	845 µL	100 µL (1:10)	55 µL	20 µM
005	845 µL	50 µL (1:10)	105 µL	10 µM

¹ Composition of the metabolite master mix can be found in Table 16; ² Exemplary concentration of ATP for respective standard; ³ standards not used for method validation.

Calculation of intracellular metabolite concentrations

Intracellular metabolite concentrations were calculated based on the amount of extracted metabolites and the total cell volume in the extracted sample. To determine the amount of the extracted metabolite from the sampled cell suspension, the concentration of the respective metabolite in the reconstituted extract $CM_{analyte}$, determined by LC-MS measurement was multiplied with the reconstitution volume (V_{rec}). The total cell volume in the cell culture sample was calculated from the viable cell volume (VCV) (Equation 4) and the volume of the sampled cell suspension (V_s) (Equation 6).

$$CM_{cell} = \frac{CM_{analyte} \cdot V_{rec}}{VCV \cdot V_s} \quad \text{with } V_s = 2 \text{ mL} \quad (\text{Equation 6})$$

3.4 Calculations and statistics

3.4.1 Calculations

Adenylate energy charge

The adenylate energy charge (AEC) gives an impression of the energy status of a viable cell. It is calculated from the concentrations of the three major energy nucleotides ATP, ADP and AMP (Equation 7). The sum of ATP, ADP and AMP is considered the total adenylate concentration (AXP).

$$AEC = \frac{ATP + 0.5 ADP}{AXP} = \frac{ATP + 0.5 ADP}{ATP + ADP + AMP} \quad (\text{Equation 7})$$

Specific metabolite consumption/production

The cell specific consumption or production rates of metabolites defines the uptake and release of substrates or products for the average cell. With a constant working volume, the specific rate is defined by the time differential of the extracellular metabolite concentration normalized on the biomass concentration (VCC). Macroscopically the metabolic rates are calculated from the difference of the extracellular concentration and the integral of the viable cell concentration between two time points (Equation 8).

$$q_{S/P} = \frac{1}{VCC} \frac{\partial C_{S/P}}{\partial t} = \frac{C_{S2/P2} - C_{S1/P1}}{\int_{t1}^{t2} VCC dt} \quad (\text{Equation 8})$$

Specific virus yield

The cell specific virus yield (CSVY) represents the virus concentration/ titer (Tv) normalized on the maximal viable cell concentration (VCC_{max}) post infection (Equation 9). It represents capacity of the average cell for the production of virus particles. Due to the differences in virus quantification assays, the HA titer have to be converted to total virus particle concentration (Equation 5) to calculate the $CSVY_{HA}$ for total virus particles (Equation 10). The TCID₅₀ titer was used directly to calculate the respective $CSVY_{TCID}$ (Equation 11). The error for the CSVY was calculated by error propagation (Equation 17) based on the individual assay errors estimated previously. The respective intra-assay error (relative standard deviation) was calculated to be at 12 % and 42 % for $CSVY_{HA}$ and $CSVY_{TCID}$, respectively. The Inter-assay error for $CSVY_{HA}$ was based on the assay (HA) validation was 19 %.

$$CSVY = \frac{Tv}{VCC_{max}} \quad (\text{Equation 9})$$

$$CSVY_{HA} = \frac{CV_T}{VCC_{max}} \quad (\text{Equation 10})$$

$$CSVY_{TCID} = \frac{TCID_{50}}{VCC_{max}} \quad (\text{Equation 11})$$

Accumulated virus titer

In semi-perfusion- cell culture-based virus production, centrifugation is used to separate cells and cultivation medium in the permeate. With the centrifugation force used in this process, virus particles are not separated from the permeate and are removed from the cultivation with every perfusion step. In order to evaluate the true produced virus amount and to compare virus dynamics with batch infections the accumulated virus titer (Tv_{acc}) was calculated (Equation 12). This titer simulates a theoretical virus titer in the same cultivation volume without any removal of virus particles from the cultivation. For the logarithmic HA titer, however, only the linear HA-units can be used to calculate the accumulated HA titer (HA_{acc}) (Equation 13).

$$Tv_{acc} = Tv_S + \sum \frac{V_P \cdot Tv_P}{V_W} \quad (\text{Equation 12})$$

$$HA_{acc} = \lg \left(10^{HA_S} + \sum \frac{V_P \cdot 10^{HA_P}}{V_W} \right) \quad (\text{Equation 13})$$

Space time yield

The space time yield (STY) is used in this work as a reference value for process productivity. It represents the amount of total product produced per cultivation volume (V_C) and production time (t_p). In our case of virus particles as desired product, the virus amount is calculated by multiplying the total (accumulated) virus concentration (CV_T) with the working volume (V_w) ((Equation 14). For cultivations in semi-perfusion the accumulated virus concentration has to be calculated. (Equation 5 & Equation 13). The error (relative standard deviation) of the STY corresponds to the assay error of the virus quantification, in this case 10 % (intra-assay) or 19% (inter-assay) (CV_T).

$$STY = \frac{P}{t_p \cdot V_C} = \frac{C_p \cdot V_W}{t_p \cdot V_C} \quad (\text{Equation 14})$$

$$STY = \frac{CV_T \cdot V_W}{t_p \cdot V_C} \quad \text{Perfusion: } CV_T = CV_{Tacc} \quad (\text{Equation 15})$$

3.4.2 Errors and statistics

Standard deviation (sample)

The standard deviation (σ_s) of a measured sample was determined from observed values of the sample items (z) with a sample size (N) of at least three samples (Equation 16). Sample standard deviation was used in the visualization of sample errors in the form of error bars.

$$\sigma_s = \sqrt{\frac{1}{N-1} \sum_{i=1}^N (z_i - \bar{z})^2} \quad (\text{Equation 16})$$

Error propagation

Error propagation was used to calculate the obtained error for a value calculated with the function f , where f contained m variables (x_i) with a respective standard deviation (σ_{x_i}) (Equation 17). Error propagation was used for the calculation of the error (SD) for the calculated values of intracellular metabolite concentrations (Equation 6), adenylate energy charge (Equation 7) and the CSVY (Equation 9).

$$\sigma_f = \sqrt{\sum_{i=1}^m \left(\frac{\partial f}{\partial x_i} \cdot \sigma_{x_i} \right)^2} \quad \text{with } f(x_1, x_2, \dots, x_m) \quad (\text{Equation 17})$$

t-Test

To evaluate the statistical significance between two sample sets, the Welch's t-test was used with a null hypothesis of an equal mean of the two populations. The test assumes two independent data sets with a normal distribution within each set and different variance (σ^2) for the sample sets. In order to calculate the t-value, mean (X), variance and size (N) of the two sample sets are used (Equation 18). With the t-value and the degree of freedom (ν) (Equation 19) the p-value can be determined. Final p-values for the null hypothesis were calculated with the Origin-Pro software. Confidence intervals higher than 95 % ($p < 0.05$) were considered statistically significant.

$$t = \frac{\bar{X}_1 - \bar{X}_2}{\sqrt{\frac{\sigma_1^2}{N_1} + \frac{\sigma_2^2}{N_2}}} \quad (\text{Equation 18})$$

$$v \approx \left(\frac{\sigma_1^2}{N_1} + \frac{\sigma_2^2}{N_2} \right)^2 \cdot \left(\frac{(\sigma_1^2)^2}{N_1^3 - N_1} + \frac{(\sigma_2^2)^2}{N_2^3 - N_2} \right)^{-1} \quad (\text{Equation 19})$$

4 Results and discussion

4.1 A new medium for influenza virus production

In 2015, Huang et al. demonstrated with a new cultivation medium a MDCK suspension cell line growing as single cell suspension to surprisingly high viable cell concentrations both in shake flasks and STR systems [172]. Very high virus titers obtained for IAV infections opened the question, whether this medium or cell line would be applicable for other processes as well. Due to unavailability of the cell line (at first), the medium was obtained thanks to a collaboration between the MPI, the East China University of Science and Technology (ECUST) and the company Shanghai BioEngine Sci-Tech Co., LTD. The initial research covered in this chapter was performed with the serum-free version of the Xeno medium (Xeno-SFM) and the MDCK suspension cell line MDCK.S8.E as well as the new developed MDCK.Xe.E. Some of the results presented in this chapter were obtained together with two master students (Adrian Mihut & Johannes Fritsch) and have been partly covered in their master theses [293,294]. Results presented in the following chapter were first published in the Vaccine journal (Bissinger et al., 2019) and parts of the original publication are used hereafter [295].

4.1.1 Adaptation of MDCK suspension cells to Xeno-SFM

The original MDCK.S8.E cell line cultivated in Smif8 medium had an average doubling time of 24-26 h (Figure 6 A) growing in small cell aggregates of variable size (Figure 6 B). A direct adaptation of this cell line to Xeno-SFM medium failed. MDCK.S8.E cells were not able to grow after a total or 50 % medium exchange with the Xeno-SFM medium. Therefore, a slower adaptation method was applied in order to leave the cells time over many passages to fully adapt to the new medium composition. Using this adaptation method, the fraction of new Xeno-SFM medium was slowly increased or kept constant until MDCK cells were able to grow in pure Xeno-SFM medium with a promising growth performance. Over the whole adaptation period, the viability of MDCK cells remained over 90 %. It seemed that the adaptation had a strong effect on the specific growth rate, but only minor effect on the overall viability of the cell population. The whole adaptation process was divided into three phases. In the first one (0-31 days), cell growth was similar or better compared to pure Smif8 cultivations (Figure 6 A). Size of cell aggregates increased, and a higher maximum cell concentration was reached (Figure 6 B). In the second adaptation phase (31-66 days), cell growth

dramatically decreased with increasing Xeno-SFM content (Figure 6 A). Additionally, cellular aggregates disappeared, and MDCK cells grew as single cells (Figure 6 B). After the second adaptation phase, MDCK cells were growing in pure Xeno-SFM medium with a lower doubling time compared to the original culture (24 vs 34 h). In the third adaptation phase (66-180 days), cells were cultivated over multiple passages in pure Xeno-SFM medium to generate the cell line finally selected for process intensification studies (after 180 days). During this adaptation phase, no morphological changes were observed, but cell metabolism seemed improved leading to better cell specific growth rate, higher cell concentrations and lower lactate as well as ammonium accumulation. The last adaptation phase could also be considered a selection phase, where a (sub)population of cells was selected for more efficient and faster growth. Fully adapted cells (passage 60) were used to create a cell bank for further experiments. The long adaptation time (>50 passages, 180 days) of the MDCK.S8.E cell line to a stable MDCK.Xe.E cell line with optimal growth in Xeno-SFM medium was rather surprising. In particular, the time period required for cell adaptation was in a comparable range as establishment of the original suspension cell line from adherent MDCK cells (>40 passages) [53,171]. As both media were developed for suspension cell growth, we expected a rather fast adaptation of the MDCK.Xe.E cell. However, metabolic and morphological changes as well as a (sub)population selection seemed to have increased the adaptation time. Earlier clonal selection processes (e.g. from 60 d), as already applied for the selection of industrial production cell lines, might have accelerated the adaptation process in pure Xeno-SFM medium. Furthermore, clonal selection might be necessary in any case, if such a cell line is to be used in a commercial process.

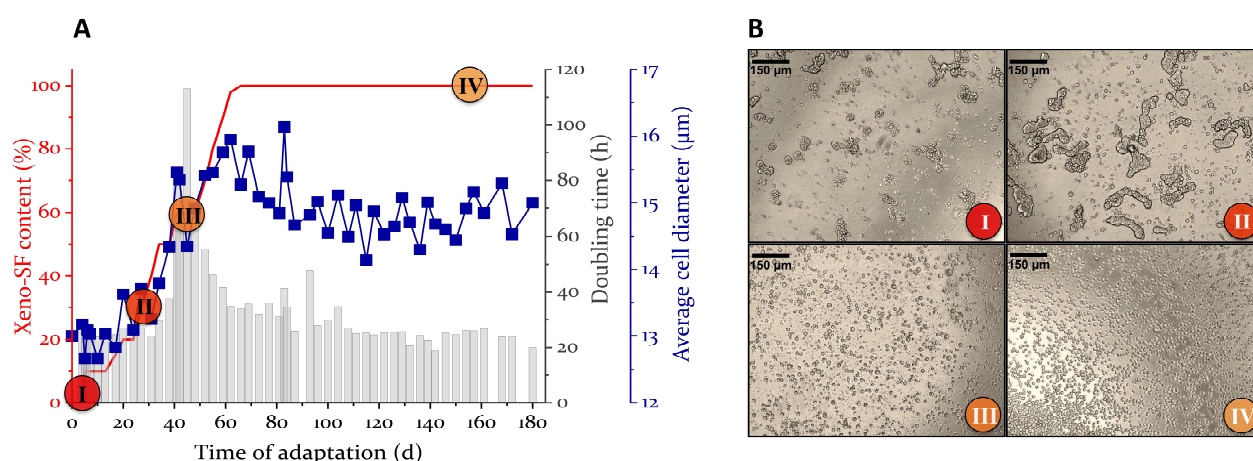


Figure 6: Adaptation of MDCK.S8.E cells from Smif8 to Xeno-SFM medium (MDCK.Xe.E).

MDCK.S8.E cells were monitored over 60 passages during the adaptation to Xeno-SFM medium. **A:** average doubling time (grey bars) and average cell diameter (blue squares) were analyzed over the adaptation time with increasing Xeno-SFM medium content (red line). **B:** Phase contrast microscopy pictures of MDCK suspension cells for morphological evaluation in different medium composition (I: 0 % Xeno-SFM; II: 30 % Xeno-SFM; III: 60 % Xeno-SFM; IV: 100 % Xeno-SFM).

4.1.2 MDCK.Xe.E: cell growth and influenza A virus production

Fully adapted MDCK.Xe.E cells were able to grow in Xeno-SFM medium to cell concentrations above 13×10^6 cells/mL in shake flasks (Figure 7 A). This was a significant improvement compared to MDCK.S8.E cells growing in Smif8 medium, where cells usually reach maximum cell concentrations between $6\text{--}8 \times 10^6$ cells/mL. Additionally, MDCK.Xe.E cells were able to grow with a much higher specific growth rate (μ_{\max} : 0.036 1/h), leading to the accumulation of more biomass in a shorter time period. Viability was stable over the cell growth phase (95 %) and only decreased after a short stationary phase together with the viable cell concentration (Figure 7 A). Due to a higher concentration of the main energy metabolites, glucose and glutamine in the Xeno-SFM medium (Figure 7 B), an increase in cell concentrations was not surprising. Moreover, in the Xeno-SFM medium, single MDCK cells could utilize the available metabolites more efficiently to fuel growth demands. Interestingly, in the middle of the cultivation (~ 72 h), we observed a metabolic shift from lactate production to lactate consumption. A high glutamine concentration and tryptone supplement (5 g/L) in the Xeno-SFM medium led to a much higher accumulation of ammonium of up to 6 mM at 72 h of cultivation (Figure 7 B). After an initial increase during the lag phase, the average cell diameter decreased after 48 h of cultivation. Here, changes in substrate concentration and decrease in osmolality due to lactate and substrate (i.e. glucose & AAs) consumption (from 320 to 270 mOsm/kg) could have led to variations in the average cell diameter.

To evaluate the potential of MDCK.Xe.E suspension cells for IAV production, cells were inoculated in shake flasks with 0.5×10^6 cells/mL, cultivated for 72 h and infected with APR8 (APR_O) after media exchange. The previously reported trypsin amount based on cell concentration (10^{-5} U/cell) [53] was not applicable for the MDCK.Xe.E cells due to higher cell concentrations. Trypsin activity over 50 U/mL led to cell lysis, visible by a fast decrease in cell concentration with stable cell viability. Therefore, a trypsin amount based on volumetric activity (U/mL) rather than cell-based activity (U/cell) was used, which enabled a better comparison of infections between different cell lines and infection strategies. Different trypsin activity (10–40 U/mL) and MOIs ($10^{-2}\text{--}10^{-4}$) were tested for MDCK.Xe.E cells, however, all tested conditions had limited effect on the final HA titer [294]. Finally, moderate MOI (10^{-3}) and trypsin activity (30 U/mL) were used to infect MDCK.Xe.E cells with IAV. With the chosen trypsin activity MDCK.Xe.E cells continued to grow for the first 24 hours post infection (hpi), reaching 11×10^6 cells/mL, followed by a fast drop in cell concentration (Figure 7 C). With the start of virus accumulation at 24 hpi, the average cell diameter decreased by 3–4 μm until the end of the infection. Influenza virus titer rose rapidly after infection (<20 hpi) to a maximal total virus titer of 3.6 lg(HAU) at 48 hpi. Infectious virus titers exceeding 10^9 TCID₅₀/mL were detected as soon as 24 hpi with a maximum at 30 hpi (2.7×10^9 TCID₅₀/mL). Afterwards, the

infectious virus titer declined and was finally reduced by three orders of magnitude at 60 hpi (Figure 7 D). Both dynamics for infectious titer and total number of virus particles (based on HA) were very reproducible between the experiments, and higher variations were observed for cell concentration, viability and cell diameter during cell death after virus production (>24 hpi) (Figure 7 C). For these experiments, the mean $CSVY_{HA}$ (8200 ± 1100 virions/cell) was comparable to previously reported $CSVY$ for MDCK suspension cell lines in the range between 7,000-10,000 virions/cell [44,53]. Even though higher virus titers have been reported already for MDCK cell lines [162,172], an influenza virus A titer of 3,6 lg(HAU) was the highest titer reached with batch or fed-batch experiments at the MPI. Due to their better cell specific growth rate, higher maximum cell concentration and single cell suspension, MDCK.Xe.E cells easily outperformed not only MDCK.S8.E cells, but also other MDCK suspension cell lines [50-53,55,172]. The only drawback was the production of high amounts of ammonium, which potentially can have a negative influence on virus replication, but which was not an issue for the conducted experiments described here [296-298].

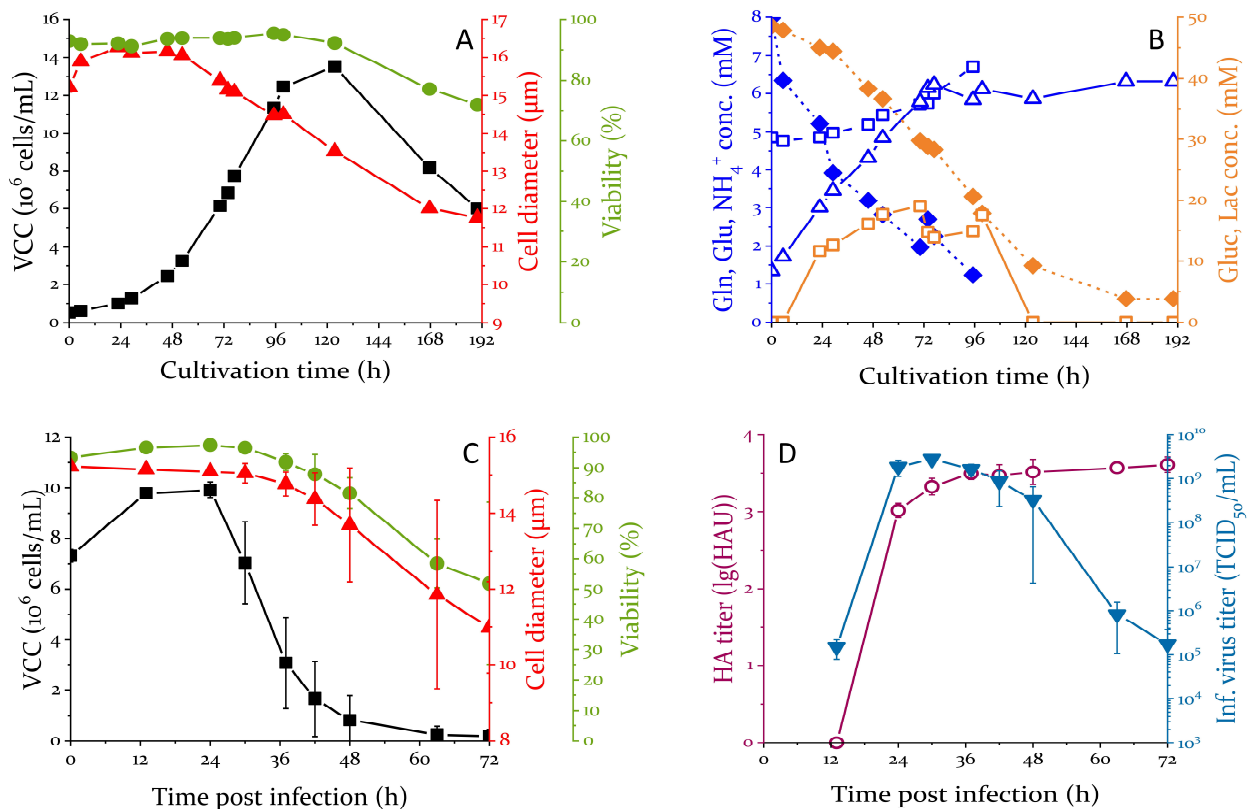


Figure 7: Cell growth and influenza A virus production of MDCK.Xe.E cells in Xeno-SFM.

MDCK cells were cultivated in shake flasks in Xeno-SFM medium (A&B). Cell growth (A) and extracellular metabolites (B) were monitored during batch cultivation. MDCK cells were cultivated for 72 h and infected with IAV (C&D). After infection, viable cell concentration (VCC), viability and cell diameter (C) as well as HA and TCID_{50} (D) were monitored. ■ viable cell concentration, ▲ average cell diameter, ● viability, ○ HA titer, ▼ infectious virus titer (TCID_{50}); ◆ glutamine (Gln), □ glutamate (Glu), ▲ ammonium (NH_4^+), ◆ glucose (Glc), □ lactate (Lac); Error bars: SD of three independent experiments.

4.1.3 Cultivation and infection of MDCK.Xe.E cells at high cell density

The very promising results obtained in batch infections encouraged us to investigate the potential of the MDCK.Xe.E cell line in Xeno-SFM for intensified processes. A semi-perfusion strategy was evaluated in shake flasks to achieve even higher cell concentrations ($> 15 \times 10^6$ cells/mL) and to investigate options regarding the establishment of bioreactor processes in perfusion mode. In particular, we wanted to verify whether IAV production with MDCK.Xe.E cells was possible at high cell densities without a reduction in CSVY (the so-called “high cell density effect”) [299]. In first attempts, the feeding strategy was optimized towards the extension of the exponential cell growth phase with high cell specific growth rates. In preliminary scouting experiments, a CSPR of 2.5 pL/(cell h) was determined to allow high cell densities with MDCK.Xe.E cells (data not shown). Applying this feeding strategy, it was possible to reach cell concentrations of 40×10^6 cells/mL in 7 days (0.5×10^6 cells/mL seeding cell concentration) (Figure 8 B). In order to reach these high cell concentrations, 4-5 times of the working volume (200-250 mL) of Xeno-SFM medium was needed over the whole perfusion process (Figure 8 A). By continued semi-perfusion, even higher cell concentrations were possible ($>60 \times 10^6$ cells/mL), but this was not followed up due to process instability (lower specific cell growth rate, viability) and handling issues. With higher cell concentrations, the time interval between perfusion steps decreased becoming limiting at a certain time ($\Delta t < 4$ h). Variations of medium temperature, pH and osmolality could have potentially created cell stress, thus, reducing cell growth and viability. For these reasons, a cell density of 40×10^6 cells/mL was considered optimal to investigate IAV infection in high cell density conditions. Accordingly, in another set of three experiments, MDCK.Xe.E cells were cultivated to 40×10^6 cells/mL and infected with IAV (APR_SFM) with a MOI of 10^{-3} (HCD₁) and 10^{-1} (HCD₂, HCD₃) (Figure 8). The higher MOI was chosen to limit cell growth post infection and to reduce the effect of perfusion (virus dilution) in the early infection phase. By using low MOI infection conditions (MOI 10^{-3}) (Figure 8 black circles), similar infection dynamics concerning HA and TCID₅₀ titer were observed as for HCD₂ and HCD₃ performed at a MOI of 10^{-1} . Using the lower MOI, cells continued to grow post infection to a maximum cell concentration of 60×10^6 cells/mL and started to die with the onset of virus accumulation (24 hpi). For higher MOI infections, virus release started earlier, but cells died rapidly after infection (< 12 hpi), which resulted in fast virus accumulation and lower maximum cell concentrations (Figure 8 B). All infections showed very high virus titers (> 4 lg(HAU)). Considering the multiple harvests performed in each perfusion step, the calculated accumulated titer exceeded 4.3 lg(HAU), reaching the maximum at 30 hpi (MOI 10^{-1}) and 48 hpi (MOI 10^{-3}), respectively. For the best performing experiment (HCD 2), a HA titer of 4.2 lg(HAU) was reached, which corresponded to an accumulated titer of almost 4.5 lg(HAU). For the

same cultivation, an accumulated infectious virus titer of 10^{10} TCID₅₀/mL was obtained. Regarding HA titers, these were the highest values reported for IAV production in animal cell culture. HA titers over 10,000 HAU (4 lg(HAU)) were neither achieved with other MDCK-based processes [44,51,162,172], nor with other cell lines in high cell density culture [159,300]. Only the combination of high cell density cultivation and high cell specific productivity of MDCK.Xe.E cells allowed the improvement of virus titers by this extent (Table 10). The two infection experiments performed at a MOI of 10^{-1} not only showed the highest virus titers but also a better overall performance compared to the low MOI infection. With this strategy, it was possible to improve CSVY_{HA} to over 10,000 virions/cell, compared to conventional batch experiments with only 8,000 virions/cell. Additionally, the volumetric productivity of these two experiments was similar to the batch experiment (Table 10), proving this approach was not only valuable for increasing virus titers but also commercially feasible with respect to medium consumption. The lower productivity and cell specific virus titer for the low MOI infection (10^{-3}) might be caused by feeding issues (medium limitations) at cell concentrations of 60×10^6 cells/mL as already described earlier.

Table 10: Comparison of influenza A virus production in batch and semi-perfusion culture.

	VCC _{max}	V _m	Max. virus titer		Acc. virus titer		CSVY _{HA}	STY
			HA	TCID ₅₀	HA	TCID ₅₀	HA based	HA based
	cells/mL	mL	lg(HAU)	TCID ₅₀ /mL	lg(HAU)	TCID ₅₀ /mL	vir./cell	vir./(L d)
Batch	9.3×10^6	75	3.60	2.2×10^9	3.60	2.2×10^9	8,200	1.6×10^{13}
HCD 1	58.7×10^6	487	4.08	4.2×10^9	4.33	6.0×10^9	7,300	4.9×10^{13}
HCD 2	45.6×10^6	448	4.19	7.5×10^9	4.49	9.4×10^9	13,600	7.6×10^{13}
HCD 3	41.5×10^6	373	4.16	4.2×10^9	4.35	4.3×10^9	10,800	5.6×10^{13}

HCD1-3 Cultivations of MDCK.Xe.E in high cell density; HCD1: MOI 10^{-3} , HCD2&3: MOI 10^{-1} (Figure 8); V_m: overall volume of used cultivation medium; CSVY_{HA}: cell specific virus yield (based on HA); STY.: space time yield (based on HA)

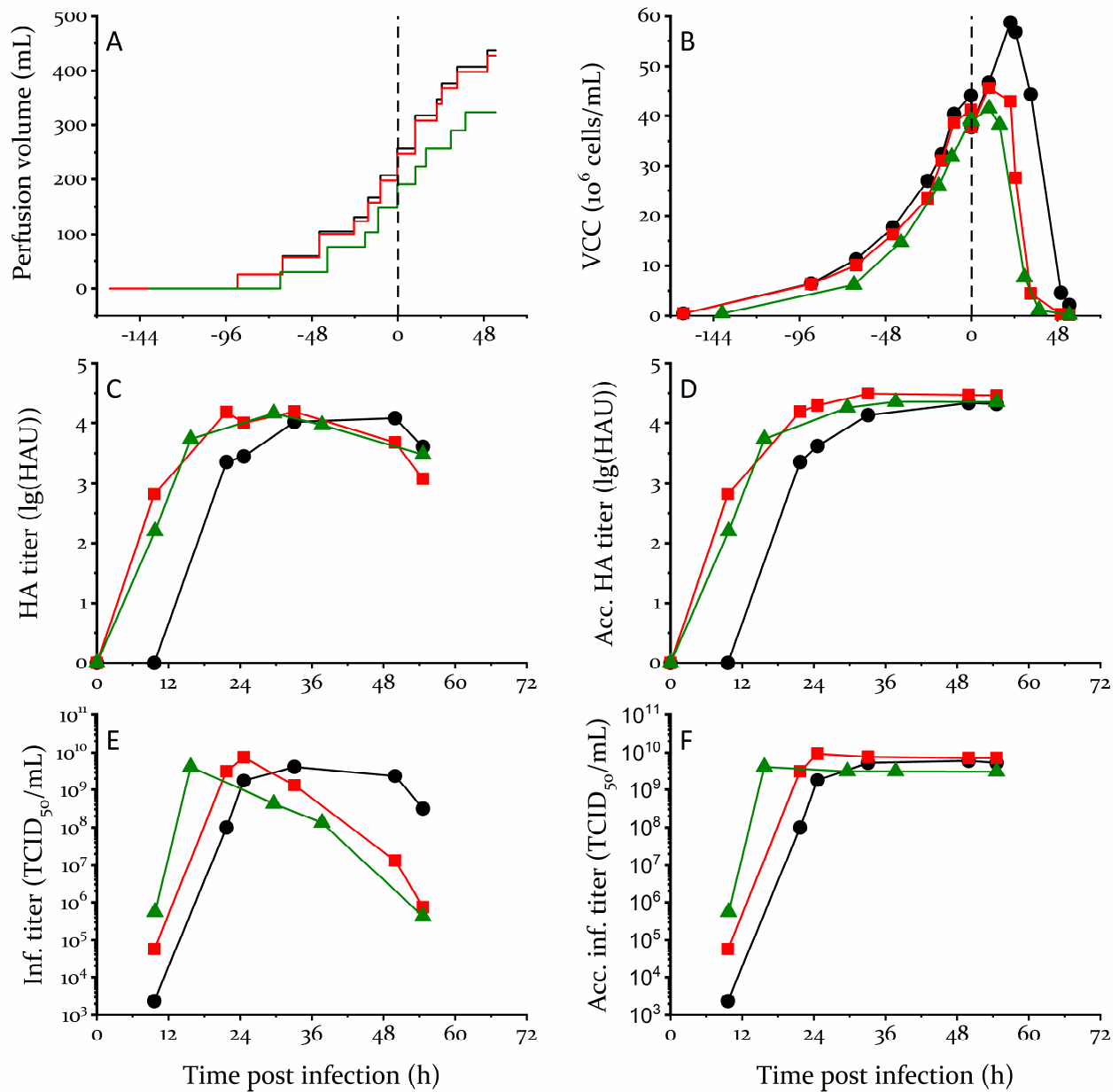


Figure 8 Influenza A virus production with MDCK.Xe.E cells in high cell density culture.

MDCK.Xe.E cells were cultivated in semi-perfusion shake flask experiments to 40×10^6 cells/mL and evaluated for the production of IAV. Accumulated virus titers were determined from total virus titers produced in perfusion steps based on the fixed working volume (50 mL). **A:** total volume of Xeno-SFM medium used for perfusion; **B:** viable cell concentration (VCC); **C:** virus titer (HA) in cell suspension; **D:** accumulated virus titer of multiple harvests (HA); **E:** infectious virus titer (TCID₅₀) in cell suspension; **F:** accumulated infectious virus titer of multiple harvests (TCID₅₀) ● HCD1 (MOI 10^{-3}), ■ HCD2 and ▲ HCD3 (MOI 10^{-1}).

4.1.4 Summary: MDCK.Xe.E cells for influenza A virus production

Overall, the observations in this section demonstrate the impact of advanced cultivation media on process development and intensification with MDCK suspension cell lines. Massive changes of cell line performance were possible without the need of any genetic manipulation of the host cell line. Unfortunately, the medium component(s) responsible for adapting this specific MDCK.Xe.E phenotype remain unclear, since medium composition was not disclosed and detailed studies regarding uptake and release of all medium components and metabolic by-products were not possible. Traditionally, the optimization of MDCK-based influenza vaccine manufacturing has often focused on genetic modifications of the MDCK cell line or improved cultivation technologies to increase productivity [48,162,301-304]. Only limited research was dedicated to medium development. Nevertheless, Huang et. al., introduced this new cell culture medium for the cultivation of MDCK suspension cells, which enabled us to achieve high virus titer (3.6 lg(HAU)) and improve productivity significantly. The newly established cell line (MDCK.Xe.E) grew faster and to higher cell concentration than other MDCK suspension cells [50-53,55,172] and showed various changes of central metabolism as well as of cell morphology compared to the original cell line (MDCK.S8.E). For process intensification, semi-perfusion enabled for the first time the cultivation of MDCK cells at a very high cell concentration. Here, we were able to show cell concentrations up to 60×10^6 cells/mL, producing an IAV titer of up 4.2 lg(HAU). Both cell concentration (for MDCK.Xe.E) and IAV titer are the highest reported for conventional MDCK cultivations [44,159,172] and intensified processes [159,162,300]. A short process time in semi-perfusion (< 8 days) led to a process with similar volumetric productivity compared to batch culture, despite high medium consumption (5-7 \times volume of batch cultivations). The productivity based on the working volume (space time yield) was up to five times higher in the high cell density cultivation. Further optimization of perfusion strategy or medium composition could allow an even more efficient utilization of perfusion medium and a further increase in process productivity for both cells and viruses [159,300,305-307]. In particular, with use of capacitance sensors for on-line measurement of cell concentrations and feeding control the implementation of highly productive continuous perfusion cultures should be feasible. With the achieved virus yields very competitive cell culture-based influenza vaccine manufacturing processes can be implemented to overcome limitations of egg-based production systems and contribute significantly to reduce time for pandemic preparedness in case of an influenza epidemic.

4.2 Comparison of MDCK cell lines for influenza A virus production

After the good performance of the newly developed MDCK.Xe.E cell line in Xeno-SFM medium, we were wondering how the original cell line from ECUST with an ATCC background would compare to the cell line generated at the MPI. In order to do that the MDCK suspension cell line from ECUST (MDCK.Xe.A) was transferred to the MPI through an extended research stay of an ECUST PhD student (Yixiao Wu) to Magdeburg. Furthermore, a chemically defined version of the Xeno medium (Xeno-CDM) was developed and used as a replacement for the Xeno-SFM medium. The transfer from Xeno-SFM to Xeno-CDM was performed for both cell lines by changing the medium in four passages (25, 50, 75, 100 %) without major alteration of cell growth or morphology. MDCK cells transferred from Xeno-SFM to Xeno-CDM were not considered a new cell line and the same names are used in this work. For a true comparison of the cell lines and cultivation media however, the adaptation of the newly obtained MDCK.Xe.A cell line to the Smif8 medium was needed.

4.2.1 Adaptation of MDCK.Xe.A to Smif8 medium

With the previous experience using MDCK.Xe.E cells and preliminary studies with the MDCK.Xe.A cell line in Xeno-CDM a further improvement of cell growth or IAV productivity by adapting the MDCK.A cells to the Smif8 medium was not expected. However, to evaluate the impact of the media on metabolism, growth and virus production capacity of the respective cell lines, it was necessary to develop the MDCK.S8.A cell line. According to the generation of the MDCK.Xe.E cell line, adaptation was performed by exchanging small fractions of the medium (10 %) per passage until the cells were growing in pure Smif8 medium. Similar to the previous adaptation, this transformation process required a lot of time (>4 months), thus being separated in similar phases: primary adaptation, intermediate adaptation, and an extended third adaptation period in pure smif8 medium. In some phases of adaptation, cellular viability was dropping slightly, but recovered in the following passages. Interestingly, the adaptation of MDCK.S8.A cells also showed an adaptation period with very low growth rate at around 50 days of adaptation. During this time, MDCK cells were already “growing” in pure Smif8 medium (Figure 9). The morphological changes between the two media were not as significant as for the MDCK.E cells, despite the generation of some smaller and some bigger cell aggregates in Smif8 medium. Cell aggregates were smaller and appeared less dense as for MDCK.S8.E cells (Figure 9 B). However, cells in Smif8 medium attached to the inner material of the shake flask, forming a cell rim at the medium–air interface. Therefore, the shake flask had to be periodically replaced in order to limit negative effects of dead or lysing cells on the whole cell population. As the MDCK.S8.E cells, fully adapted MDCK.S8.A cells had to be trypsinized in order to determine the cell concentration with a cell counter. Cell growth improved slightly in

the third adaptation period (80-140 d), but growth rate was quite unsteady between passages and doubling time stayed over 24 h (Figure 9 A). In the following experiments the MDCK.S8.A cell line was used as a reference to differentiate between cell line and medium effects.

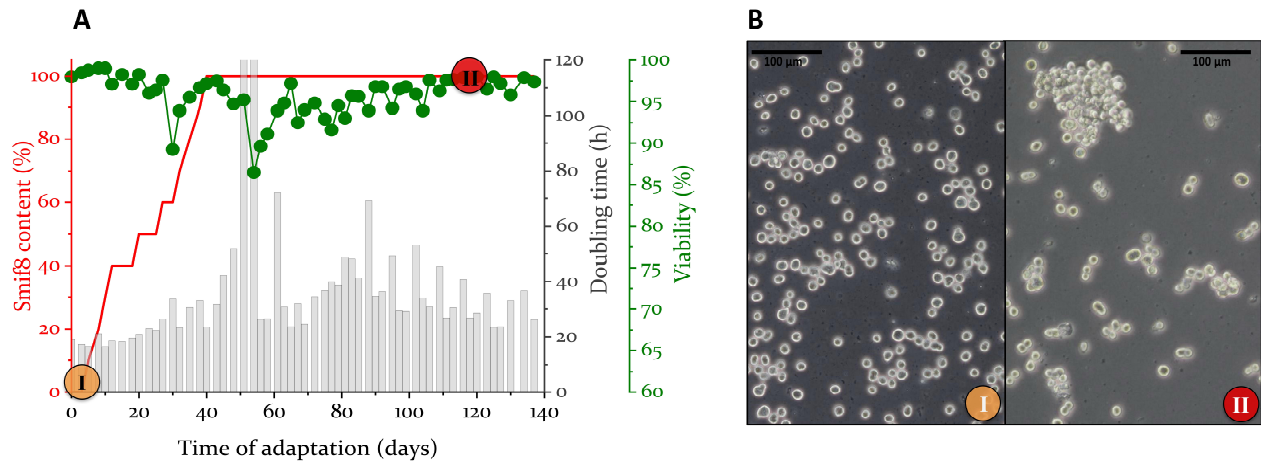


Figure 9: Adaptation of MDCK.Xe.A cells to Smif8 medium.

MDCK.Xe.A cell adaptation to Smif8 medium over multiple passages to generate the new MDCK.S8.A cell line. A: average doubling time (grey bars) and cell viability (●) were analyzed over the adaptation time with increasing Smif8 medium content (-). B: Phase contrast microscopy pictures of MDCK.A suspension cells for morphological evaluation in different medium (I: Xeno-CDM; II: Smif8).

4.2.2 Cell growth and metabolism

To compare the different MDCK suspension cells in the two different cultivation media (Smif8 & Xeno-CDM), the four fully adapted cell lines (MDCK.Xe.A, MDCK.Xe.E, MDCK.S8.A and MDCK.S8.E) were each cultivated in three parallel shake flasks and infected with the respective adapted APR8 seed virus. Cultivation, and infection conditions were chosen to mimic an IAV production process divided in a cell growth phase (72 h), followed by a feeding (dilution) step to start the virus infection phase. To allow for an exponential cell growth phase, all cells were inoculated with the same cell concentration (0.8×10^6 cells/mL).

Cell growth for the two cell lines in Xeno-CDM medium was significant higher, leading to higher cell concentrations, compared to the cells cultivated in Smif8 medium. Between the two cell lines in the same cultivation medium, only minor differences in the overall growth profile were observed (Figure 10 D). Both cell lines grew to similar cell concentrations in Smif8 ($5-6 \times 10^6$ cells/mL) and Xeno-CDM ($8-9 \times 10^6$ cells/mL) medium, respectively (Figure 10 A). MDCK cells in Xeno-CDM medium were consistently larger, reaching cell diameters of 14-15 µm in comparison to slightly

smaller MDCK cells (12.5–13.5 μm) in Smif8 medium (Figure 10 C). But size differences between the media could be due to cell aggregates, trypsinization for Smif8 cells or differences of medium properties. Most likely, the differences were caused by a different medium osmolality (Smif8: 320 mOsm/kg, Xeno: 290 mOsm/kg), as already described for other cell lines [308]. Bigger cells are usually associated with higher cell specific productivities due to overall higher cell volume compared to smaller cells with the same cell concentration [309,310]. In our study, MDCK in Xeno-CDM medium combined both advantages of higher cell concentration and bigger cells generating roughly double the cell volume compared to the MDCK cells in Smif8. MDCK cells in Xeno-CDM grew with a similar growth rate as described earlier, but lower maximal cell concentrations were reached (i.e. 10×10^6 cells/mL for MDCK.Xe.E). As for the Xeno-SFM medium, higher growth rates and VCC were fueled by the richer Xeno-CDM medium, containing much more glucose (40 vs 20 mM) and glutamine (8 vs 4 mM), respectively. Additionally, higher metabolite concentrations were generally linked to higher substrate consumption and to an accumulation of more by-products (Figure 11). However, for lactate this general trend was only true for the initial cultivation period. MDCK cells in Xeno-CDM medium had a decreased production of lactate in the second half of growth phase, where only minor amounts of lactate were secreted. This led to lower lactate levels at time of infections, despite double the initial glucose concentration and double the biomass (Figure 11 C). When comparing the specific metabolic rates determined over the whole cell growth phase, we confirmed higher metabolic activity of MDCK cells in Xeno-CDM medium. Specifically, higher consumption rates of glucose and glutamine, as well as higher production rates of ammonium were measured for MDCK cells in Xeno-CDM medium but lower specific production rates for lactate. Additionally, significant differences between the metabolic rates of the cell lines in the same cultivation media were observed for all metabolites (Figure 12). However, no clear metabolic pattern was observed. Cells of the ATCC origin showed higher glucose consumption and lactate production rates, indicating higher glycolysis activity. Despite different metabolic rates of glucose and lactate, their conversion ratio was the same for the cell lines in the same media, but much higher for the MDCK cells cultivated in Smif8 medium (Figure 12 C). Xeno-CDM medium was able to support a metabolic switch between lactate production to consumption, or at least reduced lactate production. Lactate consumption is generally considered a beneficial phenotype for manufacturing and would be an advantage for potential intensified fed-batch processes [249,311]. MDCK cells in Smif8 did not show any indication of reduced lactate production. Metabolic rates were especially high for the MDCK.S8.A cells, consuming more substrate and producing more by-product than the MDCK.S8.E cell line. The conversion rate from glutamine to ammonium was significantly higher than all the other cell lines. For MDCK cells cultivated in Xeno-CDM medium, MDCK.Xe.A cells had a pronounced glucose and a reduced glutamine consumption compared to

the MDCK.Xe.E cells. Differences in these metabolic rates indicated slight alterations in the central carbon metabolism, where MDCK.Xe.A rely more on glycolysis and MDCK.Xe.E more on glutaminolysis to fuel cell growth. Additionally, the conversion ratio from glutamine to ammonium was slightly lower for MDCK.Xe.A cells, leading to lower ammonium accumulation despite higher cell concentrations.

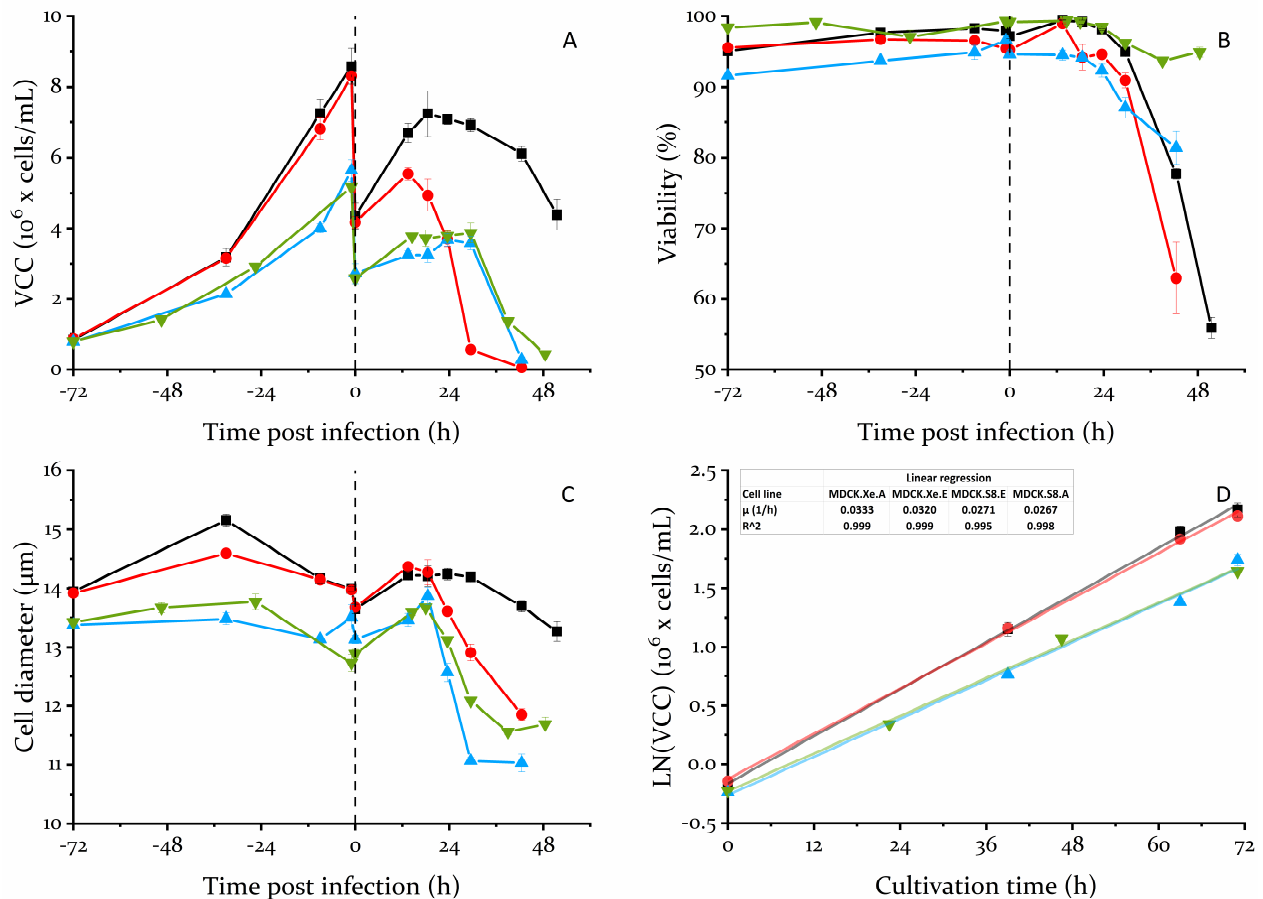


Figure 10: Growth and cell properties of MDCK cell lines in different cultivation media.

Viable cell concentration (A), cell viability (B) and average cell diameter (C) of four MDCK suspension cell lines cultivated in shake flasks for 72 h, diluted and infected with APR8 virus at an MOI of 10^{-3} . The logarithm of the viable cell concentration was plotted against the cultivation time of the exponential cell growth phase to determine the specific growth rate with a linear fit (D). ■ MDCK.Xe.A, ● MDCK.Xe.E, ▲ MDCK.S8.E, ▼ MDCK.S8.A. Dashed vertical line indicates time point of infection. Error bars represent standard deviation between three parallel cultivations in shake flasks.

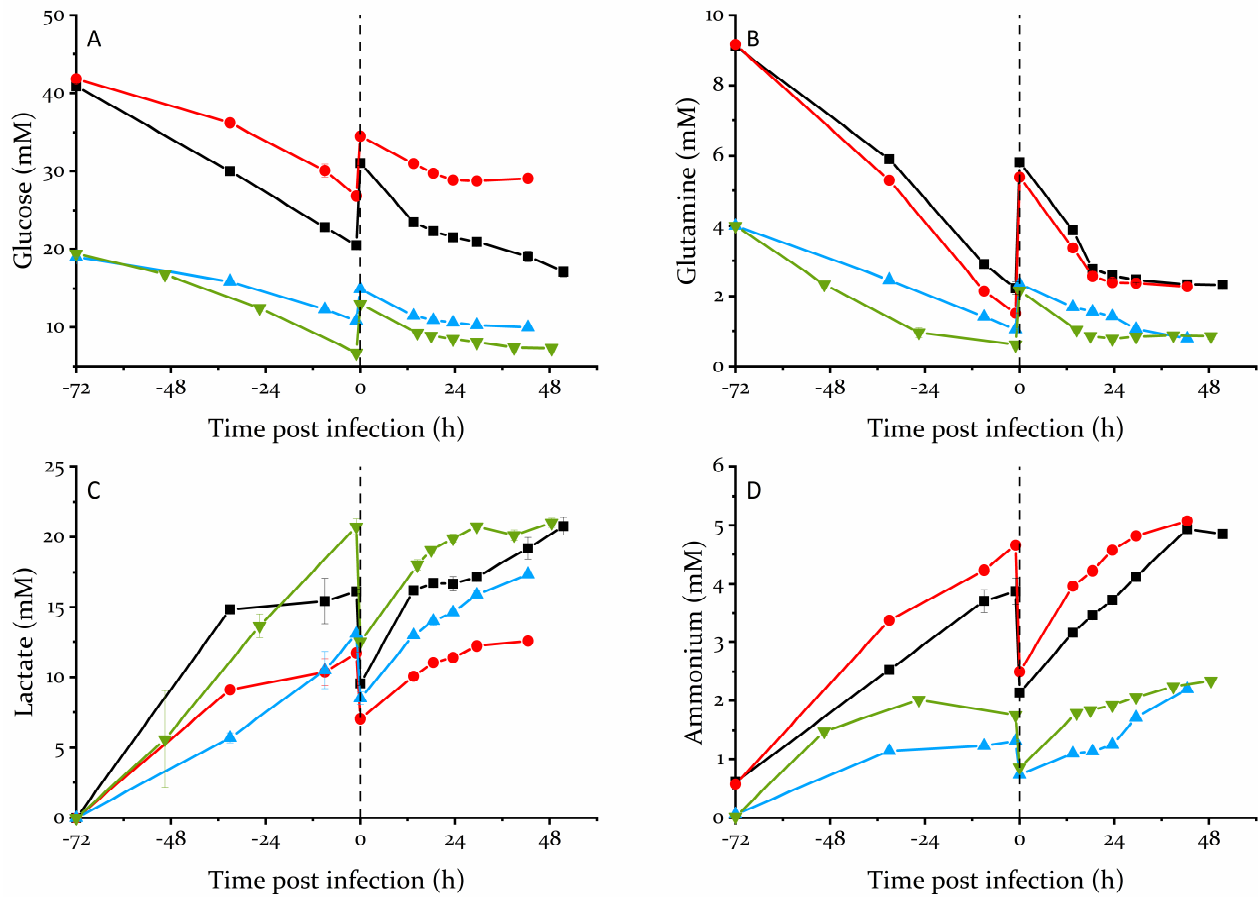


Figure 11: Main extracellular metabolites of MDCK cell lines in different cultivation media.

Concentration of main extracellular metabolites glucose (A), glutamine (B) lactate (C) and ammonium (D) in the cultivation media of four MDCK suspension cell lines cultivated in shake flasks for 72 h, diluted by half with fresh medium and infected with APR8 virus at an MOI of 10^{-3} . ■ MDCK.Xe.A, ● MDCK.Xe.E, ▲ MDCK.S8.E, ▼ MDCK.S8.A. Dashed vertical line indicates time point of infection. Error bars represent standard deviation between three parallel cultivations in shake flasks.

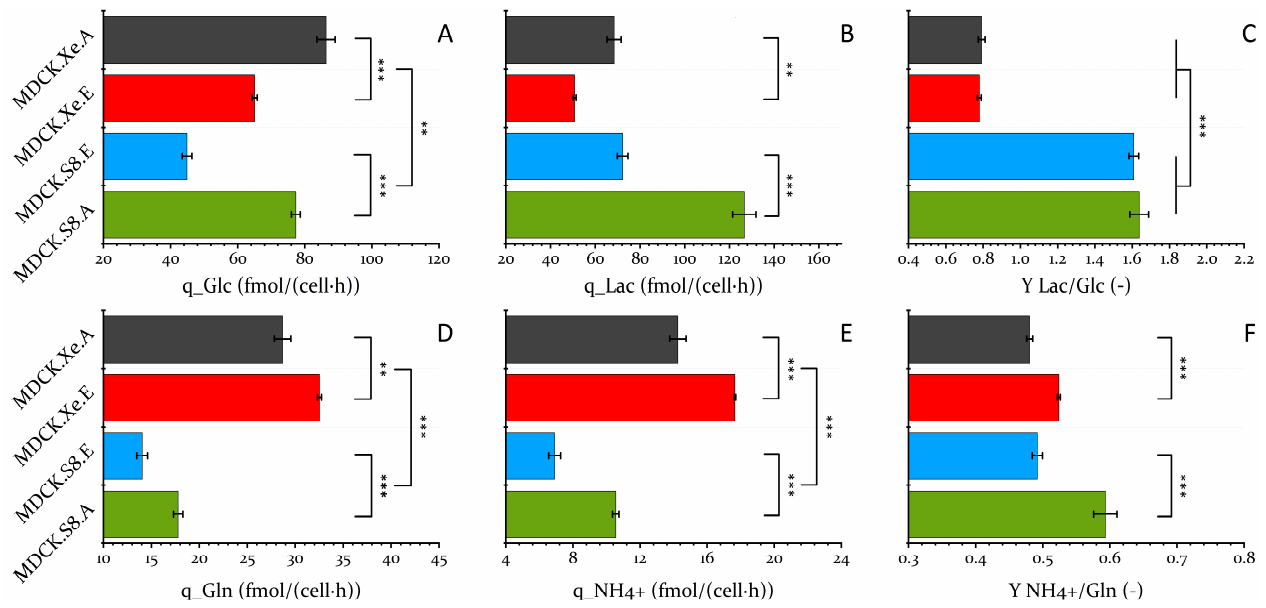


Figure 12: Metabolic rates and conversion ratios of main metabolites for different MDCK cell lines. Cell specific glucose (A) and glutamine (D) consumption rates as well as lactate (B) and ammonium (E) production rates, determined for the whole cell growth phase (-72-00 hpi) assuming exponential cell growth. For the same period metabolic conversion ratios of lactate to glucose (C) and ammonium to glutamine (F) were calculated. Error bars represent standard deviation between three parallel cultivations in shake flasks. * p < 0.05; ** p < 0.01; *** p < 0.001

4.2.3 Infection and influenza A virus production using different MDCK cell lines

As a higher cell amount generally generates a higher amount of virus particles, influenza virus titer was linked to cell concentration to a certain extent. However, the generated amount per cell (CSVY) was not constant between cell lines. To evaluate cellular productivity of total and infectious virus particles, MDCK cells were diluted and infected with APR8 influenza virus. After a short cell growth phase post infection (~24 h), where cell concentrations increased and virus infections spread over the respective cell population, cellular effects of virus infection were detected for all cell lines. Generally, viability, cell concentration and cell diameter dropped depending of the individual virus dynamic (Figure 10 A–C). MDCK.Xe.E cells showed the earliest signs of virus infection with a fast drop of cell concentration already 18 hpi, whereas MDCK.Xe.A proved to be more resilient to the infection. MDCK.Xe.A cells were able to grow up to 7×10^6 cells/mL and viability and cell diameter remained more stable, as well. For all cell lines, no major changes for the overall extracellular metabolic profile were observed for the infection phase compared to the growth phase (Figure 11). Due to different infection dynamics and differences in cell death, a detailed comparison of the cellular metabolism in this state was not considered. After the infection, influenza virus accumulated in the supernatant quite fast: a significant increase in virus titer was measured as early as 12 hpi. For the total number of virus particles (HA titer), it seemed that virus replication in Smif8 medium was slightly faster than in the Xeno-CDM medium, but higher maximal virus titer were reached in the later phase of infection (24–36 hpi) (Figure 13 A). The highest total virus titer was achieved with the MDCK.Xe.A cell line (HA > 3.6 lg(HAU)). This titer was similar to the previously obtained titer for the MDCK.Xe.E cells in the serum-free medium. However, in this experiment, the MDCK.Xe.E cells showed a significant lower titer (3.4 lg(HAU)) compared to MDCK.Xe.A cells (Figure 13 A). Most likely, this was due to different cell concentrations between the experiments (dilution vs medium exchange) and the richer Xeno-SFM medium. Interestingly, the CSVY_{HA} of the MDCK.Xe.E cells was quite similar to the previous experiment as well as the MDCK.S8.E cells. Both cells of the ATCC origin showed significant higher CSVY_{HA} under the chosen infection condition, though. Furthermore, MDCK.Xe.A cells had the highest CSVY_{HA} (12,400 virions/cell) of all the four cell lines (Figure 13 C). As for the HA-titer, infectious virus titer was increasing slightly faster for the MDCK cells in Smif8 medium, but the final titer was very similar ($\sim 10^9$ TCID₅₀/mL) for the cell lines, with exception of the MDCK.Xe.E cells. The maximal infectious titer for this cell was lower than for the other cell lines and declined rapidly after reaching a maximum slightly above 10^8 TCID₅₀/mL (Figure 13 B). This rapid decrease was already observed for the MDCK.Xe.E cells in Xeno-SFM medium. However, it was surprising in this experiment, since the infectious titer of the other cell lines was rather stable. Evidence suggests that this strong inactivation of influenza virus particles in

this situation also reduced the maximal infectious virus titer and was the reason for a significantly reduced CSVY_{TCID} for the infectious virus particles, as well (Figure 13 D). There was no explanation for the origin of this effect since neither the medium nor the cell line were linked to the fast reduction of infective virus particles directly. It might be that low pH during the cultivation or high ammonium concentration could have led to virus inactivation, but no further investigations were performed in this regard.

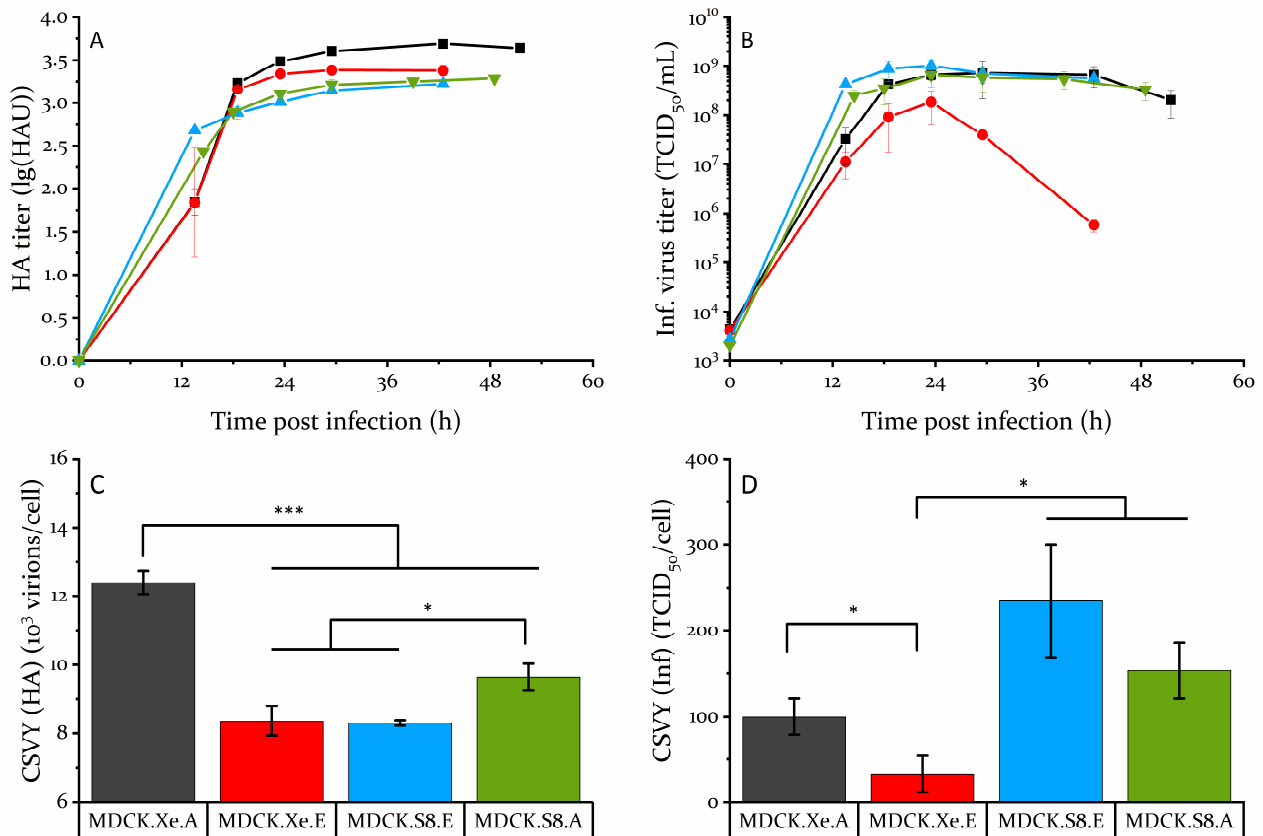


Figure 13: Influenza A virus production in different MDCK suspension cell lines

Time course of total IAV particles (A) and infectious IAV particles (B) of the four MDK suspension cell lines after infection with the respective adapted APR8 virus (MOI 10⁻³). Cell specific virus yield (CSVY) based on the HA-titer (C) and TCID₅₀ titer (D), calculate from the maximal virus titer and cell concentration, post infection. Error bars represent standard deviation between three independent infectious in shake flasks.

■ MDCK.Xe.A, ● MDCK.Xe.E, ▲ MDCK.S8.E, ▼ MDCK.S8.A. * p < 0.05; ** p < 0.01; *** p < 0.001.

4.2.4 The optimal cell line for influenza A virus production

The newly generated MDCK.S8.A cell line had major disadvantages in contrast to all the other cell lines. Even though smaller cell clumps were observed than for MDCK.S8.E cells, MDCK.S8.A attached to the plastic material of the cultivation system, resulting in problems to accurately determine the biomass. Additionally, cells grew rather unstable and produced high amounts of metabolic side products (i.e. lactate & ammonium). Further adaptation might have improved cellular performance and the metabolic efficiency, however no further time was invested since no significant improvements were expected after already spending such a long time for adaptation. By separating growth and infection phase by a feeding point for infection, we were able to analyze growth performance and virus productivity separately.

As for the previous study, the Xeno-CDM medium supported high specific growth rates and high cell concentrations, much higher than both cell lines in Smif8 medium (Table 11). Furthermore, growth rate and maximal viable cell concentration reached using the Xeno-CDM medium were the highest reported for MDCK cells in chemically defined medium in batch mode [44,53,55,312]. Additionally, the Xeno-CDM medium allowed a reduced lactate production, despite higher glucose consumption. Lactate consumption might be possible as well, in a later stage of the growth phase, as already shown for the Xeno-SFM medium and other cell lines [238,311,313,314]. High amount of extracellular ammonium generated in Xeno-CDM medium during cell growth and infection is considered a disadvantage for influenza production [296,298]. Despite this disadvantage, higher virus titers were obtained in Xeno-CDM medium, due to higher VCC. Furthermore high lactate concentration during the virus infection phase can reduce the pH of the cultivation medium, which might inactivate influenza virus particles [315]. Interestingly, the MDCK.Xe.A cells showed not only the highest cell concentration, but also the highest CSVY_{HA} exceeding 12,000 virions per cell. In our research group, such a high cell specific virus productivity was previously only obtained using adherent MDCK cells and exceeds the CSVY_{HA} of all other suspension cell lines described so far [46,49,157,160,161,312,316,317]. The combination of high VCC and CSVY_{HA} led to a very competitive virus titer of more than 3.6 lg(HAU), which is among the highest, obtained in extended batch infection experiments [44,161,172,304]. Other potential cell lines for influenza virus propagation lack a competitive growth in suspension (i.e. Vero cells), have a low cell specific productivity (i.e. AGE1.CR.pIX, HEK-293 & CAP), are biosafety level 2 (i.e. PBG.PK2.1), or their performance is only reported by industry (i.e. EB66, Per.C6) [11,42,161,316,318]. Overall, the MDCK.Xe.A cells is not only superior to the analyzed MDCK cell lines with respect to virus production, but also has the highest growth rate as single cell suspension, highest cell concentration, very high viability and superior metabolic properties of all the tested MDCK suspension cells (Table 11). Furthermore, the

MDCK.Xe.A cell line might be even superior to all other cell lines described for IAV propagation, which makes this cell line the ideal candidate for a cell culture based influenza vaccine platform.

Table 11 Cellular growth performance and influenza virus productivity for MDCK cell lines.

Cell line	Morphology	VCC _{max} [10 ⁶ c/mL]	t _D [h]	Viab. [%]	HA-titer [lg(HAU)]	CSVY _{HA} [vir/cell]
MDCK.Xe.A	Single cells	12	21.1±0.4	98±0.3	3.64±0.05	12,400
MDCK.Xe.E	Single cells	8-9	22.0±0.2	96±0.6	3.37±0.05	8,400
MDCK.S8.E	Big clumps	6-8	25.6±0.3	95±1.5	3.12±0.05	8,300
MDCK.S8.A	Small clumps	4-6	26.4±0.7	99±1.1	3.25±0.05	9,600

VCC_{max}: maximal viable cell concentration; t_D: cellular doubling time; viab: viability; CSVY_{HA}: cell specific virus yield; ±: standard deviation

4.3 Influenza A virus production in laboratory scale bioreactors

The transition from shake flasks to scalable stirred tank bioreactors is not always straight forward. In some cases, shear stress, pH control strategy or set point have significant impact on cellular growth performance or specific productivity. For MDCK suspension cells, the transfer to STR systems was a major issue, and low specific growth rates were reported using the previously applied MDCK.S8.E cell line [53]. Huang et al. demonstrated high virus titer and high cellular growth rate of their ATCC-based MDCK suspension cell line adapted to an early version of the Xeno-SFM media in stirred tank systems ($\mu \approx 0.03 \text{ h}^{-1}$) [172]. However, maximal cell concentration was limited to about 6×10^6 cells/mL. To evaluate the potential of the MDCK.Xe.A cell line cultivated in the new Xeno-CDM medium, we aimed to design a full vaccine manufacturing process in small-scale scalable STR systems. The DASGIP parallel bioreactor system available in the MPI laboratories, was the ideal platform to demonstrate performance and reproducibility of such an influenza virus production process. Here, we specifically focused on the growth and metabolism of the MDCK suspension cell lines as well as the virus production in a controlled system. Additionally, this process evaluation included virus purification and analysis of product quality. These results are further discussed elsewhere by Marichal-Gallardo[319] and Bissinger et al. (in preparation).

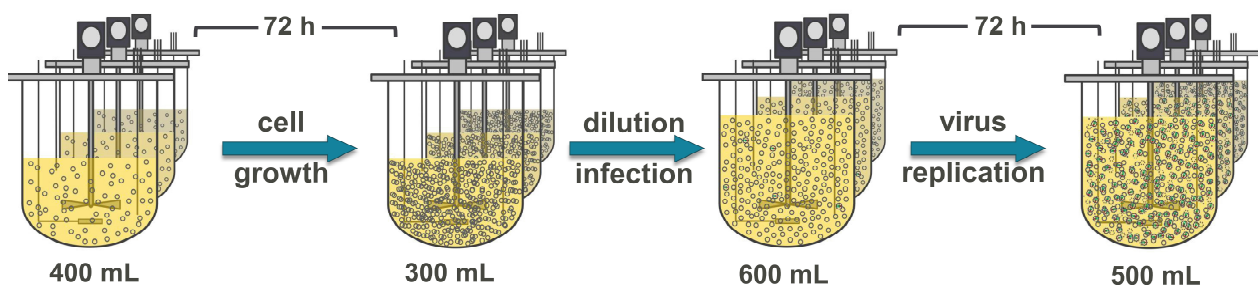


Figure 14: Schematic overview of evaluated production process for influenza A virus.

Three parallel lab scale bioreactors were inoculated from independent MDCK.Xe.A precultures at a working volume of 400 mL. Cell growth and metabolism were monitored for a cell growth phase of 72 h. For virus infection, cell suspension was diluted by half with fresh Xeno-CDM medium. Virus replication and cellular response was monitored for another 72 hpi. Reduction of the working volume during cell growth and infection phase was due to frequent sampling for extensive analytics.

4.3.1 Optimization of stirred tank bioreactor cultivations

In preliminary studies, cultivation conditions were evaluated for cell growth in STR cultivations. Different agitation speeds from 80 rpm to 140 rpm were tested for MDCK.Xe.A cultivation in DASGIP bioreactors. By comparing the respective cell growth and maximal cell concentration with different conditions, the optimal stirring speed was determined. The scale up of the MDCK.Xe.A cells from shake flasks to a STR system was unproblematic and cells grew satisfactorily without any negative impact on viability. Overall, only minor differences between cell growth of the cultivations was observed. With 80 rpm stirring speed cells grew faster and to slightly higher cell concentration than with the higher stirring speed in the three other STRs (Figure 15). Compared to shake flask cultivations, a longer lag phase was observed in the STR system, with a similar cell concentration of $11\text{-}12 \times 10^6$ cells/mL at 96 h of cultivation (Figure 15 A). No major differences for cell viability and average cell diameter were detected between bioreactor and shake flask cultivations (Figure 15 B-C). The set-points for pH (7.0) and DO (40 %) were chosen by recommendation of the medium developer. Thanks to the good growth performance in the bioreactor, there was no need for further optimization of other process conditions. For the virus infection phase, a higher pH set-point of 7.2 was used to protect influenza virus particles from inactivation at lower pH values (< 6.8). Over the whole cultivation time, pH was controlled solely by CO₂ sparging. Only in later cell death phase, when medium was depleted or influenza virus infection resulted in cell lysis, base addition was needed to keep pH stable. For IAV infection similar infection strategies were used as described earlier, to evaluate an easy and scalable process for large scale manufacturing [44].

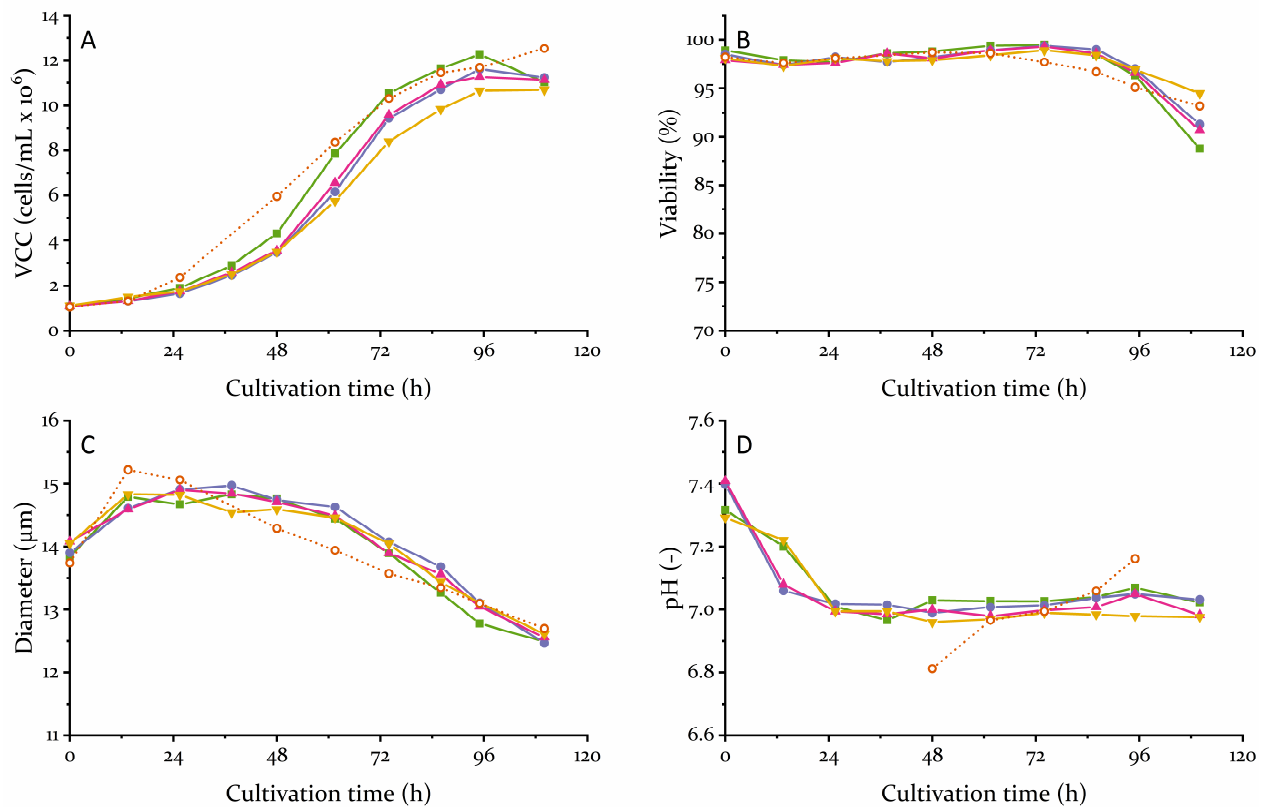


Figure 15: Optimization of stirred tank cultivation conditions for MDCK.Xe.A cells.

MDCK.Xe.A cells in Xeno-CDM medium were cultivated in bioreactors with different stirring speeds and a shake control. Viable cell concentration (A), cell viability (B), average cell diameter (C) and pH (D) were monitored of the cultivation time. 80 rpm (■), 100 rpm (●), 120 rpm (▲), 140 rpm (▼), shake flask (○).

4.3.2 MDCK.Xe.A cells in stirred tank system: growth and metabolism

MDCK.Xe.A cells were cultivated in three parallel stirred tank bioreactors to evaluate the cell growth and metabolism in a cell growth phase and an infection phase (Figure 14). In the first phase of the production process (cell growth phase), MDCK cells were grown in batch mode to amplify cellular biomass. With the used cultivation conditions, excellent growth of our MDCK.Xe.A cell line was observed. After an initial lag phase (8 h), MDCK cells were growing exponentially to almost 10×10^6 cells/mL (Figure 16 A). Due to variations in cell size, initially after inoculation and in the last 24 h of cell growth phase, the viable cell volume per cultivation volume was calculated additionally (Figure 16 B). With the VCV, effects of osmolality on cell size after inoculation and during cell growth could be considered, giving a more homogeneous growth curve and less variations between the replicates. When VCC and VCV were fitted to an exponential growth function, it was clear that for the overall cell volume unrestricted exponential growth was true for at least 64 h (Figure 16 B) and was able to cover the initial “lag phase” as well. The growth rate based on cell volume was insignificantly lower ($\mu=0.031 \text{ h}^{-1}$) compared to the growth rate based on cell concentration ($\mu=0.033 \text{ h}^{-1}$) calculated

without the initial lag phase (0.8–7.2 h). Over the whole cell growth phase, cell viability was consistently high (>97 %) and even increased slightly in the later part of the growth phase to over 98 % (Figure 16 C). To achieve productive and stable manufacturing of cell culture-based vaccines, high specific growth rate, high viability and high cell concentration are fundamental. The lack of any of these aspects reduces the productivity, scalability and costs of a large-scale manufacturing process. With the used cultivation system, we were able to control the cultivation environment to minimize process variability as little as possible (Figure 17). Scale-up was a major issue for previous reported MDCK suspension cells [51–53,55]. The possible use a MDCK cell line growing in chemically defined medium to over 10×10^6 cells/mL with a doubling time of 21 h and stable viability over 97 % in STR systems represents a big step towards a more competitive process. Additionally, growth performance of MDCK cells cultivated in Xeno-CDM medium seems to be very reproducible and resilient (Figure 15 & Figure 16), which eases scale up and reduces batch to batch variations in manufacturing.

Neither of the main substrates (Figure 18 A–B) nor most of the amino acids (Figure 20 Figure 21) showed any obvious limitation. Only the amino acids leucine, isoleucine and methionine were below the limit of quantification at the end of the growth phase (Figure 20 D–F). Accumulation of the by-products lactate and ammonium (Figure 18 C&D) were expected, and concentrations were in a reasonable range, where effects on metabolism or cell growth could be possible but were not observed [249,320,321]. Additional to lactate and ammonium, the amino acids glutamate, alanine and to a lesser extent aspartate were secreted (Figure 20 A–C). This was most likely due to the side products formation of cellular transamination reaction of glutamine [320,322]. Whereas glucose was available in excess over the whole process leading to high lactate accumulation, glutamine and other amino acids were almost depleted in the end of the cultivation phase and were restored partly by fresh medium feed at time point of infection. Despite lactate accumulation (max.: 42 mM), there was no or minor impact on medium osmolality (Figure 17). Consumption rates of glucose increased in the initial phase of cultivation significantly until the glucose concentration was falling below 30 mM, followed by a strong decrease in specific glucose consumption until the end of the growth phase. Similarly, glutamine consumption increased slightly, then stayed stable and decreased 24 h post inoculation for the whole growth phase (Figure 19 A–B). Overall, specific consumption rate of glutamine stayed rather stable in comparison to glucose consumption, which changed almost with a factor of two during the growth phase. The production rate of the main by-products (lactate & ammonium) was decreasing massively directly from inoculation to the end of the growth phase. This resulted in a reduction of the conversion ratio of Lac/Gluc and NH_4^+ /gln over the cultivation

(Figure 19 C–D). Cell metabolism seemed to respond to reduced substrate and increased by-product concentration and switched to a more “efficient” metabolism.

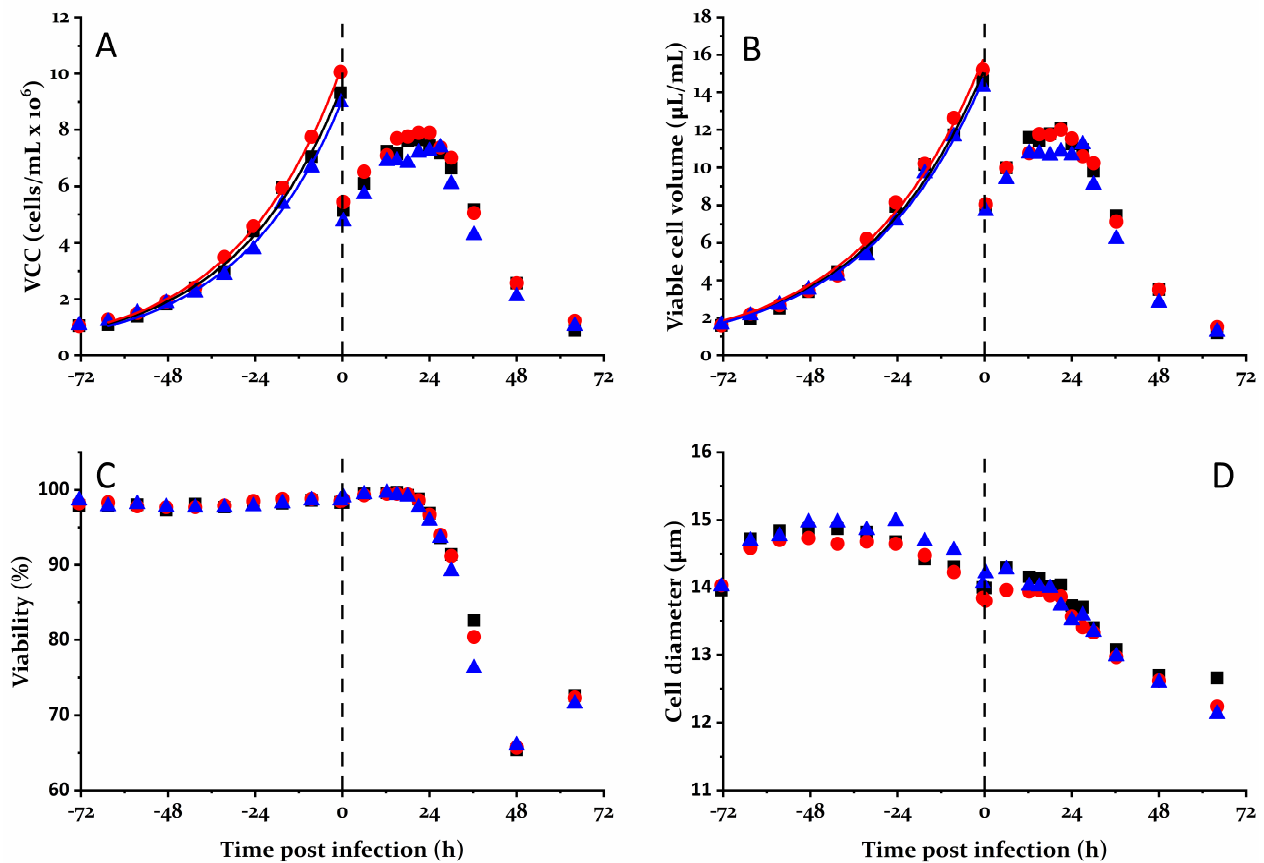


Figure 16: Cell count and properties of MDCK.Xe.A cells in three parallel stirred tank bioreactors. Viable cell concentration (A), viable cell volume (B), cell viability (C) and average cell diameter (D) were monitored over the whole process time (144 h). Cellular biomass was fitted to an exponential growth function (curves) to determine the specific growth rate based on cell concentration and cell volume. Vertical lines indicate time of infection. All three bioreactors were run in parallel and inoculated from three separated precultures. STR1 (■), STR2 (●), STR3 (▲)

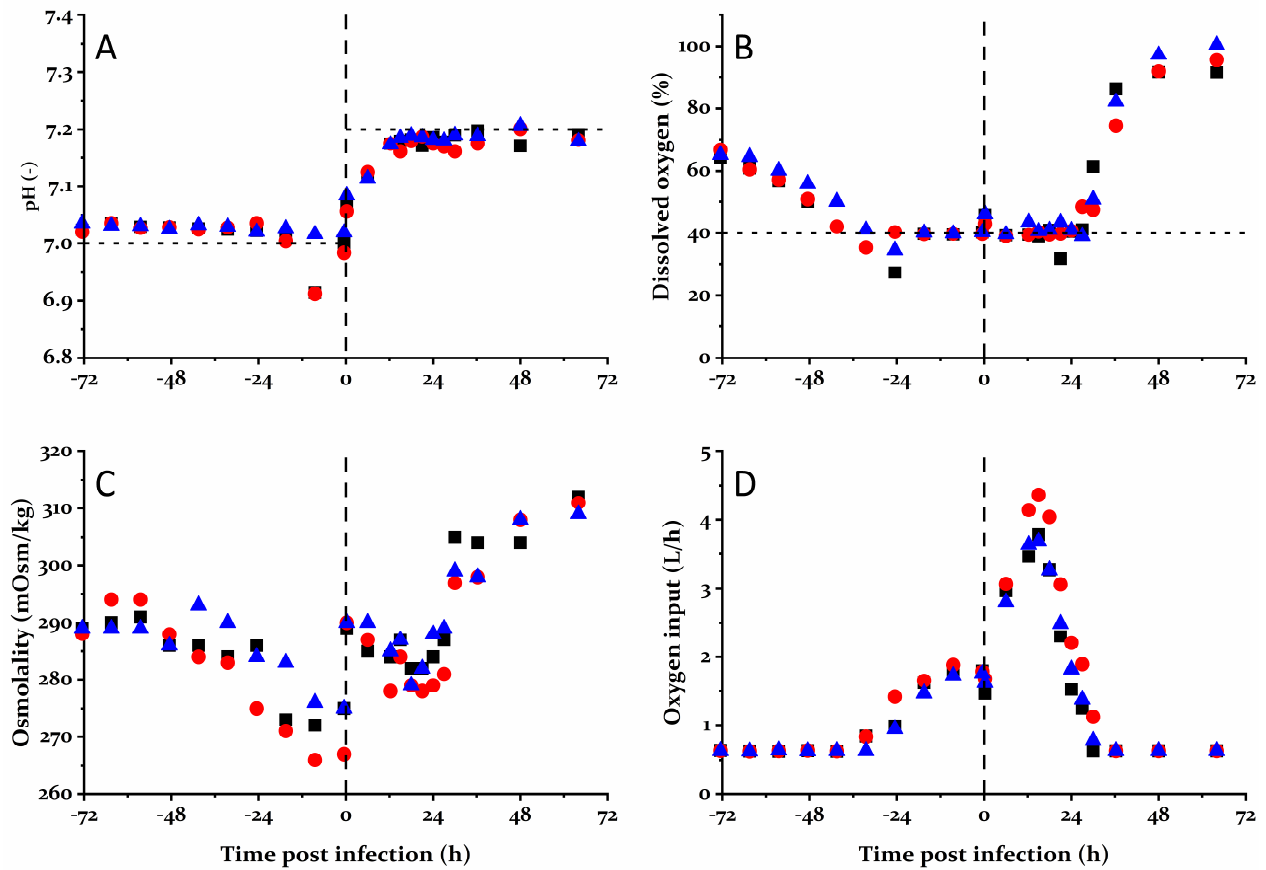


Figure 17: Process parameters of MDCK.Xe.A cell cultivations in three parallel bioreactors.

Physical process parameter pH (A), dissolved oxygen (B), osmolality (C) and overall oxygen input: QO_2 (D) were monitored for the whole cultivation process. pH and dissolved oxygen (DO) were controlled, horizontal dashed lines indicate controller set-points. Vertical lines indicate time point of infection. Values for pH, DO and QO_2 were extracted from online data at the respective time points. All three bioreactors were run in parallel and inoculated from three separated precultures. STR1 (■), STR2 (●), STR3 (▲)

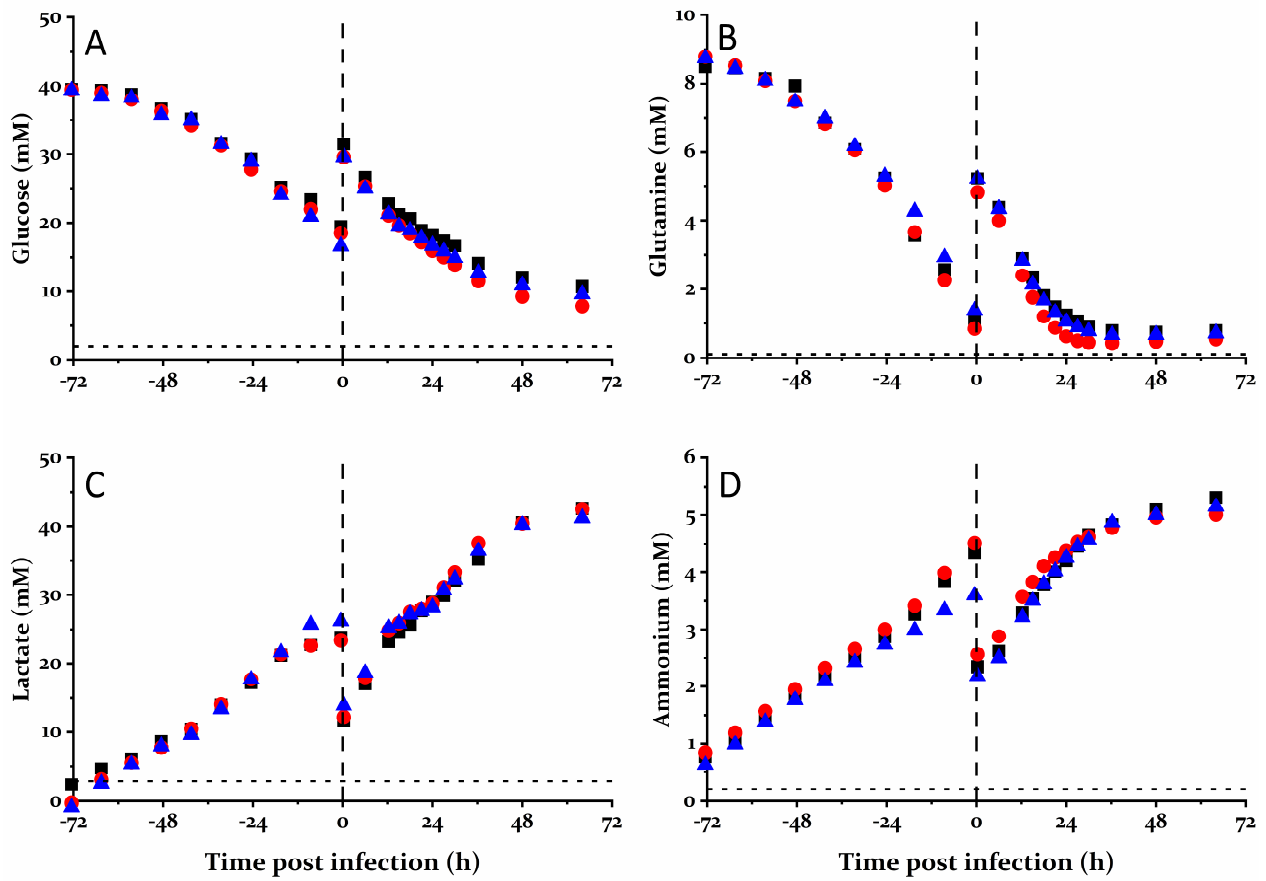


Figure 18: Main extrac. metabolites of MDCK.Xe.A cell cultivations in three parallel bioreactors. Concentrations of the main metabolites glucose (A), glutamine (B), lactate (C) and ammonium (D) in the culture medium over the process time (144 h). Vertical lines indicate time point of infection. Horizontal dashed lines indicate limit of quantification of the respective metabolite. All three bioreactors were run in parallel and inoculated from three separated precultures. STR₁ (■), STR₂ (●), STR₃ (▲).

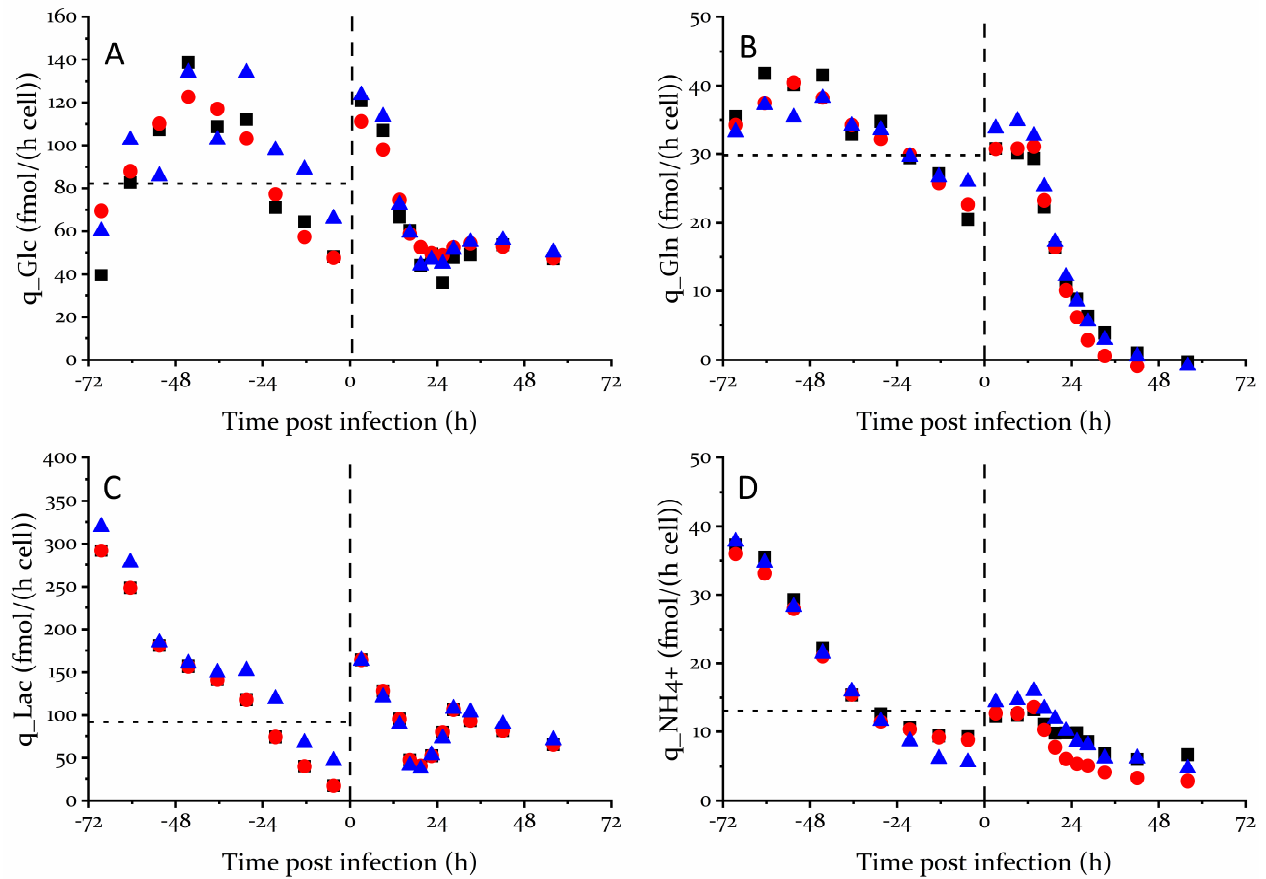


Figure 19: Metabolic rates of MDCK.Xe.A cell cultivations in three parallel bioreactors.

Cell specific consumption rates of glucose (A) and glutamine (B) as well as specific production rates of lactate (C) and ammonium (D) calculated for each time interval over the whole process time (144 h). Vertical lines indicate time point of infection. Horizontal dotted lines indicate average metabolic rate calculated for the whole growth phase (-72 - 00 h). All three bioreactors were run in parallel and inoculated from three separated precultures. STR₁ (■), STR₂ (●), STR₃ (▲)

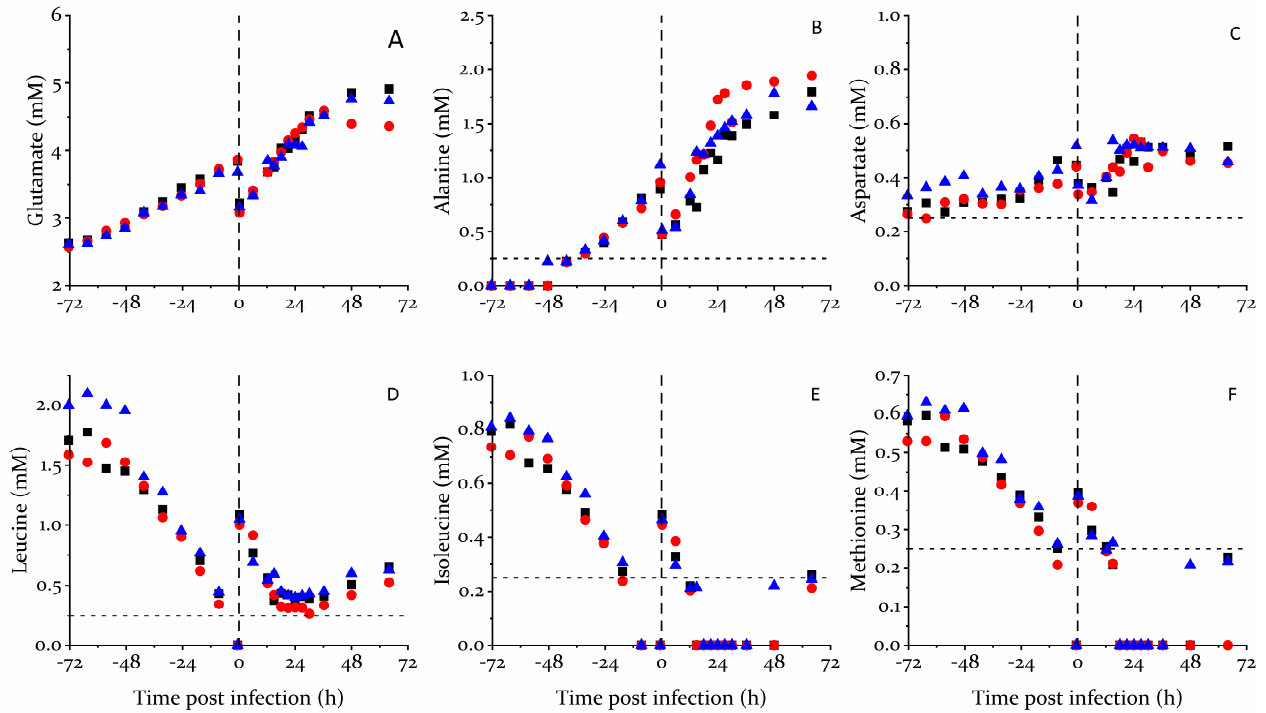


Figure 20: Selected amino acids of MDCK.Xe.A cell cultivations in three parallel bioreactors.

The concentration of the amino acids glutamate (A), alanine (B) and aspartate (C), leucine (D), isoleucine (E) and methionine (F) in the cultivation medium were quantified over the process time (144 h). Vertical lines indicate time point of infection. Horizontal dashed lines indicate limit of quantification of the respective metabolite. All three bioreactors were run in parallel and inoculated from three separated precultures. STR1 (■), STR2 (●), STR3 (▲).

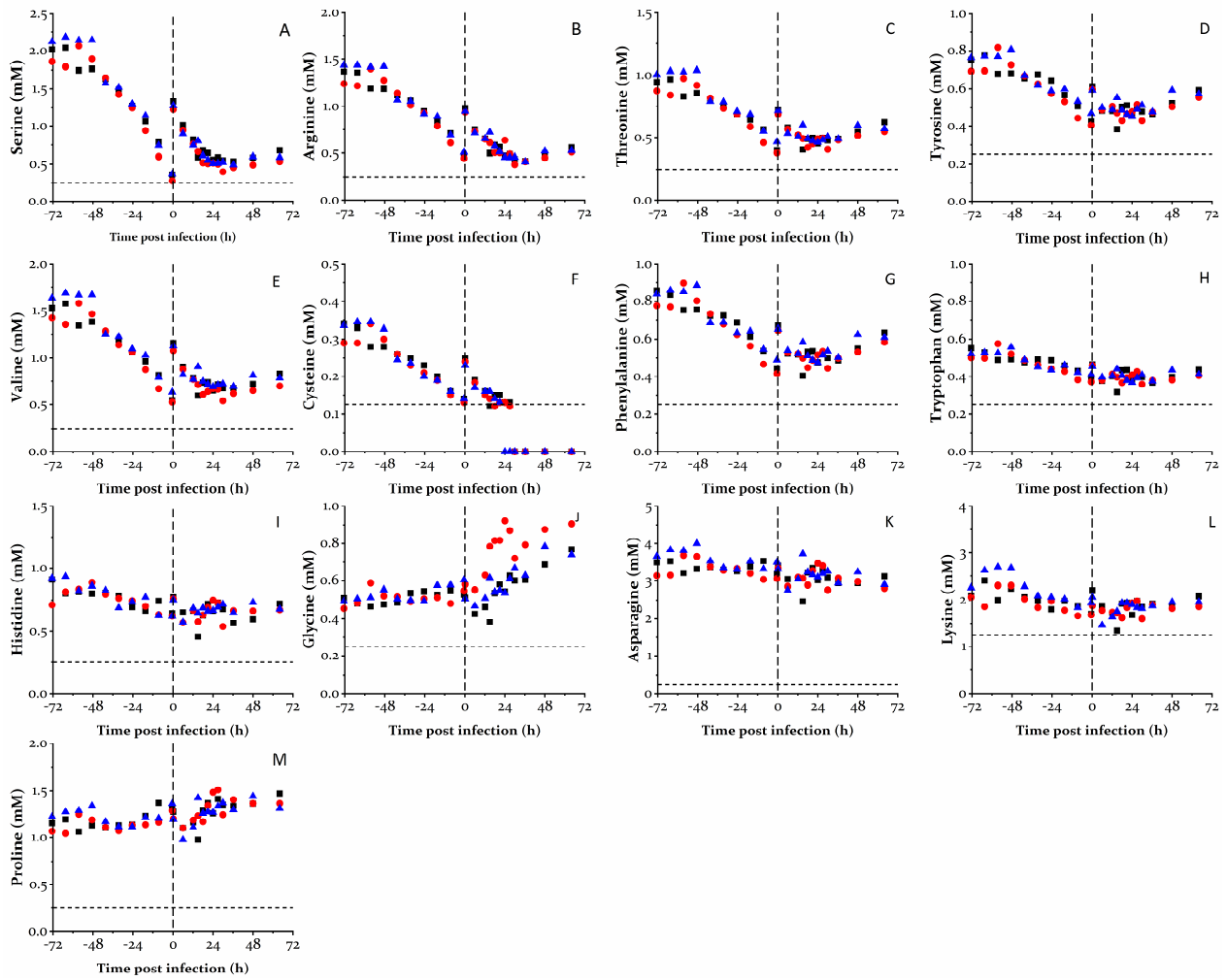


Figure 21 Extracellular amino acids of MDCK.Xe.A cell cultivations in three parallel bioreactors. Concentrations of consumed (A–G) or relatively constant (H–M) amino acids in cultivation medium, analyzed over the process time (144 h). Vertical lines indicate time point of infection. Horizontal dashed lines indicate limit of quantification for the respective amino acid. All three bioreactors were run in parallel and inoculated from three separated precultures. STR₁ (■), STR₂ (●), STR₃ (▲).

4.3.3 MDCK.Xe.A cells in stirred tank system: influenza A virus production

MDCK cells continued to grow post infection as IAV propagated and infected the whole cell population (18 hpi), reaching a maximal cell concentration of approximately 7×10^6 cells/mL at 21 hpi. After that, viable cell concentration started to decrease. Cell viability initially increased to over 99 % and started to decrease with the onset of virus accumulation (>21 hpi). Similarly, cell size decreased significantly during virus production (Figure 16), due to the onset of virus induced apoptosis (Figure 22 D) and cell lysis. In this case, reduced cell size cannot be attributed to changes in medium osmolality which was increasing after 24 hpi (Figure 17 C). Due to media addition and the increase in working volume at time of infection, the level of nutrients recovered to some extent, and accumulated by-products were diluted. Similar to the growth phase, no significant limitation of main metabolites was found, and even though ammonium and lactate accumulated rapidly after infection, concentrations remained rather moderate, increasing not over 45 mM and 6 mM, respectively in the late infection phase (Figure 18). Most of the main amino acids were sufficiently added in the feed to fuel the MDCK.XE.A cells in the infection phase as well: only isoleucine and methionine decreased below the limit of quantification (>18 hpi). Other amino acids (i.e. glutamate, alanine, and glycine) showed a strong increase during the infection phase (Figure 20 & Figure 21). Consumption/production rates of main metabolites increased significantly after dilution with fresh medium due to sudden increase in substrate concentration. However, metabolic rates of glucose and lactate decreased rapidly, while rates for glutamine and ammonium remained stable until 15 hpi. With full infection of the cell population at 15-18 hpi (Figure 22 C), MDCK cells consumed more glucose and produced more lactate, but glutamine consumption and ammonium production declined rapidly (Figure 19). Lactate continued to accumulate in the end of infection, probably due to cell lysis.

The combination of image stream and virus quantification assays enabled to follow the virus replication dynamics both for the host cells and the produced virus particles. Very fast virus replication led to a fast increase of infectious virus titer and infected cell population, with a maximum at 18-27 hpi and 15-18 hpi respectively (Figure 22 B-C). The delay of the virus accumulation dynamic to infection spreading in the cell population corresponds roughly to the 6 h needed for intracellular virus replication [283]. Very high infectious virus titer ($>2 \times 10^9$ TCID₅₀/mL) were measured at this time (21 hpi), followed by a titer reduction due to virus inactivation (>27 hpi). Total virus particles (HA titer) were not detectable in the initial infection phase due to the detection limit of the assay and were only quantified during in the later infection phase (> 12 hpi). HA titer rose rapidly, reaching a plateau at about 24 hpi with roughly 3.6 lg(HAU) (Figure 22 A). With the

infection spreading over the cell population, the proportion of apoptotic cells started increasing at 12 hpi, and reached a maximum (approx. 80 %) in the end of the infection (Figure 22 D).

Identification of optimal harvest point

Investigating the optimal process time for harvest to transfer from virus production to virus purification was of great importance for process integration. With the rise of virus titers, we observed a significant increase in total protein and host cell DNA (HC-DNA) concentrations in the cell culture supernatant. After infection total protein concentration “only” increased fivefold whereas the DNA content increased by two order of magnitudes compared to the uninfected MDCK.Xe.A cells (Figure 23). Total protein concentrations were already rising during growth phase and increased rapidly in the later part of infection due to virus release (viral proteins) and cell death (HCP) (Figure 23 A). HC-DNA levels, however, remained stable (≈ 100 ng/mL) during growth phase, but rose after trypsin addition (time of infection). Trypsin was leading to minor cell lysis, preferably of “dead” cells resulting in an artificial increase of cellular viability (>99 %) and the release of cellular DNA. In the later stage of infection, a high level of HC-DNA (> 2 $\mu\text{g/mL}$) was measured due to extensive virus induced cell lysis (Figure 23 C). Due to the strong dynamic of host cell contaminants, the optimal harvest point was determined by analyzing the ratio of HA unit (HAU) to the main contaminant levels (HC-DNA & total protein). This ratio showed a strong maximum at 21-24 hpi, both for DNA and total protein (Figure 23 B & D), where it was possible to achieve high virus titers. Furthermore, cell concentration as well as viability were quite stable and the percentage of apoptotic cell population was still relatively small (approx. 25 %) (Figure 22 D). In general, cell damage should be limited due to cell-derived contaminations (e.g. histones), which are challenging to deplete in additional downstream purification technologies. Reduction of cell debris, DNA and protein contaminations from the host cells improves purification and can reduce the number of purification steps for an overall improved productivity. At the optimal harvest time, the major amount of released HC-DNA might actually be due to the trypsin effect and not due to virus-induced cell lysis. However, this observed effect was already the optimal condition of trypsin type (trypsin and TPCK trypsin tested) and trypsin activity to minimize DNA release and optimize virus replication. Other type of proteases or expression of proteases in the host cell system may reduce this effect and ease purification. For harvested material at 21 & 24 hpi, downstream DNA digestion, inactivation (β -PL) and SXC purification were applied which is not described in this work. For the inactivated material an average ratio of 350-400 HAU/ $(\mu\text{g/mL})$ was determined by SRID measurements [319,323].

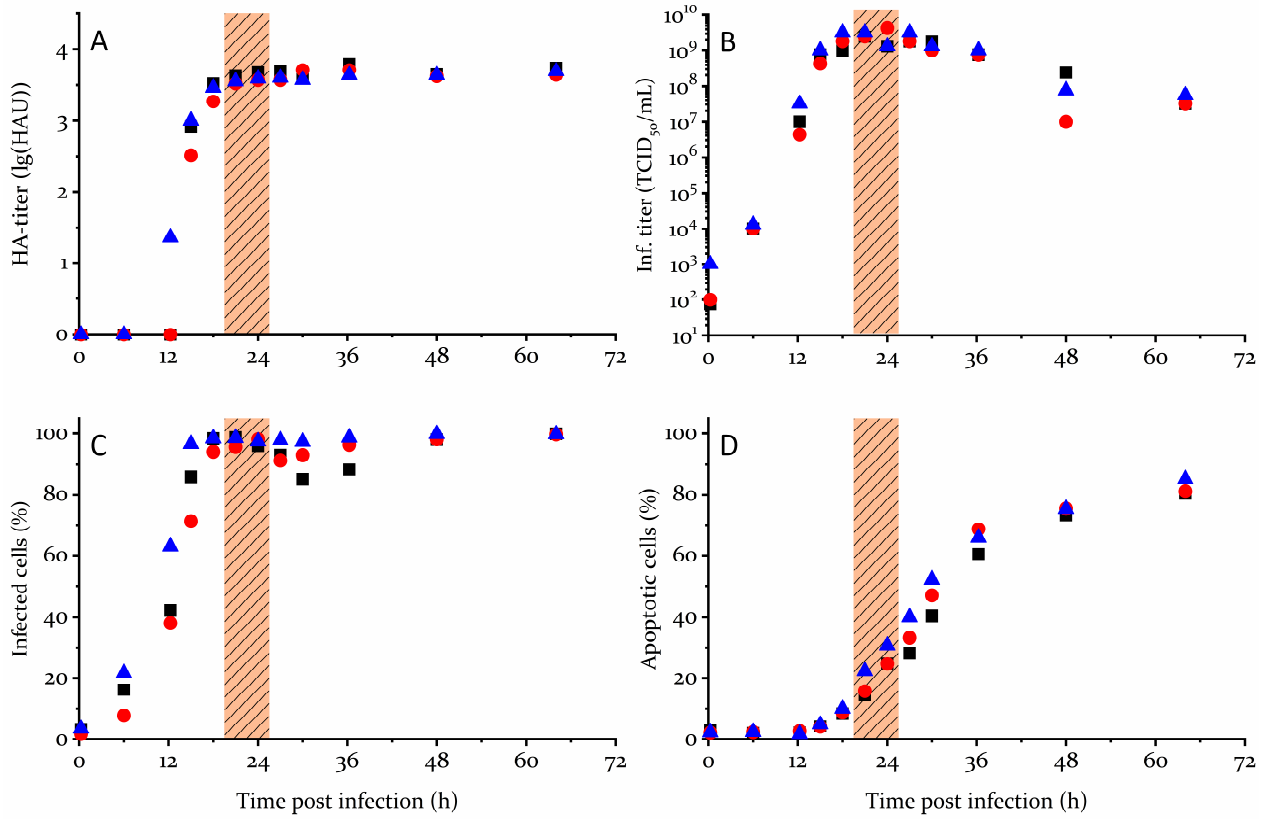


Figure 22: Influenza A virus infection of MDCK.Xe.A cell cultivations in parallel bioreactors. Total virus titer based on hemagglutination activity (A), infectious virus titer based on TCID₅₀ assay (B), percentage of infected (C) and apoptotic (D) MDCK cells analyzed after infection with IAV. Shaded area represents suggested optimal harvest time. All three bioreactors were run in parallel and inoculated from three separated precultures. STR₁ (■), STR₂ (●), STR₃ (▲).

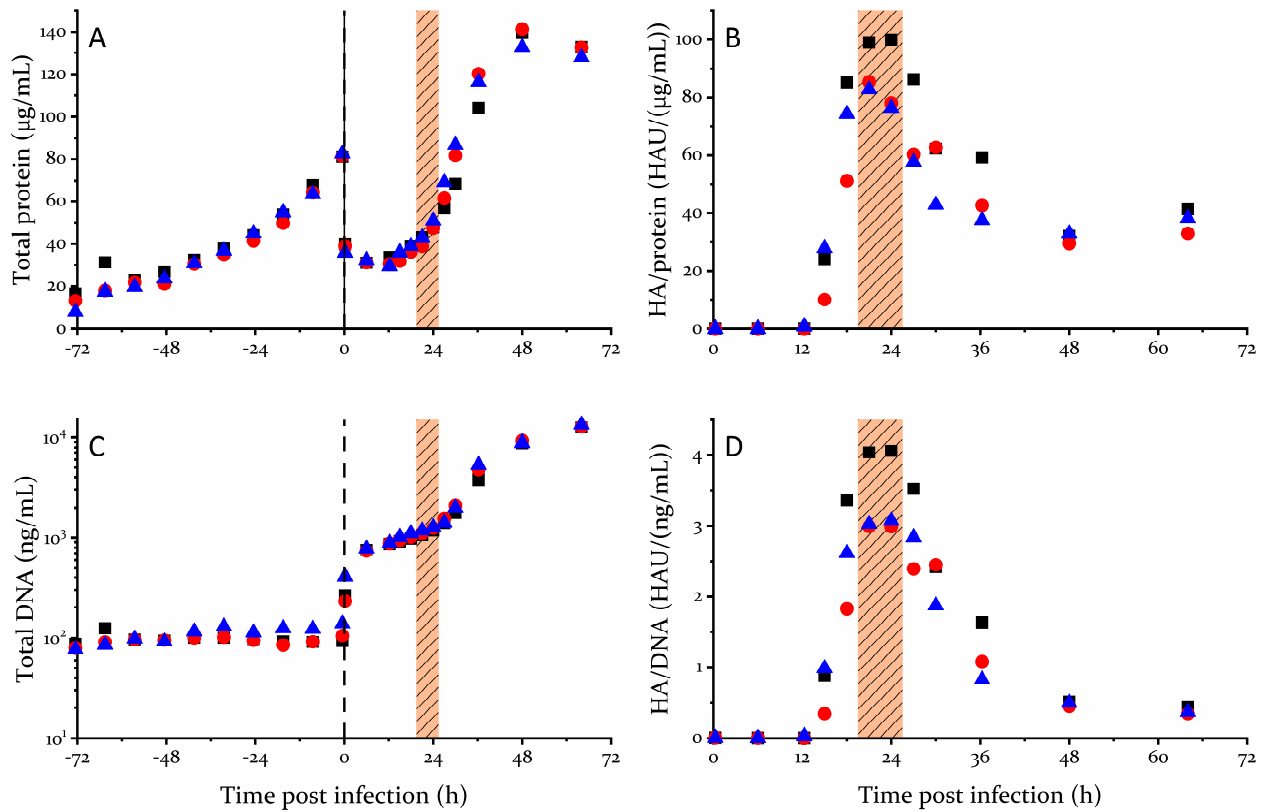


Figure 23: Total protein and DNA profiles of MDCK.Xe.A cells cultivations in parallel bioreactors. Total protein (A) and total DNA (C) were measured as an indication for host cell contamination during the cultivation process. A ratio of total protein (B) and DNA (D) over virus titer (HA-assay) was used to identify optimal harvest point after infection (shaded area). Vertical lines indicate time point of infection. All three bioreactors were run in parallel and inoculated from three separated precultures. STR1 (■), STR2 (●), STR3 (▲).

4.3.4 Process performance in stirred tank bioreactors

Scale-up of MDCK.Xe.A cell cultivation and infection was straightforward without major adjustments to the overall process design. Cell growth, cell concentrations, metabolism, and virus titers were comparable to the small scale shake flask infections carried out in the previous chapter (4.2.). Metabolic rates and metabolic conversion ratios calculated over the whole cell growth phase were similar between the scales, except for lactate. Lactate production rate and conversion ratio ($Y_{\text{Lac/Glc}}$) were significantly higher in the bioreactor cultivations compared to the previous cultivation in shake flasks (Table 12). Despite the strong reduction of lactate production rate over the MDCK cultivation in the bioreactors, lactate release seemed to be higher than in shake flask cultivations of MDCK cells in Xeno-CDM medium. In the uncontrolled shake flask cultivation, pH variation could have induced a metabolic shift, which we did not observe in this extent in the bioreactor cultivations. As described already for CHO cell cultivations, pH reduction can favor lactate consumption under certain process conditions [238,314]. For additional process intensification, the use of a designed feed medium for an extend growth phase (fed- batch mode) and infection phase might be able to further increase IAV titer and overall process productivity. Reduced substrate concentrations (i.e. glucose or glutamine) might reduce lactate and ammonium accumulation [249,324,325]. Alternatively, glutamine and glucose could be replaced with other substrates to reduce by-product formation [239,273,326,327]. Nevertheless, there was no indication of cell growth inhibition or reduced virus replication due to lactate or ammonium accumulation, in the designed process.

The MDCK.Xe.A cell line showed great potential for a productive and scalable IAV production process. With the exception of the infective virus titer, all relevant parameters for the cell specific and overall productivity of IAV particles were matching between the small scale shake flask and the laboratory scale STR cultivations (Table 13). Higher infectious virus titers and $\text{CSVY}_{\text{TCID}}$ were obtained for the STR cultivations, most likely due to better control of the pH (i.e. 7.2) during the infection phase. High cell concentrations in combination with outstanding CSVY allowed high IAV titer ($3.6 \pm 0.06 \text{ Lg(HAU)}$) at the potential harvest point (21-24 hpi). These are one of the highest IAV titers for batch or extended batch processes and are the highest titers for cultivations in STR systems with chemically defined medium reported so far [44,172,295,316,328,329]. Fast virus replication and high cell growth rates reduced the production time for USP from seven to four days, compared to adherent MDCK cells [46,47,49]. Especially for pandemic vaccine manufacturing, fast scale-up and high productivity are crucial to provide billions of vaccine doses as fast as possible. Here, high cell growth rates are essential to speed up large-scale production. With the presented cell line, we would estimate a lead time of three weeks (22 days) and six passages (cryo; 0.02; 0.1; 2; 25; 500 L) to reach

10,000 L manufacturing scale. Compared to other cell lines with lower growth rate and maximal cell density (e.g. tD 30h; VCC 5×10^6 cells/mL), four weeks (28 days) and seven to eight passages would be required to reach a similar scale [53]. Furthermore, the demonstrated production process is faster and more productive than processes using other MDCK suspension cell lines [44,53,172,312]. With an estimated HA antigen content of roughly 10 $\mu\text{g/mL}$ in the USP harvest (400 HAU/ $(\mu\text{g/mL})$) and a traditional vaccine dose of 15 $\mu\text{g/dose}$, a potential batch productivity of 660 vaccine doses per liter of cultivation broth is estimated. However, product losses in downstream processing operations, vaccine optimization with respect to antigen stability and reduction of antigen dosage with the addition of adjuvants could change the overall process productivity. With advanced membrane-based purification technologies, only minimal (0-20 %) product loss is expected for each unit operation [153,154]. In downstream purification experiments using membrane-based capture technology (SXC), inactivation and DNA digestion was reducing recovery to a much higher extend than SXC based purification. Here, an overall productivity (USP & DSP) of 300 doses/L was determined based on a four step purification process (clarification, DNA digestion, inactivation, SXC capture) [319,323]. Following the overall trend of bio-manufacturing to run processes as single use operation, a production scale of 2,000 L would be feasible, resulting in estimated potential 1.2 million vaccine doses per USP batch. In order to increase manufacturing capacity, multiple single use bioreactors could be run in parallel or perfusion technology could be applied, as already demonstrated for MDCK.Xe.E cells and other cell lines and in previous experiments [159-161,300]. High cell density manufacturing would not only increase virus titers but improve overall productivity as well. However, viral downstream technologies still have to prove their potential for sufficient virus purification with similar recovery and product quality as in batch processes.

Table 12: Comparison of metabolic activity of MDCK cells between bioreactor and shake flask.

	q_{Glc}^2	q_{Gln}^2	q_{Lac}^2	$q_{NH_4}^2$	$Y_{Glc/Lac}^2$	$Y_{NH_4/Gln}^2$
	fmol/(cell h)	fmol/(cell h)	fmol/(cell h)	fmol/(cell h)	-	-
SF ¹	86.3±2.7	28.7±0.9	68.4±3.1	14.3±0.5	0.79±0.02	0.48±0.05
STR	82.4±9.4	29.8±0.8	91.9±13.4	13.1±0.9	1.11±0.04	0.45±0.04

¹ Cultivation from chapter 4.2, ² over whole growth phase (72 h), SF: shake flask, ±: standard deviation

Table 13: Bioreactor and shake flask process performance for influenza A virus production.

	STR₁	STR₂	STR₃	STR_{AV}	SF_{AV}
HA titer (lg(HAU))	3.68	3.55	3.57	3.61±0.06	3.60±0.03
Inf. virus titer (TCID₅₀/mL)	2.4×10^9	2.4×10^9	3.2×10^9	$2.7 \pm 0.5 \times 10^9$	$0.7 \pm 0.5 \times 10^9$
CSVY_{HA} ¹ (virions/cell)	$13,1 \times 10^3$	$11,2 \times 10^3$	$11,6 \times 10^3$	$11.9 \pm 1.0 \times 10^3$	$12.4 \pm 0.3 \times 10^3$
CSVY_{TCID}} (virions/cell)	320	310	440	360±70	100±21
STY (virions/(L d))	2.4×10^{13}	1.8×10^{13}	1.9×10^{13}	$2.1 \pm 0.3 \times 10^{13}$	$1.9 \pm 0.1 \times 10^{13}$
STY_{VD}} (doses/(L d)) ²	190	150	150	160±20 ²	-

¹ average of maximal titers, ² based on 15 µg of HA antigen per dose, ±: standard deviation CSVY: cell specific virus yield, STY: space time yield for USP batch based on HA titer, STY_{VD}: space time yield for USP batch based on vaccine dose estimate, STR_{AV}: average value of the three bioreactors, SF_{AV}: average value of the three shake flasks (chapter 4.2)

4.4 Metabolic profiling of MDCK suspension cells

Metabolic profiling of animal suspension cells was a major part of this thesis from the very beginning. Due to the time needed to establish the appropriate experimental set-up, conducting the experiments, sample processing, LC-MS metabolite quantification and data analysis, additional experiments were performed as described in the previous chapters. Initially different quenching methods reported for mammalian suspension cell lines were evaluated, in order to find the optimal method for metabolic profiling of MDCK suspension cell lines. In the final experimental set up, the metabolism of MDCK.S8.E cells were monitored for growth and on parallel IAVs infection. Intracellular metabolite pools were quantified for infected and uninfected MDCK cells in regular time steps. Additionally, cell count, cell size, extracellular metabolites, total virus titer (HA assay), intracellular virus replication and apoptosis were monitored (Figure 24).

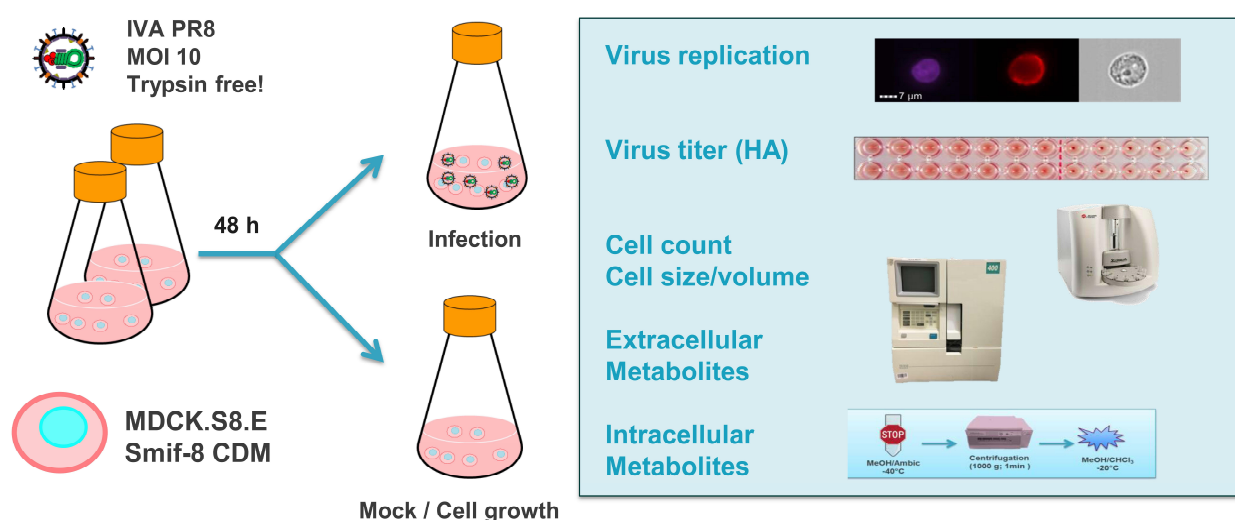


Figure 24: Experimental set-up for metabolic profiling of MDCK.S8.E cells.

Suspension MDCK cells, cultivated for 48 h were infected with IAV at high MOI (10) to enable synchronous infection. Cell count, cell size, intra- and extracellular metabolites were quantified for infected and mock-infected cells. For infected cell population, intracellular virus replication was monitored in addition to virus titer (HA-titer).

4.4.1 Evaluation of quenching methods for MDCK.S8.E and MDCK.Xe.E cells

In order to find the most appropriate quenching method for metabolic profiling experiments with MDCK suspension cells, three different methods were evaluated. All methods were already applied for metabolic profiling of other mammalian suspension cells [287,288,290,292,330]. Centrifugation quenching (CQ) was developed in house, whereas direct quenching (DQ) and filtration quenching (FQ) were developed in other research groups [287,290,292]. For this purpose, two MDCK suspension cell lines (MDCK.S8.E and MDCK.Xe.E) were cultivated for three days in shake flasks to test the different quenching methods in mid exponential phase. At the time of analysis, MDCK.S8.E and MDCK.Xe.E cells were growing to a VCC of 4.5×10^6 cells/mL (VCV: $6.5 \mu\text{L/mL}$) and 5.6×10^6 cells/mL (VCV: $9.5 \mu\text{L/mL}$), respectively. Since metabolites of the central carbon metabolism were the focus of following investigations, metabolic profiles of glycolysis and TCA were evaluated in addition to AEC and adenylate recovery. This study was part of a bigger investigation of seven animal suspension cells, where the metabolic profile was analyzed with the three quenching methods. The optimization and implementation of quenching methods was part of a master thesis by Jonas Ringeisen, supervised in the process of this thesis [330].

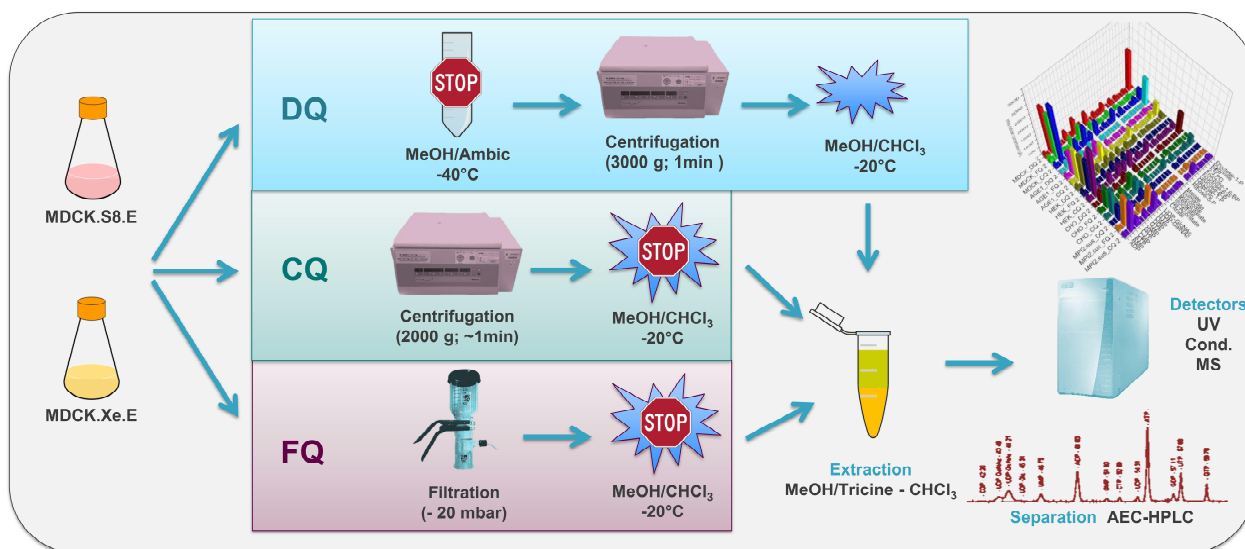


Figure 25: Experimental design for the evaluation of quenching methods.

Three quenching methods, direct quenching (DQ), centrifugation quenching (CQ) and filtration quenching (FQ) were tested for two MDCK suspension cell lines for metabolic profiling. Extracted metabolites were separated by ion chromatography and quantified by conductivity, UV and MS detection.

Sampling and quenching rate

Quenching methods for metabolic profiling strongly effect the “reality” of the metabolite composition and feasibility of implementing a cheap and fast sampling technique. All three evaluated methods were designed for fast and high throughput sampling of animal suspension cells; there are differences in sampling time and necessary equipment, though. Centrifugation quenching only needed basic laboratory equipment, whereas for filtration- and direct quenching additional equipment was necessary (Table 14). Fast filtration was applied commonly for prokaryotic cells, where high vacuum pressure can be applied. However, for animal cells the vacuum has to be tightly controlled (ideally with a pressure controller) to maximize flow and limit cell damage [287,331]. Additionally, appropriate filter materials (i.e. glass filter) and filter holders have to be used. Concerning the speed of the methods we distinguished between the time needed from sampling to quenching (quenching), from sampling to storage in liquid nitrogen (sampling) and the time between two samples (processing) (Table 14). Due to the repeated centrifugation steps in CQ, quenching speed was much lower compared to DQ and FQ methods. DQ samples were quenched basically immediately by adding the sample directly to -40 °C quenching solution but overall the processing time was the longest for DQ. Samples quenched with FQ were processed very quickly, but due to the installation and equilibration of fresh filters, time between sampling was increased. However, a filter device with the capability to process multiple samples simultaneously could reduce time between sampling significantly. Overall, the FQ is a quite good compromise between the need for specialized equipment on the one hand and sampling and quenching speed on the other side. This might be one of the reason for its application in different studies over many research groups [287-289,331].

Table 14: Overview of equipment and time necessary for the different quenching methods.

Method	Equipment	Quenching ¹	Processing ²	Sample to sample ³
CQ	Centrifuge (4 °C)	1.9 min	2.0 min	2.2 min
DQ	Centrifuge (-20 °C) Cryostat (-40 °C)	~0.1 min	2.4 min	2.6 min
FQ	Filtration unit Vacuum controller	0.5 min	0.6 min	1.8 min

¹ time between sampling and quenching; ² time between sampling and liquid nitrogen, ³ time between two samples.

Energy charge and metabolite recovery

The adenylate energy charge (AEC) is an intracellular indicator for the cell to balance its metabolic pathways and control ATP production and consumption [332]. To assess quenching efficiency, the AEC of the cell is considered a good indicator for the speed a quenching method to stop cellular metabolic reactions [333]. ATP, ADP and AMP (AXP) are ubiquitously involved in biochemical reactions leading to a very fast turnover rate, compared to the AXP synthesis or degradation. We can assume, that the AXP concentration stays constant over a short time period (<5 min) and changes in AXP concentration are due to leakage or degradation during cell quenching. For both MDCK cell lines CQ showed the highest AXP levels compared to the other quenching methods. Differences in AXP recovery between the quenching methods were more pronounced for the MDCK.Xc.E cells were only 50-60 % of the AXP were recovered for FQ. MDCK.S8.E seemed to be more robust and differences in AXP levels were much lower over all three methods, and there was basically no difference between the DQ and CQ methods (Figure 26 B). For both MDCK cell lines we observed a high AEC (> 0.9) with all quenching methods, but the AEC for the CQ and DQ methods showed a consistent higher value (0.95–0.96) compared to the FQ method (0.93–0.94) (Figure 26 A). Between the two MDCK cell lines similar AEC values were determined for the respective quenching method. For the MDCK.S8.E cell line, both CQ and DQ seemed to have similar recovery and quenching efficiency. FQ in contrast showed inferior AXP recovery and quenching efficiency for both cell lines.

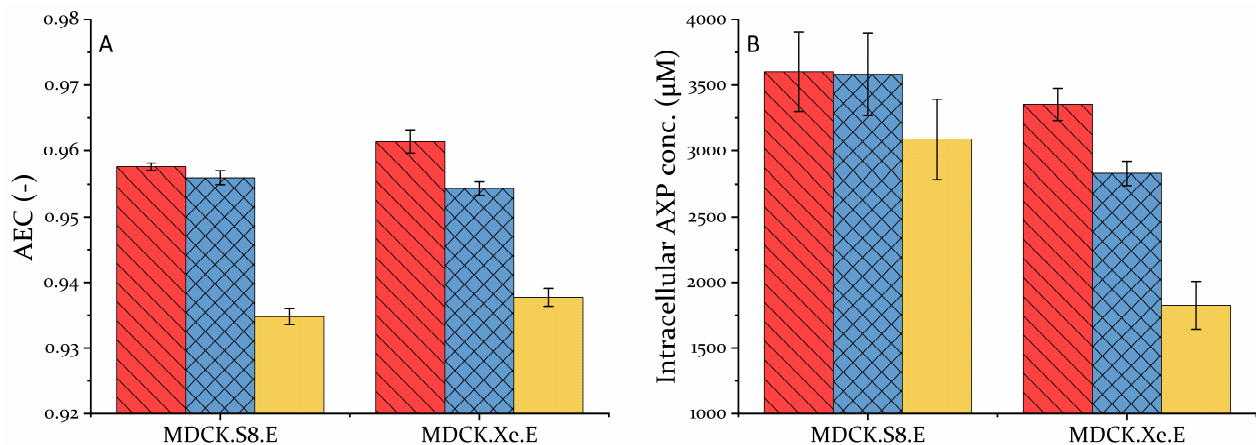


Figure 26: Energy charge and adenylate recovery of quenched MDCK suspension cells.

Adenylate energy charge (A) and intracellular AXP concentration (B) of two MDCK suspension cell lines calculated from intracellular ATP, ADP and AMP concentrations. Red striped bar: CQ, blue crossed bar: DQ, yellow dotted bar: FQ. Error bars: standard deviation of technical triplicates.

Quantification of metabolites from glycolysis

Glycolytic metabolites are crucial for metabolic profiling of the MDCK suspension cells due to the key function of central carbon metabolism. Metabolite pools of the glycolytic pathway appeared to be very different between the different quenching methods. Due to the linear connection of the upper glycolysis to the extracellular glucose the metabolites are quite sensitive to glucose limitation. It seemed that this was especially true for the CQ method, where the cells are exposed to PBS for an extended period of time compared to the other methods. For the CQ methods G6P and F6P are reduced slightly, whereas F16BP and 3PG accumulate compared to the other quenching methods. Short processing time during fast filtration (FQ) and direct metabolic inactivation during direct quenching (DQ) seemed to be faster in quenching enzyme activity and preserving metabolite pools for both MDCK cell lines. No major differences were observed for the metabolite pools of PEP. (Figure 27). The shift of metabolite pools for CQ significantly altered the overall metabolic profile as well, F16BP and 3PG were the dominant pools and the remaining metabolites had much lower levels. For DQ and FQ the metabolite pools were much more balanced with the exception of PEP, which was quite low for all methods and cell lines. Additionally, metabolite pools were quite similar for DQ and FQ for the two analyzed MDCK cell lines, despite the significant differences in cell growth as well as uptake and release of extracellular metabolites, as shown in the previous chapter (Chapter 4.2). To evaluate the glycolytic metabolites accurately DQ and FQ seemed to be more suitable due to faster cellular quenching (DQ) and faster sampling (FQ), respectively.

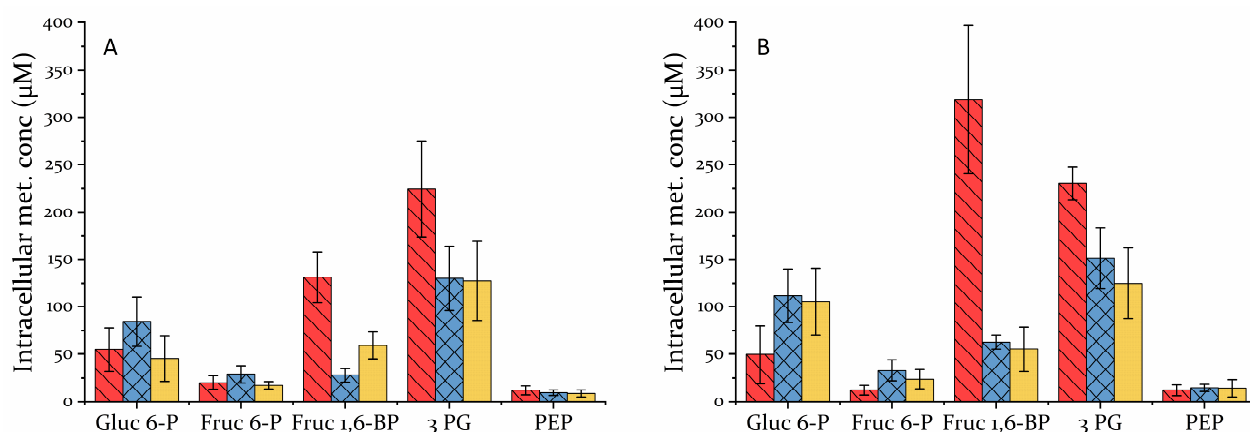


Figure 27: Intracellular metabolites of glycolysis for quenched MDCK suspension cells.

Intracellular profile of glycolytic metabolites quantified for MDCK.S8.E (A) and MDCK.Xe.E (B) cell lines in mid exponential phase (~72 h) using three different quenching methods. Red striped bar: CQ, blue crossed bar: DQ, yellow dotted bar: FQ. Error bars: standard deviation of technical triplicates.

TCA-metabolites

Measured values for TCA metabolite pools were more similar between the different quenching methods, compared to the metabolites of the glycolysis. With the exception of Suc in MDCK.Xe.E cells, there were no significant differences between the metabolites pools both between the cell lines and the different quenching methods. For most metabolites slightly reduced levels were observed for FQ samples which might be due to lower overall metabolite recovery. Surprising were the consistently high levels of citrate and malate, which were much higher compared to other metabolite pools, especially isocitrate. These high levels could be explained by a high activity of the citrate malate shuttle to support fatty acid synthesis that might lead to significant metabolite pools of malate and citrate in the cytoplasm. With the used methods it was not possible to distinguish between intracellular metabolites in the mitochondria and the cytoplasm. Due to the much higher volume of the cytoplasm and colocalization of malate and citrate in the cytoplasm and mitochondria higher overall levels could also be explained, even though a more balanced distribution of the TCA metabolite concentration is expected in the mitochondria [289,334-336]. Since no major differences were observed between the measured metabolite pools (especially between DQ and CQ) these metabolites did not have a major influence for choosing the optimal quenching method for subsequent experiments.

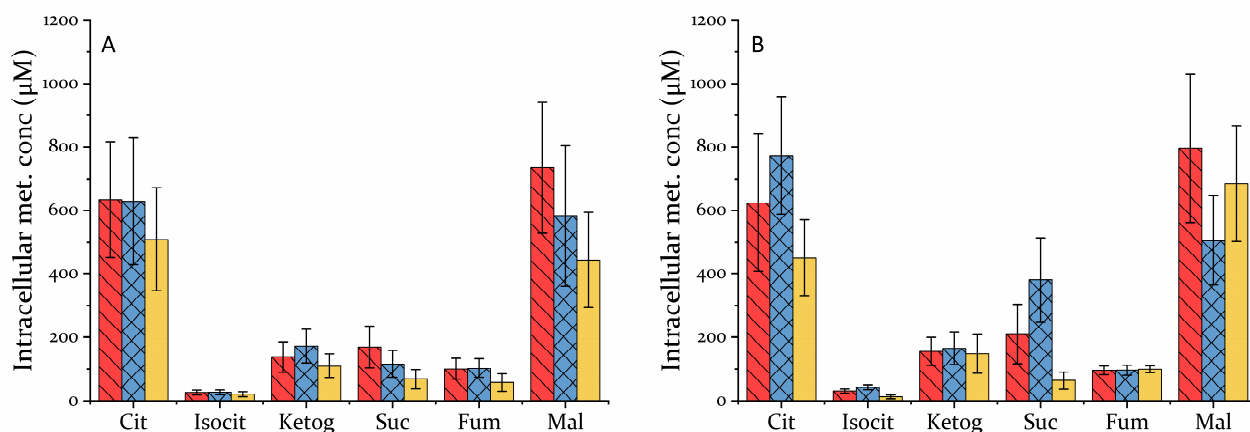


Figure 28: Intracellular metabolites of TCA for quenched MDCK suspension cells.

Intracellular profile of TCA metabolites quantified for MDCK.S8.E (A) and MDCK.Xe.E (B) cell lines in mid exponential phase (~72 h) using three different quenching methods. Red striped bar: CQ, blue crossed bar: DQ, yellow dotted bar: FQ. Error bars: standard deviation of technical triplicates.

Optimal quenching method for MDCK suspension cells

With the conducted experiments direct quenching (DQ) was identified as the optimal quenching method for metabolic profiling of both MDCK cell lines. With the instant temperature reduction to $-40\text{ }^{\circ}\text{C}$ enzymatic activity was stopped instantly and high amounts of relevant metabolites were recovered. In general, high recovery was observed for both MDCK cell lines, but for the MDCK.S8.E cell line both AEC and AXP concentration were basically identical. Despite good quenching and washing speed, which enabled a realistic metabolite spectrum of glycolysis, filtration quenching (FQ) was not considered for further metabolic profiling experiments due to massive reduction of the AEC and AXP recovery. High sample processing time and high demand for additional experimental equipment, like a cryostat were the only disadvantages of this method. As an alternative, ethanol could have been cooled in a $-80\text{ }^{\circ}\text{C}$ freezer to reach quenching temperatures between -40 to $-45\text{ }^{\circ}\text{C}$. Thus DQ was consequently applied for metabolic profiling experiments of MDCK.S8.E cells to analyze metabolic dynamics during a growth curve and upon IAV infection.

4.4.2 Cell growth and extracellular metabolites of MDCK.S8.E cells

Cell growth

Viable cell concentration, viability and average diameter of MDCK.S8.E cells cultivated in shake flasks were evaluated to depict both the extended growth curve and effects of IAV infection for two independent experiments (I & II). Despite similar initial seeding cell concentration and at least theoretically identical medium composition, MDCK.S8.E cells grew much faster and to higher cell concentration in the second sample set. In the exponential growth phase (< 84 h) MDCK cells of the first experiment grew significantly slower with a doubling time of 33 h ($\mu = 0.021 \text{ h}^{-1}$) compared to a doubling time of 29 h ($\mu = 0.024 \text{ h}^{-1}$) for the same time period in the second experiment. However, the two parallel cultivations (infection & mock) grew very similar prior to the virus infection (< 48 h). Cellular viability and average cell diameter were much more similar between the two experiments as well as the technical replicates, showing much lower variations between the individual samples (error bars) (Figure 29). In consequence to the lower growth rate for MDCK.S8.E cells (Mock.I), there was an extended growth phase (> 100 h) in the first experiment.

Both cell lines reached surprisingly high maximal cell concentrations compared to previous cultivations for this cell line [44,337], which might be due to a different cultivation scale or the volume adjustment to replace evaporated water, which was not routinely performed in previous cultivation experiments (Figure 29 A). Faster cell growth and higher cell concentration in the second experiment was probably due to a higher initial pyruvate concentration (Smif8 medium), an increased pyruvate consumption rate as well as a metabolic switch to lactate consumption for experiment II (mock). It was not clear why there was such a significant difference in initial pyruvate concentration between the different Smif8 media lots (Figure 30 E). Either pyruvate was not supplemented in the first medium batch, or batch to batch variations between the basal medium powder resulted in this issue. Higher pyruvate concentration led to higher lactate production and subsequent lactate consumption in later cell growth phase of the MockII culture (Figure 30 B). This metabolic switch in Smif8 medium was not observed for the first experiment and usually was not described for previous MDCK.S8.E cultivations [53,162]. Either higher pyruvate concentration, variations in medium lot or the addition of small amounts of Xeno-SFM medium together with the seed virus might have led to lactate consumption. The influence of the cultivation conditions and medium compositions on lactate consumption is rather complex and multiple parameters (i.e. pH, pCO₂, osmolarity, redox potential, pyruvate concentration) can affect the metabolic shift towards lactate consumption [238,243,311,314,338]. The higher availability of pyruvate and lactate as a carbon

source might have led to faster cell growth and higher maximal cell concentration. The other metabolites did not show a significant variation in the start concentration.

Influenza A virus infection

For all cellular parameters almost immediate effect of the high MOI influenza virus infection was visible. Viable cellular concentration and cellular viability stayed either relatively constant, or decreased 3-6 hpi (Figure 29). In the first experiment (Inf.I) infected cells continued to grow slightly, followed by an immediate reduction in viable cell concentration, whereas in the second experiment (Inf.II) cell concentration remained rather stable for 12 hpi. During this time (0-12 hpi) cell diameter as well as cellular viability remained stable followed with a significant reduction for both experiments at 12 hpi. Reduction of cell concentration, is usually linked to a reduction of viability and cell diameter as shown in the late stage of mock cultivations, and is not necessarily directly associated with virus replication.

Differences in the extracellular metabolite dynamics between the two experiments (Exp.I & Exp.II) where primarily defined by metabolic differences in the growth phase prior to the infection. Significant differences in glucose, lactate and pyruvate concentrations existed already pre-infection, but the overall dynamics of the respective metabolites during virus replication were quite similar for both experiments (Figure 30). Obviously, metabolite consumption changed after influenza virus infection, primarily due to the fast growth arrest and the reduction of viable biomass shortly after the infection. However, cell specific consumption and production rates of the major metabolites seemed to be quite consistent in the first 24 hpi compared to the mock infected control (Figure 31). Cell specific lactate production was slightly increased in both infection experiments (Figure 31 B). For the other metabolites (glucose, glutamine, ammonium) there were no consistent alterations between the two experiments in substrate consumption and product formation, respectively (Figure 31 A, C, D). Major differences between the two experiments (Exp.I & Exp. II) concerning the glutamine consumption and ammonium production might be due to the different pyruvate levels, which could have influenced glutaminolysis in MDCK cells [339]. An increase in lactate production after complete infection of the cell population was already documented for MDCK.Xe.A cells in the bioreactor experiments and seemed to be specific to IAV and MDCK cells rather than the used infection conditions (4.2.2.). For MDCK adherent an increased lactate production rate was already showed in a similar study [76]. However, Ritter et al. demonstrated almost a doubled lactate production rate for infected MDCK cells coupled to an increased glucose consumption rate. Since adherent MDCK cells were infected during complete confluency leading to growth arrest and switch to maintenance metabolism, a direct comparison is rather difficult.

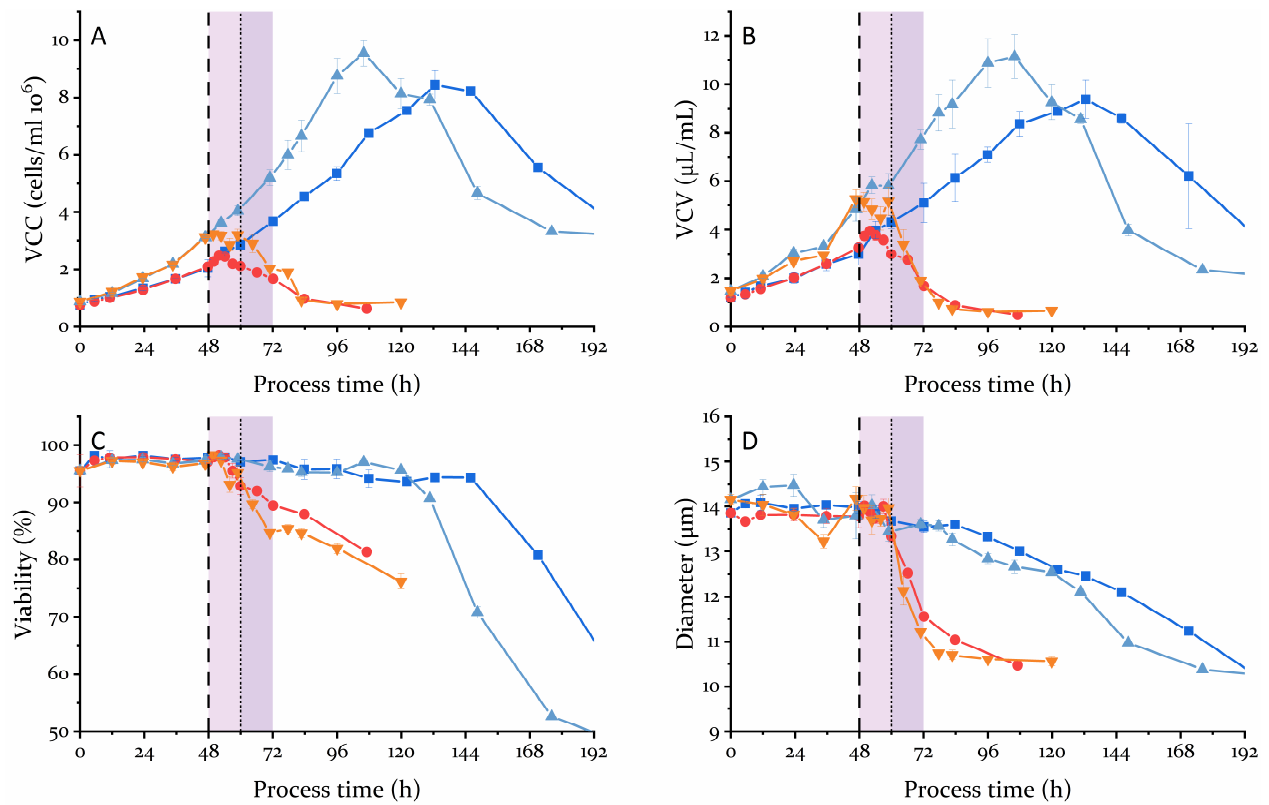


Figure 29 Cell concentration, cell size and viability for IAV infected and mock infected MDCK cells. Viable cell concentration (A) and cell volume (B), as well as cell viability (C) and average cell diameter (D) were monitored of mock (\blacksquare , \blacktriangle) and IAV infected (\bullet , \blacktriangledown) MDCK.S8.E cells in two independent experiments (ExpI: \blacksquare , \bullet ; ExpII: \blacktriangle , \blacktriangledown). Influenza A virus (ExpI: APR_O; ExpII: APR_SFM) was added for infection two days post inoculation (vertical dashed line). Early infection phase (48-60 h) and late infection phase (60-72 h) are highlighted in light and dark purple, respectively. Error bars: standard deviation of samples measured in triplicate.

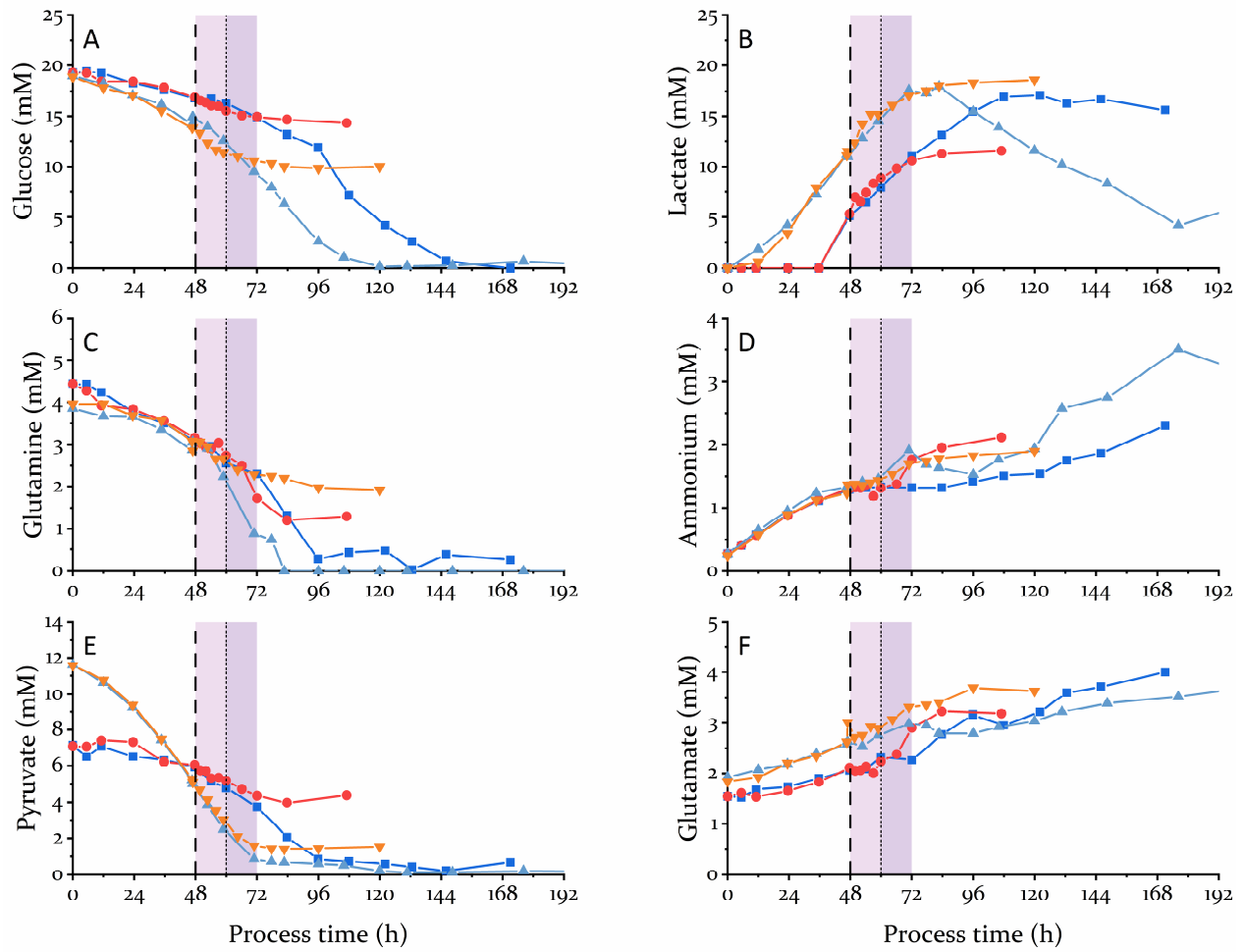


Figure 30: Main extracellular metabolites for IAV infected and mock infected MDCK cells.

The extracellular substrates glucose (A), glutamine (C) and pyruvate (E) as well as the metabolic side-products lactate (B), ammonium (D) and glutamate (F) were analyzed of mock (■, ▲) and IAV infected (●, ▼) MDCK.S8.E cells in two independent experiments (ExpI: ■, ●; ExpII: ▲, ▼). Influenza A virus (ExpI: APR_O; ExpII: APR_SFM) was added for infection two days post inoculation (vertical dashed line). Early infection phase (48-60 h) and late infection phase (60-72 h) are highlighted in light and dark purple, respectively.

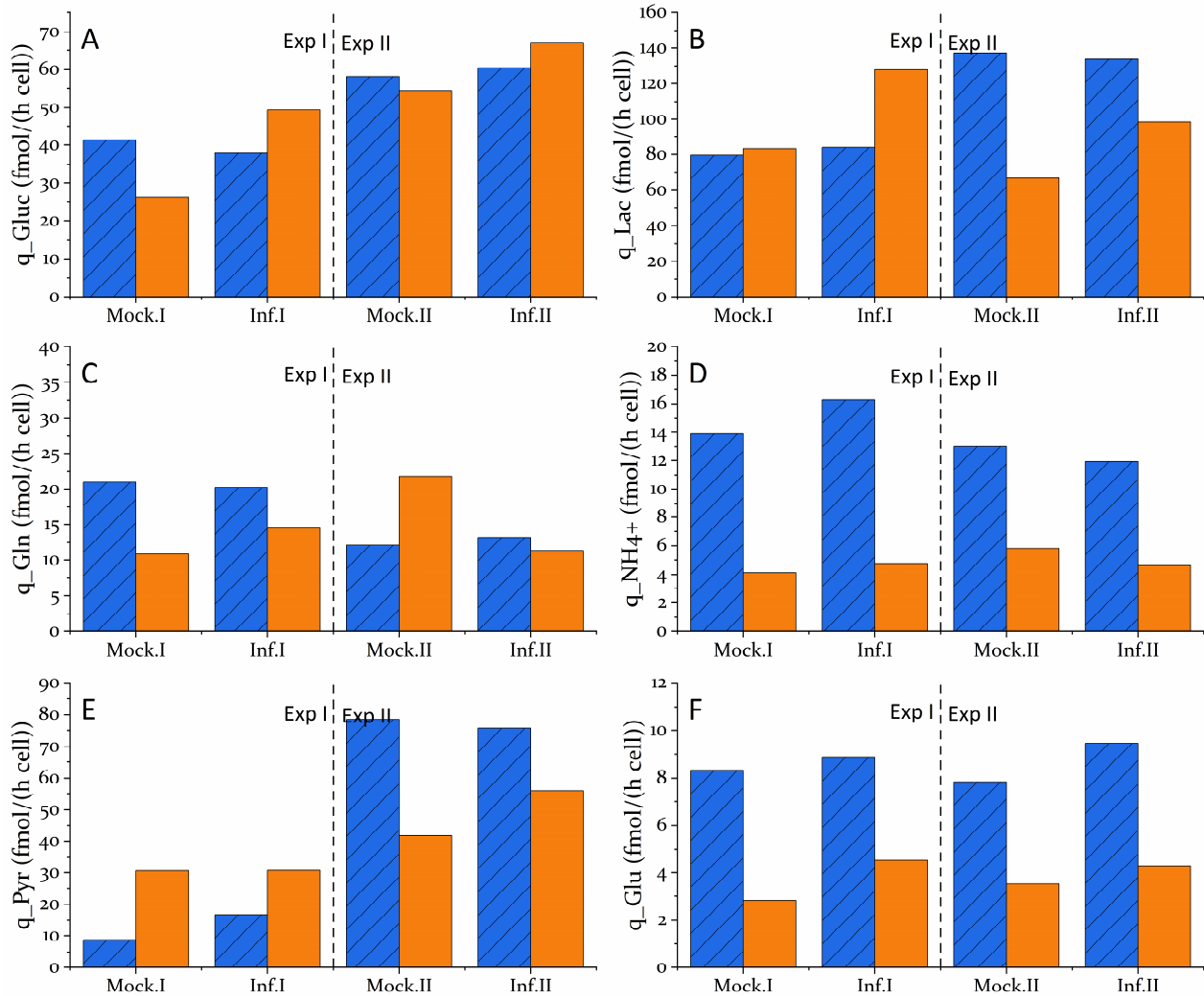


Figure 31: Specific metabolic rates of main metabolites for infected and mock infected MDCK cells. Cell specific consumption rates of glucose (A), glutamine (C) and pyruvate (E) as well as specific production rates of lactate (B), ammonium (D) and glutamate (F) were calculated for IAV infected (Inf) and mock infected (Mock) MDCK.S8.E cells in two independent experiments (I & II). Metabolic rates were determined in 48 h before infection (■) and 12 hpi (■).

4.4.3 Influenza A virus replication in MDCK.S8.E cells

Virus replication was analyzed both for the extracellular accumulation of total virus particles (HA-assay) and intracellular detection of vRNPs and cellular apoptosis signals. Extracellular influenza virus accumulation was detected almost instantly, with only a small delay in the first experiment. The overall dynamic, however, was very similar and a similar final titer was reached (Figure 32 A). For both infection experiments, an instant synchronous infection was confirmed by the detection of intracellular viral proteins (vRNP) basically in the total cell population immediately after the infection (Figure 32 B). Similar to the previously reported dynamics in adherent MDCK cells, vRNPs

were spread initially over the whole cell, then transported to the nucleus, (2-4 hpi) and subsequently were relocated from the nucleus to the cytoplasm and cell membrane [283]. Cellular apoptosis was detected quite late after infection, (12 hpi), when virus production was detected extracellularly was almost at its maximum. After 24 h the apoptotic cell population reached a maximum of 60 % and 80 %, respectively (Figure 32 B). Overall, both the dynamics of extracellular virus particles, the dynamics of intracellular vRNP proteins and apoptosis under high MOI conditions were similar to the dynamics observed for adherent MDCK cells [283]. A vRNP positive population of almost 100 %, directly after infection confirmed a synchronous infection of all cells with one replication cycle. Surprisingly, a high cell specific productivity was calculated for both experiments (10,000 virions/cell), comparable to low MOI (10^{-3}) infections performed with the same cell line, but with slower infection dynamics and the use of trypsin containing medium (Chapter 4.2.3). With the presence of defective interfering particles (DIPs), lower cell specific productivity would have been expected due to a higher probability for coinfections of the MDCK cells [340]. With the used seed viruses, DIPs (if present) had no or only minor effects on the final virus titer. Seed virus quality was checked by DIP PCR, confirming low DIP content qualitatively (data not shown) [294]. This observation underlines the importance of high-quality seed viruses rather than low MOI for efficient IAV production. Seed virus of lower “quality” might have had a higher DIP content and a higher impact on virus dynamics and virus titers [340]. For commercial, large scale IAV production, however, low MOIs (10^{-3} – 10^{-5}) are much more feasible and more economic.

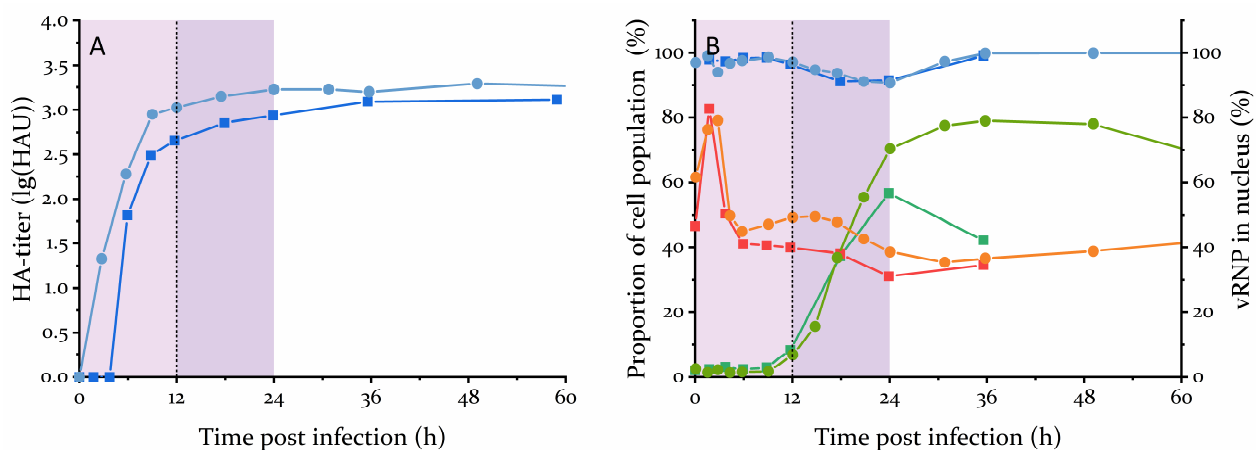


Figure 32 Influenza A virus titer and image stream analysis of infected MDCK cells.

Virus replication of two high MOI infections was monitored via HA titer of newly produced virus particles (A) and the intracellular virus replication dynamics of the vRNP particles and virus induced apoptosis quantified by image stream analysis (B). Experiment I: squares; experiment II circles. ■, ●: vRNP positive /infected cells; ■, ●: apoptotic cell; ■, ●: vRNP signal located in the nucleus. Early infection phase (48-60 h) and late infection phase (60-72 h) are highlighted in light and dark purple, respectively.

4.4.4 Dynamics of intracellular metabolite pools in MDCK.S8.E cells

Intracellular metabolites of the central carbon metabolism were quantified to analyze respective pool dynamics during cell growth phase in batch mode, as well as during IAV infection. Originally, we hoped to determine the impact of influenza virus infection on central carbon metabolism and identify possible metabolic bottlenecks for influenza virus replication. Therefore, high MOI infection for a synchronous infection was used to isolate effects of viral infection and compare these effects directly to a noninfected population. The resulting fast virus replication led to an almost immediate impact of the infection on the cellular growth and limited the time for sufficient data generation to approximately 24 h.

Energy metabolites and energy charge

Metabolite pools of the adenylate sugar nucleotides were quite stable during the cell growth lasting for at least 96 h for the growth curve and 24 hours for the infection cultivation, respectively. Strong effects on the energy metabolites were visible upon the later phase of the growth curve when cells were dying and in the late phase (12-24 hpi) of IAV infection (cellular apoptosis). Directly after infection metabolite pools and the adenylate energy charge stayed relatively stable for 12 hpi followed by a significant drop of ATP pools (Figure 33 A). In the first experiment almost no effect of virus infection on the AEC was visible whereas there was a significant drop of the energy charge in the second experiment at 12 hpi (Figure 33 D). It also seemed that the infection dynamic was slightly faster in the 2nd infection experiment, leading to a faster and more significant impact on all energy metabolites. In neither of the infection experiments a strong increase in ADP or AMP pools could be observed, like mock infected cells at the end of cultivation due to intracellular starvation responds (Figure 33 B,D). Since there was no substrate limitation for the infected cells the decrease in intracellular energy metabolites are due to virus induced changes, cellular apoptosis and necrosis. Interestingly, no stimulating effect on the general energy homeostasis was visible in the short time period after viral infection until significant virus release and the first apoptotic signals were detected (approx. 12 hpi). The collapse of energy supply in the later phase (12-24 hpi) of the infection was probably induced by cellular response to virus replication and cellular death or apoptosis respectively. Compared to adherent MDCK cells both AEC and adenosyl pools of MDCK.S8.E cells remained relatively stable, after influenza virus infection. For MDCK adherent cells strong reduction of AEC and ATP pools as well as an increase in intracellular ADP and AMP concentration was demonstrated [76]. It seemed that despite the massive effect of virus infection on cell growth and overall cellular biomass, no significant effect on the energy homeostasis of the cell was detected. This means that the cellular mechanism was able to keep intracellular energy supply intact which

might be necessary to maximize virus yield. However, this assumption is quite speculative since other studies with less productive cell lines are missing, and no other documented metabolic analysis using suspension cells has been published so far.

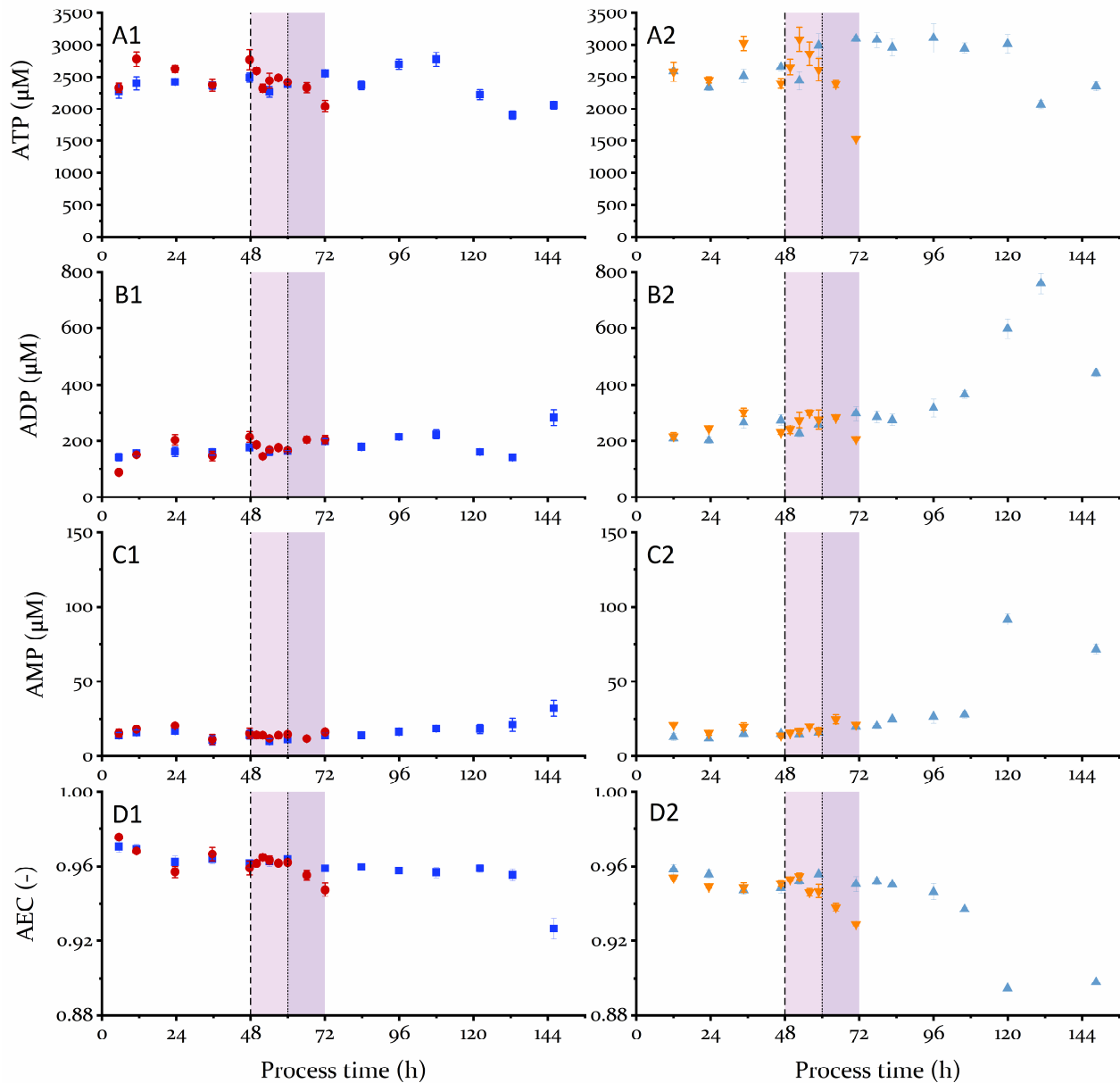


Figure 33: Intracellular metabolite pools of energy metabolites in MDCK cells.

Intracellular metabolite pools of ATP (A), ADP (B), AMP (C), and adenylate energy charge (D) of infected (●/▼) and mock infected (■/▲) MDCK.S8.E cells. Influenza A virus (ExpI: APR_O; ExpII: APR_SFM) was added for infection two days post inoculation (vertical line). Exp. I: first column (●/■); Exp. II: second column (▼/▲). Early infection phase (48-60 h) and late infection phase (60-72 h) are highlighted in light and dark purple, respectively. Error bars: standard deviation of technical triplicates.

Metabolites of glycolysis

The overall results of the intracellular metabolite pools of the glycolysis were similar between the two independent experiments. A depletion of basically all glycolytic pools was observed in the late phase of the mock infected cells, where cell growth stopped and viability started to drop (ExpI: 140 h; ExpII: 120 h) (Figure 29). This correlated nicely with the depletion of extracellular glucose for both experiments (Figure 30 A). Metabolite pools of the early glycolysis (G6P, F6P) especially showed a consistent trend between ExpI and ExpII both for mock and infected cells. Despite massive effects of virus infection on cell growth, viability and cellular biomass, G6P and F6P pools of infected cells remained surprisingly comparable to the respective pools of the mock infected cells (Figure 34 A,B). It seemed that these pools were more defined by the concentration of extracellular metabolites (i.e. glucose) rather than downstream metabolic activity. Similarly, an uncoupled upper glycolysis would lead to high concentrations of G6P and F6P, despite the fast depletion of downstream metabolite pools of glycolysis. However, this would suggest a virus induced reduced glucose consumption, which was not observed for infected MDCK cells (Figure 31 A). For metabolites of the lower glycolysis (F16BP, 3PG & PEP) a much more pronounced reduction, sometimes complete depletion of metabolites was detected in the 12 hpi, which in the most cases did not recover in the later infection phase (12-24 hpi) (Figure 34 C-E). In the first set of experiments this effect was much more visible, which might be due to a slower infection dynamic and a more pronounced effect in this case. The reduction of metabolite pools could either be induced by higher downstream demand and subsequent pool depletion which cannot be fueled via a faster glucose import. Alternatively, a fast reduction of PFK activity, could have led to an accumulation of G6P and F6P metabolites and downstream depletion of glycolytic metabolites. Higher demand for the glycosylation of viral surface proteins could increase the demand for metabolites of the hexosamine pathway which is branching from the glycolysis over F6P. Without the help of more detailed isotope-based flux analysis of the specific metabolites, or mathematical modelling it is impossible to draw further conclusions of what exactly the discrepancy between the upper and lower glycolysis is based on.

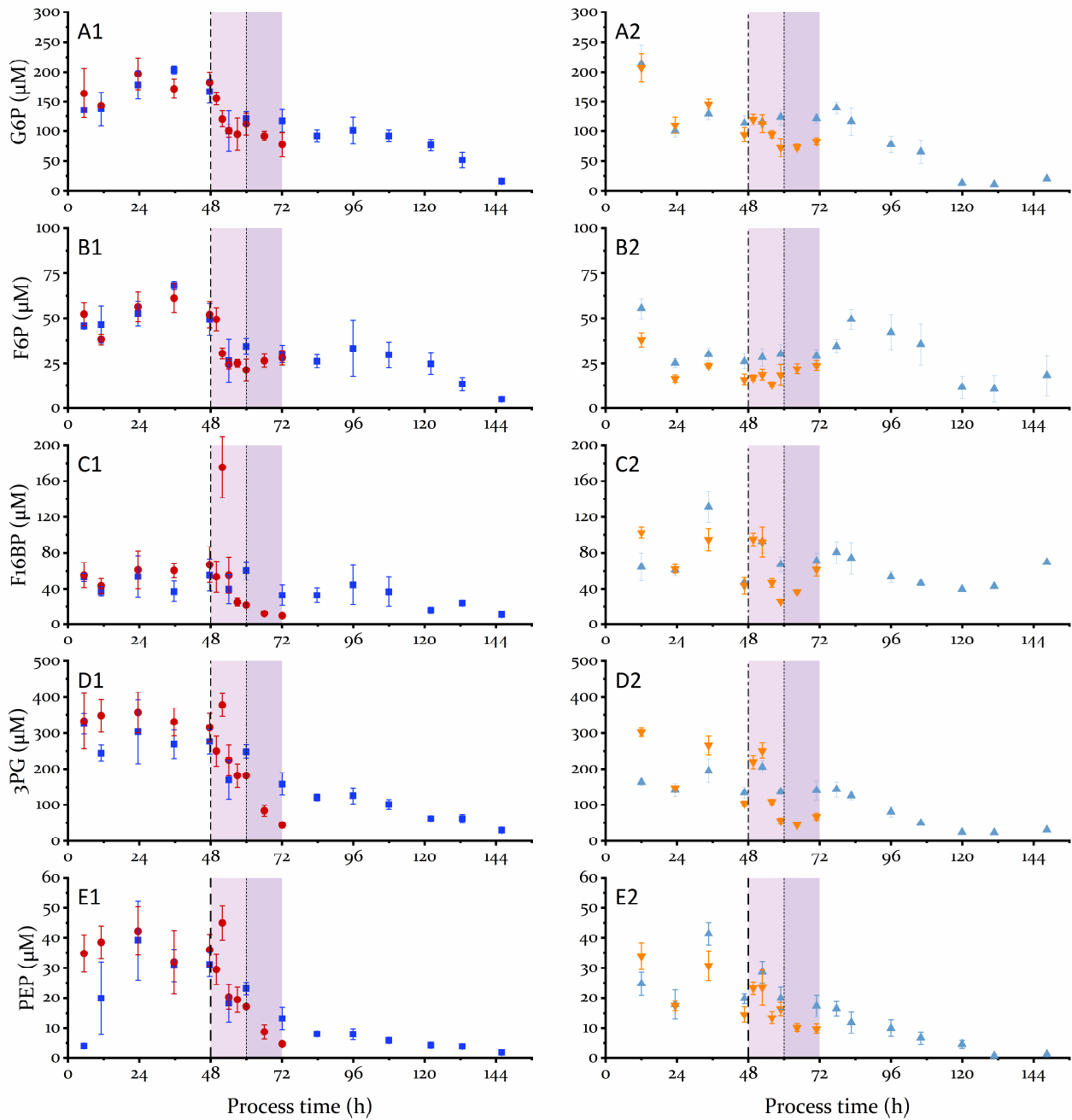


Figure 34: Intracellular metabolite pools of glycolytic metabolites in MDCK cells.

Intracellular concentration of glucose 6-P (A), fructose 6-P (B), fructose 1,6-BP (C), 3-phosphoglycerate (D), and phosphoenolpyruvate (E) of infected (●/▼) and mock infected (■/▲) MDCK.S8.E cells. Influenza A virus (ExpI: APR_O; ExpII: APR_SFM) was added for infection two days post inoculation (vertical line). Exp. I: first column (●/■); Exp. II: second column (▼/▲). Early infection phase (48-60 h) and late infection phase (60-72 h) are highlighted in light and dark purple, respectively. Error bars: standard deviation of technical triplicates.

TCA metabolites

Overall the metabolite pool dynamics of the TCA metabolites were comparable, both between the independent experiments and the infected and mock infected control (Figure 35). The only exception was succinate (Suc), where an accumulation was observed in the second experiment, whereas the pool in the first experiment was very low over the whole cultivation time (Figure 35 C). In the case of citrate, metabolite pools were basically identical despite major differences in cell growth between infected and mock infected MDCK.S8.E cells for both experiments. Due to the importance of the TCA for cellular anabolism it is quite surprising that a reduced cell growth and with this a reduced demand for precursors for cellular biomass did not lead to a reduced activity in the TCA. It seems that the virus replication replaces the demand of metabolites used both for energy supply and anabolism for the generation of biomass. Our observations also confirmed previous results obtained for MDCK adherent cells, where there was basically no differences between TCA metabolites (with exception of succinate) between citrate and α -ketoglutarate as representative metabolites of the TCA [76]. Other studies in A549 cells suggested an increased lipid metabolism which was fueled by TCA intermediates (i.e. citrate) as well [267]. However, our observation indicated no major alterations in this pathway.

Nucleotide sugars & ribose 5-phosphate

The only intermediate of the pentose phosphate pathway that could be quantitatively analysed was ribose 5-phosphate. In contrast to the upstream G6P metabolite pools of the glycolysis, R5P metabolite pools depleted shortly after virus infection (Figure 36 A). Due to the quite complex metabolic pathway of the PPP and an additional connection to the glycolysis over GAP a direct conclusion for the whole PPP-activity only based on R5P was not possible. However, higher demand of nucleotides, phospholipids as well as reduction equivalents for virus biosynthesis might have led to a depletion of this metabolite pool. Similar to R5P, UDP-glucose was reduced after IAV infection (Figure 36 B), both in the early (<12 hpi) and late (>12 hpi) infection phase. Since UDP-glucose is a precursor for glycogen biosynthesis, pool reduction could either be impacted by a depletion of cellular glycogen or a disconnection of the glycan biosynthesis and the glycolysis, reducing the UDP-glucose influx and maintaining high fructose 6-P levels. Intracellular concentration of UDP-GlcNAc and UDP-GalNAc were comparable to the mock control in the early infection phase (<12hpi). In case of ExpI both pools increased in the infection phase (Figure 36 C, D). Due to their involvement as precursors for the glycan biosynthesis (hexosamine pathway), an active glycan biosynthesis might be necessary to support the production of complex glycan structures of viral surface proteins (i.e.

HA). Both a reduction of UDP-glucose and R5P was not observed for adherent MDCK cells, where both pools remained stable upon influenza virus infection [76].

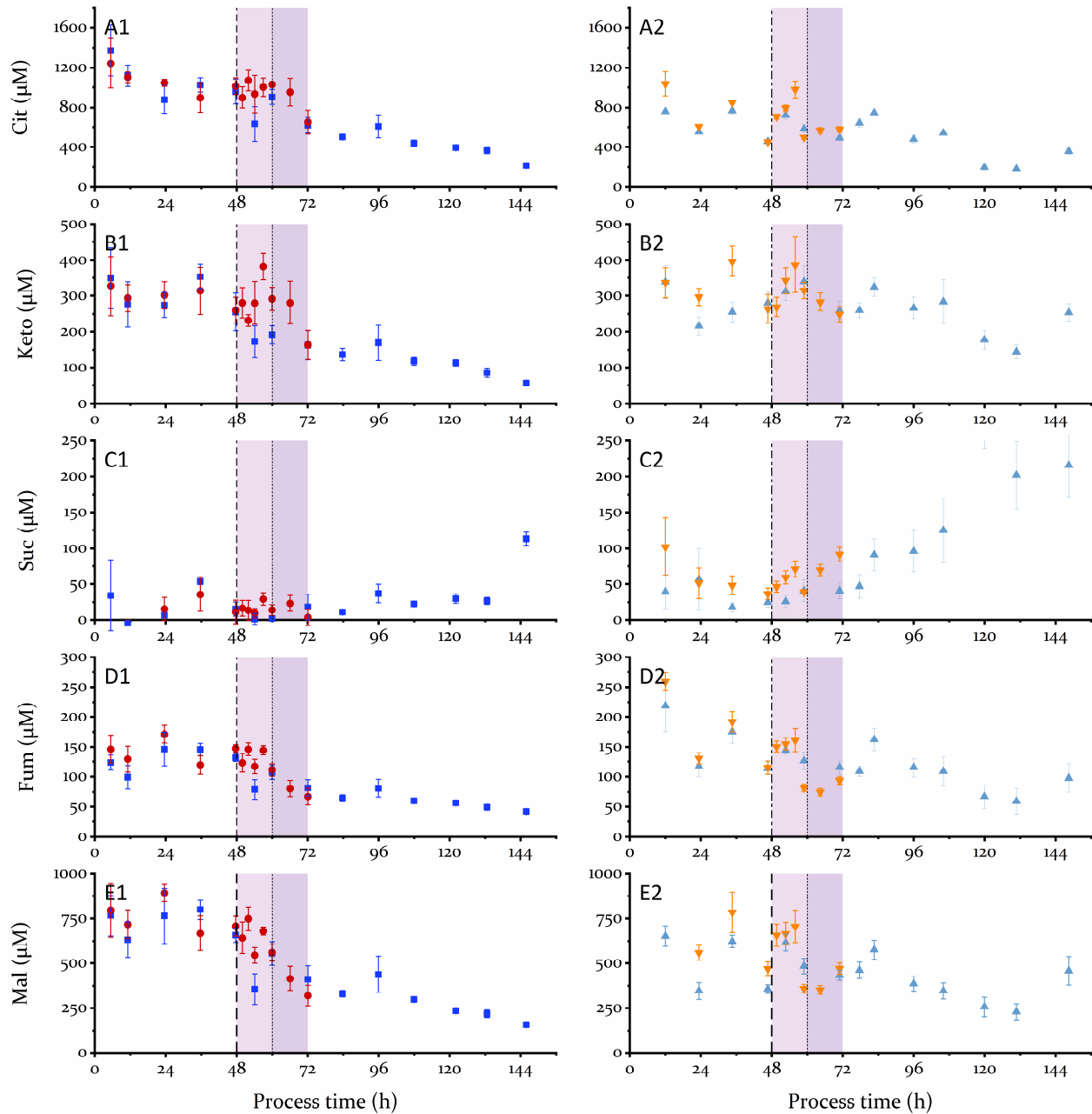


Figure 35: Intracellular metabolite pools of TCA metabolites in MDCK cells.

Intracellular concentration of citrate (A), α -ketoglutarate (B), succinate (C), fumarate (D), and malate (E) of infected (\bullet / ∇) and mock infected (\blacksquare / \blacktriangle) MDCK.S8.E cells. Influenza A virus (ExpI: APR_O; ExpII: APR_SFM) was added for infection two days post inoculation (vertical line). Exp. I: first column (\bullet / \blacksquare); Exp. II: second column (∇ / \blacktriangle). Early infection phase (48-60 h) and late infection phase (60-72 h) are highlighted in light and dark purple, respectively. Error bars: standard deviation of technical triplicates.

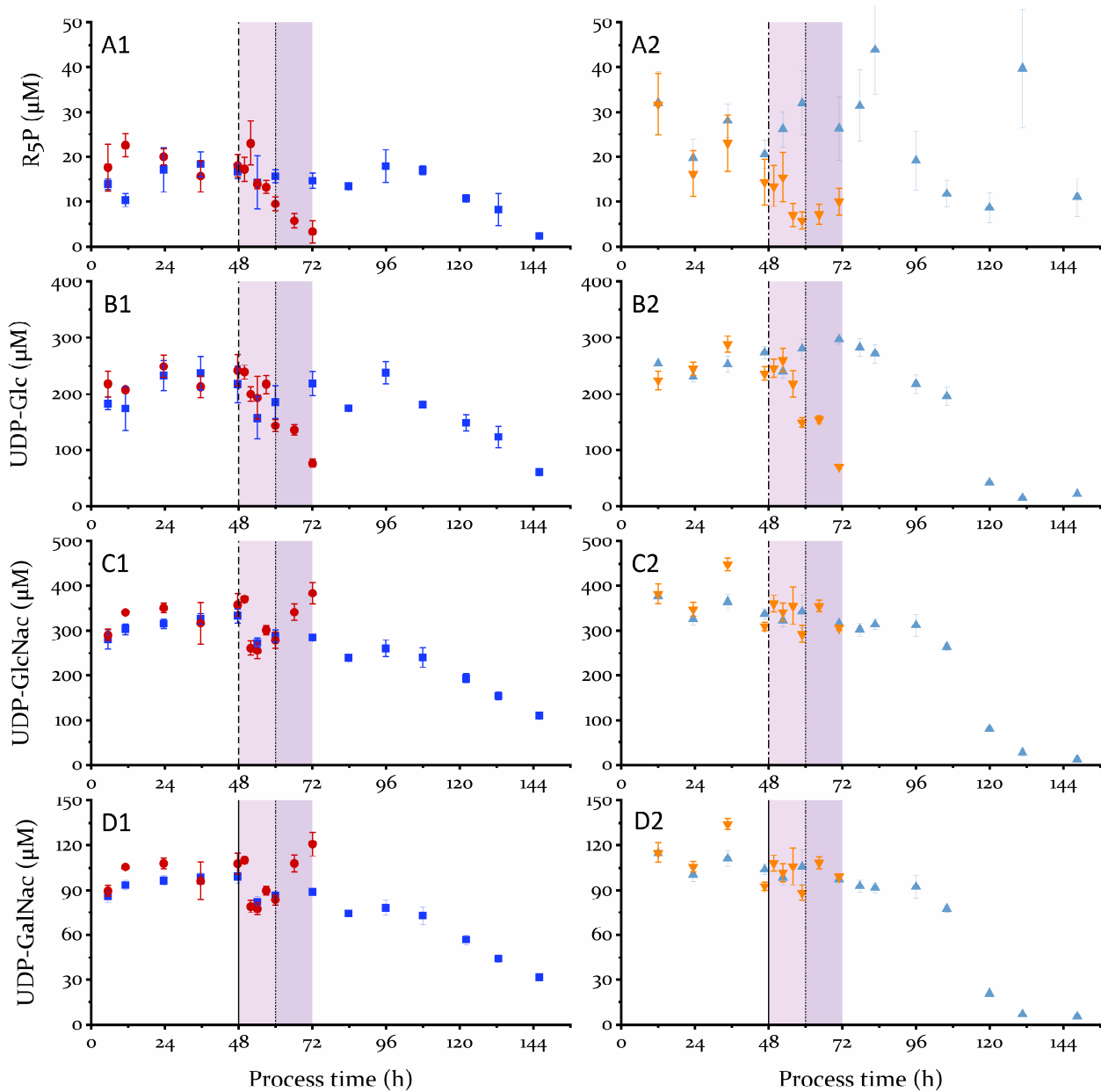


Figure 36: Intracellular metabolite pools of nucleotide sugars and ribose-P in MDCK cells.

Intracellular concentration of ribose 5-P (A), UDP-glucose (B), UDP-N-acetylglucosamine (C), UDP-N-acetylgalactosamine (D) of infected (●/▼) and mock infected (■/▲) MDCK.S8.E cells. Influenza A virus (ExpI: APR_O; EXP II: APR_SF M) was added for infection two days post inoculation (vertical line). Exp. I: first column (●/■); Exp. II: second column (▼/▲). Early infection phase (48-60 h) and late infection phase (60-72 h) are highlighted in light and dark purple, respectively. Error bars: standard deviation of technical triplicates.

4.4.5 Overall effects of influenza A virus infection on MDCK metabolism

Similar to the MDCK adherent cells, direct effects of IAV infection on the central carbon metabolism were quite limited during period of virus replication (12 h), before the onset of virus induced apoptosis [76]. Intracellular metabolite pools suggested some effect on the lower glycolysis, pentose phosphate pathway and glycogen metabolism. Since they are all fueled over G6P and F6P of the upper glycolysis we can assume some kind of virus induced alteration at this stage. Surprisingly, the specific glucose consumption rate of the infected cells was only slightly increased after infection what would suggest a redirection of metabolites to other pathways. Part of the consumed glucose might have been funneled to the glycan biosynthesis which did not show any signs of altered pool content. Other pathways like the TCA seemed not to be affected at all by the virus infection and metabolite pool concentrations were basically identical between infected and mock infected MDCK cells for many intermediates. Due to the massive impact of the virus on cell growth, no or only minor alterations of intracellular metabolite pools is quite surprising. It seemed the IAV replication uses cellular resources to switch the cellular metabolism from a cell division state to a virus production state, with only small alterations of the central carbon metabolism in general. With a SCVY of 10,000 virus particles per host cell the estimated total virus volume only comprises 0.2 % of the cell volume. However, this tiny volume fraction contains roughly 2 % of the cellular protein and 50 % of the cellular surface area. Nevertheless, theoretical evaluation of IAV replication indicate that the energetic burden of the virus production should be neglectable (1 %) compared to the energy capacity of the host cell [341]. This might explain the small metabolite pool alterations observed in our experiments. Furthermore, small changes of the metabolite pools might have been overshadowed by intracellular pool dynamics caused by changes in substrate concentrations.

5 Conclusion

The aim of this thesis was to elucidate the potential of a new MDCK cultivation medium for MDCK based influenza vaccine manufacturing and to investigate the metabolic effects of IAV infection on MDCK suspension cells. The new cultivation medium for MDCK suspension cells (Xeno-CDM) solved many limitations observed with the MDCK suspension cell line (MDCK.S8.E) used previously in our research laboratory (i.e. low μ , low VCC_{max} , cell aggregates, bad scalability to STR). This cultivation medium enabled significant improvements in productivity, higher cellular biomass in standard batch processes and it enabled (for the first time) the establishment of (semi-) perfusion processes for MDCK suspension cells. With the help of metabolic profiling, we hoped to identify metabolic bottlenecks of virus replication in MDCK cells to identify options for cell line engineering for a cell line with improved virus replication capabilities.

Improved productivity for influenza A virus production with MDCK cells

Fast virus replication and high cell specific virus productivity has made the MDCK cells to one of the best candidates for influenza virus propagation and is already used for cell culture-based vaccine manufacturing [31]. With the use of the new cultivation media (Xeno) for MDCK suspension cells, the overall cell growth performance and virus productivity was improved significantly. In Xeno medium MDCK suspension cells were growing as single cells with a higher growth rate and to higher cell concentrations than in other reported media before. This enabled the cultivation of MDCK cells in high cell density in semi-perfusion, reaching the highest documented cell concentration for MDCK cells (60×10^6 cells/mL). In addition, this small-scale experiment proved that intensified, high cell density processes are able to improve both overall virus titer and productivity significantly, avoiding the high cell density effect. Despite the fact, that perfusion processes were already reported for other cell lines used for IAV production, the lack of high cell specific virus productivity ($> 10,000$ virions/cell) was limiting virus titers and hence productivity. Only the combination of fast growing, highly productive MDCK suspension cells (i.e. MDCK.Xe.E) and high cell density (semi-)perfusion process enabled HA titers exceeding 4 lg(HAU). This exceeded results reported previously for MDCK cell-based influenza virus propagation by far and is suggesting MDCK cells-based perfusion cultures as valid process option to intensify viral vaccine manufacturing.

With the acquisition of the ATCC derived MDCK suspension cell line and a chemically defined version of the Xeno medium from our cooperation partner, it was possible to directly compare both cell lines (ATCC and ECACC derived) adapted to both Smif8 and Xeno medium. Despite the long time needed for adaptation, the cellular morphology and growth profile were quite similar between the cell lines in the same cultivation medium. The medium clearly had major effects on the cell morphology, cell growth, metabolism and maximal cell concentration. In direct comparison of Smif8 and Xeno-CDM medium, the latter supported higher growth rate, higher cell concentration, lactate consumption and single cell suspension. Differences between the cell lines in the same cultivation medium were minor. However, cell specific virus yield depended more on the cell line than the cultivation medium. Of all the analyzed cell lines the MDCK.Xe.A cell lines had the highest cell specific productivity (HA based), resulting in combination with high cell concentration in the highest virus titer of the analyzed cell lines. Furthermore, the cultivation of the MDCK.Xe.A cell line was easily transferable to a lab scale bioreactor, which is crucial for possible application in large scale manufacturing.

The MDCK.Xe.A suspension cell line, showed excellent growth performance in STR systems, enabling the batch cultivation of MDCK suspension cells in chemically defined media up to 12×10^6 cells/mL in a bioreactor, for the first time. This led to the development of a robust, scalable and productive manufacturing process for an influenza vaccine candidate with a simple fed-batch process design. A fully characterized upstream process with respect to cell growth, intracellular and extracellular virus propagation, cellular metabolism as well as main host cell contaminants, eased the identification of an optimal harvest point for process integration. The optimization of the whole process stream allowed us to reduce host cell contaminants from harvest and final purified IAV product and improved product quality significantly compared to a process used previously. High productivity, process simplicity and low cost is crucial for the application of such a production process for fast influenza vaccine manufacturing in a pandemic scenario. Most likely, this process can be applied for large scale manufacturing with only minor adjustments to boost production capabilities for influenza vaccines for pandemic preparedness. Furthermore, such an cell culture-based process with similar productivity might be economically competitive to egg-based manufacturing as well. Since many developing countries are seeking to establish new national vaccine manufacturing concepts for a still increasing demand, the findings of this work are important to shape future influenza vaccine manufacturing strategies.

Metabolic profiling of influenza A virus infected MDCK cells

Metabolic profiling of MDCK suspension cells during IAV infection as well as for a standard batch growth curve did not yield obvious metabolic bottlenecks for cell growth or influenza virus replication. The interpretation of the intracellular pool dynamics without a holistic interpretation strategy using metabolic network modeling was difficult. Advanced mathematical modelling of metabolic networks requires further computational skills and therefore the modelling is part of another PhD project (João Rodrigues Correia Ramos). Furthermore, fast influenza virus replication limited the analysis space to a very short time period (12 h) to evaluate intracellular metabolite pools of infected MDCK suspension cells. Similar problems were already addressed in the metabolic analysis of infected adherent MDCK cells in a previous study. In neither of these studies major metabolic alterations caused by viral infection were identified, which would support either medium supplementation or metabolic engineering strategies to improve virus titer. Advanced metabolic flux analysis might give a better understanding about the specific metabolic flux distribution as already shown for other cell lines [215,342-344]. This might lead to a better insight, however, there is no concrete evidence supporting further investigations in this area which could lead to an improved cell specific virus productivity. It is also not clear, if differences in metabolic activity can truly be quantified with the help of metabolic profiling. When analyzing the two MDCK cell lines MDCK.S8.E and MDCK.Xe.E for the development of the quenching methods, no major differences in the metabolite pools of the central carbon metabolism were detected, despite major differences in cellular performance in the different media. We would have expected to see these differences also reflected in the metabolite pools. The major challenge to profile the metabolism of IAV infected cells, MDCK specifically, was the very fast virus replication. It seemed that the viral replication machinery took over, at least part of the cellular metabolism used for the generation of cellular biomass. For influenza virus a fast replication might be evolutionary beneficial, especially in an artificial replication system like mammalian cells, where the cellular interferon system is the only line of defense against pathogens. Fast virus replication, however, doesn't give a lot of room for significant virus metabolic changes that might in the end not improve virus replication due to an induced interferon response. Consequently, viruses with a slower replication cycle (e.g. yellow fever virus or Modified Vaccinia Ankara) might give more possibility to investigate metabolic changes due to the virus replication.

6 Outlook

Although the metabolic profiling of MDCK suspension cells did not lead to obvious targets for metabolic engineering, further knowledge might be generated with the help of metabolic network modeling. A metabolic model would ease the comparison of the whole system dynamics between an infected and non-infected cell population. Metabolic profiling proved to be a good tool to analyze and model the metabolic network of mammalian cells responding to extracellular and intracellular stimuli in normal cultivation scenario. For the investigation of metabolic affects in an influenza virus infected MDCK cell, however, this might come to its limits. Metabolic flux analysis, preferably supported by isotope labeled substrates, might be able to elucidate changes in intracellular fluxes due to viral infection. However, a comparatively large analytical effort would be necessary with only minor chances to find metabolic engineering targets for improved virus productivity.

If we look at the potential of media design, cell line development, and process engineering for higher product titer and increased productivity, it is not expected that metabolic engineering will lead to significant improvements. Especially, the use of perfusion processes can help to boost space time yield significantly, reducing the need for large process scales (> 10.000 L). For this, the scale-up of the designed perfusion process into a lab-scale bioreactor would be the logical next step, to confirm both cell growth and virus yields in a scalable system. In a “real” perfusion system with filtration retention devices (i.e. ATF and TFF), where the virus can be retained in the cultivation broth, similar virus titers as for the accumulated virus titer calculated for semi-perfusion cultures are to be expected. Other retention devices (i.e. inclined & acoustic settler) [345-347], where the virus can be transferred to the permeate, might be beneficial to remove virus continuously from the bioreactor. Additionally, even higher cell concentrations should be feasible with a continuous controlled perfusion flow, to further improve process productivity. In the very end of this thesis such a process was already successfully established together with a PhD student from ECUST, and further characterization will be part of her PhD thesis [348].

Similar to the designed fed-batch production process an integrated process optimization might give additional insights in potential challenges for vaccine manufacturing using perfusion. High host cell contaminations, viral antigen stability in extended culture, product recovery from permeate, cell retention devices as well as product quality might be addressed in such a study. So far, perfusion processes are mainly applied for recombinant protein production and are not yet used in

commercial vaccine manufacturing. Detailed research in this area might not only give information of additional and innovative production methods but also support other cell culture-based commercial virus production. Furthermore, this kind of investigation might give useful results not only for the vaccine manufacturing industry but also for the growing gene-therapy and oncolytic virus sectors where similar challenges for the generation of high dose applications have to be addressed.

For a more detailed characterization of influenza viruses derived from the different MDCK cell lines, the analysis of the viral glycosylation and immunogenicity might give additional insight into the role of HA and NA glycan for the efficacy of a cell culture-derived vaccine. In a preliminary study (not shown in this work), the glycan profiles of the HA-antigen showed significant differences between the used cultivation media and MDCK cell lines. It would be important to know, if these differences affect the efficacy of a whole virus, split, or subunit vaccines for the use of an appropriate host cell line and the design of an improved virus replication medium. A detailed comparison of the viral glycan structures in combination with animal immunization studies might give new insights into the role of viral glycan structures for vaccine efficacy.

7 References

1. Blume, S.; Geesink, I. A Brief History of Polio Vaccines. *Science* **2000**, *288*, 1593-1594, doi:10.1126/science.288.5471.1593.
2. Barrett, P.N.; Mundt, W.; Kistner, O.; Howard, M.K. Vero cell platform in vaccine production: moving towards cell culture-based viral vaccines. *Expert Review of Vaccines* **2009**, *8*, 607-618, doi:10.1586/erv.09.19.
3. Birch, J.R.; Onakunle, Y. Biopharmaceutical Proteins. In *Therapeutic Proteins: Methods and Protocols*, **2005**, 1-16, doi:10.1385/1-59259-922-2:001.
4. Ecker, D.M.; Jones, S.D.; Levine, H.L. The therapeutic monoclonal antibody market. *mAbs* **2015**, *7*, 9-14, doi:10.4161/19420862.2015.989042.
5. Alldread, R.M.; Birch, J.R.; Metcalfe, H.K.; Farid, S.; Racher, A.J.; Young, R.J.; Khan, M. Large Scale Suspension Culture of Mammalian Cells. In *Industrial Scale Suspension Culture of Living Cells* **2014**, 410-462, doi:10.1002/9783527683321.ch12.
6. Wurm, F.M. Production of recombinant protein therapeutics in cultivated mammalian cells. *Nature Biotechnology* **2004**, *22*, 1393-1398, doi:10.1038/nbt1026.
7. Chon, J.H.; Zarbis-Papastoitis, G. Advances in the production and downstream processing of antibodies. *New Biotechnology* **2011**, *28*, 458-463, doi:10.1016/j.nbt.2011.03.015.
8. Kim, J.Y.; Kim, Y.G.; Lee, G.M. CHO cells in biotechnology for production of recombinant proteins: Current state and further potential. *Applied microbiology and biotechnology* **2012**, *93*, 917-930, doi:10.1007/s00253-011-3758-5.
9. Ginn, S.L.; Amaya, A.K.; Alexander, I.E.; Edelstein, M.; Abedi, M.R. Gene therapy clinical trials worldwide to 2017: An update. *The Journal of Gene Medicine* **2018**, *20*, e3015, doi:10.1002/jgm.3015.
10. Merten, O.-W.; Gaillet, B. Viral vectors for gene therapy and gene modification approaches. *Biochemical Engineering Journal* **2016**, *108*, 98-115, doi:10.1016/j.bej.2015.09.005.
11. Genzel, Y. Designing cell lines for viral vaccine production: Where do we stand? *Biotechnology Journal* **2015**, *10*, 728-740, doi:10.1002/biot.201400388.
12. Butler, M. Animal cell cultures: recent achievements and perspectives in the production of biopharmaceuticals. *Applied microbiology and biotechnology* **2005**, *68*, 283-291, doi:10.1007/s00253-005-1980-8.
13. Gallo-Ramirez, L.E.; Nikolay, A.; Genzel, Y.; Reichl, U. Bioreactor concepts for cell culture-based viral vaccine production. *Expert Rev Vaccines* **2015**, *14*, 1181-1195, doi:10.1586/14760584.2015.1067144.
14. Sharon, D.; Kamen, A. Advancements in the design and scalable production of viral gene transfer vectors. *Biotechnology and bioengineering* **2018**, *115*, 25-40, doi:10.1002/bit.26461.
15. Merten, O.W.; Bakker, W.A.; Vorlop, J.; Reiter, M.; Visnovsky, G.; Jäger, V.; Merabishvili, M.; Reichl, U. Virus Production Under Suspension Conditions. In *Industrial Scale Suspension Culture of Living Cells*, **2014**, 503-554.
16. Griffiths, B. Scale-up of suspension and anchorage-dependent animal cells. *Applied Biochemistry and Biotechnology - Part B Molecular Biotechnology* **2001**, *17*, 225-238, doi:10.1385/MB:17:3:225.
17. Legmann, R.; Schreyer, H.B.; Combs, R.G.; McCormick, E.L.; Russo, A.P.; Rodgers, S.T. A predictive high-throughput scale-down model of monoclonal antibody production in CHO cells. *Biotechnology and bioengineering* **2009**, *104*, 1107-1120, doi:10.1002/bit.22474.
18. Chisti, Y.; Moo-Young, M. Bioprocess intensification through bioreactor engineering. *Chemical Engineering Research and Design* **1996**, *74*, 575-583.
19. Tapia, F.; Vázquez-Ramírez, D.; Genzel, Y.; Reichl, U. Bioreactors for high cell density and continuous multi-stage cultivations: options for process intensification in cell culture-based viral vaccine production. *Applied microbiology and biotechnology* **2016**, *100*, 2121-2132, doi:10.1007/s00253-015-7267-9.
20. Walther, J.; Godawat, R.; Hwang, C.; Abe, Y.; Sinclair, A.; Konstantinov, K. The business impact of an integrated continuous biomanufacturing platform for recombinant protein production. *Journal of biotechnology* **2015**, *213*, 3-12, doi:10.1016/j.jbiotec.2015.05.010.

21. Rameez, S.; Mostafa, S.S.; Miller, C.; Shukla, A.A. High-throughput miniaturized bioreactors for cell culture process development: Reproducibility, scalability, and control. *Biotechnology progress* **2014**, *30*, 718-727, doi:10.1002/btpr.1874.
22. Shukla, A.A.; Hubbard, B.; Tressel, T.; Guhan, S.; Low, D. Downstream processing of monoclonal antibodies-Application of platform approaches. *Journal of Chromatography B: Analytical Technologies in the Biomedical and Life Sciences* **2007**, *848*, 28-39, doi:10.1016/j.jchromb.2006.09.026.
23. Wolf, M.W.; Reichl, U. Downstream processing of cell culture-derived virus particles. *Expert Review of Vaccines* **2011**, *10*, 1451-1475, doi:10.1586/erv.11.111.
24. Warikoo, V.; Godawat, R.; Brower, K.; Jain, S.; Cummings, D.; Simons, E.; Johnson, T.; Walther, J.; Yu, M.; Wright, B., et al. Integrated continuous production of recombinant therapeutic proteins. *Biotechnology and bioengineering* **2012**, *109*, 3018-3029, doi:10.1002/bit.24584.
25. Shukla, A.A.; Gottschalk, U. Single-use disposable technologies for biopharmaceutical manufacturing. *Trends in biotechnology* **2013**, *31*, 147-154, doi:10.1016/j.tibtech.2012.10.004.
26. Farid, S.S.; Washbrook, J.; Titchener-Hooker, N.J. Decision-support tool for assessing biomanufacturing strategies under uncertainty: Stainless steel versus disposable equipment for clinical trial material preparation. *Biotechnology progress* **2005**, *21*, 486-497, doi:10.1021/bp049692b.
27. Langer, E.S.; Rader, R.A. Single-use technologies in biopharmaceutical manufacturing: A 10-year review of trends and the future. *Engineering in Life Sciences* **2014**, *14*, 238-243, doi:10.1002/elsc.201300090.
28. Hildinger, M.; Baldi, L.; Stettler, M.; Wurm, F.M. High-titer, serum-free production of adeno-associated virus vectors by polyethyleneimine-mediated plasmid transfection in mammalian suspension cells. *Biotechnology letters* **2007**, *29*, 1713-1721, doi:10.1007/s10529-007-9441-3.
29. Clément, N.; Knop, D.R.; Byrne, B.J. Large-scale adeno-associated viral vector production using a herpesvirus-based system enables manufacturing for clinical studies. *Human Gene Therapy* **2009**, *20*, 796-806, doi:10.1089/hum.2009.094.
30. Ansoerge, S.; Lanthier, S.; Transfiguracion, J.; Durocher, Y.; Henry, O.; Kamen, A. Development of a scalable process for high-yield lentiviral vector production by transient transfection of HEK293 suspension cultures. *The Journal of Gene Medicine* **2009**, *11*, 868-876, doi:10.1002/jgm.1370.
31. Doroshenko, A.; Halperin, S.A. Trivalent MDCK cell culture-derived influenza vaccine Optaflu® (Novartis Vaccines). *Expert Review of Vaccines* **2009**, *8*, 679-688, doi:10.1586/erv.09.31.
32. Trombetta, C.M.; Marchi, S.; Manini, I.; Lazzeri, G.; Montomoli, E. Challenges in the development of egg-independent vaccines for influenza. *Expert Review of Vaccines* **2019**, *18*, 737-750, doi:10.1080/14760584.2019.1639503.
33. Buckland, B.C. The development and manufacture of influenza vaccines. *Human Vaccines & Immunotherapeutics* **2015**, *11*, 1357-1360, doi:10.1080/21645515.2015.1026497.
34. Audsley, J.M.; Tannock, G.A. The role of cell culture vaccines in the control of the next influenza pandemic. *Expert Opinion on Biological Therapy* **2004**, *4*, 709-717, doi:10.1517/14712598.4.5.709.
35. Genzel, Y.; Reichl, U. Continuous cell lines as a production system for influenza vaccines. *Expert Review of Vaccines* **2009**, *8*, 1681-1692, doi:10.1586/erv.09.128.
36. Skowronski, D.M.; Janjua, N.Z.; De Serres, G.; Sabaiduc, S.; Eshaghi, A.; Dickinson, J.A.; Fonseca, K.; Winter, A.-L.; Gubbay, J.B.; Krajdén, M., et al. Low 2012-13 Influenza Vaccine Effectiveness Associated with Mutation in the Egg-Adapted H3N2 Vaccine Strain Not Antigenic Drift in Circulating Viruses. *PLoS one* **2014**, *9*, e92153, doi:10.1371/journal.pone.0092153.
37. Schild, G.C.; Oxford, J.S.; de Jong, J.C.; Webster, R.G. Evidence for host-cell selection of influenza virus antigenic variants. *Nature* **1983**, *303*, 706-709, doi:10.1038/303706a0.
38. Zost, S.J.; Parkhouse, K.; Gumina, M.E.; Kim, K.; Diaz Perez, S.; Wilson, P.C.; Treanor, J.J.; Sant, A.J.; Cobey, S.; Hensley, S.E. Contemporary H3N2 influenza viruses have a glycosylation site that alters binding of antibodies elicited by egg-adapted vaccine strains. *Proceedings of the National Academy of Sciences* **2017**, *114*, 12578-12583, doi:10.1073/pnas.1712377114.
39. Ernest, M.; Kamen, A.A. Current and Emerging Cell Culture Manufacturing Technologies for Influenza Vaccines. *BioMed Research International* **2015**, *11*, doi:10.1155/2015/504831.
40. Cox, M.M.J.; Hollister, J.R. FluBlok, a next generation influenza vaccine manufactured in insect cells. *Biologicals* **2009**, *37*, 182-189, doi:10.1016/j.biologicals.2009.02.014.
41. Pau, M.G.; Ophorst, C.; Koldijk, M.H.; Schouten, G.; Mehtali, M.; Uytdehaag, F. The human cell line PER.C6 provides a new manufacturing system for the production of influenza vaccines. *Vaccine* **2001**, *19*, 2716-2721, doi:10.1016/S0264-410X(00)00508-9.

-
42. Genzel, Y.; Behrendt, I.; Rödig, J.; Rapp, E.; Kueppers, C.; Kochanek, S.; Schiedner, G.; Reichl, U. CAP, a new human suspension cell line for influenza virus production. *Applied microbiology and biotechnology* **2013**, *97*, 111-122, doi:10.1007/s00253-012-4238-2.
 43. Schuind, A.; Segall, N.; Drame, M.; Innis, B.L. Immunogenicity and Safety of an EB66 Cell-Culture-Derived Influenza A/Indonesia/5/2005(H5N1) AS03-Adjuvanted Vaccine: A Phase 1 Randomized Trial. *The Journal of Infectious Diseases* **2015**, *212*, 531-541, doi:10.1093/infdis/jiv091.
 44. Peschel, B.; Frentzel, S.; Laske, T.; Genzel, Y.; Reichl, U. Comparison of influenza virus yields and apoptosis-induction in an adherent and a suspension MDCK cell line. *Vaccine* **2013**, *31*, 5693-5699, doi:10.1016/j.vaccine.2013.09.051.
 45. Dukes, J.D.; Whitley, P.; Chalmers, A.D. The MDCK variety pack: choosing the right strain. *BMC Cell Biology* **2011**, *12*, 43, doi:10.1186/1471-2121-12-43.
 46. Genzel, Y.; Olmer, R.M.; Schäfer, B.; Reichl, U. Wave microcarrier cultivation of MDCK cells for influenza virus production in serum containing and serum-free media. *Vaccine* **2006**, *24*, 6074-6087, doi:10.1016/j.vaccine.2006.05.023.
 47. Hu, A.Y.-C.; Weng, T.-C.; Tseng, Y.-F.; Chen, Y.-S.; Wu, C.-H.; Hsiao, S.; Chou, A.-H.; Chao, H.-J.; Gu, A.; Wu, S.-C., et al. Microcarrier-based MDCK cell culture system for the production of influenza H5N1 vaccines. *Vaccine* **2008**, *26*, 5736-5740, doi:10.1016/j.vaccine.2008.08.015.
 48. Bock, A.; Sann, H.; Schulze-Horsel, J.; Genzel, Y.; Reichl, U.; Möhler, L. Growth behavior of number distributed adherent MDCK cells for optimization in microcarrier cultures. *Biotechnology progress* **2009**, *25*, 1717-1731, doi:doi:10.1002/btpr.262.
 49. Genzel, Y.; Fischer, M.; Reichl, U. Serum-free influenza virus production avoiding washing steps and medium exchange in large-scale microcarrier culture. *Vaccine* **2006**, *24*, 3261-3272, doi:10.1016/j.vaccine.2006.01.019.
 50. Huang, D.; Zhao, L.; Tan, W. Adherent and single-cell suspension culture of Madin-Darby canine kidney cells in serum-free medium. *Sheng Wu Gong Cheng Xue Bao* **2011**, *27*, 645-652.
 51. Chu, C.; Lugovtsev, V.; Golding, H.; Betenbaugh, M.; Shiloach, J. Conversion of MDCK cell line to suspension culture by transfecting with human siat7e gene and its application for influenza virus production. *Proceedings of the National Academy of Sciences* **2009**, *106*, 14802-14807, doi:10.1073/pnas.0905912106.
 52. van Wielink, R.; Kant-Eenbergen, H.C.M.; Harmsen, M.M.; Martens, D.E.; Wijffels, R.H.; Coco-Martin, J.M. Adaptation of a Madin-Darby canine kidney cell line to suspension growth in serum-free media and comparison of its ability to produce avian influenza virus to Vero and BHK21 cell lines. *Journal of Virological Methods* **2011**, *171*, 53-60, doi:10.1016/j.jviromet.2010.09.029.
 53. Lohr, V.; Genzel, Y.; Behrendt, I.; Scharfenberg, K.; Reichl, U. A new MDCK suspension line cultivated in a fully defined medium in stirred-tank and wave bioreactor. *Vaccine* **2010**, *28*, 6256-6264, doi:10.1016/j.vaccine.2010.07.004.
 54. Gröner, A.; Vorlop, J. Animal cells and processes for the replication of influenza viruses. *International patent* **1997**, WO 97/37000.
 55. Castro, R.; Fernandes, P.; Laske, T.; Sousa, M.F.Q.; Genzel, Y.; Scharfenberg, K.; Alves, P.M.; Coroadinha, A.S. Production of canine adenovirus type 2 in serum-free suspension cultures of MDCK cells. *Applied microbiology and biotechnology* **2015**, *99*, 7059-7068, doi:10.1007/s00253-015-6636-8.
 56. Sharfstein, S.T. Advances in Cell Culture Process Development: Tools and Techniques for Improving Cell Line Development and Process Optimization. *Biotechnology progress* **2008**, *24*, 727-734, doi:10.1021/bp070471q.
 57. Heath, C.; Kiss, R. Cell Culture Process Development: Advances in Process Engineering. *Biotechnology progress* **2007**, *23*, 46-51, doi:10.1021/bp060344e.
 58. Lewis, A.M.; Abu-Absi, N.R.; Borys, M.C.; Li, Z.J. The use of 'Omics technology to rationally improve industrial mammalian cell line performance. *Biotechnology and bioengineering* **2016**, *113*, 26-38, doi:10.1002/bit.25673.
 59. Datta, P.; Linhardt, R.J.; Sharfstein, S.T. An 'omics approach towards CHO cell engineering. *Biotechnology and bioengineering* **2013**, *110*, 1255-1271, doi:10.1002/bit.24841.
 60. Kildegaard, H.F.; Baycin-Hizal, D.; Lewis, N.E.; Betenbaugh, M.J. The emerging CHO systems biology era: harnessing the 'omics revolution for biotechnology. *Current opinion in biotechnology* **2013**, *24*, 1102-1107, doi:10.1016/j.copbio.2013.02.007.
 61. Griffin, T.J.; Seth, G.; Xie, H.; Bandhakavi, S.; Hu, W.-S. Advancing mammalian cell culture engineering using genome-scale technologies. *Trends in biotechnology* **2007**, *25*, 401-408, doi:10.1016/j.tibtech.2007.07.004.

62. Wuest, D.M.; Harcum, S.W.; Lee, K.H. Genomics in mammalian cell culture bioprocessing. *Biotechnology Advances* **2012**, *30*, 629-638, doi:10.1016/j.biotechadv.2011.10.010.
63. Gupta, P.; Lee, K.H. Genomics and proteomics in process development: opportunities and challenges. *Trends in biotechnology* **2007**, *25*, 324-330, doi:10.1016/j.tibtech.2007.04.005.
64. Vishwanathan, N.; Le, H.; Le, T.; Hu, W.-S. Advancing biopharmaceutical process science through transcriptome analysis. *Current opinion in biotechnology* **2014**, *30*, 113-119, doi:10.1016/j.copbio.2014.06.011.
65. Schaub, J.; Clemens, C.; Schorn, P.; Hildebrandt, T.; Rust, W.; Mennerich, D.; Kaufmann, H.; Schulz, T.W. CHO gene expression profiling in biopharmaceutical process analysis and design. *Biotechnology and bioengineering* **2010**, *105*, 431-438, doi:10.1002/bit.22549.
66. Meleady, P. Proteomic profiling of recombinant cells from large-scale mammalian cell culture processes. *Cytotechnology* **2007**, *53*, 23-31, doi:10.1007/s10616-007-9052-9.
67. Dickson, A.J. Enhancement of production of protein biopharmaceuticals by mammalian cell cultures: the metabolomics perspective. *Current opinion in biotechnology* **2014**, *30c*, 73-79, doi:10.1016/j.copbio.2014.06.004.
68. Vernardis, S.I.; Goudar, C.T.; Klapa, M.I. Metabolic profiling reveals that time related physiological changes in mammalian cell perfusion cultures are bioreactor scale independent. *Metabolic engineering* **2013**, *19*, 1-9, doi:10.1016/j.ymben.2013.04.005.
69. Aranibar, N.; Reily, M.D. NMR Methods for Metabolomics of Mammalian Cell Culture Bioreactors. In *Animal Cell Biotechnology: Methods and Protocols*, Pörtner, R., Ed. Humana Press **2014**, 223-236, doi:10.1007/978-1-62703-733-4_15.
70. Patti, G.J.; Yanes, O.; Siuzdak, G. Innovation: Metabolomics: the apogee of the omics trilogy. *Nature reviews. Molecular cell biology* **2012**, *13*, 263-269, doi:10.1038/nrm3314.
71. Patti, G.J.; Yanes, O.; Siuzdak, G. Innovation: Metabolomics: the apogee of the omics trilogy. *Nature Reviews Molecular Cell Biology* **2012**, *13*, 263-269, doi:10.1038/nrm3314.
72. Gao, Y.; Ray, S.; Dai, S.; Ivanov, A.R.; Abu-Absi, N.R.; Lewis, A.M.; Huang, Z.; Xing, Z.; Borys, M.C.; Li, Z.J., et al. Combined metabolomics and proteomics reveals hypoxia as a cause of lower productivity on scale-up to a 5000-liter CHO bioprocess. *Biotechnology Journal* **2016**, *11*, 1190-1200, doi:10.1002/biot.201600030.
73. Selvarasu, S.; Ho, Y.S.; Chong, W.P.K.; Wong, N.S.C.; Yusufi, F.N.K.; Lee, Y.Y.; Yap, M.G.S.; Lee, D.Y. Combined in silico modeling and metabolomics analysis to characterize fed-batch CHO cell culture. *Biotechnology and bioengineering* **2012**, *109*, 1415-1429, doi:10.1002/bit.24445.
74. Dietmair, S.; Hodson, M.P.; Quek, L.E.; Timmins, N.E.; Chrysanthopoulos, P.; Jacob, S.S.; Gray, P.; Nielsen, L.K. Metabolite profiling of CHO cells with different growth characteristics. *Biotechnology and bioengineering* **2012**, *109*, 1404-1414, doi:10.1002/bit.24496.
75. Stolfa, G.; Smonskey, M.T.; Boniface, R.; Hachmann, A.B.; Gulde, P.; Joshi, A.D.; Pierce, A.P.; Jacobia, S.J.; Campbell, A. CHO-Omics Review: The Impact of Current and Emerging Technologies on Chinese Hamster Ovary Based Bioproduction. *Biotechnology Journal* **2018**, *13*, doi:10.1002/biot.201700227.
76. Ritter, J.B.; Wahl, A.S.; Freund, S.; Genzel, Y.; Reichl, U. Metabolic effects of influenza virus infection in cultured animal cells: Intra- and extracellular metabolite profiling. *BMC systems biology* **2010**, *4*, 61, doi:10.1186/1752-0509-4-61.
77. Petiot, E.; Cuperlovic-Culf, M.; Shen, C.F.; Kamen, A. Influence of HEK293 metabolism on the production of viral vectors and vaccine. *Vaccine* **2015**, *33*, 5974-5981, doi:10.1016/j.vaccine.2015.05.097.
78. Rodrigues, A.F.; Formas-Oliveira, A.S.; Bandeira, V.S.; Alves, P.M.; Hu, W.S.; Coroadinha, A.S. Metabolic pathways recruited in the production of a recombinant enveloped virus: Mining targets for process and cell engineering. *Metabolic engineering* **2013**, *20*, 131-145, doi:10.1016/j.ymben.2013.10.001.
79. Dueñas-Carrera, S. Hepatitis C virus and lipid metabolism: Their implications in vaccine development and treatment. *Biotechnologia Aplicada* **2011**, *28*, 1-5.
80. Shaw, M.L.; Palese, P. Orthomyxoviridae. In *Fields Virology*, 6 ed.; Kipe, D.M., Howley, P.M., Eds. Lippincott Williams & Wilkins. **2013**; Vol. 1, 1151-1185.
81. Wright, P.F.; Neumann, G.; Kawaoka, Y. Orthomyxoviruses. In *Fields Virology*, 6 ed.; Kipe, D.M., Howley, P.M., Eds. Lippincott Williams & Wilkins **2013**, Vol. 1, 1186-1243.
82. Krammer, F.; Smith, G.J.D.; Fouchier, R.A.M.; Peiris, M.; Kedzierska, K.; Doherty, P.C.; Palese, P.; Shaw, M.L.; Treanor, J.; Webster, R.G., et al. Influenza. *Nature Reviews Disease Primers* **2018**, *4*, 3, doi:10.1038/s41572-018-0002-y.
83. Häggström, L. Cell Metabolism, Animal. In *Encyclopedia of Cell Technology*, Spier, R.E., Ed. John Wiley & Sons **2000**, Vol. 1, 392-410.

-
84. Amable, P.; Butler, M. Cell metabolism and its control in culture. In *Animal Cell Technology: From Biopharmaceuticals to Gene Therapy*, 1 ed.; Castillho, L.R., Moraes, A.M., Augusto, E.F.P., Butler, M., Eds. Taylor & Francis Group **2008**, 75-110.
85. Vasin, A.V.; Temkina, O.A.; Egorov, V.V.; Klotchenko, S.A.; Plotnikova, M.A.; Kiselev, O.I. Molecular mechanisms enhancing the proteome of influenza A viruses: An overview of recently discovered proteins. *Virus Research* **2014**, *185*, 53-63, doi:10.1016/j.virusres.2014.03.015.
86. Calder, L.J.; Wasilewski, S.; Berriman, J.A.; Rosenthal, P.B. Structural organization of a filamentous influenza A virus. *Proceedings of the National Academy of Sciences* **2010**, *107*, 10685-10690, doi:10.1073/pnas.1002123107.
87. Hayden, F.G. Newer influenza antivirals, biotherapeutics and combinations. *Influenza and other Respiratory Viruses* **2013**, *7*, 63-75, doi:10.1111/irv.12045.
88. De Clercq, E.; Li, G. Approved Antiviral Drugs over the Past 50 Years. *Clinical Microbiology Reviews* **2016**, *29*, 695-747, doi:10.1128/cmr.00102-15.
89. Garten, W.; Klenk, H.D. Cleavage activation of the influenza virus hemagglutinin and its role in pathogenesis. In *Monographs in Virology*, **2008**, Vol. 27, 156-167.
90. Böttcher, E.; Matrosovich, T.; Beyerle, M.; Klenk, H.-D.; Garten, W.; Matrosovich, M. Proteolytic Activation of Influenza Viruses by Serine Proteases TMPRSS2 and HAT from Human Airway Epithelium. *Journal of virology* **2006**, *80*, 9896-9898, doi:10.1128/jvi.01118-06.
91. Peitsch, C.; Klenk, H.D.; Garten, W.; Böttcher-Friebertshäuser, E. Activation of influenza A viruses by host proteases from swine airway epithelium. *Journal of virology* **2014**, *88*, 282-291, doi:10.1128/JVI.01635-13.
92. Galloway, S.E.; Reed, M.L.; Russell, C.J.; Steinhauer, D.A. Influenza HA Subtypes Demonstrate Divergent Phenotypes for Cleavage Activation and pH of Fusion: Implications for Host Range and Adaptation. *PLoS Pathogens* **2013**, *9*, doi:10.1371/journal.ppat.1003151.
93. Zhirnov, O.P.; Klenk, H.D.; Wright, P.F. Aprotinin and similar protease inhibitors as drugs against influenza. *Antiviral Research* **2011**, *92*, 27-36, doi:10.1016/j.antiviral.2011.07.014.
94. Prevention, C.f.D.C.a. Types of Influenza Viruses. Available online: <https://www.cdc.gov/flu/about/viruses/types.htm> (accessed on 28 April 2020).
95. Tate, M.D.; Job, E.R.; Deng, Y.-M.; Gunalan, V.; Maurer-Stroh, S.; Reading, P.C. Playing hide and seek: how glycosylation of the influenza virus hemagglutinin can modulate the immune response to infection. *Viruses* **2014**, *6*, 1294-1316, doi:10.3390/v6031294.
96. Roedig, J.V.; Rapp, E.; Höper, D.; Genzel, Y.; Reichl, U. Impact of host cell line adaptation on quasispecies composition and glycosylation of influenza a virus hemagglutinin. *PloS one* **2011**, *6*, doi:10.1371/journal.pone.0027989.
97. Sun, S.; Wang, Q.; Zhao, F.; Chen, W.; Li, Z. Glycosylation site alteration in the evolution of influenza a (H1N1) viruses. *PloS one* **2011**, *6*, doi:10.1371/journal.pone.0022844.
98. Das, S.R.; Puigbo, P.; Hensley, S.E.; Hurt, D.E.; Bennink, J.R.; Yewdell, J.W. Glycosylation focuses sequence variation in the influenza a virus H1 hemagglutinin globular domain. *PLoS Pathogens* **2010**, *6*, doi:10.1371/journal.ppat.1001211.
99. Sun, X.; Jayaraman, A.; Maniprasad, P.; Raman, R.; Houser, K.V.; Pappas, C.; Zeng, H.; Sasisekharan, R.; Katz, J.M.; Tumpey, T.M. N-linked glycosylation of the hemagglutinin protein influences virulence and antigenicity of the 1918 pandemic and seasonal H1N1 influenza A viruses. *Journal of virology* **2013**, *87*, 8756-8766, doi:10.1128/JVI.00593-13.
100. Das, S.R.; Hensley, S.E.; David, A.; Schmidt, L.; Gibbs, J.S.; Puigbo, P.; Ince, W.L.; Bennink, J.R.; Yewdell, J.W. Fitness costs limit influenza A virus hemagglutinin glycosylation as an immune evasion strategy. *Proceedings of the National Academy of Sciences of the United States of America* **2011**, *108*, E1417-E1422, doi:10.1073/pnas.1108754108.
101. Zhang, Y.; Zhu, J.; Li, Y.; Bradley, K.C.; Cao, J.; Chen, H.; Jin, M.; Zhou, H. Glycosylation on Hemagglutinin Affects the Virulence and Pathogenicity of Pandemic H1N1/2009 Influenza A Virus in Mice. *PloS one* **2013**, *8*, doi:10.1371/journal.pone.0061397.
102. Wu, C.-Y.; Lin, C.-W.; Tsai, T.-I.; Lee, C.-C.D.; Chuang, H.-Y.; Chen, J.-B.; Tsai, M.-H.; Chen, B.-R.; Lo, P.-W.; Liu, C.-P., et al. Influenza A surface glycosylation and vaccine design. *Proceedings of the National Academy of Sciences* **2017**, *114*, 280-285, doi:10.1073/pnas.1617174114.
103. Taubenberger, J.K.; Morens, D.M. 1918 Influenza: the Mother of All Pandemics. *Emerging Infectious Diseases* **2006**, *12*, 15-22, doi:10.3201/eid1201.050979.

104. Newman, L.P.; Bhat, N.; Fleming, J.A.; Neuzil, K.M. Global influenza seasonality to inform country-level vaccine programs: An analysis of WHO FluNet influenza surveillance data between 2011 and 2016. *PLoS one* **2018**, *13*, e0193263, doi:10.1371/journal.pone.0193263.
105. World Health Organization. Up to 650 000 people die of respiratory diseases linked to seasonal flu each year. Available online: <http://www.who.int/en/news-room/detail/14-12-2017-up-to-650-000-people-die-of-respiratory-diseases-linked-to-seasonal-flu-each-year> (accessed on 29 September 2019).
106. Iuliano, A.D.; Roguski, K.M.; Chang, H.H.; Muscatello, D.J.; Palekar, R.; Tempia, S.; Cohen, C.; Gran, J.M.; Schanzer, D.; Cowling, B.J., et al. Estimates of global seasonal influenza-associated respiratory mortality: a modelling study. *The Lancet* **2018**, *391*, 1285-1300, doi:10.1016/S0140-6736(17)33293-2.
107. Hussain, A.; Ali, S.; Ahmed, M.; Hussain, S. The Anti-vaccination Movement: A Regression in Modern Medicine. *Cureus* **2018**, *10*, e2919-e2919, doi:10.7759/cureus.2919.
108. Plotkin, S. History of vaccination. *Proceedings of the National Academy of Sciences* **2014**, *111*, 12283-12287, doi:10.1073/pnas.1400472111.
109. Strassburg, M.A. The global eradication of smallpox. *American Journal of Infection Control* **1982**, *10*, 53-59, doi:10.1016/0196-6553(82)90003-7.
110. Baxby, D. Edward Jenner's inquiry after 200 years. *BMJ* **1999**, *318*, 390-390, doi:10.1136/bmj.318.7180.390.
111. Pasteur, L. Méthode pour prévenir la rage après morsure. *C. R. Acad. Sci.* **1885**, *101*, 765-772.
112. Sellard, A.W.; Laigret, J. Vaccination de l'homme contre la fièvre jaune. *C. R. Acad. Sci.* **1932**, *194*, 1609-1611.
113. Plotkin, S.A. Vaccines, Vaccination, and Vaccinology. *The Journal of Infectious Diseases* **2003**, *187*, 1349-1359, doi:10.1086/374419.
114. Theiler, M.; Smith, H.H. The effect of prolonged cultivation in vitro upon the pathogenicity of yellow fever virus. *The Journal of Experimental Medicine* **1937**, *65*, 767-786, doi:10.1084/jem.65.6.767.
115. Thomas, F.; Magill, T.P. Vaccination of Human Subjects with Virus of Human Influenza. *Proceedings of the Society for Experimental Biology and Medicine* **1936**, *33*, 604-606, doi:10.3181/00379727-33-8467P.
116. Enders, J.F.; Weller, T.H.; Robbins, F.C. Cultivation of the Lansing Strain of Poliomyelitis Virus in Cultures of Various Human Embryonic Tissues. *Science* **1949**, *109*, 85-87, doi:10.1126/science.109.2822.85.
117. Rey, M.; Girard, M.P. The global eradication of poliomyelitis: Progress and problems. *Comparative Immunology, Microbiology and Infectious Diseases* **2008**, *31*, 317-325, doi:10.1016/j.cimid.2007.07.013.
118. Zahoor, M.A.; Khurshid, M.; Qureshi, R.; Naz, A.; Shahid, M. Cell culture-based viral vaccines: current status and future prospects. *Future Virology* **2016**, *11*, 549-562, doi:10.2217/fvl-2016-0006.
119. Valenzuela, P.; Medina, A.; Rutter, W.J.; Ammerer, G.; Hall, B.D. Synthesis and assembly of hepatitis B virus surface antigen particles in yeast. *Nature* **1982**, *298*, 347-350, doi:10.1038/298347a0.
120. Cox, M.M.J.; Patriarca, P.A.; Treanor, J. FluBlok, a recombinant hemagglutinin influenza vaccine. *Influenza and Other Respiratory Viruses* **2008**, *2*, 211-219, doi:10.1111/j.1750-2659.2008.00053.x.
121. Kirnbauer, R.; Booy, F.; Cheng, N.; Lowy, D.R.; Schiller, J.T. Papillomavirus L1 major capsid protein self-assembles into virus-like particles that are highly immunogenic. *Proceedings of the National Academy of Sciences of the United States of America* **1992**, *89*, 12180-12184, doi:10.1073/pnas.89.24.12180.
122. Guy, B.; Guirakhoo, F.; Barban, V.; Higgs, S.; Monath, T.P.; Lang, J. Preclinical and clinical development of YFV 17D-based chimeric vaccines against dengue, West Nile and Japanese encephalitis viruses. *Vaccine* **2010**, *28*, 632-649, doi:10.1016/j.vaccine.2009.09.098.
123. Henao-Restrepo, A.M.; Camacho, A.; Longini, I.M.; Watson, C.H.; Edmunds, W.J.; Egger, M.; Carroll, M.W.; Dean, N.E.; Diatta, I.; Doumbia, M., et al. Efficacy and effectiveness of an rVSV-vectored vaccine in preventing Ebola virus disease: final results from the Guinea ring vaccination, open-label, cluster-randomised trial (Ebola Ça Suffit!). *The Lancet* **2017**, *389*, 505-518, doi:10.1016/S0140-6736(16)32621-6.
124. Ulmer, J.B.; Sadoff, J.C.; Liu, M.A. DNA vaccines. *Current Opinion in Immunology* **1996**, *8*, 531-536, doi:10.1016/S0952-7915(96)80042-2.
125. Ulmer, J.B.; Mason, P.W.; Geall, A.; Mandl, C.W. RNA-based vaccines. *Vaccine* **2012**, *30*, 4414-4418, doi:10.1016/j.vaccine.2012.04.060.
126. Lundstrom, K. Latest development on RNA-based drugs and vaccines. *Future Science OA* **2018**, *4*, doi:10.4155/fsoa-2017-0151.
127. Geall, A.J.; Ulmer, J.B. Introduction to RNA-based vaccines and therapeutics. *Expert Review of Vaccines* **2015**, *14*, 151-152, doi:10.1586/14760584.2015.1001244.

-
128. Hobernik, D.; Bros, M. DNA Vaccines-How Far From Clinical Use? *International journal of molecular sciences* **2018**, *19*, 3605, doi:10.3390/ijms19113605.
129. Kresse, H.; Rovini, H. Influenza vaccine market dynamics. *Nature Reviews Drug Discovery* **2009**, *8*, 841, doi:10.1038/nrd3026.
130. Orenstein, W.A.; Schaffner, W. Lessons Learned: Role of Influenza Vaccine Production, Distribution, Supply, and Demand—What It Means for the Provider. *The American Journal of Medicine* **2008**, *121*, S22-S27, doi:10.1016/j.amjmed.2008.05.004.
131. Gerdil, C. The annual production cycle for influenza vaccine. *Vaccine* **2003**, *21*, 1776-1779, doi:10.1016/S0264-410X(03)00071-9.
132. Giezeman, K.M.; Nauta, J.; de Bruijn, I.A.; Palache, A.M. Trivalent inactivated subunit influenza vaccine Influvac[®]: 25-Year experience of safety and immunogenicity. *Vaccine* **2009**, *27*, 2414-2417, doi:10.1016/j.vaccine.2009.02.008.
133. Carter, N.J.; Curran, M.P. Live attenuated influenza vaccine (FluMist[®]; Fluenz[™]): A review of its use in the prevention of seasonal influenza in children and adults. *Drugs* **2011**, *71*, 1591-1622, doi:10.2165/11206860-000000000-00000.
134. Harding, A.T.; Heaton, N.S. Efforts to Improve the Seasonal Influenza Vaccine. *Vaccines* **2018**, *6*, 19, doi:10.3390/vaccines6020019.
135. U.S. Food & Drug Administration. Vaccines, Blood & Biologics. Available online: <https://www.fda.gov/biologicsbloodvaccines/vaccines/approvedproducts/ucm335836.htm> (accessed on 28 August 2019).
136. Liu, Y.-J.; Wu, S.-L.; Love, K.R.; Hancock, W.S. Characterization of Site-Specific Glycosylation in Influenza A Virus Hemagglutinin Produced by Spodoptera frugiperda Insect Cell Line. *Analytical chemistry* **2017**, *89*, 11036-11043, doi:10.1021/acs.analchem.7b03025.
137. Henry, C.; Palm, A.-K.E.; Utset, H.A.; Huang, M.; Ho, I.Y.; Zheng, N.-Y.; Fitzgerald, T.; Neu, K.E.; Chen, Y.-Q.; Krammer, F., et al. Monoclonal antibody responses after recombinant HA vaccine versus subunit inactivated influenza virus vaccine: a comparative study. *Journal of virology* **2019**, *10.1128/jvi.01150-19*, JVI.01150-01119, doi:10.1128/jvi.01150-19.
138. King, J.C.; Cox, M.M.; Reisinger, K.; Hedrick, J.; Graham, I.; Patriarca, P. Evaluation of the safety, reactogenicity and immunogenicity of FluBlok[®] trivalent recombinant baculovirus-expressed hemagglutinin influenza vaccine administered intramuscularly to healthy children aged 6–59 months. *Vaccine* **2009**, *27*, 6589-6594, doi:10.1016/j.vaccine.2009.08.032.
139. Ping, J.; Lopes, T.J.S.; Neumann, G.; Kawaoka, Y. Development of high-yield influenza B virus vaccine viruses. *Proceedings of the National Academy of Sciences* **2016**, *113*, E8296-E8305, doi:10.1073/pnas.1616530113.
140. Ping, J.; Lopes, T.J.S.; Nidom, C.A.; Ghedin, E.; Macken, C.A.; Fitch, A.; Imai, M.; Maher, E.A.; Neumann, G.; Kawaoka, Y. Development of high-yield influenza A virus vaccine viruses. *Nature communications* **2015**, *6*, 8148, doi:10.1038/ncomms9148.
141. Johnson, A.; Chen, L.-M.; Winne, E.; Santana, W.; Metcalfe, M.G.; Mateu-Petit, G.; Ridenour, C.; Hossain, M.J.; Villanueva, J.; Zaki, S.R., et al. Identification of Influenza A/PR/8/34 Donor Viruses Imparting High Hemagglutinin Yields to Candidate Vaccine Viruses in Eggs. *PloS one* **2015**, *10*, e0128982, doi:10.1371/journal.pone.0128982.
142. Kilbourne, E.D. Future influenza vaccines and the use of genetic recombinants. *Bull World Health Organ* **1969**, *41*, 643-645.
143. Au - Brauer, R.; Au - Chen, P. Influenza Virus Propagation in Embryonated Chicken Eggs. *JoVE* **2015**, doi:10.3791/52421, e52421, doi:doi:10.3791/52421.
144. Tree, J.A.; Richardson, C.; Fooks, A.R.; Clegg, J.C.; Looby, D. Comparison of large-scale mammalian cell culture systems with egg culture for the production of influenza virus A vaccine strains. *Vaccine* **2001**, *19*, 3444-3450, doi:10.1016/S0264-410X(01)00053-6.
145. Montomoli, E.; Khadang, B.; Piccirella, S.; Trombetta, C.; Mennitto, E.; Manini, I.; Stanzani, V.; Lapini, G. Cell culture-derived influenza vaccines from Vero cells: a new horizon for vaccine production. *Expert Review of Vaccines* **2012**, *11*, 587-594, doi:10.1586/erv.12.24.
146. Wolff, M.W.; Reichl, U. Downstream Processing: From Egg to Cell Culture-Derived Influenza Virus Particles. *Chemical Engineering & Technology* **2008**, *31*, 846-857, doi:doi:10.1002/ceat.200800118.
147. Mischler, R.; Metcalfe, I.C. Inflflexal[®]V a trivalent virosome subunit influenza vaccine: production. *Vaccine* **2002**, *20*, B17-B23, doi:10.1016/S0264-410X(02)00512-1.

148. Reisinger, K.S.; Block, S.L.; Izu, A.; Groth, N.; Holmes, S.J. Subunit Influenza Vaccines Produced from Cell Culture or in Embryonated Chicken Eggs: Comparison of Safety, Reactogenicity, and Immunogenicity. *The Journal of Infectious Diseases* **2009**, *200*, 849-857, doi:10.1086/605506.
149. Wong, S.-S.; Webby, R.J. Traditional and New Influenza Vaccines. *Clinical Microbiology Reviews* **2013**, *26*, 476-492, doi:10.1128/cmr.00097-12.
150. Tregoning, J.S.; Russell, R.F.; Kinnear, E. Adjuvanted influenza vaccines. *Human Vaccines & Immunotherapeutics* **2018**, *14*, 550-564, doi:10.1080/21645515.2017.1415684.
151. Schild, G.C.; Wood, J.M.; Newman, R.W. A single radial immunodiffusion technique for the assay of influenza haemagglutinin antigen. Proposals for an assay method for the haemagglutinin content of influenza vaccines. *Bulletin of the World Health Organization* **1975**, *52*, 223-231.
152. Kalbfuss-Zimmermann, B.; Reichl, U. Viral Vaccines Purification. In *Wiley Series in Biotechnology and Bioengineering*, 1 ed.; Wen, E.P., Ellis, R., Pujar., N.S., Eds. John Wiley & Sons, Inc., **2015**, 97-180.
153. Marichal-Gallardo, P.; Pieler, M.M.; Wolff, M.W.; Reichl, U. Steric exclusion chromatography for purification of cell culture-derived influenza A virus using regenerated cellulose membranes and polyethylene glycol. *Journal of Chromatography A* **2017**, *1483*, 110-119, doi:10.1016/j.chroma.2016.12.076.
154. Fortuna, R.A.; van Teeffelen, S.; Ley, A.; Fischer, L.M.; Taft, F.; Genzel, Y.; Villain, L.; Wolff, M.M.; Reichl, U. Use of sulfated cellulose membrane adsorbers for chromatographic purification of cell cultured-derived influenza A and B viruses. *Separation and Purification Technology* **2019**, *10.1016/j.seppur.2019.05.101*, doi:10.1016/j.seppur.2019.05.101.
155. Hegde, N.R. Cell culture-based influenza vaccines: A necessary and indispensable investment for the future. *Hum Vaccin Immunother* **2015**, *11*, 1223-1234, doi:10.1080/21645515.2015.1016666.
156. Fineberg, H.V. Pandemic Preparedness and Response — Lessons from the H1N1 Influenza of 2009. *New England Journal of Medicine* **2014**, *370*, 1335-1342, doi:10.1056/NEJMra1208802.
157. Lohr, V.; Rath, A.; Genzel, Y.; Jordan, I.; Sandig, V.; Reichl, U. New avian suspension cell lines provide production of influenza virus and MVA in serum-free media: studies on growth, metabolism and virus propagation. *Vaccine* **2009**, *27*, 4975-4982, doi:10.1016/j.vaccine.2009.05.083.
158. Naruse, T.; Fukuda, T.; Tanabe, T.; Ichikawa, M.; Oda, Y.; Tochiwara, S.; Kimachi, K.; Kino, Y.; Ueda, K. A clinical phase I study of an EB66 cell-derived H5N1 pandemic vaccine adjuvanted with AS03. *Vaccine* **2015**, *33*, 6078-6084, doi:10.1016/j.vaccine.2015.09.022.
159. Genzel, Y.; Vogel, T.; Buck, J.; Behrendt, I.; Ramirez, D.V.; Schiedner, G.; Jordan, I.; Reichl, U. High cell density cultivations by alternating tangential flow (ATF) perfusion for influenza A virus production using suspension cells. *Vaccine* **2014**, *32*, 2770-2781, doi:10.1016/j.vaccine.2014.02.016.
160. Coronel, J.; Behrendt, I.; Bürgin, T.; Anderlei, T.; Sandig, V.; Reichl, U.; Genzel, Y. Influenza A virus production in a single-use orbital shaken bioreactor with ATF or TFF perfusion systems. *Vaccine* **2019**, *10.1016/j.vaccine.2019.06.005*, doi:10.1016/j.vaccine.2019.06.005.
161. Gränicher, G.; Coronel, J.; Pralow, A.; Marichal-Gallardo, P.; Wolff, M.; Rapp, E.; Karlas, A.; Sandig, V.; Genzel, Y.; Reichl, U. Efficient influenza A virus production in high cell density using the novel porcine suspension cell line PBG.PK2.1. *Vaccine* **2019**, *10.1016/j.vaccine.2019.04.030*, doi:10.1016/j.vaccine.2019.04.030.
162. Tapia, F.; Vogel, T.; Genzel, Y.; Behrendt, I.; Hirschel, M.; Gangemi, J.D.; Reichl, U. Production of high-titer human influenza A virus with adherent and suspension MDCK cells cultured in a single-use hollow fiber bioreactor. *Vaccine* **2014**, *32*, 1003-1011, doi:10.1016/j.vaccine.2013.11.044.
163. Trucchi, C.; Paganino, C.; Amicizia, D.; Orsi, A.; Tisa, V.; Piazza, M.F.; Icardi, G.; Ansaldi, F. Universal influenza virus vaccines: what needs to happen next? *Expert Opinion on Biological Therapy* **2019**, *19*, 671-683, doi:10.1080/14712598.2019.1604671.
164. Lee, L.Y.Y.; Izzard, L.; Hurt, A.C. A Review of DNA Vaccines Against Influenza. *Front Immunol* **2018**, *9*, 1568-1568, doi:10.3389/fimmu.2018.01568.
165. Scorza, F.B.; Pardi, N. New kids on the block: RNA-based influenza virus vaccines. *Vaccines* **2018**, *6*, doi:10.3390/vaccines6020020.
166. Gaush, C.R.; Hard, W.L.; Smith, T.F. Characterization of an Established Line of Canine Kidney Cells (MDCK). *Proceedings of the Society for Experimental Biology and Medicine* **1966**, *122*, 931-935, doi:10.3181/00379727-122-31293.
167. Simmons, N.L. Cultured monolayers of MDCK cells: A novel model system for the study of epithelial development and function. *General Pharmacology: The Vascular System* **1982**, *13*, 287-291, doi:10.1016/0306-3623(82)90047-7.

-
168. Tsai, H.-C.; Lehman, C.W.; Lin, C.-C.; Tsai, S.-W.; Chen, C.-M. Functional evaluation for adequacy of MDCK-lineage cells in influenza research. *BMC Research Notes* **2019**, *12*, 101, doi:10.1186/s13104-019-4134-2.
169. Zuccotti, G.V.; Fabiano, V. Influvac, a trivalent inactivated subunit influenza vaccine. *Expert Opinion on Biological Therapy* **2011**, *11*, 89-98, doi:10.1517/14712598.2011.541436.
170. Rubio, A.P.; Eiros, J.M. Cell culture-derived flu vaccine: Present and future. *Human Vaccines and Immunotherapeutics* **2018**, *14*, 1874-1882, doi:10.1080/21645515.2018.1460297.
171. Kluge, S.; Benndorf, D.; Genzel, Y.; Scharfenberg, K.; Rapp, E.; Reichl, U. Monitoring changes in proteome during stepwise adaptation of a MDCK cell line from adherence to growth in suspension. *Vaccine* **2015**, *33*, 4269-4280, doi:10.1016/j.vaccine.2015.02.077.
172. Huang, D.; Peng, W.J.; Ye, Q.; Liu, X.P.; Zhao, L.; Fan, L.; Xia-Hou, K.; Jia, H.J.; Luo, J.; Zhou, L.T., et al. Serum-Free Suspension Culture of MDCK Cells for Production of Influenza H1N1 Vaccines. *PloS one* **2015**, *10*, e0141686, doi:10.1371/journal.pone.0141686.
173. Shoji, T. The Recruitment Model of Metabolic Evolution: Jasmonate-Responsive Transcription Factors and a Conceptual Model for the Evolution of Metabolic Pathways. *Frontiers in Plant Science* **2019**, *10*, doi:10.3389/fpls.2019.00560.
174. Fani, R.; Fondi, M. Origin and evolution of metabolic pathways. *Physics of Life Reviews* **2009**, *6*, 23-52, doi:10.1016/j.plrev.2008.12.003.
175. Fiehn, O. Metabolomics - The link between genotypes and phenotypes. *Plant Molecular Biology* **2002**, *48*, 155-171, doi:10.1023/A:1013713905833.
176. Fell, D.A. Evolution of Central Carbon Metabolism. *Molecular cell* **2010**, *39*, 663-664, doi:10.1016/j.molcel.2010.08.034.
177. Buchakjian, M.R.; Kornbluth, S. The engine driving the ship: metabolic steering of cell proliferation and death. *Nature reviews. Molecular cell biology* **2010**, *11*, 715-727, doi:10.1038/nrm2972.
178. Koppenol, W.H.; Bounds, P.L.; Dang, C.V. Otto Warburg's contributions to current concepts of cancer metabolism. *Nature reviews. Cancer* **2011**, *11*, 325-337, doi:10.1038/nrc3038.
179. Zhou, W.; Capello, M.; Fredolini, C.; Racanicchi, L.; Piemonti, L.; Liotta, L.A.; Novelli, F.; Petricoin, E.F. Proteomic analysis reveals Warburg effect and anomalous metabolism of glutamine in pancreatic cancer cells. *Journal of proteome research* **2012**, *11*, 554-563, doi:10.1021/pr2009274.
180. Buchsteiner, M.; Quek, L.E.; Gray, P.; Nielsen, L.K. Improving culture performance and antibody production in CHO cell culture processes by reducing the Warburg effect. *Biotechnology and bioengineering* **2018**, *115*, 2315-2327, doi:10.1002/bit.26724.
181. Macheda, M.L.; Rogers, S.; Best, J.D. Molecular and cellular regulation of glucose transporter (GLUT) proteins in cancer. *Journal of Cellular Physiology* **2005**, *202*, 654-662, doi:10.1002/jcp.20166.
182. WEINHOUSE, S.; WARBURG, O.; BURK, D.; SCHADE, A.L. On Respiratory Impairment in Cancer Cells. *Science* **1956**, *124*, 267-272, doi:10.1126/science.124.3215.267.
183. DeBerardinis, R.J.; Lum, J.J.; Hatzivassiliou, G.; Thompson, C.B. The Biology of Cancer: Metabolic Reprogramming Fuels Cell Growth and Proliferation. *Cell Metabolism* **2008**, *7*, 11-20, doi:10.1016/j.cmet.2007.10.002.
184. Cork, G.K.; Thompson, J.; Slawson, C. Real Talk: The Inter-play Between the mTOR, AMPK, and Hexosamine Biosynthetic Pathways in Cell Signaling. *Frontiers in Endocrinology* **2018**, *9*, doi:10.3389/fendo.2018.00522.
185. Patra, K.C.; Hay, N. The pentose phosphate pathway and cancer. *Trends in Biochemical Sciences* **2014**, *39*, 347-354, doi:10.1016/j.tibs.2014.06.005.
186. Stincone, A.; Prigione, A.; Cramer, T.; Wamelink, M.M.C.; Campbell, K.; Cheung, E.; Olin-Sandoval, V.; Grüning, N.-M.; Krüger, A.; Tauqeer Alam, M., et al. The return of metabolism: biochemistry and physiology of the pentose phosphate pathway. *Biological Reviews* **2015**, *90*, 927-963, doi:10.1111/brv.12140.
187. Schell, John C.; Olson, Kristofor A.; Jiang, L.; Hawkins, Amy J.; Van Vranken, Jonathan G.; Xie, J.; Egnatchik, Robert A.; Earl, Espen G.; DeBerardinis, Ralph J.; Rutter, J. A Role for the Mitochondrial Pyruvate Carrier as a Repressor of the Warburg Effect and Colon Cancer Cell Growth. *Molecular cell* **2014**, *56*, 400-413, doi:10.1016/j.molcel.2014.09.026.
188. Baffy, G. Mitochondrial uncoupling in cancer cells: Liabilities and opportunities. *Biochimica et Biophysica Acta (BBA) - Bioenergetics* **2017**, *1858*, 655-664, doi:10.1016/j.bbabi.2017.01.005.
189. Kozłowski, L.P. Proteome-pI: proteome isoelectric point database. *Nucleic Acids Res* **2017**, *45*, D1112-D1116, doi:10.1093/nar/gkw978.

190. Bhutia, Y.D.; Ganapathy, V. Glutamine transporters in mammalian cells and their functions in physiology and cancer. *Biochimica et Biophysica Acta (BBA) - Molecular Cell Research* **2016**, *1863*, 2531-2539, doi:10.1016/j.bbamcr.2015.12.017.
191. Nicolae, A.; Wahrheit, J.; Bahnemann, J.; Zeng, A.P.; Heinzle, E. Non-stationary ¹³C metabolic flux analysis of Chinese hamster ovary cells in batch culture using extracellular labeling highlights metabolic reversibility and compartmentation. *BMC systems biology* **2014**, *8*, 50, doi:10.1186/1752-0509-8-50.
192. Xu, X.; Nagarajan, H.; Lewis, N.E.; Pan, S.; Cai, Z.; Liu, X.; Chen, W.; Xie, M.; Wang, W.; Hammond, S., et al. The genomic sequence of the Chinese hamster ovary (CHO)-K1 cell line. *Nature Biotechnology* **2011**, *29*, 735, doi:10.1038/nbt.1932.
193. Spinelli, J.B.; Yoon, H.; Ringel, A.E.; Jeanfavre, S.; Clish, C.B.; Haigis, M.C. Metabolic recycling of ammonia via glutamate dehydrogenase supports breast cancer biomass. *Science* **2017**, *358*, 941, doi:10.1126/science.aam9305.
194. Johnson, C.H.; Gonzalez, F.J. Challenges and opportunities of metabolomics. *Journal of cellular physiology* **2012**, *227*, 2975-2981, doi:10.1002/jcp.24002.
195. Aebersold, R.; Mann, M. Mass spectrometry-based proteomics. *Nature* **2003**, *422*, 198-207, doi:10.1038/nature01511.
196. Hawkins, R.D.; Hon, G.C.; Ren, B. Next-generation genomics: An integrative approach. *Nature Reviews Genetics* **2010**, *11*, 476-486, doi:10.1038/nrg2795.
197. Wang, Z.; Gerstein, M.; Snyder, M. RNA-Seq: A revolutionary tool for transcriptomics. *Nature Reviews Genetics* **2009**, *10*, 57-63, doi:10.1038/nrg2484.
198. Wu, L.; Mashego, M.R.; van Dam, J.C.; Proell, A.M.; Vinke, J.L.; Ras, C.; van Winden, W.A.; van Gulik, W.M.; Heijnen, J.J. Quantitative analysis of the microbial metabolome by isotope dilution mass spectrometry using uniformly ¹³C-labeled cell extracts as internal standards. *Analytical biochemistry* **2005**, *336*, 164-171, doi:10.1016/j.ab.2004.09.001.
199. Gil, A.; Siegel, D.; Permentier, H.; Reijngoud, D.-J.; Dekker, F.; Bischoff, R. Stability of energy metabolites—An often overlooked issue in metabolomics studies: A review. *Electrophoresis* **2015**, *36*, 2156-2169, doi:10.1002/elps.201500031.
200. Vuckovic, D. Current trends and challenges in sample preparation for global metabolomics using liquid chromatography-mass spectrometry. *Analytical and bioanalytical chemistry* **2012**, *403*, 1523-1548, doi:10.1007/s00216-012-6039-y.
201. Ritter, J.B.; Genzel, Y.; Reichl, U. High-performance anion-exchange chromatography using on-line electrolytic eluent generation for the determination of more than 25 intermediates from energy metabolism of mammalian cells in culture. *Journal of chromatography. B, Analytical technologies in the biomedical and life sciences* **2006**, *843*, 216-226, doi:10.1016/j.jchromb.2006.06.004.
202. Bannefeld, K.H.; Stass, H.; Blaschke, G. Capillary electrophoresis with laser-induced fluorescence detection, an adequate alternative to high-performance liquid chromatography, for the determination of ciprofloxacin and its metabolite desethyleneciprofloxacin in human plasma. *Journal of Chromatography B: Biomedical Sciences and Applications* **1997**, *692*, 453-459, doi:10.1016/S0378-4347(96)00539-7.
203. Purdon, M.P.; Lehman-McKeeman, L.D. Improved high-performance liquid chromatographic procedure for the separation and quantification of hydroxytestosterone metabolites. *Journal of Pharmacological and Toxicological Methods* **1997**, *37*, 67-73, doi:10.1016/S1056-8719(97)00013-0.
204. Fan, T.W.M.; Colmer, T.D.; Lane, A.N.; Higashi, R.M. Determination of Metabolites by ¹H NMR and GC: Analysis for Organic Osmolytes in Crude Tissue Extracts. *Analytical biochemistry* **1993**, *214*, 260-271, doi:10.1006/abio.1993.1486.
205. Tsikas, D. Simultaneous Derivatization and Quantification of the Nitric Oxide Metabolites Nitrite and Nitrate in Biological Fluids by Gas Chromatography/Mass Spectrometry. *Analytical chemistry* **2000**, *72*, 4064-4072, doi:10.1021/ac9913255.
206. Teerlink, T.; Nijveldt, R.J.; De Jong, S.; Van Leeuwen, P.A.M. Determination of arginine, asymmetric dimethylarginine, and symmetric dimethylarginine in human plasma and other biological samples by high-performance liquid chromatography. *Analytical biochemistry* **2002**, *303*, 131-137, doi:10.1006/abio.2001.5575.
207. Ramautar, R.; de Jong, G.J. Recent developments in liquid-phase separation techniques for metabolomics. *Bioanalysis* **2014**, *6*, 1011-1026, doi:10.4155/bio.14.51.
208. Dettmer, K.; Aronov, P.A.; Hammock, B.D. Mass spectrometry-based metabolomics. *Mass spectrometry reviews* **2007**, *26*, 51-78, doi:10.1002/mas.20108.

209. Lei, Z.; Huhman, D.V.; Sumner, L.W. Mass spectrometry strategies in metabolomics. *J Biol Chem* **2011**, *286*, 25435-25442, doi:10.1074/jbc.R111.238691.
210. Wilson, I.D.; Plumb, R.; Granger, J.; Major, H.; Williams, R.; Lenz, E.M. HPLC-MS-based methods for the study of metabonomics. *Journal of Chromatography B* **2005**, *817*, 67-76, doi:10.1016/j.jchromb.2004.07.045.
211. Xiao, J.F.; Zhou, B.; Resson, H.W. Metabolite identification and quantitation in LC-MS/MS-based metabolomics. *TrAC - Trends in Analytical Chemistry* **2012**, *32*, 1-14, doi:10.1016/j.trac.2011.08.009.
212. Nagana Gowda, G.A.; Raftery, D. Recent Advances in NMR-Based Metabolomics. *Analytical chemistry* **2016**, *89*, 490-510, doi:10.1021/acs.analchem.6b04420.
213. Kostidis, S.; Addie, R.D.; Morreau, H.; Mayboroda, O.A.; Giera, M. Quantitative NMR analysis of intra- and extracellular metabolism of mammalian cells: A tutorial. *Analytica Chimica Acta* **2017**, *980*, 1-24, doi:10.1016/j.aca.2017.05.011.
214. Zamboni, N.; Fendt, S.M.; Ruhl, M.; Sauer, U. (¹³C)-based metabolic flux analysis. *Nature protocols* **2009**, *4*, 878-892, doi:10.1038/nprot.2009.58.
215. Long, C.P.; Antoniewicz, M.R. High-resolution ¹³C metabolic flux analysis. *Nature protocols* **2019**, *10.1038/s41596-019-0204-0*, doi:10.1038/s41596-019-0204-0.
216. Bennett, B.D.; Yuan, J.; Kimball, E.H.; Rabinowitz, J.D. Absolute quantitation of intracellular metabolite concentrations by an isotope ratio-based approach. *Nature protocols* **2008**, *3*, 1299-1311, doi:10.1038/nprot.2008.107.
217. Bajad, S.U.; Lu, W.; Kimball, E.H.; Yuan, J.; Peterson, C.; Rabinowitz, J.D. Separation and quantitation of water soluble cellular metabolites by hydrophilic interaction chromatography-tandem mass spectrometry. *Journal of Chromatography A* **2006**, *1125*, 76-88, doi:10.1016/j.chroma.2006.05.019.
218. Luo, B.; Groenke, K.; Takors, R.; Wandrey, C.; Oldiges, M. Simultaneous determination of multiple intracellular metabolites in glycolysis, pentose phosphate pathway and tricarboxylic acid cycle by liquid chromatography-mass spectrometry. *Journal of Chromatography A* **2007**, *1147*, 153-164, doi:10.1016/j.chroma.2007.02.034.
219. Buescher, J.M.; Moco, S.; Sauer, U.; Zamboni, N. Ultrahigh performance liquid chromatography-tandem mass spectrometry method for fast and robust quantification of anionic and aromatic metabolites. *Analytical chemistry* **2010**, *82*, 4403-4412, doi:10.1021/ac100101d.
220. Guo, L.; Worth, A.J.; Mesaros, C.; Snyder, N.W.; Glickson, J.D.; Blair, I.A. Diisopropylethylamine/hexafluoroisopropanol-mediated ion-pairing ultra-high-performance liquid chromatography/mass spectrometry for phosphate and carboxylate metabolite analysis: utility for studying cellular metabolism. *Rapid Commun Mass Spectrom* **2016**, *30*, 1835-1845, doi:10.1002/rcm.7667.
221. Lu, W.; Bennett, B.D.; Rabinowitz, J.D. Analytical strategies for LC-MS-based targeted metabolomics. *Journal of Chromatography B: Analytical Technologies in the Biomedical and Life Sciences* **2008**, *871*, 236-242, doi:10.1016/j.jchromb.2008.04.031.
222. Roberts, L.D.; Souza, A.L.; Gerszten, R.E.; Clish, C.B. Targeted metabolomics. *Current Protocols in Molecular Biology* **2012**, *1*, doi:10.1002/0471142727.mb3002s98.
223. Gao, Y.; Chen, Y.; Yue, X.; He, J.; Zhang, R.; Xu, J.; Zhou, Z.; Wang, Z.; Zhang, R.; Abliz, Z. Development of simultaneous targeted metabolite quantification and untargeted metabolomics strategy using dual-column liquid chromatography coupled with tandem mass spectrometry. *Analytica Chimica Acta* **2018**, *1037*, 369-379, doi:10.1016/j.aca.2018.08.042.
224. Fuhrer, T.; Zamboni, N. High-throughput discovery metabolomics. *Current opinion in biotechnology* **2015**, *31*, 73-78, doi:10.1016/j.copbio.2014.08.006.
225. De Vos, R.C.H.; Moco, S.; Lommen, A.; Keurentjes, J.J.B.; Bino, R.J.; Hall, R.D. Untargeted large-scale plant metabolomics using liquid chromatography coupled to mass spectrometry. *Nature protocols* **2007**, *2*, 778-791, doi:10.1038/nprot.2007.95.
226. del Val, I.J.; Kyriakopoulos, S.; Polizzi, K.M.; Kontoravdi, C. An optimized method for extraction and quantification of nucleotides and nucleotide sugars from mammalian cells. *Analytical biochemistry* **2013**, *443*, 172-180, doi:10.1016/j.ab.2013.09.005.
227. Bonarius, H.P.J.; Hatzimanikatis, V.; Meesters, K.P.H.; de Gooijer, C.D.; Schmid, G.; Tramper, J. Metabolic flux analysis of hybridoma cells in different culture media using mass balances. *Biotechnology and bioengineering* **1996**, *50*, 299-318.
228. Wiechert, W. ¹³C Metabolic Flux Analysis. *Metabolic engineering* **2001**, *3*, 195-206, doi:10.1006/mben.2001.0187.

229. Zupke, C.; Stephanopoulos, G. Intracellular flux analysis in hybridomas using mass balances and in vitro ^{13}C nmr. *Biotechnology and bioengineering* **1995**, *45*, 292-303, doi:10.1002/bit.260450403.
230. Mancuso, A.; Sharfstein, S.T.; Tucker, S.N.; Clark, D.S.; Blanch, H.W. Examination of primary metabolic pathways in a murine hybridoma with carbon-13 nuclear magnetic resonance spectroscopy. *Biotechnology and bioengineering* **1994**, *44*, 563-585, doi:10.1002/bit.260440504.
231. Templeton, N.; Smith, K.D.; McAtee-Pereira, A.G.; Dorai, H.; Betenbaugh, M.J.; Lang, S.E.; Young, J.D. Application of ^{13}C flux analysis to identify high-productivity CHO metabolic phenotypes. *Metabolic engineering* **2017**, *43*, 218-225, doi:10.1016/j.ymben.2017.01.008.
232. Karst, D.J.; Steinhoff, R.F.; Kopp, M.R.G.; Serra, E.; Soos, M.; Zenobi, R.; Morbidelli, M. Intracellular CHO Cell Metabolite Profiling Reveals Steady-State Dependent Metabolic Fingerprints in Perfusion Culture. *Biotechnology progress* **2017**, *33*, 879-890, doi:10.1002/btpr.2421.
233. Khoo, S.H.G.; Al-Rubeai, M. Metabolic characterization of a hyper-productive state in an antibody producing NSo myeloma cell line. *Metabolic engineering* **2009**, *11*, 199-211, doi:10.1016/j.ymben.2009.02.001.
234. Vodopivec, M.; Lah, L.; Narat, M.; Curk, T. Metabolomic profiling of CHO fed-batch growth phases at 10, 100, and 1,000 L. *Biotechnology and bioengineering* **2019**, *116*, 2720-2729, doi:10.1002/bit.27087.
235. Sellick, C.A.; Croxford, A.S.; Maqsood, A.R.; Stephens, G.; Westerhoff, H.V.; Goodacre, R.; Dickson, A.J. Metabolite profiling of recombinant CHO cells: Designing tailored feeding regimes that enhance recombinant antibody production. *Biotechnology and bioengineering* **2011**, *108*, 3025-3031, doi:10.1002/bit.23269.
236. Popp, O.; Müller, D.; Didzus, K.; Paul, W.; Lipsmeier, F.; Kirchner, F.; Niklas, J.; Mauch, K.; Beaucamp, N. A hybrid approach identifies metabolic signatures of high-producers for chinese hamster ovary clone selection and process optimization. *Biotechnology and bioengineering* **2016**, *113*, 2005-2019, doi:10.1002/bit.25958.
237. Rehberg, M.; Ritter, J.B.; Reichl, U. Glycolysis is governed by growth regime and simple enzyme regulation in adherent MDCK cells. *PLoS computational biology* **2014**, *10*, e1003885, doi:10.1371/journal.pcbi.1003885.
238. Hartley, F.; Walker, T.; Chung, V.; Morten, K. Mechanisms driving the lactate switch in Chinese hamster ovary cells. *Biotechnology and bioengineering* **2018**, *115*, 1890-1903, doi:10.1002/bit.26603.
239. Freund, N.W.; Croughan, M.S. A Simple Method to Reduce both Lactic Acid and Ammonium Production in Industrial Animal Cell Culture. *International Journal of Molecular Sciences* **2018**, *19*, 385.
240. Zhou, M.; Crawford, Y.; Ng, D.; Tung, J.; Pynn, A.F.J.; Meier, A.; Yuk, I.H.; Vijayasankaran, N.; Leach, K.; Joly, J., et al. Decreasing lactate level and increasing antibody production in Chinese Hamster Ovary cells (CHO) by reducing the expression of lactate dehydrogenase and pyruvate dehydrogenase kinases. *Journal of biotechnology* **2011**, *153*, 27-34, doi:10.1016/j.jbiotec.2011.03.003.
241. Chong, W.P.K.; Reddy, S.G.; Yusufi, F.N.K.; Lee, D.-Y.; Wong, N.S.C.; Heng, C.K.; Yap, M.G.S.; Ho, Y.S. Metabolomics-driven approach for the improvement of Chinese hamster ovary cell growth: Overexpression of malate dehydrogenase II. *Journal of biotechnology* **2010**, *147*, 116-121, doi:10.1016/j.jbiotec.2010.03.018.
242. Le, H.; Vishwanathan, N.; Kantardjieff, A.; Doo, I.; Srienc, M.; Zheng, X.; Somia, N.; Hu, W.-S. Dynamic gene expression for metabolic engineering of mammalian cells in culture. *Metabolic engineering* **2013**, *20*, 212-220, doi:10.1016/j.ymben.2013.09.004.
243. Torres, M.; Altamirano, C.; Dickson, A.J. Process and metabolic engineering perspectives of lactate production in mammalian cell cultures. *Current Opinion in Chemical Engineering* **2018**, *22*, 184-190, doi:10.1016/j.coche.2018.10.004.
244. Lin, P.C.; Chan, K.F.; Kiess, I.A.; Tan, J.; Shahreel, W.; Wong, S.Y.; Song, Z. Attenuated glutamine synthetase as a selection marker in CHO cells to efficiently isolate highly productive stable cells for the production of antibodies and other biologics. *mAbs* **2019**, *11*, 965-976, doi:10.1080/19420862.2019.1612690.
245. Fan, L.; Kadura, I.; Krebs, L.E.; Hatfield, C.C.; Shaw, M.M.; Frye, C.C. Improving the efficiency of CHO cell line generation using glutamine synthetase gene knockout cells. *Biotechnology and bioengineering* **2012**, *109*, 1007-1015, doi:10.1002/bit.24365.
246. Gupta, S.K.; Shukla, P. Gene editing for cell engineering: trends and applications. *Critical Reviews in Biotechnology* **2017**, *37*, 672-684, doi:10.1080/07388551.2016.1214557.
247. Katz, L.; Chen, Y.Y.; Gonzalez, R.; Peterson, T.C.; Zhao, H.; Baltz, R.H. Synthetic biology advances and applications in the biotechnology industry: a perspective. *Journal of Industrial Microbiology and Biotechnology* **2018**, *45*, 449-461, doi:10.1007/s10295-018-2056-y.

248. Martínez-Monge, I.; Comas, P.; Triquell, J.; Casablanco, A.; Lecina, M.; Paredes, C.; Cairó, J.J. Concomitant consumption of glucose and lactate: A novel batch production process for CHO cells. *Biochemical Engineering Journal* **2019**, *10*, 1016/j.bej.2019.107358, 107358, doi:10.1016/j.bej.2019.107358.
249. Gagnon, M.; Hiller, G.; Luan, Y.-T.; Kittredge, A.; DeFelice, J.; Drapeau, D. High-End pH-controlled delivery of glucose effectively suppresses lactate accumulation in CHO Fed-batch cultures. *Biotechnology and bioengineering* **2011**, *108*, 1328-1337, doi:10.1002/bit.23072.
250. Hiller, G.W.; Ovalle, A.M.; Gagnon, M.P.; Curran, M.L.; Wang, W. Cell-controlled hybrid perfusion fed-batch CHO cell process provides significant productivity improvement over conventional fed-batch cultures. *Biotechnology and bioengineering* **2017**, *114*, 1438-1447, doi:10.1002/bit.26259.
251. Diop, F.; Vial, T.; Ferraris, P.; Wichit, S.; Bengue, M.; Hamel, R.; Talignani, L.; Liegeois, F.; Pompon, J.; Yssel, H., et al. Zika virus infection modulates the metabolomic profile of microglial cells. *PloS one* **2018**, *13*, doi:10.1371/journal.pone.0206093.
252. Munger, J.; Bajad, S.U.; Collier, H.A.; Shenk, T.; Rabinowitz, J.D. Dynamics of the cellular metabolome during human cytomegalovirus infection. *PLoS Pathogens* **2006**, *2*, 1165-1175, doi:10.1371/journal.ppat.0020132.
253. Roe, B.; Kensicki, E.; Mohnhey, R.; Hall, W.W. Metabolomic profile of hepatitis C Virus-Infected hepatocytes. *PloS one* **2011**, *6*, doi:10.1371/journal.pone.0023641.
254. Rodgers, M.A.; Saghatelian, A.; Yang, P.L. Identification of an overabundant cholesterol precursor in Hepatitis B virus replicating cells by untargeted lipid metabolite profiling. *Journal of the American Chemical Society* **2009**, *131*, 5030-5031, doi:10.1021/ja809949r.
255. Munger, J.; Bennett, B.D.; Parikh, A.; Feng, X.J.; McArdle, J.; Rabitz, H.A.; Shenk, T.; Rabinowitz, J.D. Systems-level metabolic flux profiling identifies fatty acid synthesis as a target for antiviral therapy. *Nature Biotechnology* **2008**, *26*, 1179-1186, doi:10.1038/nbt.1500.
256. Birungi, G.; Chen, S.M.; Loy, B.P.; Ng, M.L.; Li, S.F.Y. Metabolomics approach for investigation of effects of dengue virus infection using the EA.hy926 cell line. *Journal of proteome research* **2010**, *9*, 6523-6534, doi:10.1021/pr100727m.
257. Sanchez, E.L.; Lagunoff, M. Viral activation of cellular metabolism. *Virology* **2015**, *479-480*, 609-618, doi:10.1016/j.virol.2015.02.038.
258. Byers, N.M.; Fleshman, A.C.; Perera, R.; Molins, C.R. Metabolomic Insights into Human Arboviral Infections: Dengue, Chikungunya, and Zika Viruses. *Viruses* **2019**, *11*, 225.
259. Rabinowitz, J.D.; Purdy, J.G.; Vastag, L.; Shenk, T.; Koyuncu, E. Metabolomics in drug target discovery. In *Cold Spring Harbor Symposia on Quantitative Biology*, **2011**, Vol. 76, 235-246.
260. Manchester, M.; Anand, A. Chapter Two - Metabolomics: Strategies to Define the Role of Metabolism in Virus Infection and Pathogenesis. In *Advances in Virus Research*, Kielian, M., Mettenleiter, T.C., Roossinck, M.J., Eds. Academic Press: **2017**, Vol. 98, 57-81.
261. Varanasi, S.K.; Rouse, B.T. How host metabolism impacts on virus pathogenesis. *Current Opinion in Virology* **2018**, *28*, 37-42, doi:10.1016/j.coviro.2017.11.003.
262. Beale, D.J.; Oh, D.Y.; Karpe, A.V.; Tai, C.; Dunn, M.S.; Tilmanis, D.; Palombo, E.A.; Hurt, A.C. Untargeted metabolomics analysis of the upper respiratory tract of ferrets following influenza A virus infection and oseltamivir treatment. *Metabolomics* **2019**, *15*, doi:10.1007/s11306-019-1499-0.
263. Tisoncik-Go, J.; Gasper, D.J.; Kyle, J.E.; Einfeld, A.J.; Selinger, C.; Hatta, M.; Morrison, J.; Korth, M.J.; Zink, E.M.; Kim, Y.M., et al. Integrated Omics Analysis of Pathogenic Host Responses during Pandemic H1N1 Influenza Virus Infection: The Crucial Role of Lipid Metabolism. *Cell Host and Microbe* **2016**, *19*, 254-266, doi:10.1016/j.chom.2016.01.002.
264. Chandler, J.D.; Hu, X.; Ko, E.J.; Park, S.; Lee, Y.T.; Orr, M.; Fernandes, J.; Uppal, K.; Kang, S.M.; Jones, D.P., et al. Metabolic pathways of lung inflammation revealed by high-resolution metabolomics (HRM) of H1N1 influenza virus infection in mice. *American Journal of Physiology - Regulatory Integrative and Comparative Physiology* **2016**, *311*, R906-R916, doi:10.1152/ajpregu.00298.2016.
265. Sun, X.; Song, L.; Feng, S.; Li, L.; Yu, H.; Wang, Q.; Wang, X.; Hou, Z.; Li, X.; Li, Y., et al. Fatty Acid Metabolism is Associated With Disease Severity After H7N9 Infection. *EBioMedicine* **2018**, *33*, 218-229, doi:10.1016/j.ebiom.2018.06.019.
266. Cui, L.; Fang, J.; Ooi, E.E.; Lee, Y.H. Serial Metabolome Changes in a Prospective Cohort of Subjects with Influenza Viral Infection and Comparison with Dengue Fever. *Journal of proteome research* **2017**, *16*, 2614-2622, doi:10.1021/acs.jproteome.7b00173.
267. Lin, S.; Liu, N.; Yang, Z.; Song, W.; Wang, P.; Chen, H.; Lucio, M.; Schmitt-Kopplin, P.; Chen, G.; Cai, Z. GC/MS-based metabolomics reveals fatty acid biosynthesis and cholesterol metabolism in cell lines infected with influenza A virus. *Talanta* **2010**, *83*, 262-268, doi:10.1016/j.talanta.2010.09.019.

268. Carinhas, N.; Pais, D.A.M.; Koshkin, A.; Fernandes, P.; Coroadinha, A.S.; Carrondo, M.J.T.; Alves, P.M.; Teixeira, A.P. Metabolic flux profiling of MDCK cells during growth and canine adenovirus vector production. *Scientific Reports* **2016**, *6*, doi:10.1038/srep23529.
269. Monteiro, F.; Bernal, V.; Saelens, X.; Lozano, A.B.; Bernal, C.; Sevilla, A.; Carrondo, M.J.T.; Alves, P.M. Metabolic profiling of insect cell lines: Unveiling cell line determinants behind system's productivity. *Biotechnology and bioengineering* **2014**, *111*, 816-828, doi:10.1002/bit.25142.
270. Burgener, A.; Coombs, K.; Butler, M. Intracellular ATP and total adenylate concentrations are critical predictors of reovirus productivity from Vero cells. *Biotechnology and bioengineering* **2006**, *94*, 667-679, doi:10.1002/bit.20873.
271. Rodrigues, A.F.; Guerreiro, M.R.; Formas-Oliveira, A.S.; Fernandes, P.; Blechert, A.K.; Genzel, Y.; Alves, P.M.; Hu, W.S.; Coroadinha, A.S. Increased titer and reduced lactate accumulation in recombinant retrovirus production through the down-regulation of HIF1 and PDK. *Biotechnology and bioengineering* **2016**, *113*, 150-162, doi:10.1002/bit.25691.
272. Klemperer, H. Glucose breakdown in chick embryo cells infected with influenza virus. *Virology* **1961**, *13*, 68-77, doi:10.1016/0042-6822(61)90033-2.
273. Genzel, Y.; Ritter, J.B.; König, S.; Alt, R.; Reichl, U. Substitution of Glutamine by Pyruvate To Reduce Ammonia Formation and Growth Inhibition of Mammalian Cells. *Biotechnology progress* **2005**, *21*, 58-69, doi:10.1021/bp049827d.
274. Genzel, Y.; Behrendt, I.; König, S.; Sann, H.; Reichl, U. Metabolism of MDCK cells during cell growth and influenza virus production in large-scale microcarrier culture. *Vaccine* **2004**, *22*, 2202-2208, doi:10.1016/j.vaccine.2003.11.041.
275. Huang, D.; Xia-Hou, K.; Liu, X.P.; Zhao, L.; Fan, L.; Ye, Z.; Tan, W.S.; Luo, J.; Chen, Z. Rational design of medium supplementation strategy for improved influenza viruses production based on analyzing nutritional requirements of MDCK Cells. *Vaccine* **2014**, *32*, 7091-7097, doi:10.1016/j.vaccine.2014.10.067.
276. Chotteau, V. Perfusion Processes. In *Animal Cell Culture*, Al-Rubeai, M., Ed. Springer International Publishing: Cham, **2015**, 407-443, doi:10.1007/978-3-319-10320-4_13.
277. Cadena-Herrera, D.; Esparza-De Lara, J.E.; Ramírez-Ibañez, N.D.; López-Morales, C.A.; Pérez, N.O.; Flores-Ortiz, L.F.; Medina-Rivero, E. Validation of three viable-cell counting methods: Manual, semi-automated, and automated. *Biotechnology Reports* **2015**, *7*, 9-16, doi:10.1016/j.btre.2015.04.004.
278. Genzel, Y.; Reichl, U. Vaccine Production. In *Animal Cell Biotechnology: Methods and Protocols*, Pörtner, R., Ed. Humana Press: Totowa, NJ, **2007**, 457-473, doi:10.1007/978-1-59745-399-8_21.
279. Spearman, C. Review of The Method of 'Right and Wrong Cases' ('Constant Stimuli') without Gauss's Formula. *Psychological Bulletin* **1909**, *6*, 27-28, doi:10.1037/h0063767.
280. Kärber, G. Beitrag zur kollektiven Behandlung pharmakologischer Reihenversuche. *Naunyn-Schmiedebergs Archiv für experimentelle Pathologie und Pharmakologie* **1931**, *162*, 480-483, doi:10.1007/bf01863914.
281. Kalbfuss, B.; Knöchlein, A.; Kröber, T.; Reichl, U. Monitoring influenza virus content in vaccine production: Precise assays for the quantitation of hemagglutination and neuraminidase activity. *Biologicals* **2008**, *36*, 145-161, doi:10.1016/j.biologicals.2007.10.002.
282. Kalbfuss, B.; Knochlein, A.; Krober, T.; Reichl, U. Monitoring influenza virus content in vaccine production: precise assays for the quantitation of hemagglutination and neuraminidase activity. *Biologicals* **2008**, *36*, 145-161.
283. Frensing, T.; Kupke, S.Y.; Bachmann, M.; Fritzsche, S.; Gallo-Ramirez, L.E.; Reichl, U. Influenza virus intracellular replication dynamics, release kinetics, and particle morphology during propagation in MDCK cells. *Applied microbiology and biotechnology* **2016**, *100*, 7181-7192, doi:10.1007/s00253-016-7542-4.
284. Momose, F.; Kikuchi, Y.; Komase, K.; Morikawa, Y. Visualization of microtubule-mediated transport of influenza viral progeny ribonucleoprotein. *Microbes and Infection* **2007**, *9*, 1422-1433, doi:10.1016/j.micinf.2007.07.007.
285. Wood, J.M.; Schild, G.C.; Newman, R.W.; Seagroatt, V. An improved single-radial-immunodiffusion technique for the assay of influenza haemagglutinin antigen: application for potency determinations of inactivated whole virus and subunit vaccines. *Journal of biological standardization* **1977**, *5*, 237-247.
286. Opitz, L.; Lehmann, S.; Reichl, U.; Wolff, M.W. Sulfated membrane adsorbers for economic pseudo-affinity capture of influenza virus particles. *Biotechnology and bioengineering* **2009**, *103*, 1144-1154, doi:10.1002/bit.22345.

287. Volmer, M.; Northoff, S.; Scholz, S.; Thute, T.; Buntmeyer, H.; Noll, T. Fast filtration for metabolome sampling of suspended animal cells. *Biotechnology letters* **2011**, *33*, 495-502, doi:10.1007/s10529-010-0466-7.
288. Hernandez Bort, J.A.; Shanmukam, V.; Pabst, M.; Windwarder, M.; Neumann, L.; Alchalabi, A.; Krebichl, G.; Koellensperger, G.; Hann, S.; Sonntag, D., et al. Reduced quenching and extraction time for mammalian cells using filtration and syringe extraction. *Journal of biotechnology* **2014**, *182-183*, 97-103, doi:10.1016/j.jbiotec.2014.04.014.
289. Matuszczyk, J.-C.; Teleki, A.; Pfizenmaier, J.; Takors, R. Compartment-specific metabolomics for CHO reveals that ATP pools in mitochondria are much lower than in cytosol. *Biotechnology Journal* **2015**, *10*, 1639-1650, doi:10.1002/biot.201500060.
290. Sellick, C.A.; Hansen, R.; Stephens, G.M.; Goodacre, R.; Dickson, A.J. Metabolite extraction from suspension-cultured mammalian cells for global metabolite profiling. *Nature protocols* **2011**, *6*, 1241-1249, doi:10.1038/nprot.2011.366.
291. Ritter, J.B.; Genzel, Y.; Reichl, U. Simultaneous extraction of several metabolites of energy metabolism and related substances in mammalian cells: optimization using experimental design. *Analytical biochemistry* **2008**, *373*, 349-369, doi:10.1016/j.ab.2007.10.037.
292. Rath, A.G.; Rehberg, M.; Janke, R.; Genzel, Y.; Scholz, S.; Noll, T.; Rose, T.; Sandig, V.; Reichl, U. The influence of cell growth and enzyme activity changes on intracellular metabolite dynamics in AGE1.HN.AAT cells. *Journal of biotechnology* **2014**, *178*, 43-53, doi:10.1016/j.jbiotec.2014.03.012.
293. Mihut, A.N. Biotechnologische Impfstoffproduktion: Bedeutung der Zelllinie, Medien und Methoden für die Virusausbeuten im Upstream-Verfahren. Karlsruhe Institute of Technology, University Library, 2017.
294. Fritsch, J. Prozessintensivierung der zellkulturbasierten Influenza-A Produktion mittels MDCK Hochzelldichte. Otto-von-Guericke University Magdeburg, University Library, 2017.
295. Bissinger, T.; Fritsch, J.; Mihut, A.; Wu, Y.; Liu, X.; Genzel, Y.; Tan, W.-S.; Reichl, U. Semi-perfusion cultures of suspension MDCK cells enable high cell concentrations and efficient influenza A virus production. *Vaccine* **2019**, *10.1016/j.vaccine.2019.04.054*, doi:10.1016/j.vaccine.2019.04.054.
296. Eaton, M.D.; Low, I.E.; Scala, A.R.; Uretsky, S. Inhibition by ammonium ion of the growth of influenza virus in chorioallantoic tissue. *Virology* **1962**, *18*, 102-108, doi:10.1016/0042-6822(62)90182-4.
297. Eaton, M.D.; Scala, A.R. Inhibitory effect of glutamine and ammonia on replication of influenza virus in ascites tumor cells. *Virology* **1961**, *13*, 300-307, doi:10.1016/0042-6822(61)90149-0.
298. Eaton, M.D.; Scala, A.R. Ammonium chloride and viral penetration. *Archiv für die gesamte Virusforschung* **1967**, *20*, 411-420, doi:10.1007/bfo1275221.
299. Bernal, V.; Carinhas, N.; Yokomizo, A.Y.; Carrondo, M.J.; Alves, P.M. Cell density effect in the baculovirus-insect cells system: a quantitative analysis of energetic metabolism. *Biotechnology and bioengineering* **2009**, *104*, 162-180, doi:10.1002/bit.22364.
300. Petiot, E.; Jacob, D.; Lanthier, S.; Lohr, V.; Ansoerge, S.; Kamen, A.A. Metabolic and Kinetic analyses of influenza production in perfusion HEK293 cell culture. *BMC biotechnology* **2011**, *11*, 84, doi:10.1186/1472-6750-11-84.
301. George, M.; Farooq, M.; Dang, T.; Cortes, B.; Liu, J.; Maranga, L. Production of cell culture (MDCK) derived live attenuated influenza vaccine (LAIV) in a fully disposable platform process. *Biotechnology and bioengineering* **2010**, *106*, 906-917, doi:10.1002/bit.22753.
302. Aggarwal, K.; Jing, F.; Maranga, L.; Liu, J. Bioprocess optimization for cell culture based influenza vaccine production. *Vaccine* **2011**, *29*, 3320-3328, doi:10.1016/j.vaccine.2011.01.081.
303. Wen, Z.; Wu, C.; Chen, W.; Zeng, X.; Shi, J.; Ge, J.; Chen, H.; Bu, Z. Establishment of MDCK Stable Cell Lines Expressing TMRSS2 and MSPL and Their Applications in Propagating Influenza Vaccine Viruses in Absence of Exogenous Trypsin. *Biotechnology Research International* **2015**, *2015*, 1-9, doi:10.1155/2015/402628.
304. Feng, L.; Tang, Y.; Wu, P.; Chu, X.; Wang, W.; Hou, J. H9 subtype influenza vaccine in MDCK single-cell suspension culture with stable expression of TMRSS2: Generation and efficacy evaluation. *Engineering in Life Sciences* **2016**, *16*, 795-807, doi:10.1002/elsc.201600110.
305. Mercier, S.M.; Diepenbroek, B.; Martens, D.; Wijffels, R.H.; Streefland, M. Characterization of apoptosis in PER.C6® batch and perfusion cultures. *Biotechnology and bioengineering* **2015**, *112*, 569-578, doi:10.1002/bit.25459.
306. Bielser, J.-M.; Wolf, M.; Souquet, J.; Broly, H.; Morbidelli, M. Perfusion mammalian cell culture for recombinant protein manufacturing – A critical review. *Biotechnology Advances* **2018**, *36*, 1328-1340, doi:10.1016/j.biotechadv.2018.04.011.

307. Nikolay, A.; Léon, A.; Schwamborn, K.; Genzel, Y.; Reichl, U. Process intensification of EB66® cell cultivations leads to high-yield yellow fever and Zika virus production. *Applied microbiology and biotechnology* **2018**, *102*, 8725-8737, doi:10.1007/s00253-018-9275-z.
308. Kiehl, T.R.; Shen, D.; Khattak, S.F.; Jian Li, Z.; Sharfstein, S.T. Observations of cell size dynamics under osmotic stress. *Cytometry Part A* **2011**, *79A*, 560-569, doi:10.1002/cyto.a.21076.
309. Pan, X.; Dalm, C.; Wijffels, R.H.; Martens, D.E. Metabolic characterization of a CHO cell size increase phase in fed-batch cultures. *Applied microbiology and biotechnology* **2017**, *101*, 8101-8113, doi:10.1007/s00253-017-8531-y.
310. Lloyd, D.R.; Holmes, P.; Jackson, L.P.; Emery, A.N.; Al-Rubeai, M. Relationship between cell size, cell cycle and specific recombinant protein productivity. *Cytotechnology* **2000**, *34*, 59-70, doi:10.1023/a:1008103730027.
311. Mulukutla, B.C.; Gramer, M.; Hu, W.S. On metabolic shift to lactate consumption in fed-batch culture of mammalian cells. *Metabolic engineering* **2012**, *14*, 138-149, doi:10.1016/j.ymben.2011.12.006.
312. Wang, H.; Guo, S.; Li, Z.; Xu, X.; Shao, Z.; Song, G. Suspension culture process for H9N2 avian influenza virus (strain Re-2). *Archives of Virology* **2017**, *162*, 3051-3059, doi:10.1007/s00705-017-3460-8.
313. Ma, N.; Ellet, J.; Okediadi, C.; Hermes, P.; McCormick, E.; Casnocha, S. A single nutrient feed supports both chemically defined NSo and CHO fed-batch processes: Improved productivity and lactate metabolism. *Biotechnology progress* **2009**, *25*, 1353-1363, doi:10.1002/btpr.238.
314. Ivarsson, M.; Noh, H.; Morbidelli, M.; Soos, M. Insights into pH-induced metabolic switch by flux balance analysis. *Biotechnology progress* **2015**, *31*, 347-357, doi:10.1002/btpr.2043.
315. Scholtissek, C. Stability of infectious influenza A viruses to treatment at low pH and heating. *Archives of Virology* **1985**, *85*, 1-11, doi:10.1007/BF01317001.
316. Le Ru, A.; Jacob, D.; Transfiguracion, J.; Ansorge, S.; Henry, O.; Kamen, A.A. Scalable production of influenza virus in HEK-293 cells for efficient vaccine manufacturing. *Vaccine* **2010**, *28*, 3661-3671, doi:10.1016/j.vaccine.2010.03.029.
317. Petiot, E.; Proust, A.; Traversier, A.; Dourous, L.; Dappozze, F.; Gras, M.; Guillard, C.; Balloul, J.M.; Rosa-Calatrava, M. Influenza viruses production: Evaluation of a novel avian cell line DuckCelt(R)-T17. *Vaccine* **2018**, *36*, 3101-3111, doi:10.1016/j.vaccine.2017.03.102.
318. Shen, C.F.; Guilbault, C.; Li, X.; Elahi, S.M.; Ansorge, S.; Kamen, A.; Gilbert, R. Development of suspension adapted Vero cell culture process technology for production of viral vaccines. *Vaccine* **2019**, *37*, 6996-7002, doi:10.1016/j.vaccine.2019.07.003.
319. Gallardo, P.M. Chromatographic purification of biological macromolecules by their capture on hydrophilic surfaces with the aid of non-ionic polymers. Otto von Guericke University Magdeburg, 2019.
320. Schneider, M.; Marison, I.W.; von Stockar, U. The importance of ammonia in mammalian cell culture. *Journal of biotechnology* **1996**, *46*, 161-185, doi:10.1016/0168-1656(95)00196-4.
321. Slivac, I.; Blajić, V.; Radošević, K.; Kniewald, Z.; Gaurina Srček, V. Influence of different ammonium, lactate and glutamine concentrations on CCO cell growth. *Cytotechnology* **2010**, *62*, 585-594, doi:10.1007/s10616-010-9312-y.
322. Eagle, H. Amino Acid Metabolism in Mammalian Cell Cultures. *Science* **1959**, *130*, 432-437, doi:10.1126/science.130.3373.432.
323. Bissinger, T.; Wu, Y.; Marichal-Gallardo, P.; Riedel, D.; Liu, X.; Genzel, Y.; Tan, W.-S.; Reichl, U. Integrated manufacturing of an influenza vaccine candidate with MDCK suspension cells. *In preparation* **2020**.
324. Ljunggren, J.; Häggström, L. Catabolic control of hybridoma cells by glucose and glutamine limited fed batch cultures. *Biotechnology and bioengineering* **1994**, *44*, 808-818, doi:10.1002/bit.260440706.
325. Maranga, L.; Goochee, C.F. Metabolism of PER.C6TM cells cultivated under fed-batch conditions at low glucose and glutamine levels. *Biotechnology and bioengineering* **2006**, *94*, 139-150, doi:10.1002/bit.20890.
326. Altamirano, C.; Paredes, C.; Cairó, J.J.; Gòdia, F. Improvement of CHO Cell Culture Medium Formulation: Simultaneous Substitution of Glucose and Glutamine. *Biotechnology progress* **2000**, *16*, 69-75, doi:10.1021/bp990124j.
327. Christie, A.; Butler, M. The adaptation of bhk cells to a non-ammoniogenic glutamate-based culture medium. *Biotechnology and bioengineering* **1999**, *64*, 298-309, doi:10.1002/(sici)1097-0290(19990805)64:3<298::Aid-bit6>3.o.Co;2-u.

-
328. Hu, A.Y.-C.; Tseng, Y.-F.; Weng, T.-C.; Liao, C.-C.; Wu, J.; Chou, A.-H.; Chao, H.-J.; Gu, A.; Chen, J.; Lin, S.-C., et al. Production of Inactivated Influenza H5N1 Vaccines from MDCK Cells in Serum-Free Medium. *PLoS one* **2011**, *6*, e14578, doi:10.1371/journal.pone.0014578.
329. Bock, A.; Schulze-Horsel, J.; Schwarzer, J.; Rapp, E.; Genzel, Y.; Reichl, U. High-density microcarrier cell cultures for influenza virus production. *Biotechnology progress* **2011**, *27*, 241-250, doi:10.1002/btpr.539.
330. Ringeisen, J. Comparison of quenching methods for metabolic profiling of animal suspension cell lines. University of Applied Life Sciences Emden/Leer, University Library, 2016.
331. Bordag, N.; Janakiraman, V.; Nachtigall, J.; González Maldonado, S.; Bethan, B.; Laine, J.-P.; Fux, E. Fast Filtration of Bacterial or Mammalian Suspension Cell Cultures for Optimal Metabolomics Results. *PLoS one* **2016**, *11*, e0159389-e0159389, doi:10.1371/journal.pone.0159389.
332. Atkinson, D.E. The Energy Charge of the Adenylate Pool as a Regulatory Parameter. Interaction with Feedback Modifiers. *Biochemistry* **1968**, *7*, 4030-4034, doi:10.1021/bio0851a033.
333. Faijes, M.; Mars, A.E.; Smid, E.J. Comparison of quenching and extraction methodologies for metabolome analysis of *Lactobacillus plantarum*. *Microbial Cell Factories* **2007**, *6*, doi:10.1186/1475-2859-6-27.
334. Gravel, S.P.; Andrzejewski, S.; Avizonis, D.; St-Pierre, J. Stable isotope tracer analysis in isolated mitochondria from Mammalian systems. *Metabolites* **2014**, *4*, 166-183, doi:10.3390/metabo4020166.
335. Chen, W.W.; Freinkman, E.; Wang, T.; Birsoy, K.; Sabatini, D.M. Absolute Quantification of Matrix Metabolites Reveals the Dynamics of Mitochondrial Metabolism. *Cell* **2016**, *166*, 1324-1337 e1311, doi:10.1016/j.cell.2016.07.040.
336. Pan, D.; Lindau, C.; Lagies, S.; Wiedemann, N.; Kammerer, B. Metabolic profiling of isolated mitochondria and cytoplasm reveals compartment-specific metabolic responses. *Metabolomics : Official journal of the Metabolomic Society* **2018**, *14*, 59-59, doi:10.1007/s11306-018-1352-x.
337. <conversion of MDCK cell line to suspension culture by transfecting with human siat7e gene and its application for influenza virus production.pdf>.
338. Brunner, M.; Doppler, P.; Klein, T.; Herwig, C.; Fricke, J. Elevated pCO₂ affects the lactate metabolic shift in CHO cell culture processes. *Engineering in Life Sciences* **2018**, *18*, 204-214, doi:10.1002/elsc.201700131.
339. Sidorenko, Y.; Wahl, A.; Dauner, M.; Genzel, Y.; Reichl, U. Comparison of metabolic flux distributions for MDCK cell growth in glutamine- and pyruvate-containing media. *Biotechnology progress* **2008**, *24*, 311-320, doi:10.1021/bpo702673.
340. Frensing, T.; Pflugmacher, A.; Bachmann, M.; Peschel, B.; Reichl, U. Impact of defective interfering particles on virus replication and antiviral host response in cell culture-based influenza vaccine production. *Applied microbiology and biotechnology* **2014**, *98*, 8999-9008, doi:10.1007/s00253-014-5933-y.
341. Mahmoudabadi, G.; Milo, R.; Phillips, R. Energetic cost of building a virus. *Proceedings of the National Academy of Sciences* **2017**, *114*, E4324-E4333, doi:10.1073/pnas.1701670114.
342. Dai, Z.; Locasale, J.W. Understanding metabolism with flux analysis: From theory to application. *Metabolic engineering* **2017**, *43*, 94-102, doi:10.1016/j.ymben.2016.09.005.
343. Galleguillos, S.N.; Ruckerbauer, D.; Gerstl, M.P.; Borth, N.; Hanscho, M.; Zanghellini, J. What can mathematical modelling say about CHO metabolism and protein glycosylation? *Comput Struct Biotechnol J* **2017**, *15*, 212-221, doi:10.1016/j.csbj.2017.01.005.
344. Martinez-Monge, I.; Albiol, J.; Lecina, M.; Liste-Calleja, L.; Miret, J.; Sola, C.; Cairo, J.J. Metabolic flux balance analysis during lactate and glucose concomitant consumption in HEK293 cell cultures. *Biotechnology and bioengineering* **2019**, *116*, 388-404, doi:10.1002/bit.26858.
345. Searles, J.; Todd, P.; Kompala, D. Viable Cell Recycle with an Inclined Settler in the Perfusion Culture of Suspended Recombinant Chinese Hamster Ovary Cells. *Biotechnology progress* **1994**, *10*, 198-206, doi:10.1021/bp00026a600.
346. Voisard, D.; Meuwly, F.; Ruffieux, P.-A.; Baer, G.; Kadouri, A. Potential of cell retention techniques for large-scale high-density perfusion culture of suspended mammalian cells. *Biotechnology and bioengineering* **2003**, *82*, 751-765, doi:10.1002/bit.10629.
347. Shirgaonkar, I.Z.; Lanthier, S.; Kamen, A. Acoustic cell filter: a proven cell retention technology for perfusion of animal cell cultures. *Biotechnology Advances* **2004**, *22*, 433-444, doi:10.1016/j.biotechadv.2004.03.003.
348. Wu, Y.; Bissinger, T.; Genzel, Y.; Liu, X.; Reichl, U.; Tan, W.-S. High cell density perfusion process for high yield of influenza A virus production using MDCK suspension cells. *In preparation* **2020**.

8 Appendix

8.1 Cultivation media for MDCK suspension

Xeno-S001S preparation SOP

Glutamine-free

- (1) To a mixing container add final volume of deionized or distilled water at 28-32°C.
- (2) Start the stirring, but avoid to generate bubbles.
- (3) Gently add Xeno-CD001S powder at 26.04 g/L to water, and fully mix for 20-30 min.
- (4) Adjust pH to 6.2-6.7 with 5 mol/L NaOH solution and fully mix for 10-20 min. Or add 0.25g/L NaOH powder.
- (5) Precisely weigh out sodium bicarbonate powder at 2.00 g/L and gently add to the medium, fully mix for 10-20 min.
- (6) When completely dissolved, adjust the pH to 7.0-7.4 (if needed).
- (7) Filter sterilize by 0.22 µm pore size membrane filtration.
- (8) Once the final liquid medium is sterilized, store at 2-8°C for up to one month. Protect from light.

Xeno-CD001S preparation SOP

Glutamine-free

- (1) To a mixing container add final volume of deionized or distilled water at 28-32°C.
- (2) Start the stirring, but avoid to generate bubbles.
- (3) Gently add Xeno-CD001S powder at 21.04 g/L to water, and fully mix for 20-30 min.
- (4) Adjust pH to 6.2-6.7 with 5 mol/L NaOH solution and fully mix for 10-20 min. Or add 0.25 g/L NaOH powder.
- (5) Precisely weigh out sodium bicarbonate powder at 2.00 g/L and gently add to the medium, fully mix for 10-20 min.
- (6) When completely dissolved, adjust the pH to 7.0-7.4 (if needed).
- (7) Filter sterilize by 0.22 µm pore size membrane filtration.
- (8) Once the final liquid medium is sterilized, store at 2-8°C for up to one month. Protect from light.

Working instruction Nr. M/ 03.3

Production of Smif 8 PGd- medium 2x from medium powder:

Ingredient	Reference number	Amount for 5 L
Milli-Q Water		Add to 5 L
Smif 8-PGd powder medium (FH Emden)	Ref M0-16-02 GMP	30.59 g
NaCl (Roth)	Ref P029.3	25.0 g
NaHCO₃ (Roth)	Ref HN01.2	10.0 g
Ethanolamine (98%) (Sigma)		10 µL
L-glutamic acid (Merck)	Ref 1.00291.0250	1.21 g
D-(+)-glucose water free (Roth)	Ref X997.3	18.30 g
Pluronic F68 10% (GIBCO Invitrogen)	Ref 24040-032	50 mL

Comments:

adjust pH: 7.00
Osmolality: 300 mmol/kg

8.2 LC-MS measurement

Table 15: Overview of single ion monitoring channels for metabolite quantification by MS.

Name	Mass	Span	Time range (min)	Dwell time	Polarity	Cone (V)
Sim 1: Pyr	87.0	1.0	3.5-6.5	0.1	-ve	30
Sim 2: Fum	115.0	1.0	16.0-18.5	0.1	-ve	30
Sim 3: Suc	117.0	1.0	12.0-15.0	0.1	-ve	30
Sim 4: Aconitate	129.2	1.0	28.5-33.0	0.1	-ve	50
Sim 5 Mal	133.0	1.0	12.5-15.0	0.1	-ve	35
Sim 6: α -KG	145.1	1.0	15.0-17.5	0.1	-ve	30
Sim 7: PEP	166.8	1.0	28.0-31.0	0.1	-ve	35
Sim 8: 3-PG	185.2	1.0	24.0-26.5	0.1	-ve	45
Sim 9: Cit	191.3	1.0	25.5-29.0	0.1	-ve	35
Sim 10: R5P	229.2	1.0	18.0-20.5	0.1	-ve	45
Sim 11: Hex-P	259.0	1.0	14.5-19.5	0.1	-ve	50
Sim 12: G1P	259.0	1.0	10.5-12.5	0.1	-ve	50
Sim 13: UDP-Hex	302.4	1.0	27.0-30.0	0.1	-ve	35
Sim 14: UMP	323.4	1.0	29.5-32.5	0.1	-ve	50
Sim 15: F16BP	339.1	1.0	35.0-37.5	0.1	-ve	30
Sim 16: AMP	346.1	1.0	18.5-22.0	0.1	-ve	60
Sim 17: GMP	362.2	1.0	35.0-37.0	0.1	-ve	60
Sim 18: CDP	402.0	1.0	26.5-29.0	0.1	-ve	70
Sim 19: UDP-Glc	502.0	1.0	30.0-30.0	0.1	-ve	30

Table 16: Metabolite standard mix used as standard for LC-MS analysis.

Category	Substance Name	Supplier	Product Number	CAS-Number	Lot Purity [%]	Conc. Master-Mix [μ M]	Conc. Std 155 [μ M]	Conc. Std 005 [μ M]
Additives	Sodium acetate	Sigma-Aldrich	S8750-250G	127-09-3	99.6	100	15.5	0.5
Additives	Sodium chloride	Roth	P029-3	7647-14-5	100	100	15.5	0.5
Additives	Sodium formate	Sigma-Aldrich	17841-50G	141-53-7	100	100	15.5	0.5
Additives	Sodium nitrate	Merck	1065371000	7631-99-4	99.5	100	15.5	0.5
Additives	Sodium sulfate	Roth	8631-2	7757-82-6	99	800	124	4
Nucleo-sugars	Disodium uridine-diphospho-N-acetylgalactosamine	Sigma-Aldrich	U5252-5MG	108320-87-2	100	60	9.3	0.3
Nucleo-sugars	Disodium uridine-diphospho-N-acetylglucosamine	Sigma-Aldrich	U4375-100MG	9183-98-1	99	200	31	1
Nucleo-sugars	Disodium uridine-diphosphoglucose hydrate	Sigma-Aldrich	U4625-100MG	28053-08-9	100	100	15.5	0.5
Nucleotides	Sodium adenosine-diphosphate	Sigma-Aldrich	A2754-100MG	20398-34-9	99	150	23.25	0.75
Nucleotides	Sodium adenosine-monophosphate	Sigma-Aldrich	01930-5G	4578-31-8	99.7	25	3.875	0.125
Nucleotides	Disodium adenosine-triphosphate hydrate	Sigma-Aldrich	A2383-1G	34369-07-8	99	2000	310	10
Nucleotides	Sodium cytidine-diphosphate	Sigma-Aldrich	C9755-25MG	34393-59-4	95	12.5	1.9375	0.0625
Nucleotides	Disodium cytidine-monophosphate	Sigma-Aldrich	C1006-500MG	6757-06-8	100	10	1.55	0.05
Nucleotides	Disodium cytidine-triphosphate	Sigma-Aldrich	C1506-100MG	36051-68-0	95.3	100	15.5	0.5
Nucleotides	Sodium guanosine-diphosphate	Sigma-Aldrich	G7127-100MG	43139-22-6	98	40	6.2	0.2
Nucleotides	Disodium guanosine-monophosphate hydrate	Sigma-Aldrich	G8377-500MG	5550-12-9	99.9	12.5	1.9375	0.0625
Nucleotides	Sodium guanosine-triphosphate hydrate	Sigma-Aldrich	G8877-25MG	36051-31-7	96	240	37.2	1.2
Nucleotides	Disodium uridine-diphosphate hydrate	Sigma-Aldrich	94330-100MG	27821-45-0	98.8	25	3.875	0.125
Nucleotides	Disodium uridine-monophosphate	Sigma-Aldrich	U6375-1G	3387-36-8	100	40	6.2	0.2
Nucleotides	Trisodium uridine-triphosphate hydrate	Sigma-Aldrich	U6625-100MG	19817-92-6	96	500	77.5	2.5
Organic acids	D-(-)-3-Phosphoglyceric acid disodium salt	Sigma-Aldrich	P8877-10MG	80731-10-8	93	50	7.75	0.25
Organic acids	cis-Aconitic acid	Sigma-Aldrich	A3412-1G	585-84-2	99	25	3.875	0.125
Organic acids	Citric acid monohydrate	Sigma-Aldrich	C1909-25G	5949-29-1	100	200	31	1
Organic acids	Fumaric acid	Sigma-Aldrich	F19353-25G	110-17-8	99.7	25	3.875	0.125
Organic acids	Trisodium isocitric acid hydrate	Sigma-Aldrich	I152-1G	1637-73-6	99	20	3.1	0.1
Organic acids	Sodium L-lactate	Sigma-Aldrich	L7022-5G	867-56-1	99.8	160	24.8	0.8
Organic acids	DL-Malic acid	Sigma-Aldrich	M0875-100G	6915-15-7	99	250	38.75	1.25
Organic acids	Potassium phophoenolpyruvate	Applichem	A2271,0250	4265-07-0	98	25	3.875	0.125
Organic acids	Sodium pyruvate	Sigma-Aldrich	P8574-100G	113-24-6	100	200	31	1
Organic acids	Disodium succinate	Sigma-Aldrich	224731-5G	150-90-3	99.9	100	15.5	0.5
Organic acids	α -Ketoglutaric acid	Sigma-Aldrich	K1750-100G	328-50-7	100	100	15.5	0.5
Phospho-sugars	Trisodium D-fructose-1,6-bisphosphate hydrate	Sigma-Aldrich	F6803-10MG	38099-82-0	100	150	23.25	0.75
Phospho-sugars	Fructose-1-Phosphate Sodium salt	Sigma-Aldrich	sc-214802	53823-70-4	97	35	5.425	0.175
Phospho-sugars	Disodium fructose-6-phosphate hydrate	Sigma-Aldrich	F6027-100MG	26177-86-6	100	25	3.875	0.125
Phospho-sugars	Disodium α -D-glucose-1-phosphate hydrate	Sigma-Aldrich	G7000-1G	56401-20-8	100	35	5.425	0.175
Phospho-sugars	Sodium α -D-glucose-6-phosphate	Sigma-Aldrich	G7879-500MG	54010-71-8	100	35	5.425	0.175
Phospho-sugars	Disodium ribose-5-Phosphate dihydrate	Sigma-Aldrich	83875-250MG	207671-46-3	100	25	3.875	0.125

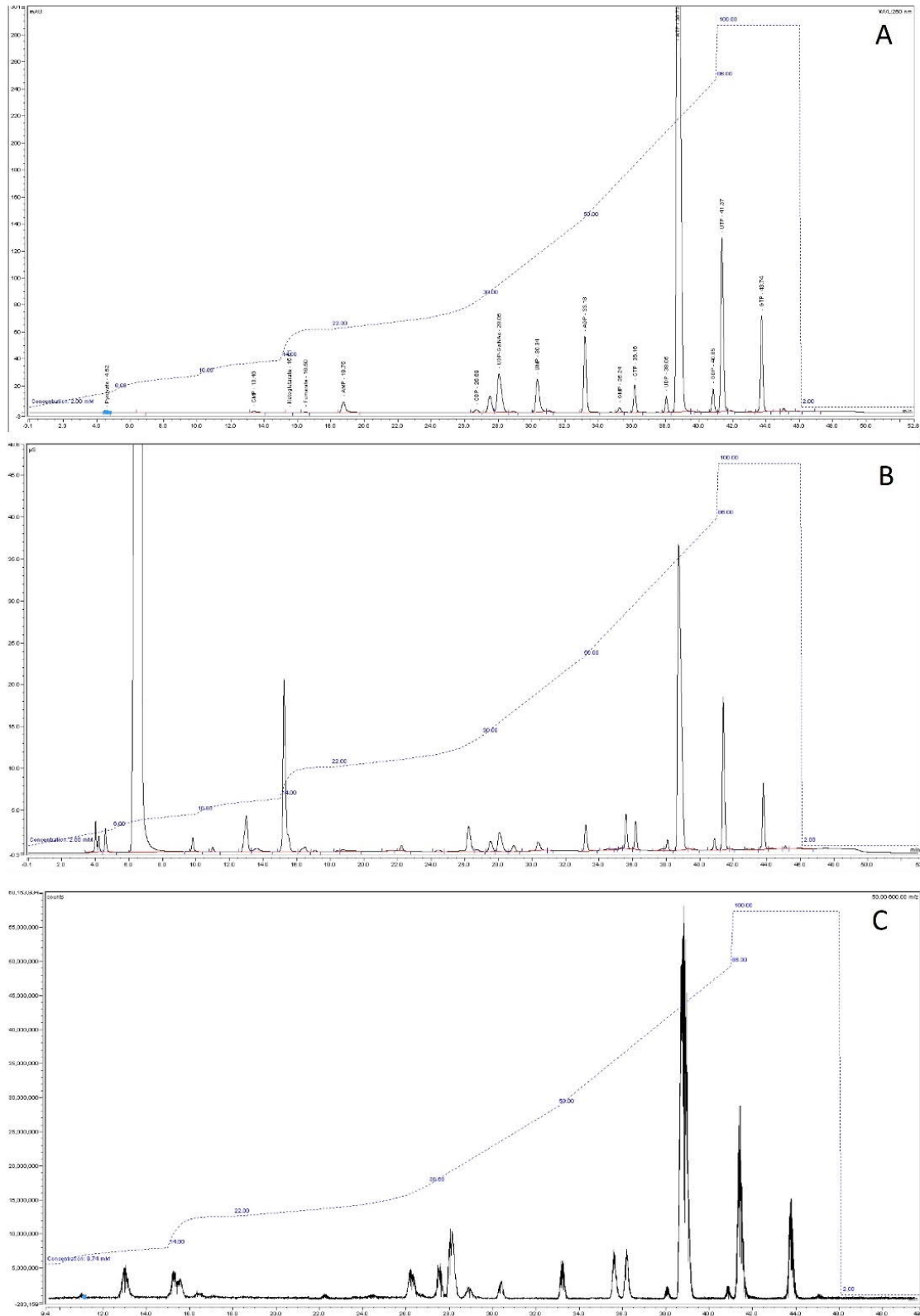


Figure 37: Chromatogram of the metabolite standard used for LC-MS analysis

Metabolite standard (105) measured with the standard LC-MS program run for the quantification of intracellular metabolites. Chromatogram of the standard from the UV-detector (A), conductivity detector (B) and the total ion chromatogram of MS-detector (C). The gradient is depicted in each chromatogram as an overlay.

8.3 Error estimation: TCID₅₀ assay

Individual measurements			Relative standard deviation	
TCID ₅₀ /mL			%	
1.00E+04	1.00E+04	1.30E+04	15.74591643	15.74591643
1.00E+07	4.30E+06	3.20E+07	94.77852404	removed (top 3)
7.60E+08	4.30E+08	1.00E+09	39.20298088	39.20298088
1.00E+09	1.80E+09	3.20E+09	55.67764363	55.67764363
2.40E+09	2.40E+09	3.20E+09	17.32050808	17.32050808
1.30E+09	4.30E+09	1.30E+09	75.30655685	75.30655685
1.80E+09	1.80E+09	3.20E+09	35.65986957	35.65986957
1.80E+09	1.00E+09	1.30E+09	29.57159915	29.57159915
7.60E+08	7.60E+08	1.00E+09	16.49572198	16.49572198
2.40E+08	1.00E+07	7.60E+07	108.9833744	removed (top 3)
3.20E+07	3.20E+07	5.60E+07	34.64101615	34.64101615
5.60E+07	1.00E+07	3.20E+07	70.43034256	70.43034256
	4.30E+08	4.30E+08	0	removed (bottom 3)
7.60E+08		5.60E+08	21.42747822	21.42747822
3.20E+08	1.30E+09	5.60E+08	70.29582662	70.29582662
1.00E+09	4.30E+08	5.60E+08	45.03308885	45.03308885
1.00E+08	1.80E+08	3.20E+08	55.67764363	55.67764363
7.60E+06	1.80E+07	7.60E+06	54.25701325	54.25701325
4.30E+07	5.60E+07	1.80E+08	81.31620456	removed (top 3)
1.00E+08	3.20E+08	1.30E+08	65.07465516	65.07465516
4.30E+07	3.20E+07	4.30E+07	16.14623634	16.14623634
4.30E+05	5.60E+05	7.60E+05	28.49704603	28.49704603
3.20E+08	2.40E+08	1.80E+08	28.47473987	28.47473987
1.80E+08	3.20E+08	5.60E+08	54.39069927	54.39069927
5.60E+08	1.00E+09	4.30E+08	45.03308885	45.03308885
7.60E+08	7.60E+08	2.40E+08	51.17422841	51.17422841
7.60E+08	3.20E+08	5.60E+08	40.29929669	40.29929669
4.30E+08	2.40E+08		40.10456371	40.10456371
4.30E+08	4.30E+08	4.30E+08	0	removed (bottom 3)
1.30E+09	7.60E+08	5.60E+08	43.83168617	43.83168617
1.30E+09	7.60E+08	1.00E+09	26.52499855	26.52499855
1.00E+09	5.60E+08	5.60E+08	35.94822431	35.94822431
5.60E+08	5.60E+08		0	removed (bottom 3)
			Average_all	Average_red
			42.34	41.19

8.4 Error estimation: HA assay

Individual measurements			Standard deviation	
lg(HAU)			lg(HAU)	
3.52	3.27	3.46	0.130511813	removed (top 3)
3.63	3.52	3.55	0.056862407	0.056862407
3.68	3.57	3.59	0.058594653	0.058594653
3.69	3.57	3.6	0.06244998	0.06244998
3.63	3.71	3.57	0.070237692	0.070237692
3.79	3.71	3.64	0.075055535	0.075055535
3.65	3.62	3.64	0.015275252	0.015275252
3.74	3.64	3.69	0.05	0.05
1.99	1.86	1.69	0.150443788	removed (top 3)
3.19	3.25	3.25	0.034641016	0.034641016
3.48	3.51	3.47	0.02081666	0.02081666
3.57	3.62	3.62	0.028867513	0.028867513
3.68	3.7	3.68	0.011547005	0.011547005
3.69	3.58	3.64	0.055075705	0.055075705
1.42	2.57	1.53	0.63458648	removed (top 3)
3.14	3.16	3.17	0.015275252	0.015275252
3.38	3.32	3.31	0.037859389	0.037859389
3.38	3.42	3.34	0.04	0.04
3.31	3.42	3.4	0.058594653	0.058594653
2.43	2.43	2.44	0.01113437	removed (bottom 3)
2.91	2.90	2.89	0.008967252	removed (bottom 3)
3.07	3.14	3.11	0.033765779	0.033765779
3.23	3.26	3.15	0.060662882	0.060662882
3.28	3.23	3.23	0.028663948	0.028663948
3.30	3.29	3.26	0.019962276	0.019962276
2.69	2.65	2.7	0.026457513	0.026457513
2.97	2.85	2.84	0.072341781	0.072341781
3.05	2.99	2.99	0.034641016	0.034641016
3.19	3.13	3.11	0.04163332	0.04163332
3.23	3.22	3.22	0.005773503	removed (bottom 3)
			Average_all	Average_red
			0.065023281	0.042053385
			RSD_all	RSD_red
			%	%
			14.97216378	9.68314963